5-2017

Sequence Stratigraphy, Chemostratigraphy, and Biostratigraphy of Lower Ordovician units in Northeastern and Western Central Utah: Regional Implications

Colter R. Davis
Utah State University

SEQUENCE STRATIGRAPHY, CHEMOSTRATIGRAPHY, AND BIOSTRATIGRAPHY OF LOWER ORDOVICIAN UNITS IN NORTHEASTERN AND WESTERN CENTRAL UTAH: REGIONAL IMPLICATIONS

by

Colter R. Davis

A thesis submitted in partial fulfillment
of the requirements for the degree

of

MASTER OF SCIENCE

in

Geology

Approved:

_____	_____
W. David Liddell, Ph.D. Major Professor	Dennis L. Newell, Ph.D. Committee Member
_____	_____
Benjamin J. Burger, Ph.D. Committee Member	Mark McLellan, Ph.D. Vice President for Research and Dean of the School of Graduate Studies

UTAH STATE UNIVERSITY
Logan, Utah

2017

ABSTRACT

Sequence Stratigraphy, Chemostratigraphy, and Biostratigraphy of

Lower Ordovician units in Northeastern and Western

Central Utah: Regional Implications

by

Colter R. Davis, Master of Science

Utah State University, 2017

Major Professor: W. David Liddell
Department: Geology

The Lower to Middle Ordovician Garden City Formation and Pogonip Group are coeval successions of mixed carbonate and siliciclastic rocks deposited under normal marine conditions on a shallow carbonate ramp on the western margin of Laurentia. The Garden City Formation was deposited in the Northern Utah Basin and the Pogonip Group was deposited in the Ibex Basin. These two basins experienced different rates of thermal subsidence following Neoproterozoic rifting along the western margin of Laurentia resulting in significant thickness differences between rock units and varying lithologic expressions of eustatic change. This study provides a unique opportunity to examine the lithologic, geochemical, and paleontological responses to eustatic oscillations of two coeval sedimentary basins in Utah that formed under different tectonic settings and subsidence rates.

The Garden City Formation is composed of fourteen lithotypes and the Pogonip Group is composed of eleven lithotypes. These lithotypes mainly represent depositional environments ranging from inner ramp and middle ramp with minor outer ramp deposits. Many lithologies appear to be storm influenced due to the presence of abundant rip-up clasts (intraclasts), fragmented bioclasts, and occasional mega-ripples. Other lithologies have been extensively bioturbated and burrowed.

Nine stratigraphic sequences have previously been identified within the Pogonip Group. Eight equivalent, albeit compressed, sequences within the Garden City Formation were located using biostratigraphic and chemostratigraphic correlations, and increases in insoluble residues often found at the bases of sequence boundaries. Sequences are expressed as deepening-upward packages containing silty/sandy lowstand deposits that transition into wackestones and lime mudstone-rich highstand deposits. Several sequence boundaries appear to coincide with conodont and/or trilobite extinction events. Important sequence boundaries mark the Sauk III-m and Sauk IV-m transition and the Ibexian-Whiterockian Series boundary. Meter-scale cycles are common and likely related to Milankovitch cyclicity.

Insoluble residue increases upsection at each location which may indicate a gradual overall drop in sea level due to the onset of the regressive upper portion of the Sauk III supersequence. Insoluble residue from the Pogonip Group ranges from 1.2 to 84.7 wt. % with an average of 16.0 wt. % ± 0.7 wt. %. Insoluble residue from the Garden City Formation ranges from 1.5 to 63.8 wt. % with an average of 13.4 wt. % ± 1.0 wt. %.

New stable carbon isotope data (δ13C) from the Garden City Formation and the

Pogonip Group range from -2.92 to 1.23 ‰ V-PDB and -2.19 to 0.56 ‰ V-PDB, respectively. Four distinct δ13C trends are recognized in both sections: 1) a drop in δ13C from positive values between 0.2-1.0 ‰ to negative values approaching -1.0 ‰ near the base of the Ordovician, 2) a 0.5 to 1.0 ‰ positive δ13C excursion near the top of the *Rossodus manitouensis* Zone, 3) a drop in δ13C values to near -2.0 ‰ through most of the *Acodus deltatus –Oneotodus costatus* Zone, and 4) a gradual increase in δ13C from -2.0 ‰ to -1.0 ‰ throughout the remainder of the sections. δ13C of the Garden City Formation and the Pogonip Group appear to be correlative based on these distinct trends. This correlative relationship was verified by the lowest occurrence of conodont species *Scolopodus filosus* and *Scalpellodus* n. sp. A of the Low Diversity Interval which coincides with the positive δ13C excursion in both the Garden City Formation and the Pogonip Group. New δ13C data likely represent global primary seawater chemistry based on the correlation of similar δ13C trends from the Argentine Precordillera and western Newfoundland.

(261 pages)

PUBLIC ABSTRACT

Sequence Stratigraphy, Chemostratigraphy, and Biostratigraphy of Lower Ordovician units in Northeastern and Western Central Utah: Regional Implications.

Colter R. Davis

The Lower to Middle Ordovician Garden City Formation and Pogonip Group are mixed carbonate and sandy marine rocks deposited on the western margin of ancestral North America. The Garden City Formation was deposited in the Northern Utah Basin and the Pogonip Group was deposited in the Ibex Basin. These two basins experienced different rates of subsidence that resulting in significant thickness differences between rock units and different rock types related to sea level change. This study provides a unique opportunity to examine changes in rock types, rock chemistry, and fossil types as sea level changed within two separate basins in Utah.

Nine cycles of sea level rise and fall have been identified within rocks of the Pogonip Group. Similar sea level cycles were located within the rocks of the Garden City Formation using fossils and rock chemistry trends that occur within both rock units. The bases of these sea level cycles often contain high concentrations of sandy and silty materials. Sea level cycles are expressed as rock packages with silty/sandy shallow water rock types at the base that transition into deeper water rock types at the top of the package. Sand and silt increase within rock types over time which may indicate a gradual overall drop in sea level.

New carbon isotope data from the Garden City Formation and the Pogonip Group range from -2.9 to 1.2 per mil and -2.2 to 0.6 per mil, respectively. Four distinct carbon isotope trends are recognized in both sections indicating a correlation between the two areas. This new carbon isotope data likely represent Ordovician global primary seawater chemistry based on the correlation of similar carbon isotope data from the Argentine Precordillera and western Newfoundland.

ACKNOWLEDGMENTS

I would like to extend a special thanks to my wife and children for their patience and support in this endeavor. Elizabeth, thank you for your many hours of painstaking review and overall assistance with this project. I would also like to thank my parents for always encouraging me to pursue an education.

I would like to express my appreciation and thanks to my advisor, Dr. W. David Liddell, who suggested this thesis topic and provided his expertise, guidance, patience, and support throughout the project. I would also like to thank my committee members, Dr. Dennis L. Newell and Dr. Benjamin J. Burger, for their expertise, assistance, suggestions, and review of this thesis. I would especially like to thank Dr. Dennis L. Newell and Andrew Lonero for their guidance and use of the stable isotope laboratory. I would like to thank Kenneth Kehoe for his field and laboratory assistance and Sarah Schulthies for her conodont extraction assistance.

Funding for this project was in part provided by the Utah State University Department of Geology, the Geological Society of America (GSA), Graymont, the Society for Sedimentary Geology (SEPM), the USU Undergraduate Research and Creative Opportunities (URCO) Grant Program, and the USU Geology Undergraduate Field Assistant Program.

Colter R. Davis

CONTENTS

Page

LIST OF TABLES

LIST OF FIGURES

INTRODUCTION

General Statement

The Garden City Formation and Pogonip Group, located within northeastern and western Utah, respectively, are mixed carbonate and siliciclastic marine rock units of the Lower and Middle Ordovician (~486-468 Ma). The Pogonip Group comprises the majority of the Ibexian Series and is often used as the North American Lower Ordovician reference section (Ross et al., 1992). It has been extensively studied in the areas of biostratigraphy, chemostratigraphy, and sequence stratigraphy. The biostratigraphy of the Garden City Formation has also been studied but to a lesser extent. These two units have been provisionally correlated using biostratigraphy (Hintze, 1951, 1953, 1954; Ross, 1951, 1953; Ethington and Clark, 1971) but little is known about the suppressed sequence architecture and rock geochemistry of the Garden City Formation.

Processes such as eustatic oscillations and tectonics (subsidence rates) resulted in a significant thickness difference of approximately 400 meters (m), different lithologies, and a suppressed stratigraphic sequence architecture in the Garden City Formation. These factors hinder a detailed correlation and comparison of facies response to eustatic change. Identifying the sequence stratigraphic framework of the Garden City Formation will facilitate a more detailed reconstruction of the paleogeography and depositional settings of the western margin of Laurentia (specifically Utah) during the Early Ordovician. This study provides an opportunity to compare excellent data sets from the Ibexian Series Pogonip Group to existing and new data obtained from the Garden City Formation to better understand the regional expressions of eustasy, sedimentation, and subsidence.

Objectives and Hypotheses

The primary objectives of this study were to examine the lithologic, geochemical, and paleontological expressions of eustatic oscillations in the different tectonic settings of the Garden City Formation and the Pogonip Group. These objectives were addressed through measurement and analysis of stratigraphic sections, stable carbon and oxygen isotope analyses, insoluble debris and total organic carbon analysis, thin section analysis, biostratigraphic analysis, facies analysis, and statistical analysis. Specific hypotheses that were tested are listed below.

- Eustatically-driven lithologic sequences preserved within the Pogonip Group will be present within the Garden City Formation, regardless of unit thickness and compositional differences.
- Fluctuations in stable $\delta^{13}C$ and $\delta^{18}O$ ratios in the Garden City Formation and the Pogonip Group will be similar despite different tectonic settings. Also, these fluctuations will be similar to global values.
- Increasing or decreasing trends in insoluble debris and total organic carbon will be similar between study areas.

Study Areas

The Garden City Formation is located throughout northern Utah and southeastern Idaho and the Pogonip Group is located throughout west central Utah and eastern Nevada. Lower to Middle Ordovician strata are common in northern and western Utah, but absent from the rest of the state (Figure 1).

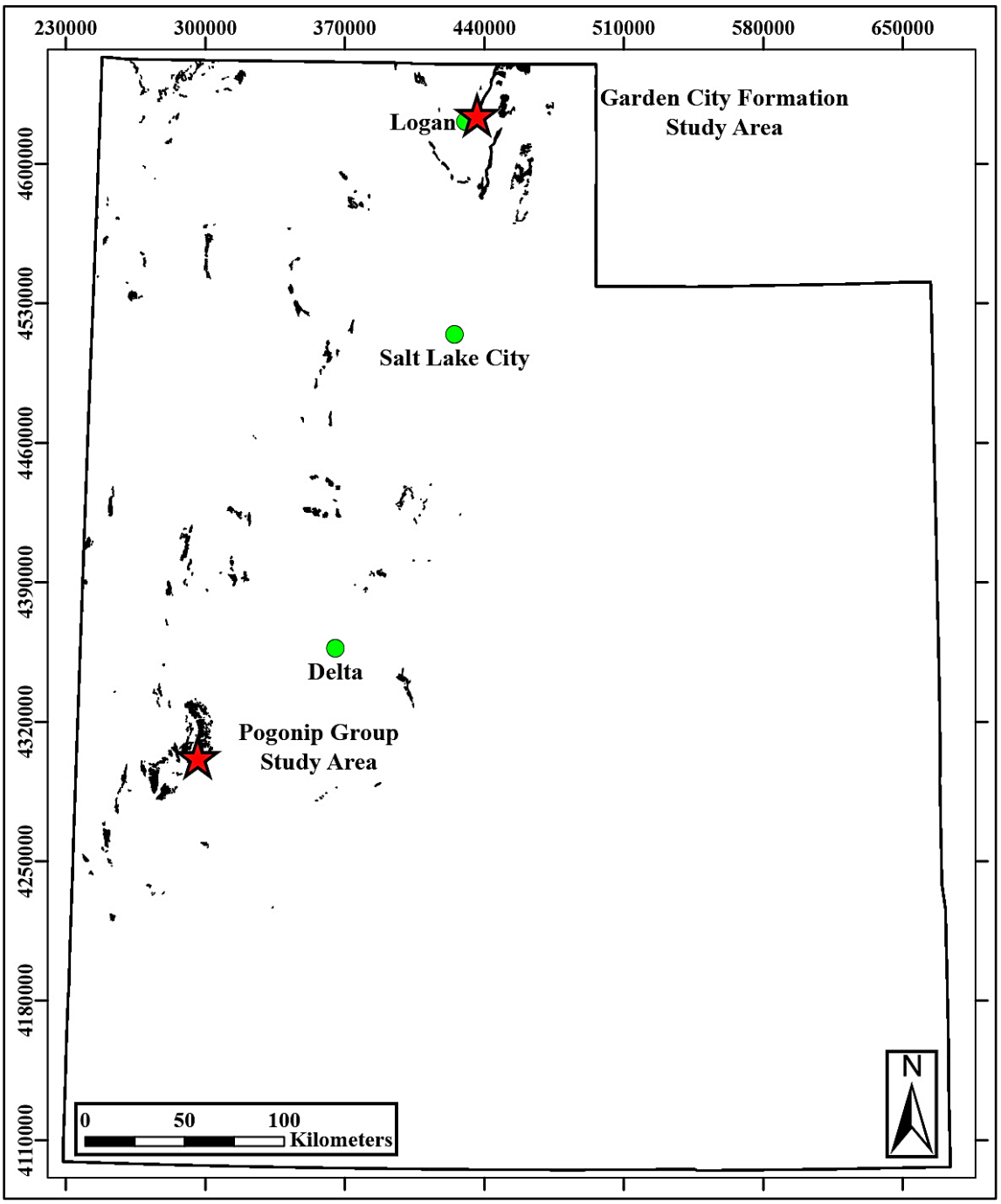

Figure 1. Overview map showing the project areas and the extent of Ordovician strata in Utah. Red stars show the study areas of the Pogonip Group and Garden City Formation. Black irregular masses show locations of exposed Ordovician strata. Green dots show city locations for reference. Figure made using Esri® ArcMap™ 10.1.

The study area for the Garden City Formation is located approximately 1.4 km up Green Canyon on the eastern flank of the Bear River Range (Sec. 19 & 20, T12N, R2 E, Smithfield, UT 7.5' quadrangle, 1998). The Universal Transverse Mercator (UTM, nad 83, zone 12) geographic coordinates of the base of the section measured of the Garden City Formation in Green Canyon is E 436,523 m; N 4,624,636 m. A detailed geologic map of this area can be found in the Smithfield 7.5' quadrangle (Lowe and Galloway, 1993). This south-facing exposure (Figure 2) is accessible from North Logan, Utah via Green Canyon Drive (E 1900 N) which transitions into Forest Service Road 050. This location was chosen due to its proximity to Logan, Utah, easy accessibility, and the completeness of the stratigraphic section.

Due to the overall thickness of the Pogonip Group (~1,060 m), five individual sections were measured and compiled to create one complete composite section (Figure 3). The Pogonip Group sections selected for this study are located approximately 80 kilometers (km) southwest of Delta Utah in the southern Confusion and House Ranges. These sections were measured by Hintze (1951, 1953, and 1973) and Hintze et al. (1988) and include the Lava Dam North (LDN) Section, the 1965 C-Section, the Mesa Section, the H-Section, and the J-Section. The LDN Section, the 1965 C-Section, and the Mesa Section are located within Tule Valley and are accessible by heading south from combined Highway 6 and 50 on Tule Valley Road (Sec. 31, T20S, R13W, Skullrock Pass, UT 7.5' quadrangle, 1991). The H-Section and the J-Section are located within Blind Valley and are accessible by heading south from combined Highway 6 and 50 on Blackham Canyon Road (Sec. 36, T20S, R14W, Hell'n Moriah Canyon, UT 7.5'

quadrangle, 1991) which transitions into Blind Canyon Road. The UTM coordinates for the bases of the measured sections for the Pogonip Group are tabulated in Table 1. A detailed geologic map of these areas can be found in the Wah Wah Mountains North 30' X 60' quadrangle (Hintze and Davis, 2002a). These locations were chosen due to good exposures and lack of structural complexity (Hintze and Davis, 2003).

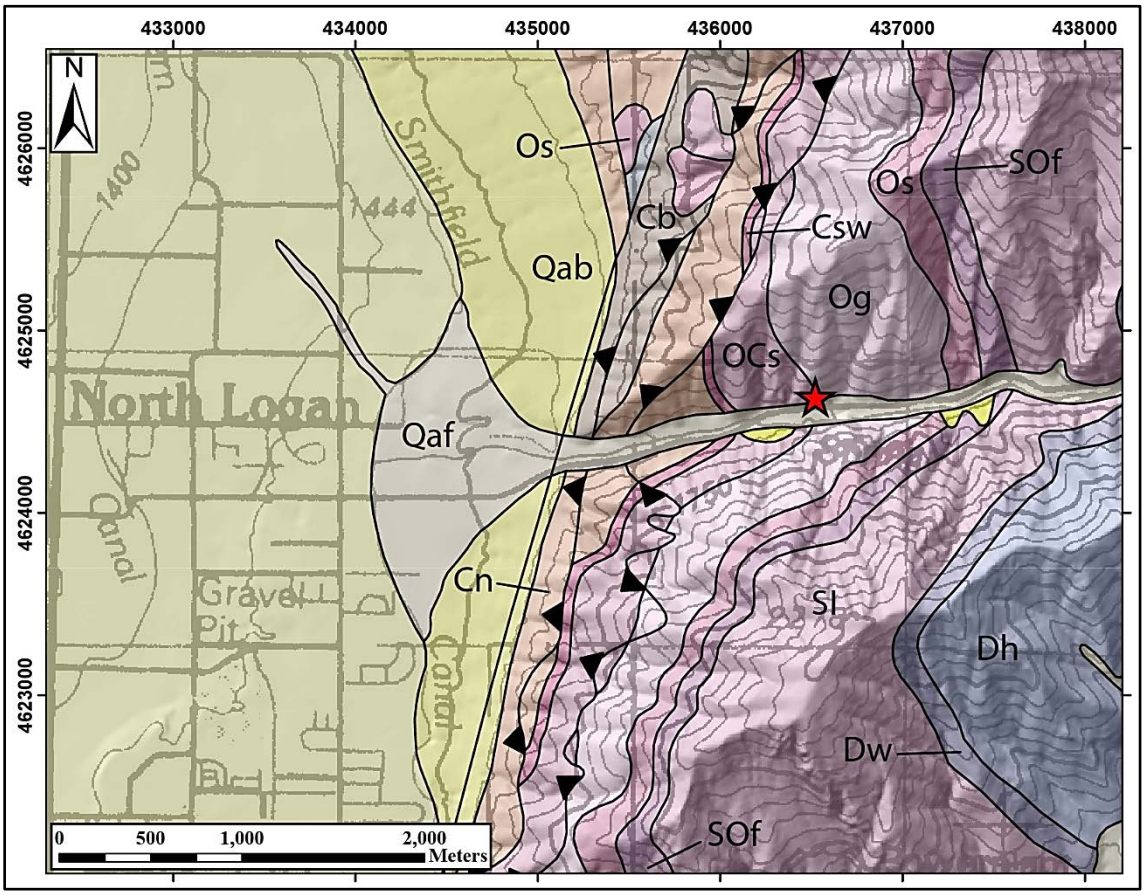

Figure 2. Geologic map of the Garden City Formation study area. Red star shows the base of the measured section in Green Canyon. Lithologic units include: Bloomington Formation (Cb), Nounan Dolomite (Cn), St. Charles Formation (Csw & OCs), Garden City Formation (Og), Swan Peak Quartzie (Os), Fish Haven Dolomite (SOf), Laketown Dolomite (SI), Water Canyon Formation (Dw), and Hyrum Dolomite (Dh). From Lowe and Galloway (1993). Figure made using Esri® ArcMapTM 10.1.

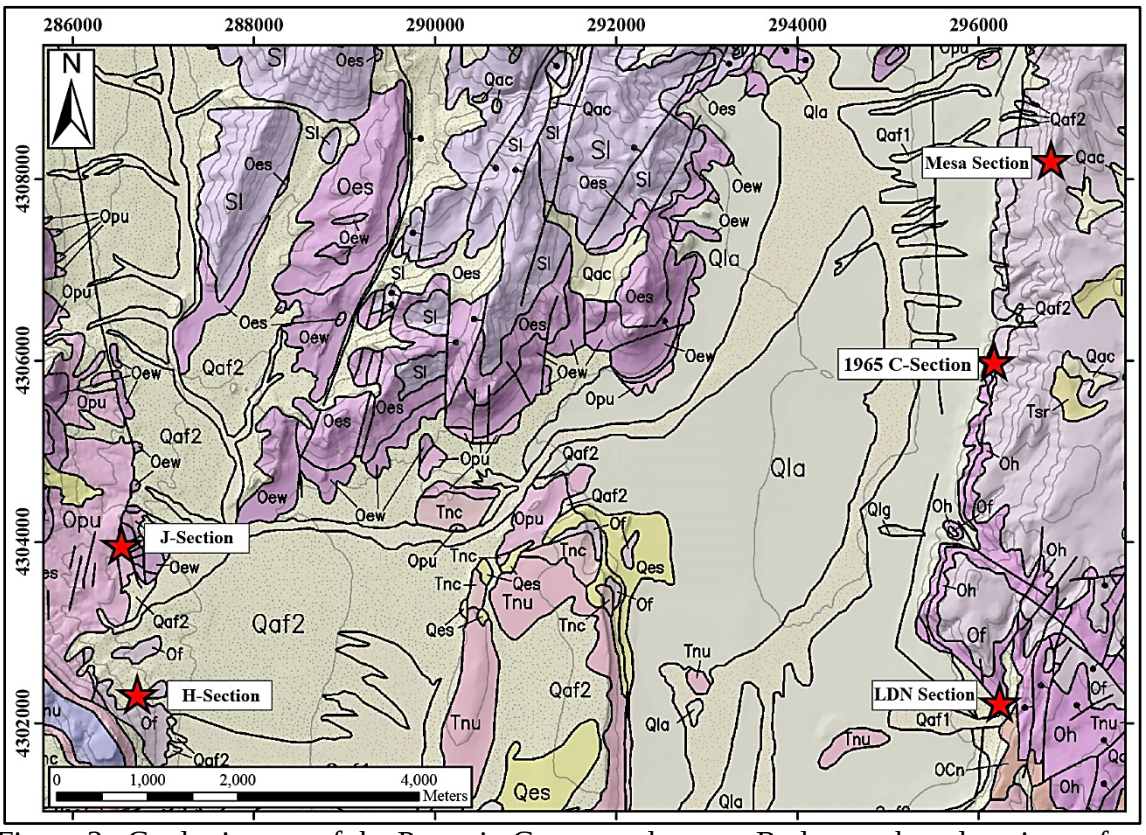

Figure 3. Geologic map of the Pogonip Group study area. Red stars show locations of sections measured for this study. Lithologic units include: Notch Peak Formation (OCn), House Limestone (Oh), Fillmore Formation (Of), Upper Pogonip Group, undivided (Opu), Eureka-Crystal Peak-Watson Ranch Formations, undivided (Oew), Ely Springs Dolomite (Oes), Laketown Dolomite (SI), Skull Rock Pass Conglomerate (Tsr), Conglomerates and landslide blocks (Tnc), Upper Needles Range Group (Tnu), Eolian Sand (Qes), Lacustrine and alluvial deposits, undifferentiated (Qla), Alluvium and colluvium, undifferentiated (Qac), Older alluvial-fan deposits (Qaf2, and Younger alluvial-fan deposits (Qaf1). From Hintze and Davis (2002a). Figure made using Esri® ArcMapTM 10.1.

Table 1. UTM coordinates for the bases of the measured sections of the Pogonip Group.

Section	UTM Coordinates
Lava Dam North Section	E 296,227 m; N 4,302,231 m
1965-C Section	E 296,164 m; N 4,305,996 m
Mesa Section	E 296,792 m; N 4,308,216 m
H Section	E 286,710 m; N 4,302,322 m
J Section	E 286,539 m; N 4,303,968 m

BACKGROUND

Geologic History

During the Early Ordovician, Laurentia (ancestral North America) was located at the equator and was rotated roughly 45° clockwise from its current orientation. The Neoproterozoic (~550 Ma) breakup of Rodinia resulted in the creation of a seafloor spreading ridge, the formation of ocean crust, the establishment of a pull-apart basin in Nevada and western Utah, and a miogeocline which later developed along the western margin of Laurentia (Sears and Price, 2003; Miller et al., 2012).

The Transcontinental Arch, a cratonic high located in present day Colorado, and the miogeocline along the western margin of Laurentia significantly influenced deposition and lithofacies development (Miller et al., 2003). For the first time, Paleozoic marine sediments were deposited eastward onto the cratonic platform (Poole et al., 1992), facilitated by sea-level rise and continued continental-margin subsidence from lithospheric cooling (Bond et al., 1984). Accommodation space generated by rapid thermal subsidence, eustatic fluctuations, and an influx of siliciclastic debris during sea level lowstands contributed to the heterolithic nature and overall thickness of the Pogonip Group (Miller et al., 2012). Differences in regional vertical tectonic adjustments from Neoproterozoic rifting further contributed to thickness differences between west central and northeastern Utah (Miller et al., 2003). Subsidence curves produced by Bond et al. (1989) indicate that subsidence was occurring more rapidly near the Ibex Basic. Subsidence creates accommodation space which can be filled with sediment. Based on these curves the Northern Utah Basin experienced approximately 450 m of subsidence

from the Late Cambrian to the Late Ordovician, whereas, approximately 750 m of subsidence occurred within the Ibex Basin during this time. This imbalance of subsidence rates and accommodation space generation resulted in a thickness difference of approximately 400 m in the age-equivalent rocks of the Garden City Formation and the Pogonip Group.

Regional tectonic elements that formed during Neoproterozoic rifting include the Northern Utah Basin, Arco Arch, Tooele Arch, House Range Embayment, Ibex Basin, and Wah Wah Arch (Oaks et al., 1977; Miller et al., 2003; Miller et al., 2012). The thickness of Middle Ordovician strata across Utah appears to have been influenced by these regional tectonic elements (Figure 4).

Ross et al. (1989) interpreted the Great Basin region as a carbonate ramp with mixed carbonate and siliciclastic sedimentation. Deposition of Middle Cambrian to Middle Ordovician strata occurred on a tropical miogeoclinal platform (Miller et al., 2012). Similarly, Hintze (1973) and Morgan (1988) indicate that Early Ordovician Utah was represented by thick limestone deposition in a broad, shallow, passive-margin sea that deepened to the west. Paleoenvironmental analyses indicate that deposition occurred in normal marine conditions near fair-weather wave base in shallow sub-tidal environments, which were influenced by storm events (Ross et al., 1989; Wilson et al., 1992; Finnegan and Droser, 2005).

The Garden City Formation and the Pogonip Group are two thick, dominantly limestone packages that were deposited on the miogeoclinal platform during the Early and Middle Ordovician. The Garden City Formation designation is used to describe the

limestones in the Northern Utah Basin and the Pogonip Group designation is used to describe the limestones and shales in the Ibex Basin (Hintze, 1959, 1973). These rock units contain intraformational conglomerates, silty layers, fossiliferous limestones, a large percentage of chert (Stokes, 1986), minor sandstones/siltstones, and low-energy shales (Ross et al., 1989; Wilson et al., 1992; Marenco et al., 2013).

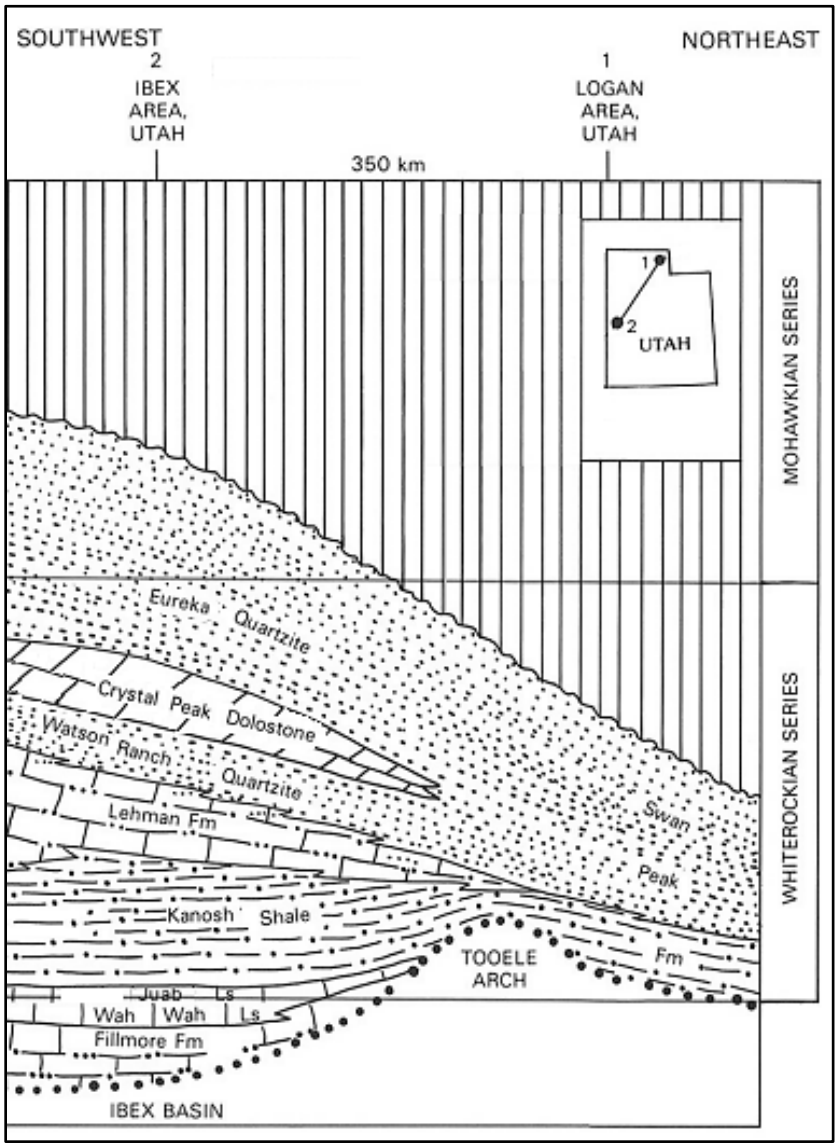

Figure 4. Middle Ordovician facies relations on the continental shelf in the Great Basin. Chronographic framework from Ross et al. (1982). Modified from Poole et al. (1992).

Structural History

Neoproterozoic rifting in Utah resulted in a SSW-NNE oriented sub-linear shelf edge of Precambrian and older crystalline cratonic rocks, known as the Cordilleran-Hingeline (Allmendinger et al., 1986; Green and Herring, 2013). The deposition of Cambrian through Late Devonian sediments west of the hingeline occurred in marine environments of a relatively shallow subsiding continental shelf. Deposition east of the hinge line was minor (or absent) and occurred at sea level on a flat surface (Green and Herring, 2013). During the Late Devonian, Laurentia began to collide with the Antler island arc complex and other landmasses encroaching from the west resulting in the development of the Roberts Mountains Thrust (RMT) system along the continental edge of Nevada (Green and Herring, 2013). The shallow shelf where the Garden City Formation and the Pogonip Group had been deposited began to warp downward and became a foreland basin where thick deposits began to collect (Green and Herring, 2013). Deposition continued in this foreland basin through the Triassic and by the Jurassic the continental plate boundary has shifted to the west of the accreted landmasses (Dickinson, 2006). Nevada and Utah experienced compressive tectonics from three overlapping orogenic events: the Nevadan (Late Jurassic to Early Cretaceous), the Sevier (Late Jurassic to Paleogene), and the Laramide (Late Cretaceous to Eocene) beginning in the Jurassic and lasting until the Eocene (Yonkee and Weil, 2011). A period of pyroclastic volcanism occurred from the Late Eocene and into the Oligo-Miocene (Green and Herring, 2013). Extensional faulting began during the Miocene (~19 Ma) initiated formation the Basin and Range Province where extension continues today (Dickinson,

2006). This extensional event produced high relief and steep fault scarps on the flanks of ranges within the province (Hose, 1977). The Basin and Range Province consists of roughly north-south trending mountain ranges and basins, and extends over a large portion of the American West. The compressional and later extensional events have resulted in exposed Lower Ordovician strata containing the Garden City Formation and the Pogonip Group.

Geology of the Garden City Formation

Stratigraphy

The Garden City Formation designation is used to describe the limestones that were deposited in the Northern Utah Basin in the Early Ordovician (Hintze, 1959, 1973). It ranges in thickness from approximately 366 m in the east to 549 m in the northwest of the Logan Quadrangle (Hansen, 1949; Ross, 1949-51; Morgan, 1988). The Garden City Formation has been informally subdivided into two informal members: the Lower Member and the Upper Cherty Member (Hansen, 1949; Ross, 1949-51; Rigby, 1958; Schaeffer, 1960; Pearce, 2012). It is bounded disconformably (diachronous disconformity with ~12 m missing from the lower Garden City Formation) by the Upper Cambrian St. Charles Formation below (Ross, 1949; Taylor and Landing, 1981; Taylor et al., 1981a; Taylor et al., 1981b) and conformably by the Swan Peak Formation above (Ross, 1949; Francis, 1972; Morgan, 1988). R. Q. Oaks, Jr. (written communication on January, 30th, 2017) suggests the presence of a low-angle regional unconformity at the contact of the Garden City Formation and the Swan Peak Formation based on a small change in the average direction and dip between the two formations at Right Hand Fork

of the Logan River in Logan Canyon. The contact between the Garden City Formation and the St. Charles Formation is a conspicuous switch from the massive dolostones of the St. Charles Formation and the limestones of the Garden City Formation (Taylor and Landing, 1981). The contact between the Garden City Formation and Swan Peak Formation is an abrupt transition from the sandy limestones of the upper Garden City Formation to the red silty/shaley sandstones of the Swan Peak Formation (Morgan, 1988). The Garden City Formation was deposited in a broad, shallow, passive-margin sea (the Panthalassic Ocean) that deepened to the west (Hintze, 1973; Morgan, 1988).

Biostratigraphy

Ross (1949, 1951, 1953, and 1968) initially divided the Lower and Middle Ordovician Garden City and Swan Peak formations of northeastern Utah and southeastern Idaho into trilobite and brachiopod assemblage zones labeled from A to M (Ross et al., 1997). New trilobite and conodont collections from the Garden City Formation in northeastern Utah and southeastern Idaho were studied by Landing (1981), Taylor and Landing (1982), and Adrain et al. (2003, 2009, and 2014).

Lithology

Morgan (1988) provides the most recent detailed stratigraphic descriptions and identified the following nine different lithofacies: nodular wackestones/mudstone with packstone lenses, green shale, laminated packstone/grainstone, cryptalgalaminite, fragmented fossiliferous packstone and whole fossil fossiliferous packstone, boundstone, *Calathium*/sponge, and burrowed fossiliferous wackestones/packstone with chert.

Morgan (1988) measured five stratigraphic sections in northeastern Utah and created a composite stratigraphic section (Figure 5).

The Lower Member of the Garden City Formation is composed of thin silty layers, argillaceous limestones, intraformational conglomerates and a few thin lime mudstone beds. Bioturbated beds alternate with non-bioturbated beds which contain intraclasts. The Lower Member contains stromatolites and a very distinct thrombolite horizon (Morgan, 1988). There is also a 20 centimeter (cm) to 5 m dolomitized section of arenaceous, argillaceous, dolomite near the St. Charles contact (Schaeffer, 1960).

The Upper Cherty Member is composed of intraformational conglomerates containing large amounts of irregularly-laminated chert beds. Bioturbated beds are common with few thin lime mudstones beds. The Upper Cherty Member also contains a dolomitized section near the Swan Peak Formation contact (Ross, 1951).

Geology of the Pogonip Group

Stratigraphy

The Pogonip Group designation is used to describe the limestones and shales that were deposited in the Ibex Basin in the Early Ordovician (Hintze, 1959, 1973). Within Millard County it ranges in thickness from approximately 343 - 513 m in the east and 1,067 m in the west (Hintze and Davis, 2003). The Pogonip Group consists of the following six lithologic units: the House Limestone, the Fillmore Formation, the Wah Wah Limestone, the Juab Limestone, the Kanosh Shale, and the Lehman Formation (Hintze, 1951) (Figure 6). The first four lithologic units (the House Limestone, the Fillmore Formation, the Wah Wah Limestone, and the Juab Limestone) correlate with the

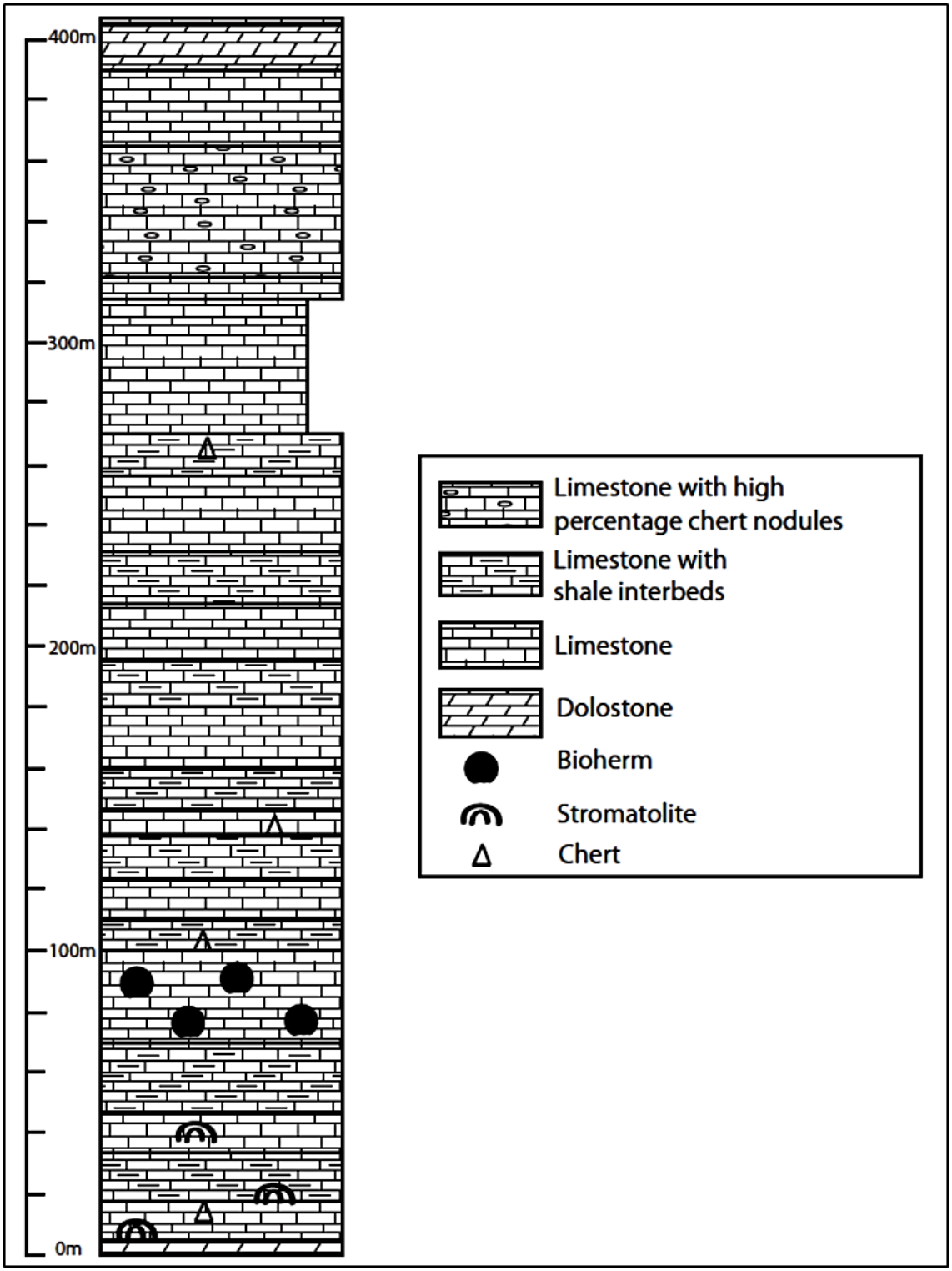

Figure 5. Stratigraphic column of the Garden City Formation. Modified from Morgan (1988).

Garden City Formation, however, the uppermost two units (the Kanosh Shale and the Lehman Formation) correlate with the Swan Peak Formation (Figure 5). The Pogonip Group is bounded disconformably by the Upper Cambrian Notch Peak Formation on the bottom and conformably by the Watson Ranch Quartzite on top (Ross and Ethington, 1992; Miller et al., 2012). The Pogonip Group was deposited in a broad, shallow, passive-margin sea (the Panthalassic Ocean) that deepened to the west (Hintze, 1973).

Biostratigraphy

The assemblage zone scheme established by Ross (1949, 1951, 1953, 1968) for Lower and Middle Ordovician rock units in northeastern Utah and southeastern Idaho was applied to the Pogonip Group in the Ibex area of west central Utah by Hintze (1951, 1953, 1954). Conodont zonal ranges for the Ibex area were established by Ethington and Clark (1981), Miller et al. (1982), and Ethington et al. (1987).

Lithology

The House Limestone has been subdivided into three members: the Barn Canyon Member (basal unit), the Burnout Canyon Member, and the Red Canyon Member (top unit) (Miller et al., 2001, 2003). The Barn Canyon Member (~ 100 m thick) contains flat-pebble conglomerates, calcarenite/grainstones, mudstones, wackestones, and sparse stromatolitic boundstones (Miller et al., 2012). The lowermost 5-10 m of the Barn Canyon Member contains a large amount (30 to 40%) of brown and white chert. The Burnout Canyon Member (~11 m thick) contains brown and white chert, flat-pebble conglomerate, and fine grainstone (Miller et al., 2012). The Red Canyon Member (~62

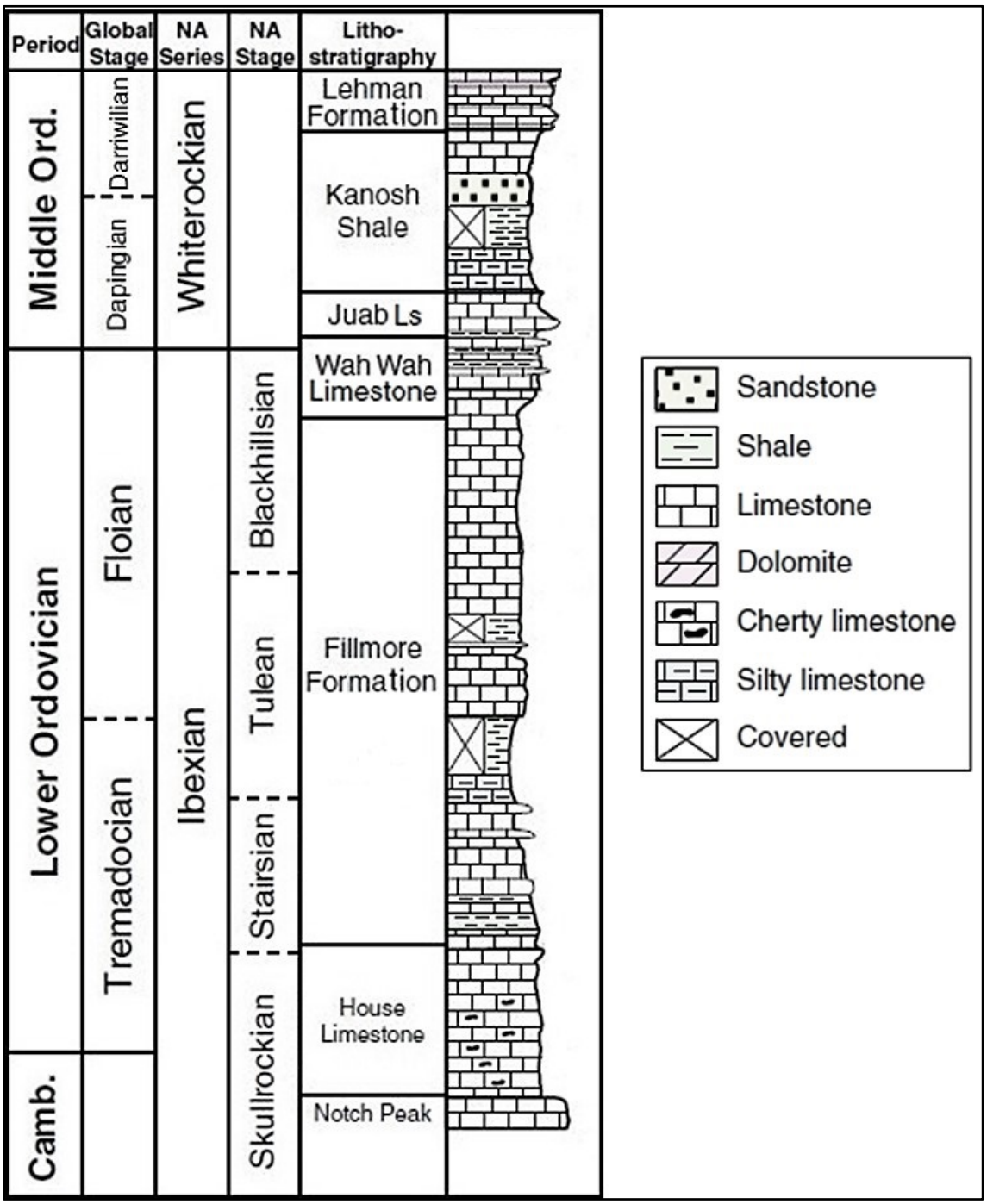

Figure 6. Stratigraphic column of the Pogonip Group. Modified from Edwards and Saltzman (2014).

m thick) contains fine-grained lime grainstone, flat-pebble conglomerate, and mudstone (Miller et al., 2012). The approximate total thickness of the House Limestone is ~173 m.

The Fillmore Formation has been subdivided into six informal members: the basal ledge-forming limestone member, the slope-forming shaley siltstone member, the light-gray ledge-forming member, the brown slope and ledge member, the calcarenite member, and the *Calathium* calcisiltite member (Hintze, 1973). The basal ledge-forming limestone member (first member, ~177 m thick) contains silty calcisiltite, flat-pebble conglomerate, siltstone, mudstone, skeletal calcarenite/grainstone, microbial boundstone, and olive-gray shale (Hintze and Davis, 2003; Miller et al., 2012). This member also contains two microbial reefs: Miller's Reef and Hintze's Reef. The slope-forming shaley siltstone member (second member, ~94 m thick) contains silty limestones, calcareous siltstone, olive-gray fissile shale, and flat pebble conglomerate. The light-gray ledge-forming member (third member, ~48 m thick) contains calcareous siltstone, mudstone, flat-pebble conglomerate, and calcilutites (Hintze and Davis, 2003; Miller et al., 2012). This member also contains a microbial reef called Church's Reef. The brown slope and ledge member (fourth member, ~92 m thick) contains primarily flat-pebble conglomerate with four mudstone/calcilutite marker beds (Hintze and Davis, 2003; Miller et al., 2012). The calcarenite member (fifth member, ~72 m thick) contains calcarenite/grainstone, flat-pebble conglomerate, calcareous siltstone, shale, and microbial patch reefs (Hintze and Davis, 2003; Miller et al., 2012). The *Calathium* calcisiltite member (sixth member, ~45 m thick) contains a ~3 m reef at its base made of *Calathium* and sponges within a micritic matrix. This member also contains calcareous siltstone and shale (Hintze and Davis,

2003; Miller et al., 2012). The approximate total thickness of the Fillmore Formation is ~529 m.

The Wah Wah Limestone consists of quartz-silty calcisiltite, flat-pebble conglomerate, and light olive fissile shale. The Wah Wah Limestone also contains three thin microbial-sponge patch reefs and a 0.6 m thick *Hesperonomiella minor* brachiopod coquina (Hintze and Davis, 2003; Miller et al., 2012). The approximate total thickness of the Wah Wah Limestone is ~62 m.

The Juab Limestone consists of calcisiltite interbedded with shale (Hintze and Davis, 2003; Miller et al., 2012). The approximate total thickness of the Juab Limestone is ~39 m.

The Kanosh Shale has been subdivided into five informal members: the lower olive shale and calcarenite member, the silty limestone member, the upper olive shale and calcarenite member, the sandstone and shale member, and the calcisiltite member (Hintze, 1973). The lower olive shale and calcarenite member (first member, ~32 m thick) consists of dark olive-gray shale interbedded with fossiliferous calcarenite/grainstone (Hintze and Davis, 2003; Miller et al., 2012). The silty limestone member (second member, ~20 m thick) consists of siltstone, calcarenite/grainstone, calcareous shale, and flat pebble conglomerate (Hintze and Davis, 2003; Miller et al., 2012). The upper olive shale and calcarenite member (third member, ~48 m thick) is similar to the lower olive shale and calcarenite member (first member) and consists of dark olive-gray shale interbedded with fossiliferous calcarenite/grainstone with the calcarenite/grainstone being more dominant than the shale (Hintze and Davis, 2003;

Miller et al., 2012). The sandstone and shale member (fourth member, ~48 m thick) consists of calcareous sandstone interbedded with fissile olive shale and fossiliferous calcarenite/grainstone (Hintze and Davis, 2003; Miller et al., 2012). The calcisiltite member (fifth member, ~46 m thick) consists of nodular calcisiltite, fossiliferous calcarenite/grainstone, and minor shale (Hintze and Davis, 2003; Miller et al., 2012). The approximate total thickness of the Kanosh Shale is ~194 m.

The Lehman Formation consists of fossiliferous calcisiltite, dolomitic limestone, and dolomitic sandstone (Hintze and Davis, 2003; Miller et al., 2012). The approximate total thickness of the Lehman Formation is ~69 m.

As previously stated, the Kanosh Shale and Lehman Formation have been correlated to the Swan Peak Formation which is located stratigraphically above the Garden City Formation (Figure 5). Descriptions of these two units have been included within this text to provide a complete, detailed description of the Pogonip Group.

Review of Previous Work

The Garden City Formation

Stratigraphic studies have been conducted on the Garden City Formation by Hansen (1949), Ross (1949, 1951), Hintze (1951, 1959, 1973), Taylor and Landing (1981), Taylor et al. (1981a), Taylor et al. (1981b), and Morgan (1988).

Paleontological studies in the Garden City Formation have been conducted on graptolites (Clark, 1935; Hansen, 1949), gastropods (Hansen, 1949), brachiopods (Hansen, 1949; Ross, 1951, 1968), trilobites (Hansen, 1949; Ross, 1949, 1951; Lee and Chatterton, 1997; Adrain et al., 2003, 2009, 2014), conodonts (Landing, 1981; Taylor and

Landing, 1981, 1982), sponges (Rigby and Gilland, 1977; Church, 1991), echinoderms (Gahn, 2006; Sprinkle, 2007), mollusks, bryozoans and various algae and bacteria (Berry, 1962; Stokes, 1986), and bioherms (Pearce, 2012). The results of these studies show that there are distinct zones in which specific biota occur and allow correlation between age equivalent rocks (e.g. The Pogonip Group).

Stable oxygen and carbon isotope studies of have not previously been conducted on the Garden City Formation. This study presents new isotopic data obtained by Kehoe et al. (2014) from Green Canyon near Logan Utah.

The Pogonip Group

Stratigraphic studies, including geologic mapping, have been conducted on the Pogonip Group by Hintze (1951, 1973, 1988), Wilson et al. (1992), Hintze and Davis (2002a-c), Hintze et al. (2003), Benner et al. (2004), Hintze and Kowalis (2009), and Miller et al. (2003, 2012). These studies of the Cambrian-Ordovician stratigraphy in Millard County provide information concerning lithology, thickness of stratigraphic units, and fossil distribution and content. The sequence stratigraphy of parts of the Cambrian-Ordovician strata in western Utah has been studied by Palmer (1981), Osleger and Read (1993), Ross and Ross (1995), and Miller et al. (2003, 2012).

Paleontological studies of the Pogonip Group have been conducted on graptolites (Braithwaite, 1969, 1976), gastropods (Dattilo, 1993; Dahl, 2012), brachiopods (Ross, 1951; Hintze, 1951, 1952, 1954; Jensen, 1967), trilobites (Ross, 1951; Hintze, 1951, 1952, 1954; Ross et al., 1997), conodonts (Miller, 1969, 1978, 1988; Ethington and Clark, 1981; Miller et al., 1982; Ethington et al., 1987), sponges (Rigby, 1962, 1965,

1971; Rigby and Gilland, 1977; Wyatt, 1979; Johns, 1994), echinoderms (Lane, 1970; Sprinkle and Guensburg, 1997), mollusks, bryozoans (Hinds, 1970) and various algae and bacteria (Ross et al., 1988; Church, 1991). The results of these studies show that there are distinct zones in which specific biota are prevalent and allow correlation between age equivalent rocks (e.g. The Garden City Formation).

Carbon and oxygen isotope ratio studies of the Pogonip Group were conducted by Ripperdan and Miller (1995), and Edwards and Saltzman (2014), however, no studies of stable carbon and oxygen isotope ratios have been performed of the Garden City Formation. Stable carbon and oxygen isotope data for the Lower and Middle Ordovician carbonates at other locations will be used for global comparison. Stable carbon and oxygen isotope ratio data of Ordovician strata have been reported by Ripperdan et al. (1992) at Black Mountain (Australia), Ripperdan and Miller (1995) at Lawson Cove (Ibex area, Utah), Buggisch et al. (2003) at the Argentine Precordillera (South American), Bassett et al. (2007) at Lange Ranch (Texas), Alvaro et al. (2008) at Montagne Noire (France), Kouchinsky et al. (2008) at the Siberian Platform, and Edwards and Saltzman (2014) at Shingle Pass (Nevada) and the Ibex area (Utah). These data provide global isotopic ratio trends which will be compared with stable carbon and oxygen isotope ratio results from the Garden City Formation and the Pogonip Group.

Overview of Sequence Stratigraphy Concepts

Sequence stratigraphy is defined as the study of repetitive, genetically-related strata within a time-stratigraphic framework, bounded by correlative conformities or unconformities (Posamentier et al., 1988; Van Wagoner, 1995). The main controls on

sediment accumulation are sea-level change (eustasy), subsidence/uplift, climate, sediment supply, basin physiography, and environmental energy (Catuneanu, 2006). Rates of eustasy and tectonic subsidence/uplift greatly affect accommodation space, which is the amount of space available to deposit sediment. Sequence stratigraphy has improved the understanding of time and space relationships between depositional factors, stratigraphic units, and facies distribution within sedimentary basins (Catuneanu, 2006).

Depositional systems, sequences, parasequences, and systems tracts are important units within sequence stratigraphy that are used to understand the sedimentary record. Depositional systems refer to the local or regional environments and depositional settings (e.g. rivers, deltas, slopes, etc.), while sequences consist of relatively conformable packages of related strata, bounded by correlative conformities or unconformities (Mitchum, 1977) and represent one cycle of relative sea-level change (rise and fall) (Emery and Myers, 1996). Sequences occur on different time scales and are classified by order (first, second, third order, etc.) with first order cycles being the greatest in duration (200-400 million years) and are composed of two of more system tracts. First order cycles are related to active global tectonism and correspond to the breakup or formation of supercontinents (e.g. Rodinia). Successive order cycles represent less time and occur in higher frequencies.

A parasequence consists of relatively conformable packages of related beds or bedsets, bounded by flooding surfaces (Van Wagoner, 1995), and generally occur in a series of parasequences. Systems tracts refer to the accumulation of strata occurring during a particular stage of shoreline shift (Catuneanu, 2006). Systems tracts include:

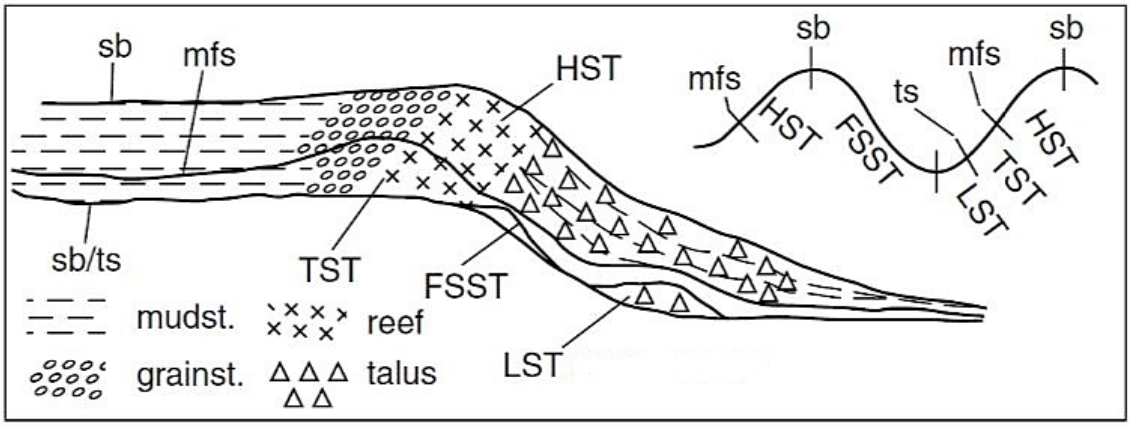

Figure 7. Simplified sequence stratigraphic model for carbonate environments and arrangement of key surfaces and system tracts. HST, FSST, TST, and LST = highstand, falling stage, transgressive, and lowstand system tracts respectively. mfs = maximum flooding surface; sb = sequence boundary; and ts = transgressive surface (modified from Figure 2 of Geology In).

Highstand System Tracts (HST), Falling-stage System Tracts (FSST), Transgressive Systems Tracts (TST), and Lowstand Systems Tracts (LST) (Figure 7).

During highstand conditions (HST) carbonate production exceeds the generation of accumulation space due to a slow rise in sea-level. Because carbonate production is more rapid than sea-level rise, seaward progradational stacking occurs. Excess carbonate sediment is deposed in deeper water by gravity flows and storms (Neumann and Land, 1975). HST are bounded on the bottom by a maximum flooding surface and at the top by portions of a subaerial unconformity, a forced regression surface, and a normal regressive surface (Catuneanu, 2006).

During falling-stage conditions (FSST), rates of sea-level fall surpass those of subsidence, leading to a forced regression or relative fall in sea-level. FSST are bounded on the bottom by a forced regression basal surface and the oldest portion of a regressive surface, and on top by a subaerial unconformity and a portion of the youngest marine

erosional regressive surface (Catuneanu, 2006). Previously submerged landward shelf and seafloor sediments are subaerially exposed creating an erosional surface known as a subaerial unconformity. Subaerial unconformities are recognized as depositional sequence boundaries which separate highstand carbonates occurring below transgressive carbonates (Catuneanu, 2006).

Lowstand conditions (LST) occur when the rate of base-level rise is slower than the rate of aggradation. Forced and normal regressions (FSST and LST) cause seaward progradation of carbonate sediments or can turn off the carbonate factory. Deep water sediment starvation and seafloor chemical precipitation may occur during the FSST-LST intervals (James and Kendall, 1992). LST are bounded on bottom by a subaerial unconformity and a correlative marine conformity, and on top by a maximum regressive surface (Catuneanu, 2006).

During transgressive conditions (TST), rates of eustasy increase and eventually outpace aggradation. Slow transgressions, those with low rates of sea-level rise, may encourage carbonate aggradation and the occupation of newly flooded surfaces. Low energy lagoons may develop between the shoreline and protective barrier reefs (Catuneanu, 2006). The carbonate platform remains submerged and within the photic zone during low rates of sea-level rise. Conversely, rapid transgressions (high rates of base-level rise) can drown carbonates when water depths of the carbonate platform exceed the photic limit. The resulting surface is referred to as a drowning unconformity and is recognized as a sequence boundary. This surface also represents the last stage in carbonate platform evolution (Catuneanu, 2006). TST are bounded on bottom by a

maximum regressive surface (mrs) and on top by a maximum flooding surface (mfs).

Sequences in carbonate depositional systems differ that those of siliciclastic environments primarily in the geometry of system tracts and sediment budget through various stages of base level rise and fall. These differences result from the dissimilar processes of sedimentation which occur in carbonate vs. siliciclastic basins (Catuneanu, 2006). In a siliciclastic depositional system sediments are derived and transported from a terrigenous source into a basin, whereas in a carbonate depositional system sediments are produced shallowly and *in situ* by the 'carbonate factory'. The rate of carbonate sediment production is influenced by such factors as: water depth, nutrient availability, rates of base-level change, illumination, climate, carbonate ramp surface area, and clastic influx (Walker and James, 1992). In short, the availability of sediment in a carbonate system is mutually tied to changes in base level, whereas in a siliciclastic system sediment supply is not (Catuneanu, 2006).

METHODS

Field Methods

The Garden City Formation and the Pogonip Group were measured using a Jacob Staff and Abney level to obtain rock unit thicknesses. Strike and dip measurements were taken using the right hand rule with a Brunton geologic compass set to a declination of 12° east. One full section of the Garden City Formation was measured in Green Canyon near Logan Utah. A composite section of the Pogonip Group was created by measuring six separate sections located in close proximity to each other. These Pogonip Group sections were measured in the southern Confusion and southern House Ranges located west of Delta Utah. Measurements (unit thicknesses, strike and dip, sample number, GPS locations, etc.), rock descriptions, and other pertinent data were carefully recorded in a field notebook. A digital camera was used to take overview and close-up photographs of rock units, lithology types, and sample locations. A photograph log which includes photograph number, description, and facing direction was kept in a field notebook. Field work was conducted with the assistance of Kenny Kehoe.

Sampling Methods

Sampling was conducted during this project to 1) characterize facies through thin section point counts; 2) create stable carbon ($\delta^{13}C$) and oxygen ($\delta^{18}O$) isotope curves; 3) create TOC curves; 4) determine the sequence stratigraphy of the Garden City Formation; and 5) establish a fine-scale (meter scale) high-resolution conodont biostratigraphy for the lower 55 m of the Garden City Formation.

Hand samples collected from both the Garden City Formation and the Pogonip Group were large enough to produce thin sections, powdered rock for stable carbon and oxygen isotope analyses, and 6 grams of powdered rock for total organic carbon (TOC) analysis. Samples were generally collected every 3 m, however, sampling intervals occasionally varied between 1 to 10 m depending on changes in lithology and extent of covered outcrop. Areas of obvious secondary alteration and mineralization were excluded from sampling. A total of 151 hand samples were collected from the Garden City Formation in Green Canyon and a total of 365 hand samples were collected from the Pogonip Group in the Ibex area.

In addition to the 151 hand samples collected from the Garden City Formation, 53 large samples (~10 kg) were collected to establish a detailed conodont biostratigraphy. These samples were collected at 1 m intervals beginning at the St. Charles and Garden City Formation contact and up through the lower 55 m of the Garden City Formation Green Canyon section.

Laboratory Analytical Methods

Carbon and Oxygen Stable Isotope Ratios

Each hand sample collected from the two project areas was cut to expose a fresh surface. Fresh surfaces were micro-drilled using a multipurpose rotary tool with a diamond bit to obtain rock powder for stable carbon and oxygen isotope analyses. Fresh surfaces consisting primarily of carbonate material were selected to be micro-drilled, whereas surfaces near veins, fractures, obvious dolomitization, and recrystallization were avoided. Micro-drilling was conducted to a depth no greater than 1-2 millimeters (mm)

to avoid sampling other fabrics. Each sample was micro-drilled over a piece of new weigh paper. Between samples the diamond bit was rinsed a minimum of three times with deionized water and then dried.

A minimum of 10 mg of powder from each sample was stored in a new glass vial. Between 140 and 160 micrograms (μg) of each sample was placed within a 12 milliliter (ml), round bottomed Exetainer® glass sample vial. Sample duplicates were made for every tenth sample to test instrument accuracy. Additionally, 10 sample vials containing 150 μg of the in-house carbonate standard, Yule 80-120 mesh (Yule 120) were placed with one between every 10 samples. Seven sample vials containing 50, 100, 150, 200, 250, 350, and 450 μg of the in-house carbonate standard Yule 42-80 mesh (Yule 80) were placed with one between every 20 samples. The Yule 120 carbonate standard was used for drift corrections, while the Yule 80 carbonate standard was used for linearity corrections. Four sample vials containing the international standards NBS 18 and 19 were placed between every 30 samples.

Each sample vial was placed within the sampling tray (heated to 50 °C) and was flushed using helium (He). After flushing each sample with He, approximately 0.1 ml 103% phosphoric acid was injected into each sample container (using needle and syringe) and allowed to react for a minimum of 2 hours. Carbon and oxygen isotope ratios were measured using a Thermoscientific Delta V Advantage Isotope Ratio Mass Spectrometer (IRMS) and a GasBench II with an auto-sampler. Ratios are reported in per mil notation relative to the Vienna Pee Dee Belemnite (V-PDB) standard (Craig, 1957).

Calibration of data and precision were monitored by analyzing in-house

laboratory standards (Yule 80 mesh and Yule 120 mesh) and the International Atomic Energy Agency (IAEA) NBS-18 and NBS-19 standards. Raw isotope ratio data was corrected for linearity and drift to produce corrected $\delta^{13}C_{PDB}$ and $\delta^{18}O_{PDB}$ values. Standard deviations for $\delta^{13}C_{PDB}$ and $\delta^{18}O_{PDB}$ are 0.06 ‰ and 0.10 ‰, respectively.

Insoluble Residue, Calcium Carbonate, and Total Organic Carbon

Samples were analyzed for insoluble residue (IR), calcium carbonate ($CaCO_3$), and total organic carbon (TOC) using the semi-quantitative method of carbonate removal and hydrogen peroxide digestion (Schumacher, 2002). This method destroys organic matter that is present in the sample through oxidation. Samples were crushed using a ROCKLABS® standard ring mill pulverizer and 6 g of crushed sample material was placed into previously weighed empty 100 ml glass sample containers. All weights obtained throughout the analysis were recorded in a Microsoft Excel® spreadsheet. A 10% hydrochloric acid (HCl) solution was added to each sample container incrementally until the sample no longer reacted to the addition of HCl. Excess HCl was decanted from the sample container and the sample was rinsed at least twice using deionized water to remove the remaining acid and salts. Excess water was decanted from the sample container and the sample was dried in an oven at a temperature of 50 °C to remove the remaining moisture. Dried samples were removed from the oven and allowed to cool to room temperature and were weighed. A 30% hydrogen peroxide (H_2O_2) solution was then added incrementally to the remaining insoluble sample material to oxidize the organic carbon. Samples were heated to 90 °C until the sample material no longer reacted with the addition of H_2O_2. The sample was rinsed, dried at 100 °C, and weighed.

The differences in weights recorded throughout the process produces TOC values.

Thin-Sections

Hand samples were cut into billets to make thin-sections. The billet surface to be mounted to the glass slide was ground smooth using first #220 and then #440 grit on mechanical laps. A glass plate and #600 grit were used to finish the mounting surface. Glass slides were prepared by frosting one side of the slide by using #600 on a glass plate. Prepared mounting surfaces were attached to the frosted side of the glass slide using clear epoxy and were placed into an oven to dry the epoxy. Excess billet material was removed from the glass slide using a thin section saw. The remaining rock material attached to the slide was ground thin using the grinder wheel on the thin section saw and then using the #220 and #440 grit mechanical laps. Thin-sections were hand finished using a glass plate and #600 grit to obtain a standard thickness of 30 microns (μm). Thin-sections were stained using alizarin red and potassium ferricyanide because dolomite is often difficult to distinguish from calcite in thin sections due to their similar crystalline properties. Alizarin red and potassium ferricyanide cause calcite to stain red, ferrocalcite (high ferrous iron) to stain scarlet/blue, ferrodolomite to stain pale blue, and dolomite resists staining. The solution used for staining was prepared as follows:

a) 0.1 g of alizarin red was dissolved in 100 cubic centimeter (cc) of 2% HCl.
b) 2 g of potassium ferricyanide was dissolved in 100 cc of distilled water and 100 cc of 2% HCl.
c) Equal parts of each solution is mixed to obtain the stain solution.

After staining the thin-section was carefully washed and dried. According to Evamy (1963) staining using alizarin red and potassium ferricyanide results in the following color and mineral combinations:

- Calcite: Red
- Ferrocalcite (low ferrous iron): Lilac (red dominant)
- Ferrocalcite (high ferrous iron): Scarlet (blue dominant)
- Dolomite: No coloring
- Ferrodolomite: Pale blue
- Ankerite: Dark blue

This complete composite test is described by Evamy (1963) and Dickson (1965). RUST-OLEUM® triple thick glaze was used in place of cover slides to finish the thin-sections. Three hundred points on each thin-section were counted using a mechanical stage to determine the classification of each sample. Sample thin-sections were classified using the Dunham classification of carbonate rocks (Dunham, 1962). Point-count data and lithologic descriptions obtained in the field were used to define lithotypes. Thin-sections (excluding 30 thin-sections made by Wagner Petrographic) were made at the Utah State University Rock Preparation Laboratory located in the Geology Building.

Conodont Element Extraction by Digestion

The 53 large samples (~10 kg) collected from the Garden City Formation were crushed using a chipmunk jaw crusher down to approximately 1-2 cm sized clasts. An Ohaus Brainweight™ B 1500 D electronic scale was used to weigh 1 kg of crushed

sample which was placed in an acid resistant container within a fume hood in preparation for acetic acid digestion. A solution of 5% acetic acid (white vinegar) was added to the crushed material and allowed to fully react. Reacted acid was decanted from the sample container prior to the addition of fresh 5% acetic acid. Once the crushed sample material no longer reacted with the addition of new acid, the remaining insoluble debris was rinsed using deionized water to remove any remaining acid. The debris were wet sieved using 2 mm, 1 mm, 180 μm, and 125 μm sized nested sieves and dried in an oven at 50 °C. The insoluble fine debris were searched (picked) using a binocular stereoscope for conodont element microfossils. Conodont elements were removed from the insoluble debris using a fine camel hair brush and were attached to a microfossil slide using Ward's Tragacanth Gum. Conodont elements types were identified by comparing picked conodont elements with scanning electron microscope (SEM) photomicrographs from Taylor and Landing (1982), and Miller et al. (2006).

Facies Analysis

The rocks of the Garden City Formation were described in the field, in hand specimen, and in thin-sections using a petrographic microscope and were classified using the Dunham (1962) classification scheme of carbonate rocks. Insoluble residue and total organic carbon (TOC) data, lithologic descriptions, and thin section petrography results were used to identify variations and repetitions of facies types, and to determine significant surfaces within the Garden City Formation and the Pogonip Group. These rock units contain meter- and member-scale cyclicity preserved as the repetition of facies (e.g. shale, carbonate, sandstone, shale, carbonate, etc.).

Statistical Tests

Statistical testing was used to detect similarities and differences in data sets from the Garden City Formation and the Pogonip Group. Descriptive statistics (e.g. grain sizes, average number of grains, percent matrix vs. grains, etc.) of data sets provided the mean, mode, median, and standard deviation. Isotope, insoluble residue, calcium carbonate, and TOC results were plotted against rock unit thickness and a best fit line was added to the plots using a 3 point running average. The 3 point running average was used to show the general trends of data values. Regression analysis using Microsoft Excel® was also conducted to test the correlation between $\delta^{13}C$ and $\delta^{18}O$ values.

The two sample Kolmogorov-Smirnov test and the two sample Mann Whitney U test are nonparametric statistical tests that were used to compare data from the Garden City Formation and the Pogonip Group. The two sample Kolmogorov-Smirnov test was used to compare isotope, insoluble residue, calcium carbonate, and TOC data. The two sample Mann Whitney U test was used to compare insoluble residue, calcium carbonate, and TOC data. Both nonparametric statistical tests were employed at significance level of alpha = 0.05. Insoluble residue, calcium carbonate, and TOC percentage data was transformed using the arcsine transformation to conduct the aforementioned statistical analyses.

The two sample Kolmogorov-Smirnov test is used to compare the cumulative distribution between two samples from the same population by comparing the two sample means. The two sample Kolmogorov-Smirnov test is defined by the following hypotheses: H_0, which states that the data follow the same distribution and H_a, which

states that the distribution of the two samples are different.

The two sample Mann Whitney U test is the alternative test to the t-test and is used to determine whether two samples come from the same population by comparing the two sample medians. The Mann Whitney U test is defined by the following hypotheses: the null hypothesis ($H_{0)}$ states that the data come from the same population and the alternative hypothesis (H_a) which states that the data come from different populations.

The thin-sections were point counted (300 points) using a microscope. Rarefaction was used to determine how many points to count. These data were used to compare the two rock units using Principle Components Analysis (PCA) and Agglomerative Hierarchical Clustering (AHC). Point count data were analyzed using Addinsoft XLSTAT Version 2016.05.33324 software suite. The Q-mode PCA and AHC - were conducted on data from point counts which were placed within a data matrix (percent of total components) to group samples that were similar. This analysis defined samples from similar environments and therefore similar lithofacies. The R-mode PCA and AHC was used to discern relationships between variables and shows which variables are affecting the analysis the most.

RESULTS

Stratigraphic Analysis

Garden City Formation Stratigraphy

A section of the Garden City Formation was measured on the south facing slope (the north side) of Green Canyon, near a previously measured section completed by Morgan (1988). The section totaled 391.5 m in thickness (Appendix A). Conodont studies by Landing (1981), Taylor et al. (1981a), Taylor and Landing (1982), and indicate that at least 12 m of erosional relief exist at the contact of the Garden City Formation and the underlying St. Charles Formation. The total measured thickness of this section plus the 12 m of erosional relief result in an adjusted total thickness of 403.5 m for the Garden City Formation at Green Canyon (Figure 8). Total exposure of the Garden City Formation in Green Canyon is 91% in this study.

Dolostones occur from 12-22 m and are the basal lithology of the Garden City Formation. Dolostones are thick-bedded and coarse-grained with sparse interbedded argillaceous silty wackestones and thin beds of intraformational conglomerates. Black and white chert nodules are also present within the dolostones.

Argillaceous nodular wackestones and mudstones occur from 22-37 m and consist of medium- to thick-bedded silty argillaceous nodular lime mudstones and wackestones with minor intraformational conglomerates. Intraclasts generally range from 5 mm to 5 cm in size and other lithologies include fossiliferous wackestones with packstone lenses, recrystallized silty mudstones, and argillaceous mudstones. Trace fossils (bioturbation), black chert nodules, fine to medium argillaceous laminations, and hummocky surfaces

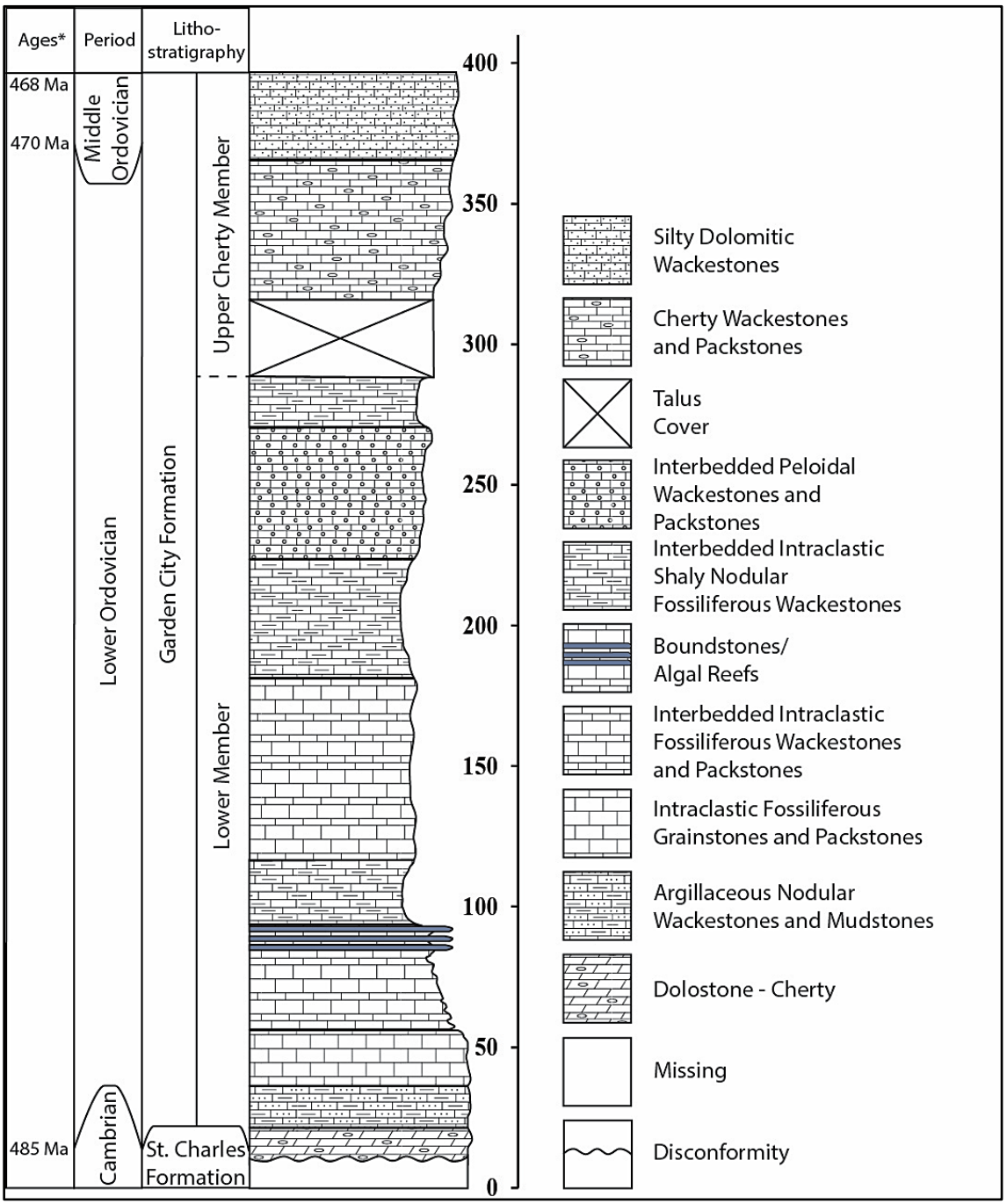

Figure 8. Stratigraphic column of the Garden City Formation. Thickness is in meters.

(Figure 9) are present within this lithotype.

Intraclastic fossiliferous packstones and grainstones occur from 37-57 m, with intraclasts ranging from 5 mm to 40 cm in size. Fine to medium argillaceous laminations, black chert beds, and ripples superimposed on mega-ripples occur within these lithotypes.

Intraclastic fossiliferous wackestones and packstones occur from 57-80 m and from118-184 m. Boundstones (algal reef) occur from 80-95 m as 6 distinct boundstone horizons separated by bioturbated interbeds of nodular wackestones. These microbial reefs often have irregular undulating undersides which appear to have compressed and distorted the underlying wackestone beds (Figure 10). Individual microbial mounds are

Figure 9. Fine to medium argillaceous laminations, and hummocky surfaces (dashed line) within the Garden City Formation. Field book for scale (14 cm by 24 cm).

rounded in shape and measure approximately 1.6 m high, 3 m in diameter, and vary in length from 1.5 to 3 m.

Intraclastic shaly nodular fossiliferous wackestones and lime mudstones occur from 95-118 m, 184-227 m, and 273-291 m. Peloidal wackestones occur from 227-273 m and contain minor packstones. Cherty wackestones and packstones occur from 320-371 m and contain abundant chert. Silty dolomitic wackestones occur from 371-403 m.

Pogonip Group Stratigraphy

Five sections were measured in the Ibex area in order to produce a composite section for the Pogonip Group. All Pogonip Group sections measured have previously

Figure 10. Microbial reef within the Garden City Formation. Irregular undulating undersides of the microbial reefs (dashed line) appear to have compressed and distorted the underlying wackestone beds of unit GC-U10. Field book for scale (14 cm by 24 cm).

been studied (Hintze, 1951, 1973; Wilson et al., 1992; Hintze and Davis, 2002a-c; Hintze et al., 2003; Benner et al., 2004; Hintze and Kowalis, 2009; and Miller et al., 2003, 2012) and the traditional formation rock unit identifications after Hintze (1951, 1973) were used while re-measuring these sections. The Pogonip Group is divided into the following six separate formations: the House Limestone, the Fillmore Formation the Wah Wah Limestone, the Juab Limestone, the Kanosh Shale, and the Lehman Formation. The Kanosh Shale and Lehman Formation have been excluded because they are coeval with the Swan Peak Formation, which overlies the Garden City Formation. The total measured thickness of the composite section is 787.3 m for the Pogonip Group in the Ibex Area (Figure 11). Total exposure of the Pogonip Group in the Ibex Area is 95 % in this study.

The Barn Canyon Member of the House Limestone - Cherty wackestones and mudstones occur within the Barn Canyon Member of the House Limestone. It also contains medium- to thick-bedded grainstones, intraformational conglomerates, lime mudstones, packstones, and wackestones, some of which are recrystallized and/or silty. Intraclasts range from mm to cm scale. Sedimentary structures within the Barn Canyon Member include: storm hummocks/mega ripples (Figure 12), cross stratification, and bioturbation. The Barn Canyon Member also contains abundant white, brown, and black chert nodules, chert beds, and irregular chert masses.

The Burnout Canyon Member of the House Limestone - The Burnout Canyon Member of the House Limestone contains mainly silty wackestones. Other lithologies include medium- to thick-bedded intraclastic packstones and wackestones, and lime mudstones.

Sedimentary structures within the Barn Canyon Member include: cross stratification, flame structures (Figure 13), and folds. Loren Babcock (Ohio State University) suggested that the soft sediment deformation features within the Burnout Canyon Member may be the result of seismic activity which distorted newly deposited unconsolidated sediments (Miller et al., 2012). Chertification appears to have occurred

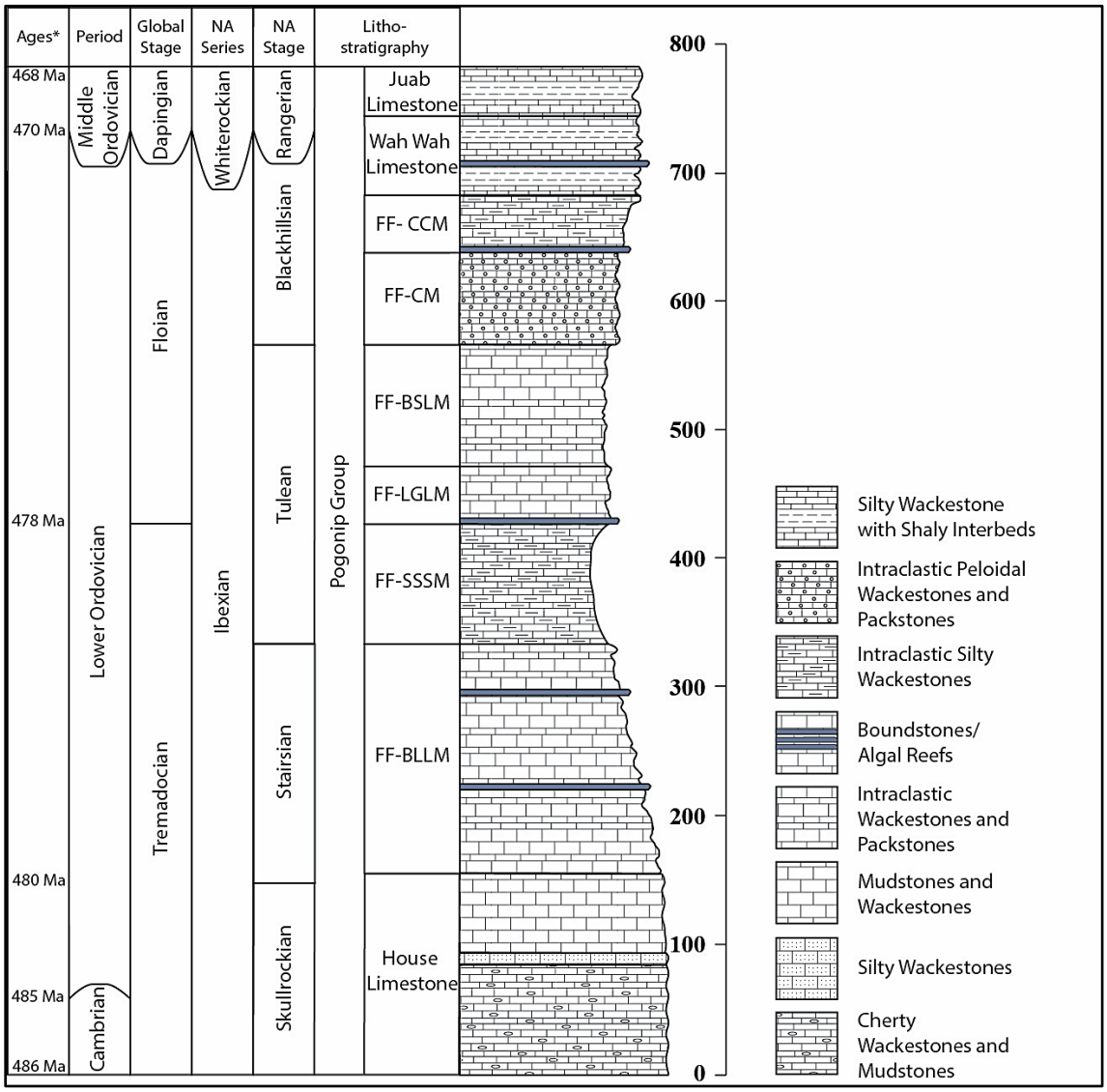

Figure 11. Stratigraphic column of the Pogonip Group. Thickness is in meters.

after the deformation of sediments. This member forms a distinctive, relatively-thin brown cliff band that is easily recognizable within the House Limestone at the Lava Dam North Section. Brown and white chert are common and often occur with the above mentioned sedimentary structures. The abundance of brown and white chert contributes to the brown color of this member.

The Red Canyon Member of the House Limestone - Mudstones and wackestones are dominant lithologies within the Red Canyon Member of the House Limestone. Other lithologies include sparse boundstones, intraclastic grainstones, packstones, and wackestones, lime mudstones, and some recrystallized and/or silty lithologies. Sedimentary structures include chert-filled burrows and truncation features such as tidal

Figure 12. Storm hummocks/mega ripples (dashed line). Found within the Barn Canyon Member of the House Limestone. Scale card for scale and orientation (9 cm by 15 cm).

channels (Figure 14). Abundant vertical and horizontal chert bodies are prevalent, which may represent chertified clastic dikes.

The Basal Ledge-Forming Limestone Member of the Fillmore Formation - The Basal Ledge-Forming Limestone Member (FF-BLLM) contains abundant intraclastic wackestones and packstones. Other lithologies include thin- to medium-bedded intraclastic rocks, silty limestones, and sparse microbial boundstones. Additional lithologies include fossiliferous grainstones, packstones, wackestones, nodular limestones, shales, and mudstones, some of which are silty and/or recrystallized. The FF-BLLM is the least fossiliferous member of the Fillmore Formation. Fossils include brachiopods, crinoids, and trilobites. Sedimentary structures include burrows (Figure 15)

Figure 13. Silicified (chert) teepee structure. Found within the Burnout Canyon Member of the House Limestone. Scale card for scale (9 cm by 15 cm) and orientation.

and some of the intraformational conglomerate clasts appear to be bored which may indicate hardground formation. Chert is not common within the FF-BLLM but it does occur in irregular masses and layers.

Two distinct thrombolite/microbial reef horizons are found within the FF-BLLM. Miller's Reef (~230 m) consists of a ~1 m thick massive layer of stromatolitic type reef with an irregular undulating underside (Figure 16). A minor microbial reef is located below Millers' Reef and contains irregular-shaped microbial masses located within a shaly nodular limestone. Hintze's Reef (~299 m) contains a massive ~3 m thick layer of large, rounded sponge-bearing microbial reef which forms a distinct light bluish-gray layer within the FF-BLLM (Figure 17).

Figure 14. Truncation feature (dashed line), likely a tidal channel. Found within the Red Canyon Member of the House Limestone. Scale card for scale (9 cm by 15 cm) and orientation.

Figure 15. Plan view of burrows and borings. Found within the FF-BLLM. Scale card for scale (9 cm by 15 cm) and orientation.

Figure 16. Miller's Reef with irregular undulating underside. Located within the FF-BLLM. 1.5 m Jacob Staff for scale.

The Slope-Forming Shaly Siltstone Member of the Fillmore Formation - The intraclastic silty wackestones dominate the Slope-Forming Shaly Siltstone Member (FF-SSSM). Minor shales occur as interbeds within the intraclastic silty wackestones. Additional lithologies include fossiliferous packstones-wackestones, intraclastic lithologies, and nodular limestones (Figure 18). The nodular limestones appear to be heavily bioturbated. Fossils include primarily brachiopods.

The Light Gray Ledge-Forming Member of the Fillmore Formation - The Light Gray Ledge-Forming Member (FF-LGLM) contains mainly intraclastic wackestones and packstones. Other lithologies include boundstones, fossiliferous wackestones, packstones, and grainstones, mudstones, nodular limestones, and shales. Many of the

Figure 17. The distinct light bluish-gray Hintze's Reef (between dashed lines). Located within the FF-BLLM. Layer is approximately 3 m thick.

wackestones and packstones contain numerous peloids. Fossils include brachiopods and crinoids. Sedimentary structures include burrows and strange syneresis-crack-like features (Figure 19). A distinct microbial reef horizon is located within the FF-LGLM at approximately 430 m. It contains subtle microbial mounds comprised of lime mud which are difficult to distinguish from other mudstones.

The Brown Slope and Ledge Member of the Fillmore Formation - The intraclastic wackestones and packstones dominate the Brown Slope and Ledge Member (FF-BSLM). Other lithologies include argillaceous limestones, fossiliferous wackestones, packstones, and grainstones, mudstones, nodular limestones, and shales. Lithologies within the FF-BSLM are slightly peloidal. Fossils include brachiopods, bryozoans, crinoids, and

Figure 18. Nodular limestones, likely from bioturbation. Found within the FF-SSSM. Field book for scale (14 cm by 24 cm).

trilobites. Sedimentary structures include black chert-filled burrows, mega-ripples, and syneresis-crack-like features similar to those of the FF-LGLM.

The Calcarenite Member of the Fillmore Formation - The Calcarenite Member (FF-CM) contains abundant intraclastic peloidal wackestones and packstones lithofacies. Additional lithologies include sparse boundstones, fossiliferous wackestones, packstones, grainstones, intraformational conglomerates, and shales. Fossils include algae, brachiopods, bryozoans, crinoids, Calathium (a receptaculitid), sponges, and silicified trilobites. Sedimentary structures include burrows, and mega-ripples. The FF-CM also contains various small microbial patch reefs.

The Calathium Calcisiltite Member of the Fillmore Formation - The *Calathium*

Figure 19. Syneresis-crack-like features. Found within the FF-LGLM. Field book for scale (14 cm by 24 cm).

Calcisiltite Member (FF-CCM) contains intraclastic silty wackestones with minor shales. Other lithologies include sparse boundstones, fossiliferous wackestones, packstones, grainstones, intraformational conglomerates, and shales with interbedded limestone nodules. Fossils include brachiopods, bryozoans, crinoids, gastropods, sponges, and trilobites. A distinct 3 m thick microbial reef horizon is located near the base of the FF-CCM (~640 m). The microbial reef is similar to Church's Reef in that it contains subtle microbial mounds comprised of lime mud but differs because it contains abundant *Calathium* (Figure 20).

The Wah Wah Limestone - The Wah Wah Limestone consists of silty wackestones with shaly interbeds. Additional lithologies include sparse boundstones, fossiliferous

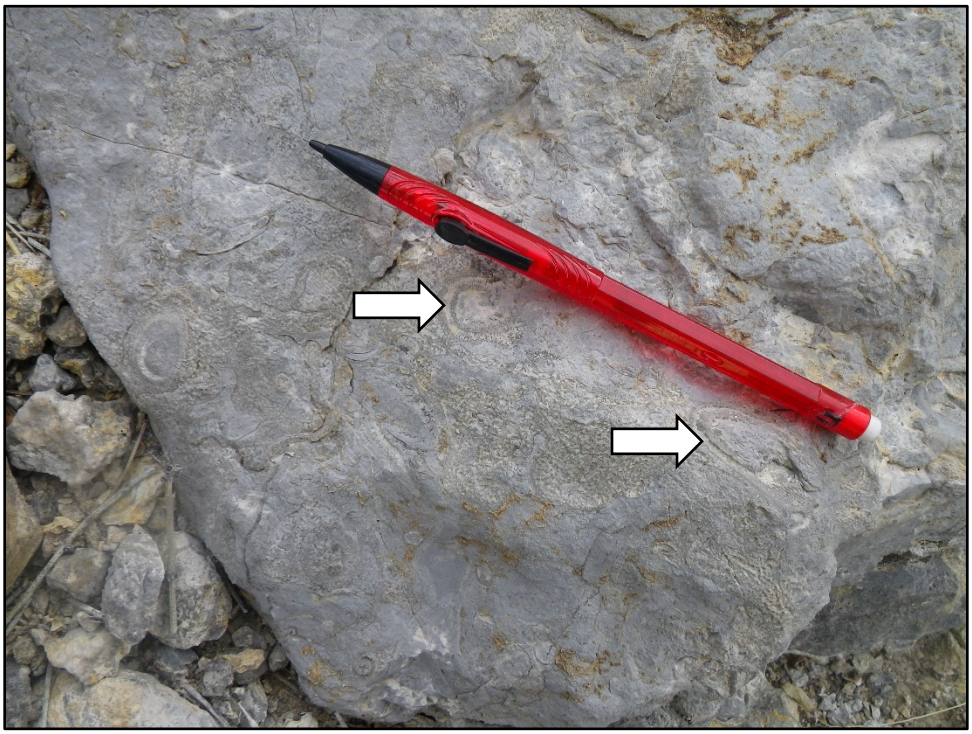

Figure 20. *Calathium* (arrows) algal reef. Located within the FF-CCM. Pencil for scale (15 cm).

wackestones, packstones, grainstones, and sparse shale. Fossils include brachiopods, bryozoans, crinoids, gastropods, graptolites, ostracods, sponges, and trilobites. A 0.7 m thick Hesperonomiella minor brachiopod coquina bed is located toward the top of the formation (Figure 21). Scattered microbial patch reefs are located within the middle to upper portion of the Wah Wah Limestone.

The Juab Limestone - The intraclastic silty wackestones with shaly interbeds occur within the Juab Limestone. Additional lithologies include silty fossiliferous wackestones and packstones. Many of the shale layers contain graptolites. Fossils include brachiopods, bryozoans, crinoids, gastropods, graptolites, ostracods, and trilobites. Sedimentary structures include burrows.

Figure 21. *Hesperonomiella minor* brachiopod coquina bed. Located within the upper Wah Wah Formation. Scale card for scale (9 cm by 15 cm) and orientation.

Garden City Formation Lithotypes and Petrography

Garden City Formation Lithotypes

Fourteen lithotypes were identified during field observations and thin section analysis of the Garden City Formation (Table 2). These lithotypes include argillaceous nodular wackestones and mudstones, boundstones, cherty wackestones and packstones, dolomitic packstones, wackestones, and mudstones, dolostones, fossiliferous packstones and wackestones, intraclastic fossiliferous grainstones, packstones, and wackestones, intraclastic shaly nodular fossiliferous wackestones, mudstones, peloidal wackestones and packstones, recrystallized packstones, wackestones, and mudstones, shales, and silty dolomitic wackestones.

Garden City Formation Petrography

Twenty-three different grain and object types were identified during the thin section analysis (Appendix B1). The majority of thin sections are varieties of wackestones and packstones. The average number of object types per sample was 8.6 with an average of 33.3 % matrix. Distinguishable fossils types identified within the thin sections include: algae, brachiopods, bryozoans, calcispheres, crinoids, gastropods, ostracods, *Nuia* (a problematic codiacean algae), radiolarians, sponges, and trilobites. Other grain/object types that were identified include: calcite crystals, dolomite crystals, intraclasts, chert, peloids/pellets, pyrite/hematite grains, quartz grains, stylolites, unknown bioclasts (unidentifiable fossils), and mineral-filled veins/fractures. Fossil grains, particularly crinoid fossils, display syntaxial overgrowth, in which large optically-continuous calcite crystals develop around an existing fossil nucleus. Additionally, some

fossil grains have been altered or recrystallized to the extent that identification is difficult or impossible.

The following lithotypes were described from thin section: boundstones, dolomitic packstones, wackestones, and mudstones, dolostones, fossiliferous packstones and wackestones, intraclastic fossiliferous grainstones, packstones, and wackestones,

Table 2. Garden City Formation lithotypes and general descriptions.

Lithotype	Description
Argillaceous nodular wackestones-mudstones	Clayey wackestones and mudstones with a distinct nodular weathering texture.
Boundstones	Calcareous mudstones with distinct fenestral fabric.
Cherty wackestones-packstones	Wackestones and packstones containing abundant black, brown, or white chert.
Dolomitic packstones-wackestones-mudstones	Packstones, wackestones, and mudstones containing greater than 10% dolomite
Dolostones	A crystalline carbonates containing primarily dolomite.
Fossiliferous packstones-wackestones	Packstones and wackestones containing greater than 10% bioclasts.
Intraclastic fossiliferous grainstones-packstones-wackestones	Grainstones, packstones, and wackestones containing greater than 10% intraclasts and greater than 10% bioclasts.
Intraclastic shaly nodular fossiliferous wackestones	Wackestones containing greater than 10% intraclasts and greater than 10% bioclasts with a distinct nodular weathering texture.
Mudstones	Predominantly calcareous mud with few or no grains.
Peloidal wackestones-packstones	Wackestones and packstones containing abundant peloids
Recrystallized packstones-wackestones-mudstones	Crystalline packstones, wackestones, and mudstones with unrecognizable (or nearly so) depositional textures.
Sandstones	Sandstones with dolomitic or calcareous cements.
Shales	Calcareous, kaolinitic shale.
Silty dolomitic wackestones	Wackestones with abundant silt-sand that contain greater than 10% dolomite rhombs.

mudstones, and recrystallized packstones, wackestones, and mudstones. All photomicrographs were taken at 40x magnification.

Boundstones - Boundstones are the primary constituent of microbial reefs within the Garden City Formation. Boundstones are a fine-grained carbonate mudstones in composition and generally display distinctive fenestral fabric, permitting them to be differentiated from other mudstones (Figure 22). Mud matrix ranges from 92-94%. Fenestral fabric consists of irregular vertical and/or horizontal openings filled with calcite or fine silt. The openings range from 0.25 mm to 1 cm across. Stylolites and sharp, parallel calcite-filled veins are also common in the boundstone lithotype. Boundstones are often finely laminated, medium gray in color, and contain sparse amounts of fine

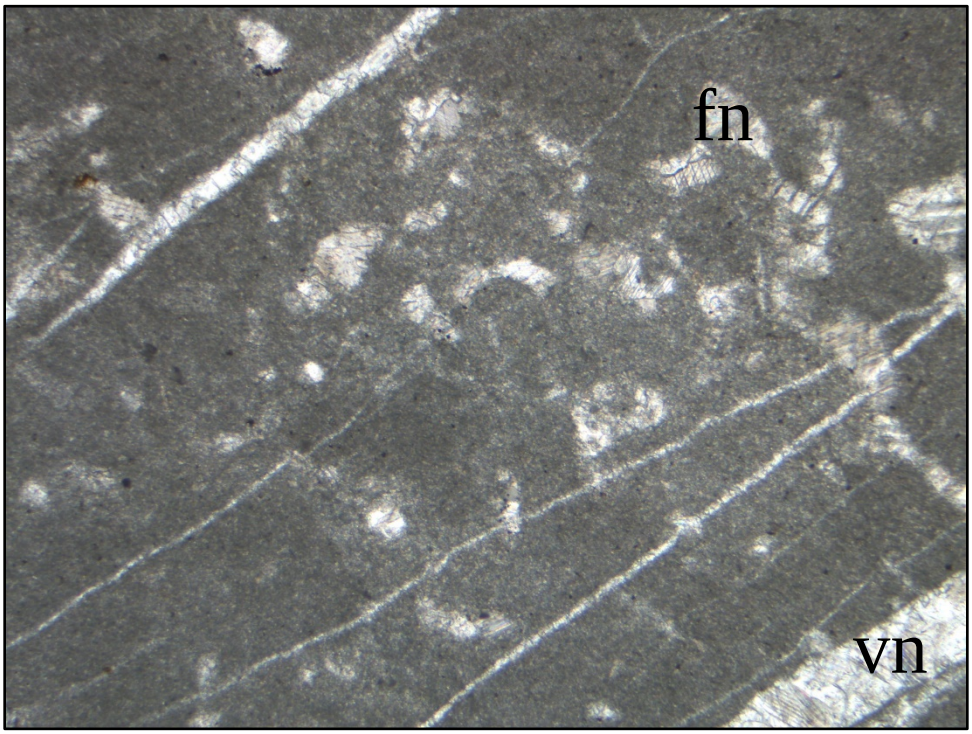

Figure 22. Plane light photomicrograph of sample GC-U10-13.5 (95.4 m). Showing fenestral fabric (fn) and parallel calcite-filled veins (vn). Bottom axis is 2.5 mm.

quartz silt. Fossils are scarce but consist of sponge spicules, *Nuia*, and crinoid fragments. Boundstones weather light gray and are gray when freshly broken.

Dolomitic Packstones, Wackestones, and Mudstones - Dolomitic packstones, wackestones, and mudstones contain more than 10% dolomite grains. Dolomitic wackestones and mudstones are often argillaceous. Dolomitic packstones, wackestones, and mudstones contain between 10% and 39% dolomite. Dolomite occurs within this lithotype as fine-grained dolomitic layers, as individual dolomite rhombohedral crystals or agglomerates of dolomite crystals. Dolomite rhombs generally show zoning evident by alternating brown and light brown/clear bands (Figure 23). The dolomite is finely- to coarsely-crystalline (0.016-0.5 mm), rhombohedral in shape, and is generally brown (but

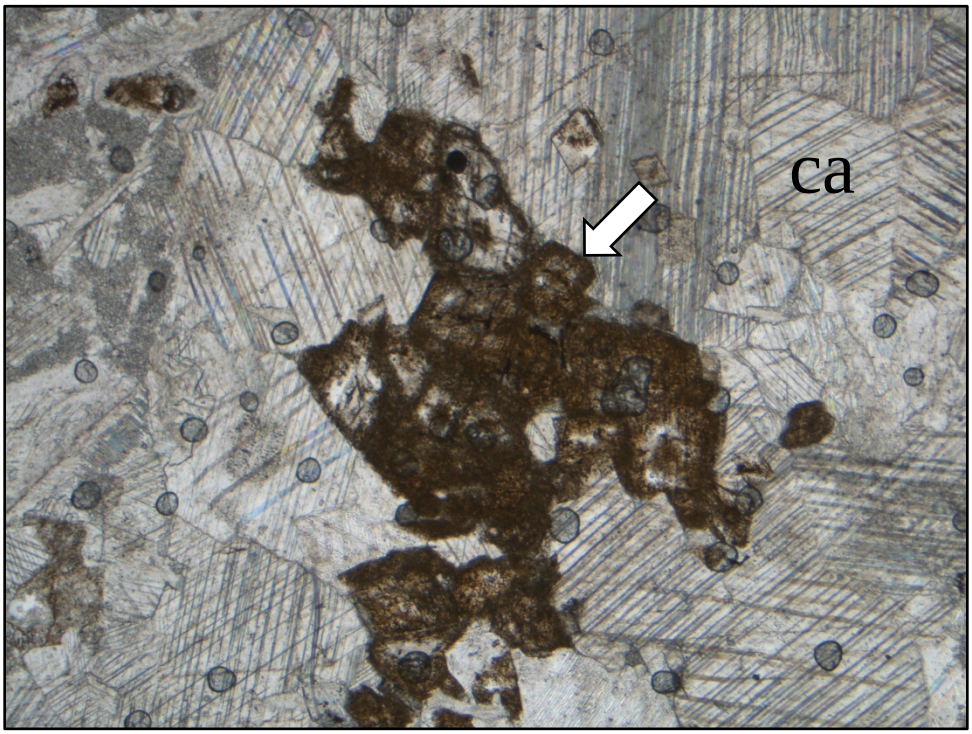

Figure 23. Plane light photomicrograph of sample GC-U5-6.0 (56.7 m). Showing an agglomerate of zoned dolomite rhombohedral crystals (arrow) and abundant twinned calcite (ca). Bottom axis is 2.5 mm.

sometimes clear) in color under plane light.

Dolomitic packstones and wackestones contain 6-20% bioclasts and range in size from 0.125-1.0 mm. Bioclast grains consist of fragmented algae, brachiopods, bryozoans, crinoids, gastropods, ostracods, *Nuia*, sponge spicules, and trilobites. Many of the crinoid grains within the packstones show syntaxial overgrowth. Calcite crystals are present in amounts ranging from 1-58% and may likely be syntaxial overgrowths with little or no remaining original organic grain structure. Crystal grains range in size from finely-crystalline (0.012-0.062 mm) to very coarsely-crystalline (1.0-4.0 mm). Other constituents that occur in minor varying amounts within the dolomitic packstones and wackestones are chert, pellets, and quartz silt. The dolomitic mudstones contain less than 10% fine crinoid fragments, *Nuia*, and sponge spicules. Minor stylolites and veins are also present. This lithotype weathers gray to brown and is dark gray to brown when freshly broken.

Dolostones - Dolostones consist primarily of the mineral dolomite ($CaMg(CO_3)_2$). Dolostones are finely to medium crystalline (0.016-0.25 mm) and retain a partial euhedral rhombohedral crystal shape. Dolomitization, the replacement of calcite with dolomite through diagenesis, has altered the original depositional texture of the rock, which is no longer recognizable. Dolostones are composed of 96-99% dolomite crystals. Dolostones in thin section appear a dusty light brown color under plane light. Stylolites and fine sand/coarse silt are often observed in thin section (Figure 24). Fossils are absent in dolostones due to the destruction of original organic structure through dolomitization. Dolostones weather light brown and are gray/light gray when freshly broken.

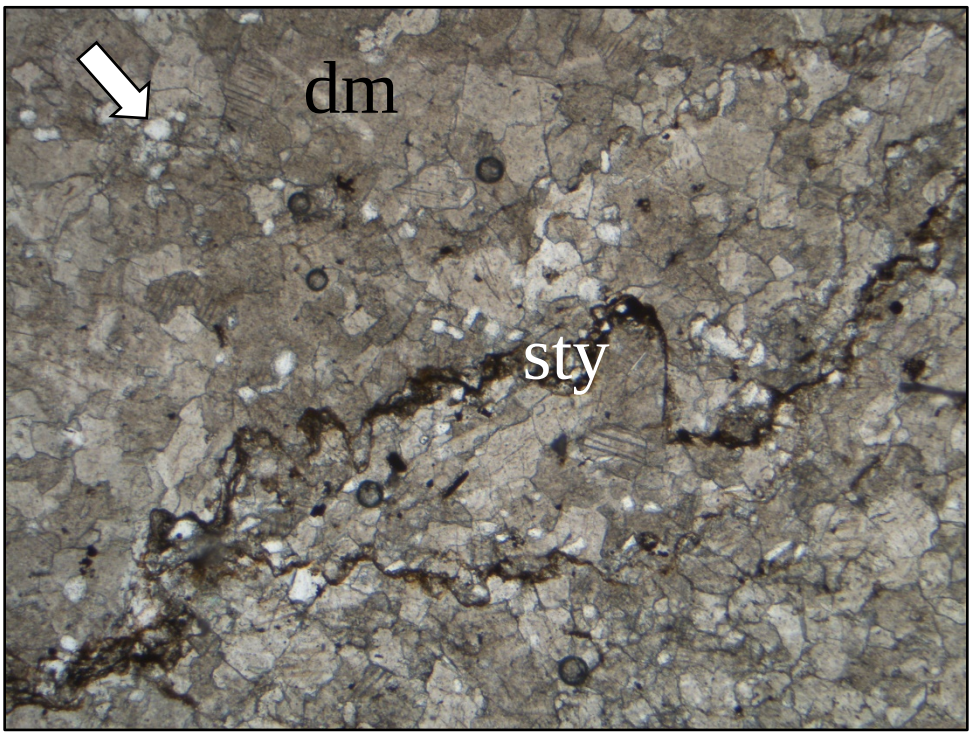

Figure 24. Plane light photomicrograph of sample GC-U0--3.0 (15 m). Showing euhedral dolomite crystals (dm), stylolites (sty), and fine sand/coarse silt (arrow). Bottom axis is 2.5 mm.

Fossiliferous Packstones and Wackestones - Fossiliferous packstones and wackestones contain more than 10% bioclast content and bioclast grains range in size from 0.125-1 mm. Bioclast content ranges from 10-77% and this lithotype generally lacks intraclasts but can contain up to 5% intraclasts. Fossiliferous packstones differ from fossiliferous wackestones in that the grains within the packstones are in contact with one another (grain supported) in the presence of carbonate mud (Figure 25). Grains within the fossiliferous wackestones are suspended within a carbonate mud matrix and are often argillaceous. Bioclast types within fossiliferous packstones-wackestones include: algae, brachiopod, bryozoans, crinoids, gastropods, ostracods, *Nuia*, sponge spicules, and trilobites. Many crinoid grains within the packstones show syntaxial overgrowths and

pellets are prevalent. Calcite crystals are present in amounts ranging from 2-67% but likely originated as bioclasts with syntaxial overgrowths. Crystal grains range in size from finely-crystalline (0.012-0.062 mm) to very coarsely-crystalline (1-4 mm). Other constituents that occur in minor varying amounts within fossiliferous packstones-wackestones are dolomite crystals, chert, pellets, and quartz silt. Many bioclasts are unrecognizable due to alteration by recrystallization, compaction, or other processes.

Intraclastic Fossiliferous Grainstones, Packstones, and Wackestones - Intraclastic fossiliferous grainstones, packstones, and wackestones contain more than 10% intraclasts and more than 10% bioclasts (fossils). Intraclastic fossiliferous wackestones are often argillaceous. Intraclast content ranges from 11-68% and bioclast content ranges from 12-

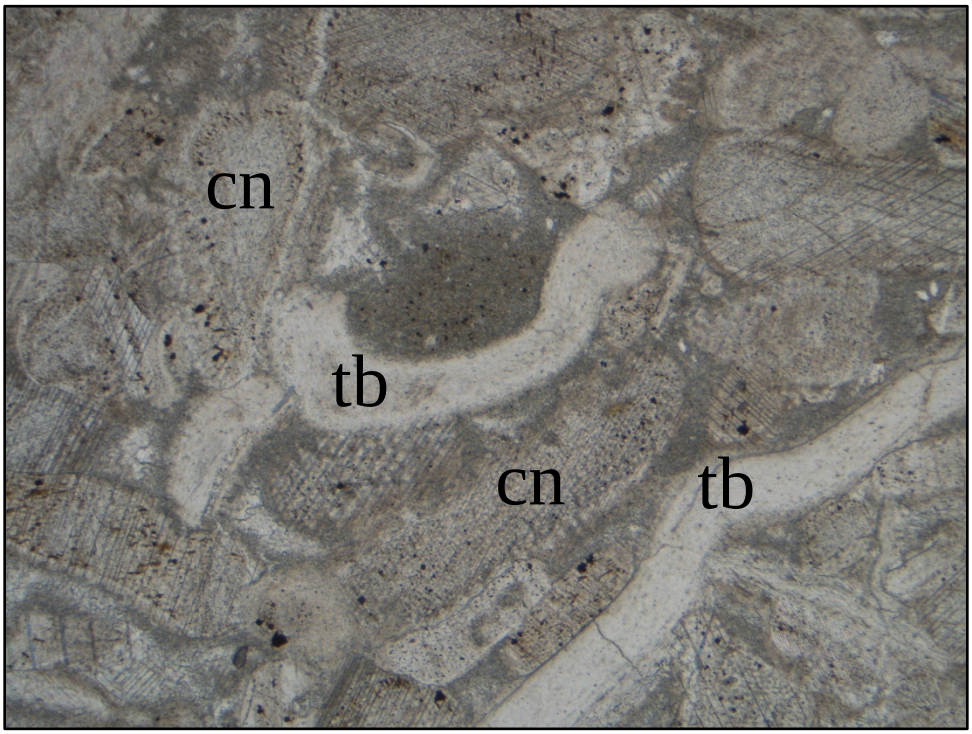

Figure 25. Plane light photomicrograph of sample GC-U13-0.4 (106 m). Showing a fossiliferous packstone with crinoids (cn) and trilobites (tb). Bottom axis is 2.5 mm.

94%. Intraclasts are held within grainstone, packstone, and wackestone matrixes composed of varying quantities of primarily brachiopods, bryozoans, crinoids, gastropods, ostracods, *Nuia*, trilobites, and carbonate mud (Figure26). Intraclasts range from several mm to several cm in length, although they can be much larger. They are generally well rounded with fossils truncated at boundaries (Figure 27), but can be subangular. Intraclasts are composed of different lithologies, but are most commonly fossiliferous wackestones and carbonate mudstones, and appear to be derived from the underlying rock beds as rip-up clasts. Bioclasts range in size from 0.125-1.0 mm. Many of the crinoid grains within the packstones show syntaxial overgrowths. Intraclastic fossiliferous grainstones, packstones, and wackestones contain calcite crystal grains

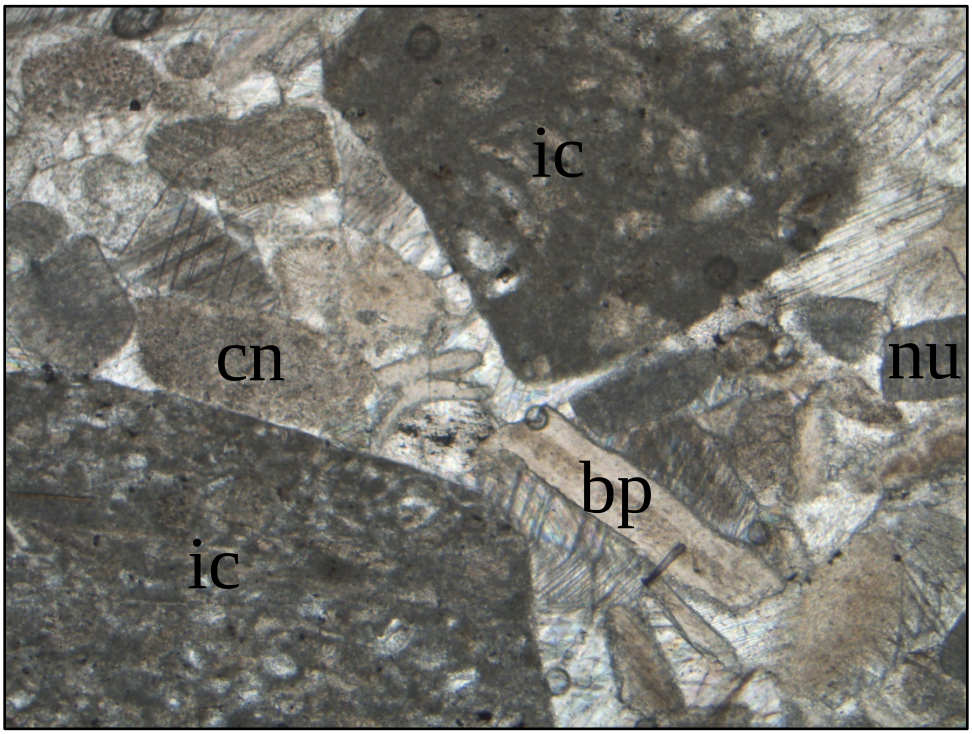

Figure 26. Plane light photomicrograph of sample GC-U3-3.0A (40.7 m). Showing an intraclastic fossiliferous grainstone with intraclasts (ic), crinoids (cn), *Nuia* (nu), trilobites (tb), brachiopods (bp). Crinoids display syntaxial overgrowths. Bottom axis is 2.5 mm.

which range from 0-45% and vary in size from finely-crystalline (0.012-0.062 mm) to very coarsely-crystalline (1-4 mm). Other constituents that occur in minor, varying amounts within the fossiliferous packstones and wackestones are dolomite crystals, chert, pellets and quartz silt. The majority of fossils in both intraclasts and matrix are fragmented and are identified using specific criteria to distinguish different fossil groups from others in thin section. Intraclastic fossiliferous grainstones, packstones, and wackestones weather light gray to light brown and are gray to light gray when freshly broken.

Mudstones - Mudstones consist of fine-grained carbonate muds containing less than 10% bioclasts or other grains (Figure 28). Mudstones contain minor silt (fine silt) and

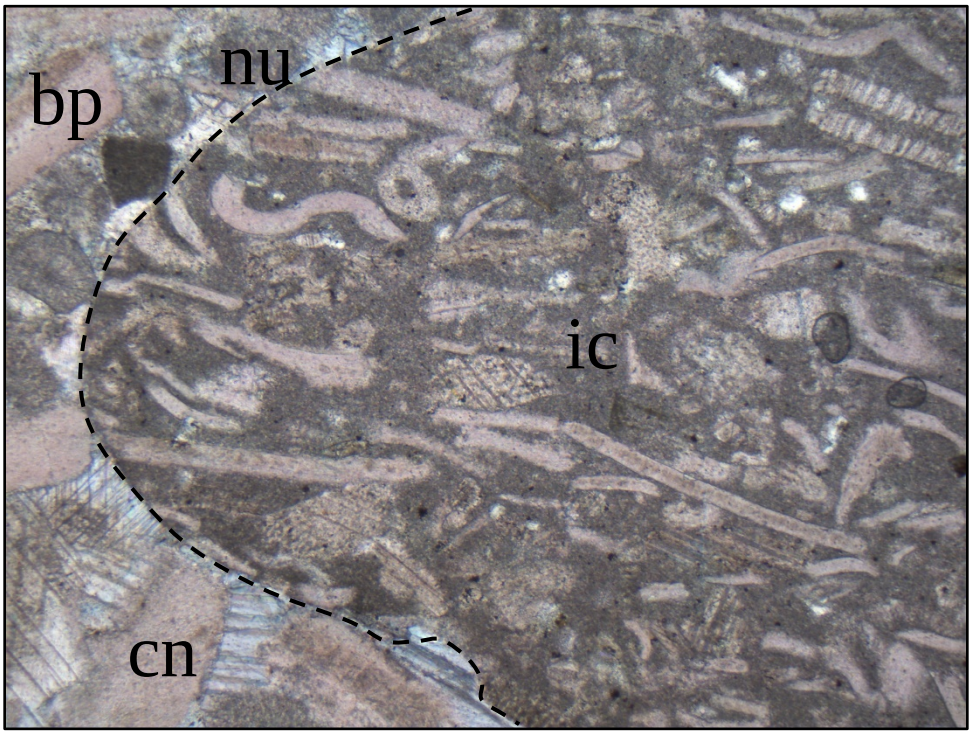

Figure 27. Plane light photomicrograph of stained sample GC-U3-3.0A (40.7 m). Showing a rounded intraclast (ic) with truncated fossils (dashed line). Fossils are mainly crinoids (cn), *Nuia* (nu), and brachiopods (bp). Bottom axis is 2.5 mm.

generally contain less than 10% bioclasts (fine crinoid fragments, *Nuia,* and sponge spicules). Occasionally mudstones are argillaceous and texture ranges from finely laminated to massive. Some mudstones display a vague peloidal fabric while others have a slight fenestral fabric, which may indicate the presence of algae. Stylolites and bioturbation are common within mudstones. Mudstones weather light gray and are dark gray when freshly broken.

Recrystallized Packstones, Wackestones, and Mudstones - Recrystallized packstones, wackestones, and mudstones consist of packstones, wackestones, and mudstones that have been recrystallized to the extent that fossil identification and the original depositional textures are difficult to discern. Recrystallized wackestones and mudstones

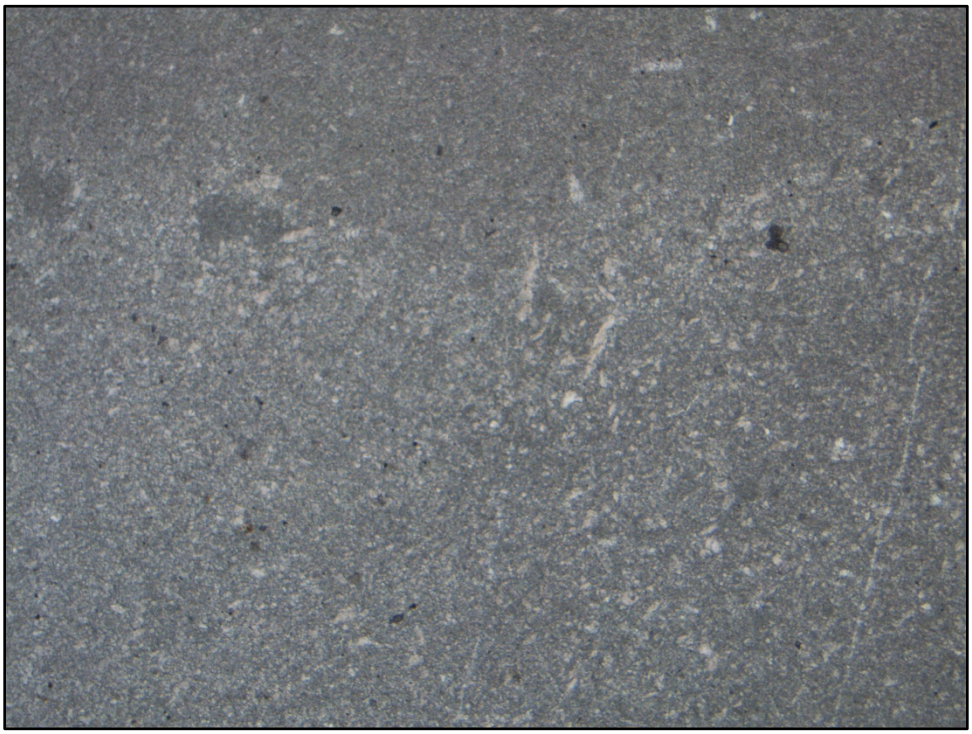

Figure 28. Plane light photomicrograph of sample GC-U12-0.0 (101.1 m). Showing a fine-grained carbonate mudstone. Bottom axis is 2.5 mm.

are often argillaceous. Recognizable bioclast content ranges from 2-17%. Some samples have undergone extensive recrystallization and under the Dunham (1962) carbonate classification scheme are classified as crystalline carbonates, due to the unrecognizable depositional texture (Figure 29). Calcite crystal grains are present and range from 9-98%. Calcite crystal grains range in size from finely-crystalline (0.012-0.062 mm) to very coarsely-crystalline (1-4 mm). Many samples contain recognizable bioclast grains and are only partially recrystallized. Varying amounts of chert, dolomite crystal grains, pellets, and silt are present within this lithotype. Recrystallized packstones, wackestones, and mudstones weather light gray to light brown and are gray when freshly broken.

Shales - Shales consist of calcareous and argillaceous shale. The primary clay mineral

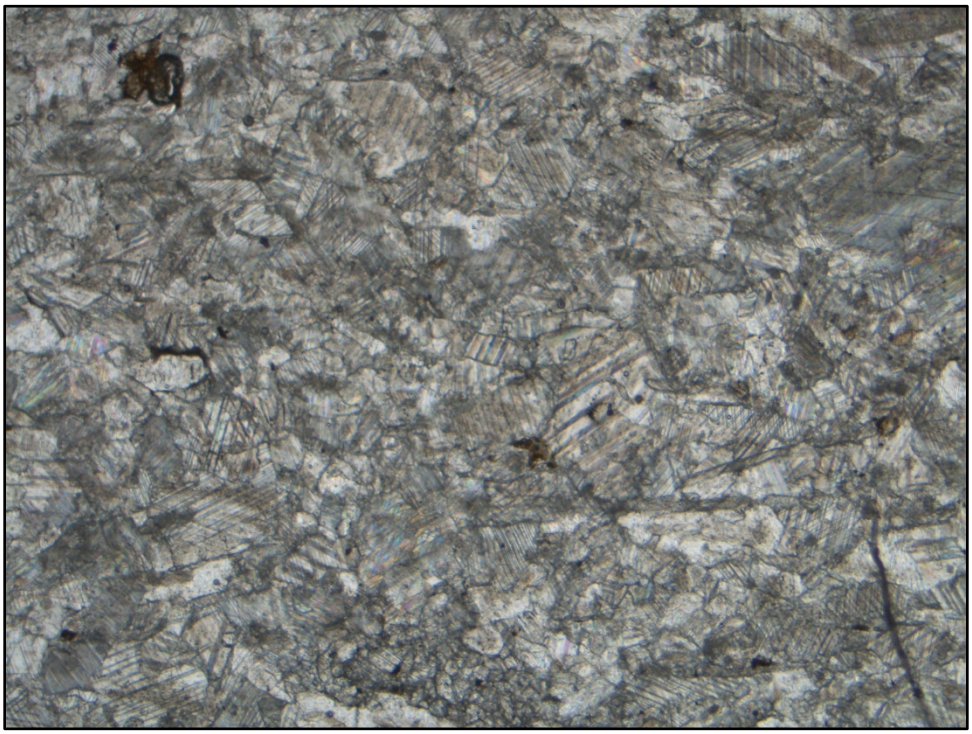

Figure 29. Plane light photomicrograph of sample GC-U6-5.1 (61.8 m). Showing a crystalline carbonate with an unrecognizable depositional texture. Bottom axis is 2.5 mm.

present within the shale lithotype is kaolinite (Morgan, 1988). Shales occur as thin interbeds and are often covered or obscured in outcrop due to their slope weathering tendencies.

Pogonip Group Lithotypes and Petrography

Pogonip Lithotypes

Eleven lithotypes were identified during field work and thin-section analysis of the Pogonip Group (Table 3). Lithotypes include boundstones, cherty wackestones and mudstones, dolomitic packstones and wackestones, fossiliferous grainstones, packstones, and wackestones, intraclastic fossiliferous grainstones, packstones, and wackestones, intraclastic peloidal wackestones and packstones, intraclastic wackestones and packstones, mudstones and wackestones, recrystallized packstones, wackestones, and mudstones, silty wackestones, and shales.

Pogonip Petrography

Twenty three different grain/object types were identified during the thin section analysis (Appendix B2). The majority of the 75 thin-sections were varieties of wackestones and packstones. The average number of object types per sample was 9.32 with an average of 41.9 % matrix. Distinguishable fossils types identified within the thin- sections include: algae, brachiopods, bryozoans, calcispheres, crinoids, gastropods, ostracods, *Nuia*, sponge spicules, and trilobites. Other object or grain types that were identified include: calcite crystals, chert, dolomite crystals, glauconite grains, gypsum crystals, intraclasts, peloids/pellets, quartz grains, stylolites, unknown bioclasts

Table 3. Pogonip Group lithotypes and general descriptions.

Lithotype	Description
Boundstone	Mound forming calcareous mudstones with distinct fenestral fabric.
Cherty wackestones-mudstones	Wackestones and mudstones with abundant chert.
Dolomitic packstones-wackestones	Packstones, wackestones, and mudstones containing greater than 10% dolomitic materials.
Fossiliferous grainstones-packstones-wackestones	Packstones and wackestones containing greater than 10% bioclasts.
Intraclastic fossiliferous grainstones-packstones-wackestones	Grainstones, packstones, and wackestones containing greater than 10% intraclasts and greater than 10% bioclasts.
Intraclastic peloidal wackestones-packstones	Wackestones and packstones containing greater than 10% intraclasts and abundant peloids.
Intraclastic wackestones-packstones	Wackestones and packstones containing greater than 10% intraclasts.
Mudstones-wackestones	Predominantly calcareous mud with few or no grains.
Recrystallized packstones-wackestones-mudstones	Crystalline packstones, wackestones, and mudstones with unrecognizable (or nearly so) depositional textures.
Silty wackestones	Wackestones containing abundant silty material.
Shales	Calcareous and argillaceous shale.

(undistinguishable fossils), and mineral-filled veins/fractures. Many thin sections are recrystallized and highly altered and crinoid fossils display syntaxial overgrowths.

The following lithotypes were described from thin section: boundstones, dolomitic packstones and wackestones, fossiliferous grainstones, packstones, and wackestones, intraclastic fossiliferous grainstones, packstones, and wackestones, mudstones, recrystallized packstones, wackestones, and mudstones, and silty wackestones. All photomicrographs were taken at 40x magnification.

Boundstones - Boundstones are the primary lithotype of microbial reefs that occur within the Pogonip Group. Boundstones within the Pogonip Group are very similar to those of

the Garden City Formation in that they are composed of fine-grained carbonate muds. Mud matrix ranges from 82-90%. Boundstones generally display distinctive fenestral fabric (Figure 30) which is more developed in the Pogonip Group than in the Garden City Formation. The fenestral fabric consists of irregular vertical and/or horizontal openings filled with calcite or silt and range from 0.25 mm up to 1.0 cm across. Compaction features are common in the boundstone lithotype and boundstones are often finely laminated, medium gray in color, and contain sparse amounts of fine quartz silt. Boundstones weather light gray to blue gray and are gray when freshly broken.

Dolomitic Packstones and Wackestones - Dolomitic packstones and wackestones contain more that 10% dolomite grains. Dolomitic packstones and wackestones contain between

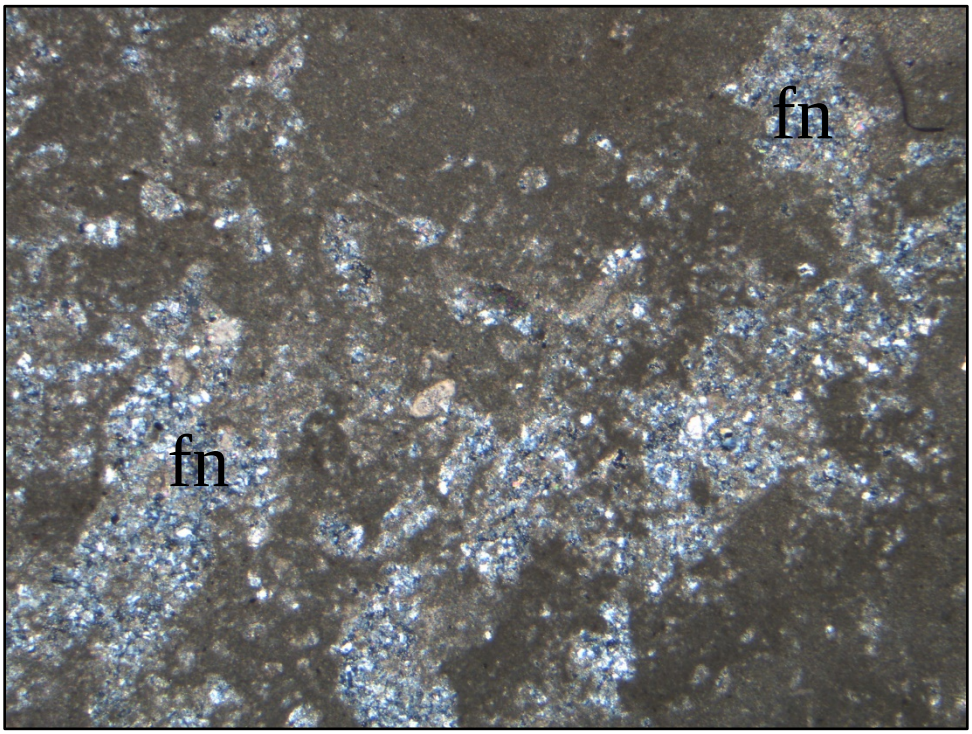

Figure 30. Polarized light photomicrograph of sample FF-BLLM-U21-1.8 (290.3 m). Showing fenestral fabric (fn) filled with fine quartz silt (black/white/gray material). Bottom axis is 2.5 mm.

10% and 35% dolomite. Dolomite occurs mainly as individual dolomite rhombohedral crystals (Figure 31). The dolomite is fine- to coarse-crystalline (0.016-0.5 mm), rhombohedral in shape, and generally brown (but sometimes clear) in color under plane light. Dolomite rhombs generally show zoning indicated by alternating brown and light brown/clear zones.

Dolomitic packstones and wackestones contain few fossils but calcite crystal grains and quartz silt are present in amounts ranging from 7-25% and 26-51%, respectively. Crystal grains range in size from finely-crystalline (0.012-0.062 mm) to very coarsely-crystalline (1-4 mm). Other constituents that occur in minor varying amounts are pellets and sparse bioclasts. Minor stylolites and veins are also present.

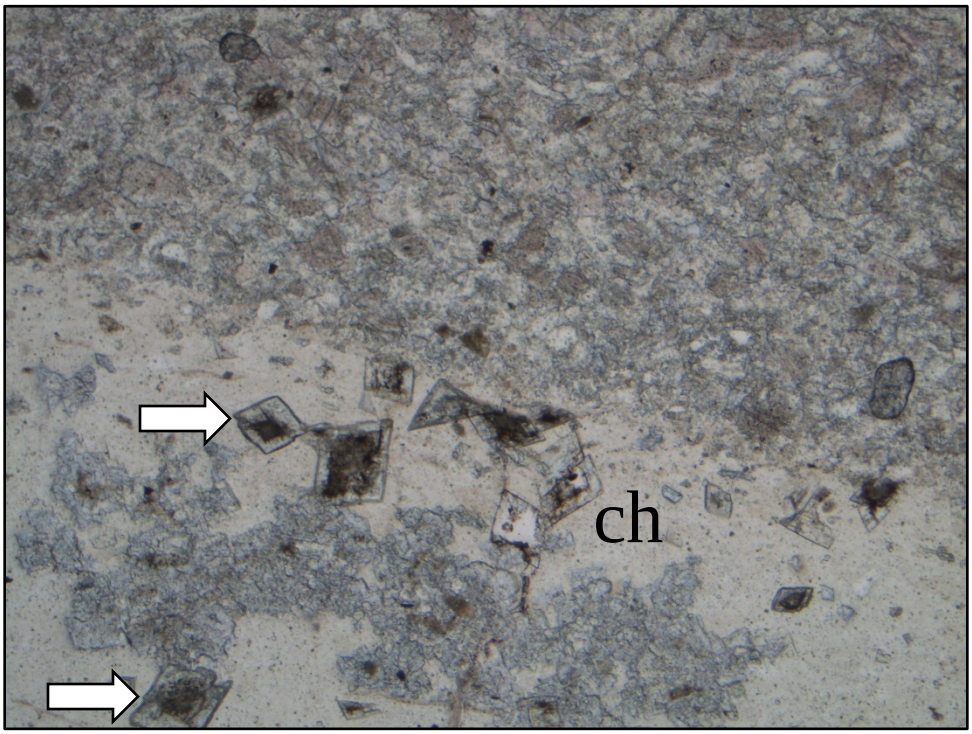

Figure 31. Plane light photomicrograph of sample HL-U5-9.0 (135.2 m). Showing individual zoned rhombohedral dolomite crystals (arrows) suspended in a chert matrix (ch). Bottom axis is 2.5 mm.

Dolomitic packstones and wackestones weather gray to brown and are dark gray when freshly broken.

Fossiliferous Grainstones, Packstones, and Wackestones - Fossiliferous grainstones, packstones, and wackestones containing more than 10% bioclasts. Bioclast content ranges from 11-69% and include: algae, brachiopod, bryozoans, crinoids, gastropods, ostracods, *Nuia*, sponge spicules, and trilobites (Figure 32). Pellets and fine quartz silt are common and range from 1-21% pellets and 0-34% quartz silt. Many of the crinoid grains within the packstones show syntaxial overgrowths. Many bioclasts are also unrecognizable due to alteration by recrystallization, compaction, or other diagenetic processes. Calcite crystals are present in amounts ranging from 4-55% and may be

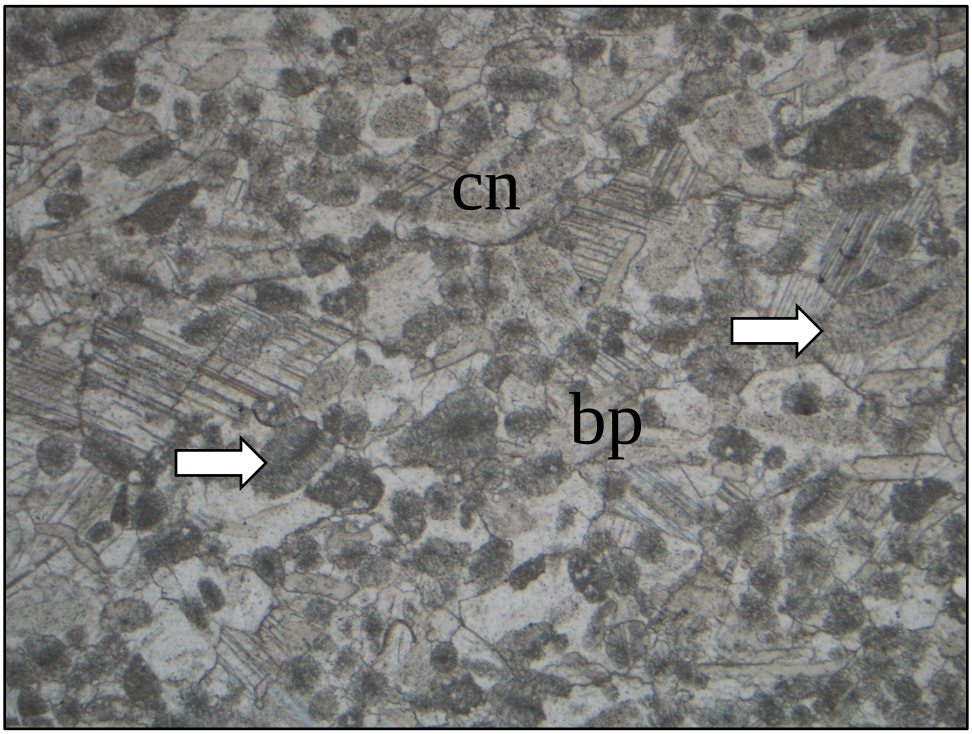

Figure 32. Plane light photomicrograph of sample HL-U4-30.0 (125.7 m). Showing *Nuia* (arrows), brachiopods (bp), and crinoids (cn). Bottom axis is 2.5 mm.

bioclasts with syntaxial overgrowths. Crystal grains range in size from finely-crystalline (0.012-0.062 mm) to very coarsely-crystalline (1-4mm). Fossiliferous grainstones, packstones, and wackestones weather light gray and are gray when freshly broken.

Intraclastic Fossiliferous Grainstones, Packstones, and Wackestones - Intraclastic fossiliferous grainstones, packstones, and wackestones containing more that 10% intraclasts and more than 10% bioclasts (fossils). Intraclastic content for this lithotype ranges from 13-64% and bioclast content ranges from 15-76%. Intraclasts are suspended within grainstone, packstone, and wackestone matrixes made of fragmented brachiopods, bryozoans, crinoids, gastropods, ostracods, *Nuia*, trilobites, and carbonate mud (Figure 33). Intraclasts range from several mm to several cm in length, but can be longer. They

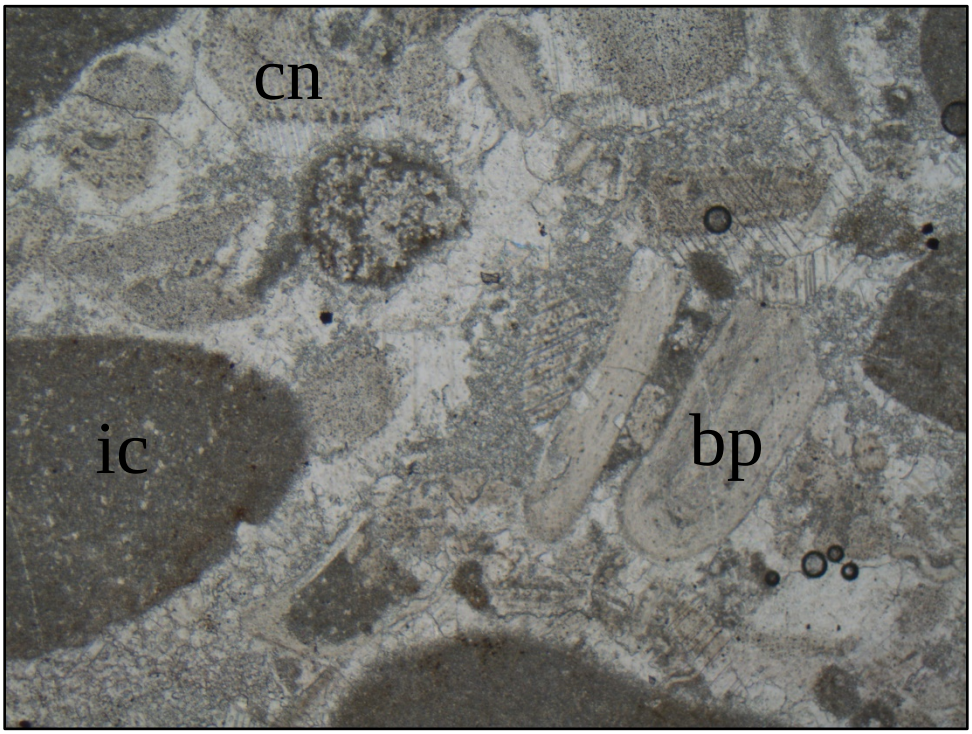

Figure 33. Plane light photomicrograph of sample FF-BSLM-U10-2.5 (555.6 m). Showing mud intraclasts (ic) suspended within packstone matrix consisting of fragmented brachiopods (bp), crinoids (cn), and carbonate mud. Bottom axis is 2.5 mm.

are generally well rounded with truncated fossils at boundaries but can be subangular. Intraclasts are composed of different lithologies but are most commonly fossiliferous wackestones and carbonate mudstones and are likely derived from the underlying rock beds as rip-up clasts. Bioclasts range in size range in size from 0.125-1.0 mm and many of the crinoid grains within the grainstones and packstones display syntaxial overgrowth. Intraclastic fossiliferous grainstones, packstones, and wackestones contain calcite crystal grains that range in size from finely-crystalline (0.012-0.062 mm) to very coarsely-crystalline (1.0-4.0mm) and vary in abundance from 7-44%. Dolomite crystal grains and pellets occur in varying amounts within this lithotype. Intraclastic fossiliferous grainstones, packstones, and wackestones weather light gray to light brown and are light gray when freshly broken.

Mudstones - Mudstones consist of fine-grained carbonate mudstones (Figure 34). Mudstones are slightly silty (fine silt) and contain less than 10% grains, usually derived from crinoid fragments, *Nuia,* and sponge spicules. Some mudstones are argillaceous and textures range from finely-laminated to massive. Stylolites and bioturbation are common within mudstones. Mudstones weather light gray and are dark gray when freshly broken.

Recrystallized Packstones, Wackestones, and Mudstones - Recrystallized packstones, wackestones, and mudstones are common within the Pogonip Group. Many samples have been recrystallized to the extent that fossil identification and the original depositional texture are difficult to discern and some samples have undergone extensive recrystallization to the degree that depositional texture is unrecognizable (Figure 35).

Recognizable bioclasts are present and are only partially recrystallized. Recognizable bioclast content ranges from 0-24%. Chert, dolomite, and fine quartz silt are present within this lithotype and range in abundance from 7-49%, 3-11%, and 1-33%, respectively.

Shales - The shale lithotype is common throughout the Pogonip Group and generally occurs as thin interbeds of calcareous and argillaceous. Shales generally occur as weathered slopes and are poorly exposed in outcrop.

Silty Wackestones - Silty wackestones contain less than 10% bioclasts and have relatively high amounts of fine quartz silt and calcite crystals (Figure 36). Fine quartz silt content ranges from 31-46% and calcite crystal content ranges from 5-50%. Silty wackestones weather light gray and are gray when freshly broken.

Figure 34. Plane light photomicrograph of sample FF-BLLM-U18-0.7 (271.7 m). Showing a fine grained carbonate mudstone with minor silt (white grains). Bottom axis is 2.5 mm.

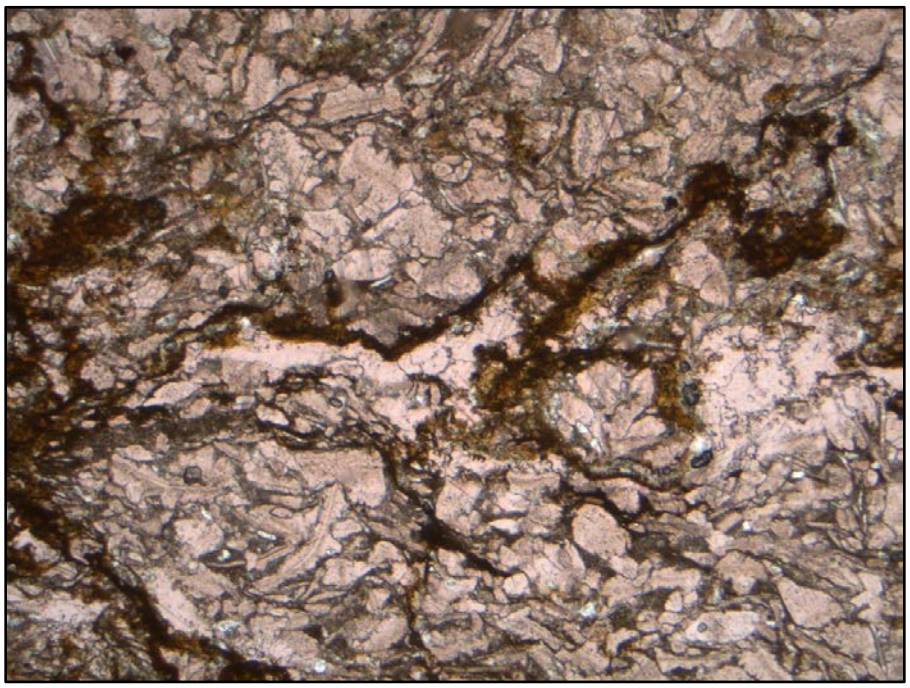

Figure 35. Plane light photomicrograph of stained sample FF-SSSM-U3-12.0 (376.2 m). Showing extensive compaction, recrystallization, and stylolitization to the degree that depositional texture is unrecognizable. Bottom axis is 2.5 mm.

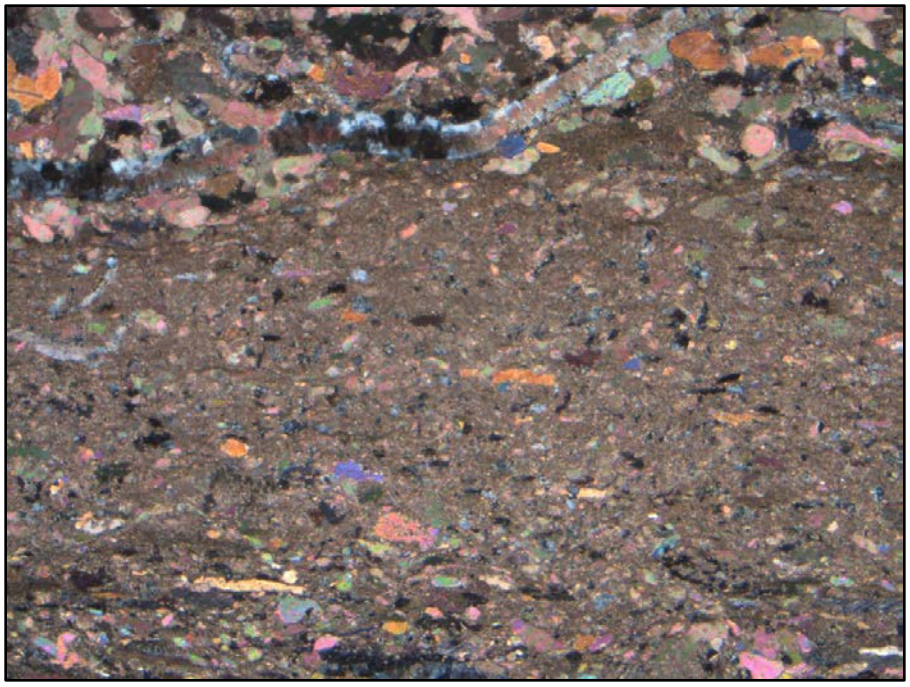

Figure 36. Polarized light photomicrograph of stained sample FF-SSSM-U2-24.0 (361.4 m). Showing relatively high amounts of fine quartz silt (high birefringence colors) and calcite crystals. Bottom axis is 2.5 mm.

Fossils of the Garden City Formation and Pogonip Group

Fossils identified during field work include microbial reefs, articulate and inarticulate brachiopods, *Calathium*, cephalopods, conodonts, crinoids, gastropods, graptolites, ostracods, sponges, and trilobites (Table 4). The majority of observable fossils in the field consist as fragmented fossil grains or fossil hash, although some are preserved as whole fossils. Many fossils (especially trilobites) have been partially replaced with silica, resulting in brown/orange weathering resistant bed surfaces covered with silicified fossils. Brachiopods, crinoids, and trilobites are by the far the most common fossils seen in the field. Cephalopods, gastropods, and ostracods occur with increased frequency higher upsection. *Calathium* occurs primarily within microbial reef horizons. *Calathium* were not observed within the Garden City Formation in Green Canyon, however, they do occur in other sections of the Garden City Formation.

Fossils identified in thin -section include dasycladacean green algae, thrombolitic algae, brachiopods and brachiopod spines, bryozoans, cephalopods, crinoids, gastropods, ostracods, *Nuia*, sponges and sponge spicules, and trilobites (Table 4). Dasycladacean green algae and bryozoans are often difficult to distinguish between in thin section due to similar skeletal structures. Brachiopods occur as impunctate, punctate, and pseudopunctate species and are common throughout the Garden City Formation and Pogonip Group. Cephalopods, gastropods, and ostracods are found mainly in thin-sections from the upper portions of both rock units. *Nuia* generally occur in large quantities vary in shape and size. Sponges are rare, however, sponge spicules commonly occur within chert-rich and fine-grained, muddy thin sections. Brachiopod, crinoid, and

trilobite fragments are by far the most common fossils found within the thin =sections from both rock units. Biogenic structures include varieties of trace fossils such as vertical burrows and horizontal burrows, as well as microbial reefs and other bioturbation features.

Table 4. Bioclastic allochems from field work and thin-section facies analysis.

Brachiopods	• Often broken down into fragments
Bryozoans	• Often broken down into fragments • Often difficult to discern from algae
Calathium	• Problematically classified as both a sponge and an algae
Cephalopods	• Occur as straight tapered fossils
Conodonts	• Occur nearly continuously throughout both rock units
Crinoids	• Often broken down into plates of single calcite crystals • Often associated with syntaxial overgrowth
Dasycladacean Green Algae	• Often broken down into fragments • Mostly shallow marine origin
Gastropods	• Occur mainly as mud molds
Graptolites	• Occur in shaly facies
Microbial reefs	• Occur as both stromatolite and lithistid sponge-Calathium reefs (microbial-dominated), and lithistid sponge-Calathium reefs (metazoan-dominated)
Nuia	• Codiacean algae which occur as round or elongate grains with radial fabric
Ostracods	• More prevalent towards the upper sections of the rock units
Trilobites	• Often broken down into elongate fragments and ‘Shepard’s crooks’
Sponges	• Often occur as only sponge spicules • Primarily associated with microbial reefs

Point Count Statistics

Garden City Formation R-Mode Cluster Analysis of Bioclasts

R-mode cluster analysis delineates communities of organisms in the Garden City Formation. These organisms include algae, brachiopods, bryozoans, calcispheres, echinoderms, gastropods, ostracods, *Nuia*, sponges, and trilobites. R-mode cluster analysis indicates that three broad groups or "communities" occur within the Garden City Formation (Figure 37). The uppermost cluster, or community, consists of ostracods, gastropods, and calcispheres. These organisms occur predominantly in the upper 30 m of the Garden City Formation. The middle cluster consists of trilobites, brachiopods, echinoderms, bryozoans, and algae. These organisms occur almost cyclically throughout the Garden City Formation and these cycles are separated by thin intervals completely lacking these fossils. The lower most cluster contains sponges and *Nuia*, which appear to occur randomly throughout the Garden City Formation.

Garden City Formation Q-Mode Cluster Analysis of Samples

Q-mode cluster analysis (based on the organisms used for R-mode cluster analysis) groups similar samples. Q-mode cluster analysis of the Garden City Formation thin-sections indicates that there are seven environments or biofacies (Figure 38). Cluster 1 contains abundant echinoderms with minor brachiopods and trilobites, however cluster 2 contains no fossil organisms. Cluster 3 contains calcispheres and echinoderms, whereas cluster 4 contains abundant brachiopods with minor trilobites and echinoderms. Cluster 5 contains mainly trilobites, and clusters 6 and 7 contain primarily *Nuia* and sponges.

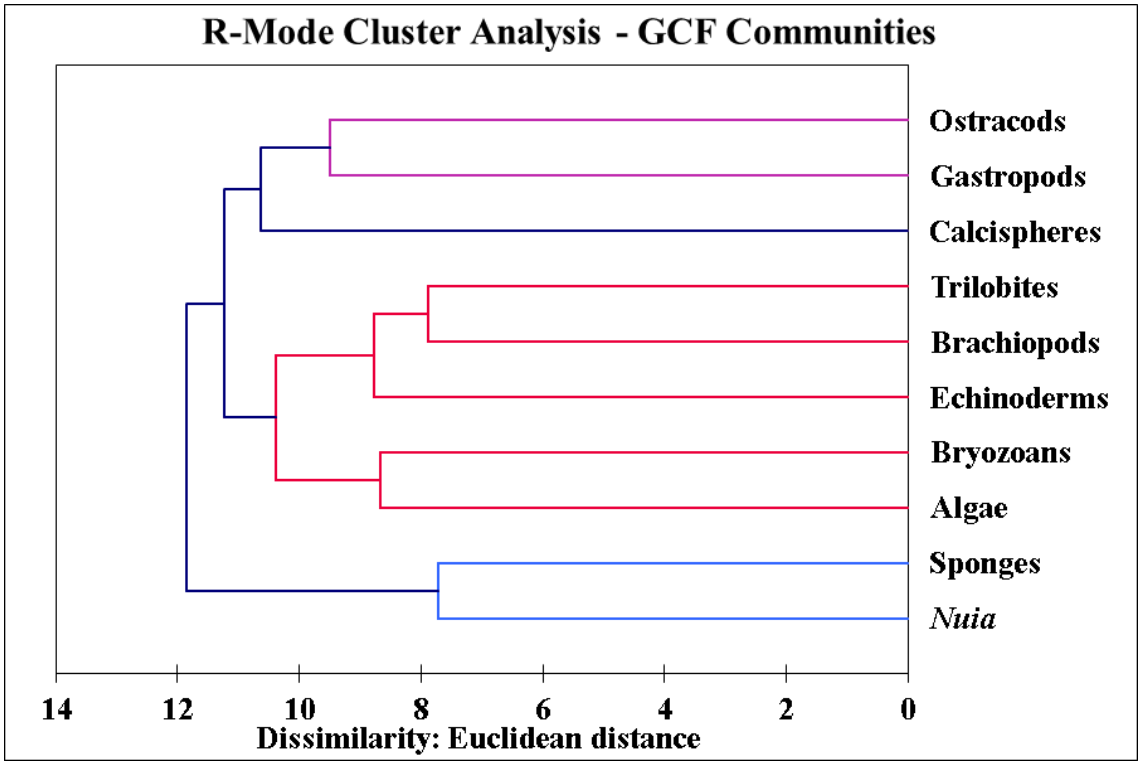

Figure 37. Garden City Formation R-mode cluster analysis showing communities. Different colors indicate different communities.

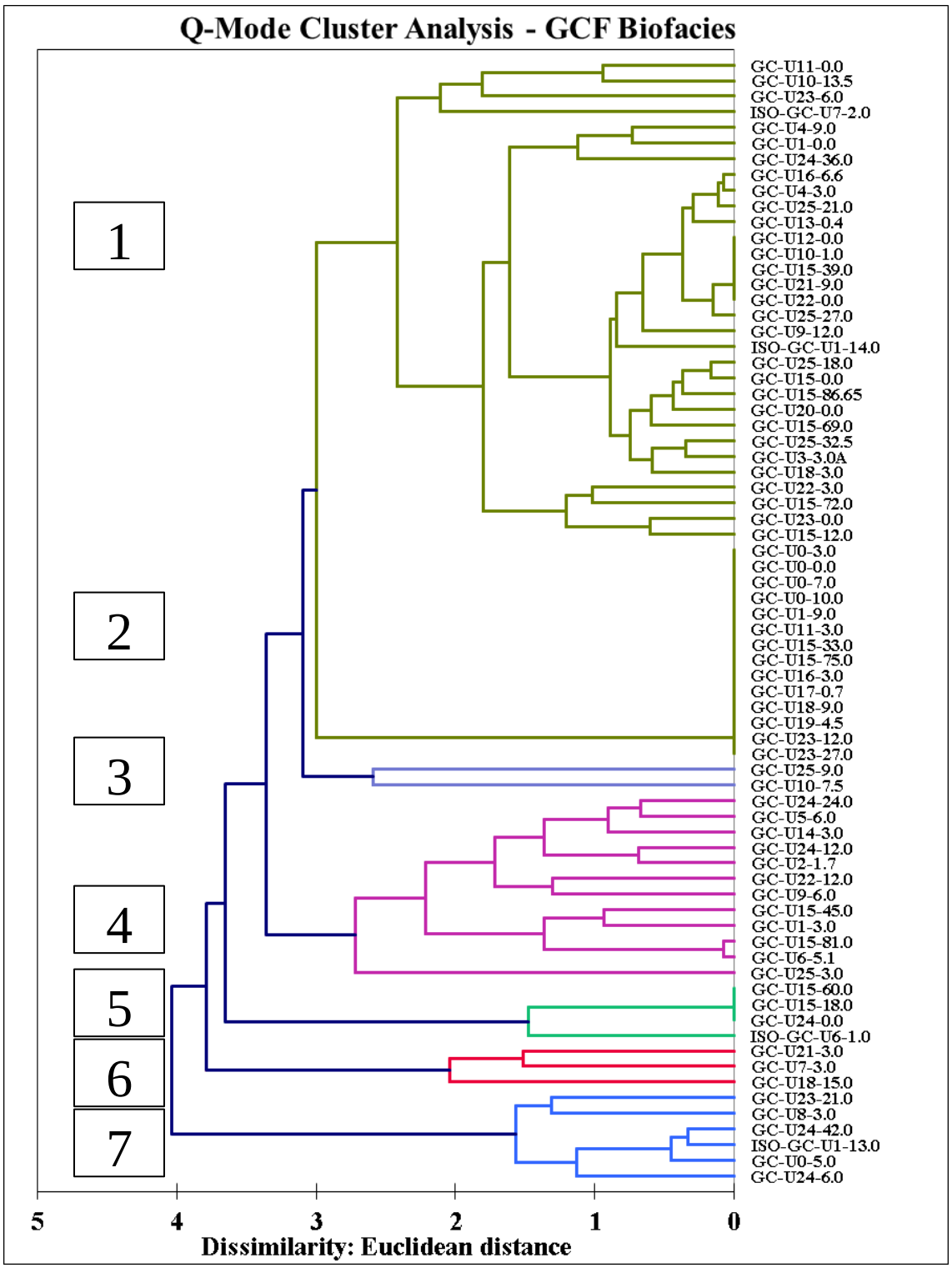

Figure 38. Garden City Formation Q-mode analysis showing biofacies. Different colors represent different environments or biofacies. Sample names are to the right of the dendrogram.

Garden City Formation Principal Components Analysis of Bioclasts

R-mode principal components analysis (PCA) for the Garden City Formation shows organisms that occur together, which represents communities. This analysis indicates that brachiopods (echinoderms and trilobites are redundant) are the most important variable affecting distribution along the factor 1 axis (x axis) and calcispheres (sponges and ostracods are redundant) are the most important variable affecting distribution along the factor 2 axis (y axis) (Figure 39). This analysis groups calcispheres, ostracods, and gastropods into a community. Bryozoans, algae, trilobites,

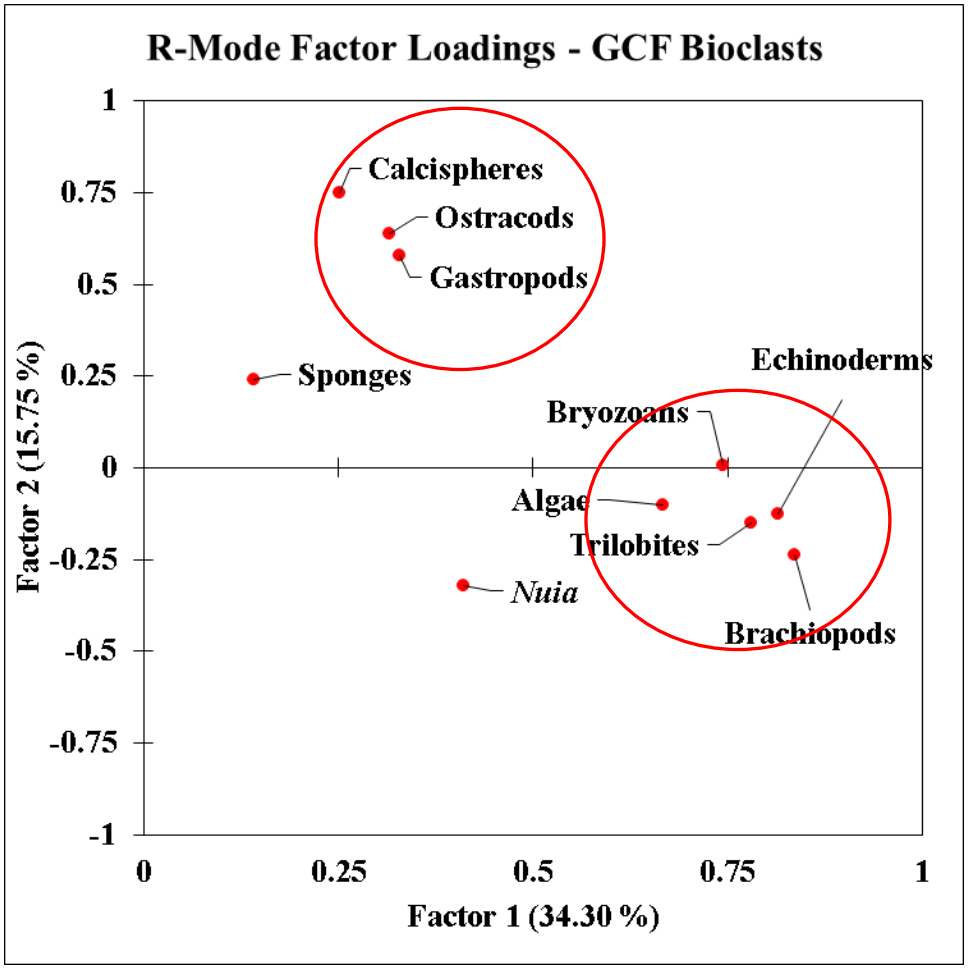

Figure 39. Garden City Formation R-mode PCA showing communities.

echinoderms, and brachiopods are also grouped into a community. However, sponges and *Nuia* appear to group separately. Similar communities are observed within the R-mode cluster analysis (Figure 37).

Q-mode PCA illustrates the grouping of samples containing similar bioclasts and should show biofacies. However, Q-mode PCA does not appear to produce obvious biofacies groups except for the cluster (red circle) that consists of samples without bioclasts (Figure 40).

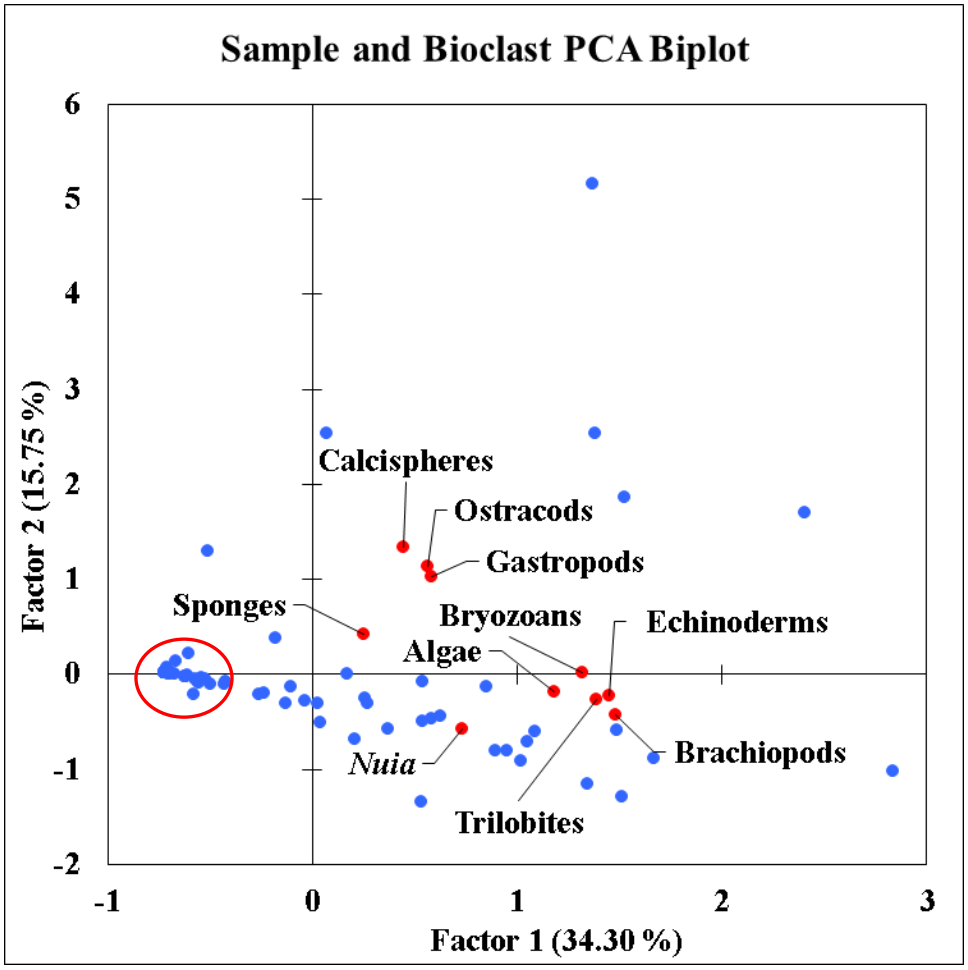

Figure 40. Garden City Formation combined sample (blue dots) and bioclast (red dots) PCA biplot.

Garden City Formation R-Mode Cluster Analysis of Important Grain Types

Twenty-three grain types were encountered during thin section analysis. Four of the main grain types, bioclasts (all taxa), intraclasts, matrix, and quartz grains, were retained for R-mode cluster analysis because they represent the bulk of point counts. R-mode cluster analysis illustrates the relationship between these four grain types and reveals 3 groups (Figure 41). Bioclasts and intraclasts group together, while matrix and quartz group independently.

Garden City Formation Q-Mode Cluster Analysis of Lithofacies

Q-mode cluster analysis illustrates the clustering of samples based on the four grain categories used in the R-mode analysis and represent different lithofacies. This

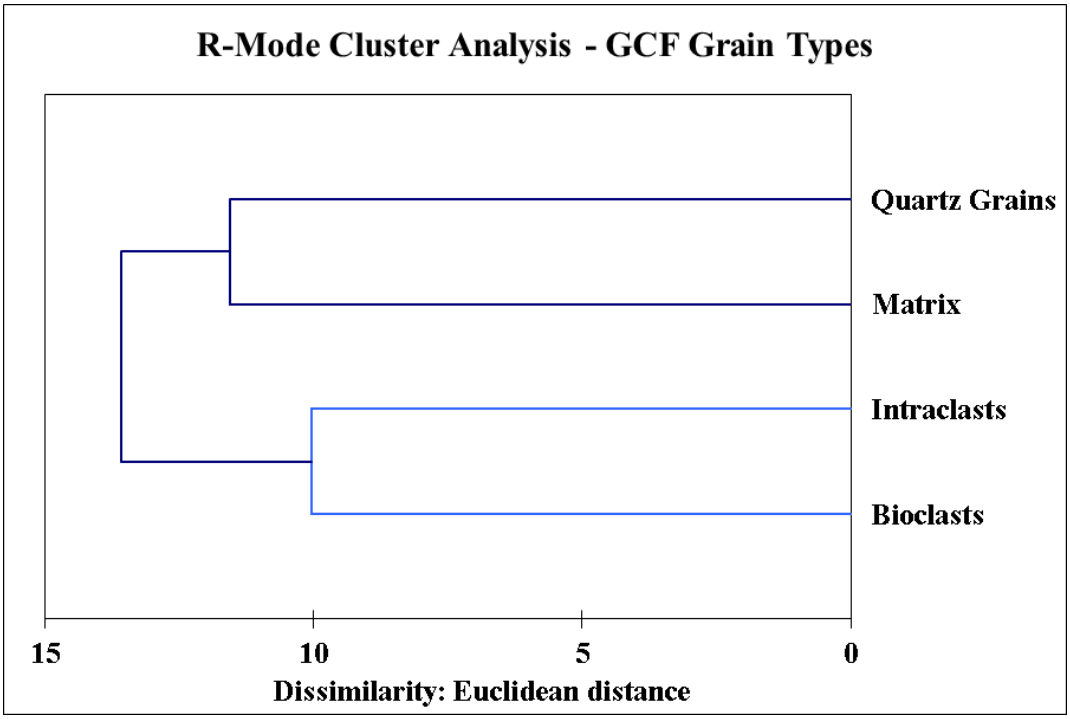

Figure 41. Garden City Formation R-mode cluster analysis showing relationships of grain types.

analysis indicates that three broad lithofacies and five specific lithofacies exist within the Garden City Formation (Figure 42).

The uppermost cluster is representative of samples grouped together due to higher quartz content and consists of two dominate subclusters. The uppermost subcluster (1a) has more matrix-sized material and consists of siliceous wackestones associated with lower energy and deeper water environments of near shore highstand deposits. The lower subcluster (1b) consists of silty dolostones, crystalline carbonates, and packstones with occasional peloids/pellets. These lithotypes contain sand and silt-sized terrigenous material that generally indicates higher energy and closer proximity to a shoreline from which the terrigenous material is derived. Higher amounts of terrigenous material is generally associated with lowstand deposits.

The middle cluster (2) is representative of samples consisting primarily of fine-grained matrix material. This cluster consists of wackestones, and mudstones with sparse boundstones and fossiliferous wackestones. These lithologies are generally deposited in lower-energy environments and likely represent highstand deposits within the Garden City Formation, with the exception of the boundstones which generally occur as lowstand or transgressive deposits. The boundstones clustered with these fine-grained lithologies because they are also composed of fine-grained material.

The bottommost cluster is representative of samples containing abundant bioclasts and intraclasts. This cluster also contains two dominate subclusters. The upper subcluster (3a) contains abundant bioclasts associated with fossiliferous wackestones and packstones. The lower subcluster (3b) contains abundant intraclasts associated with

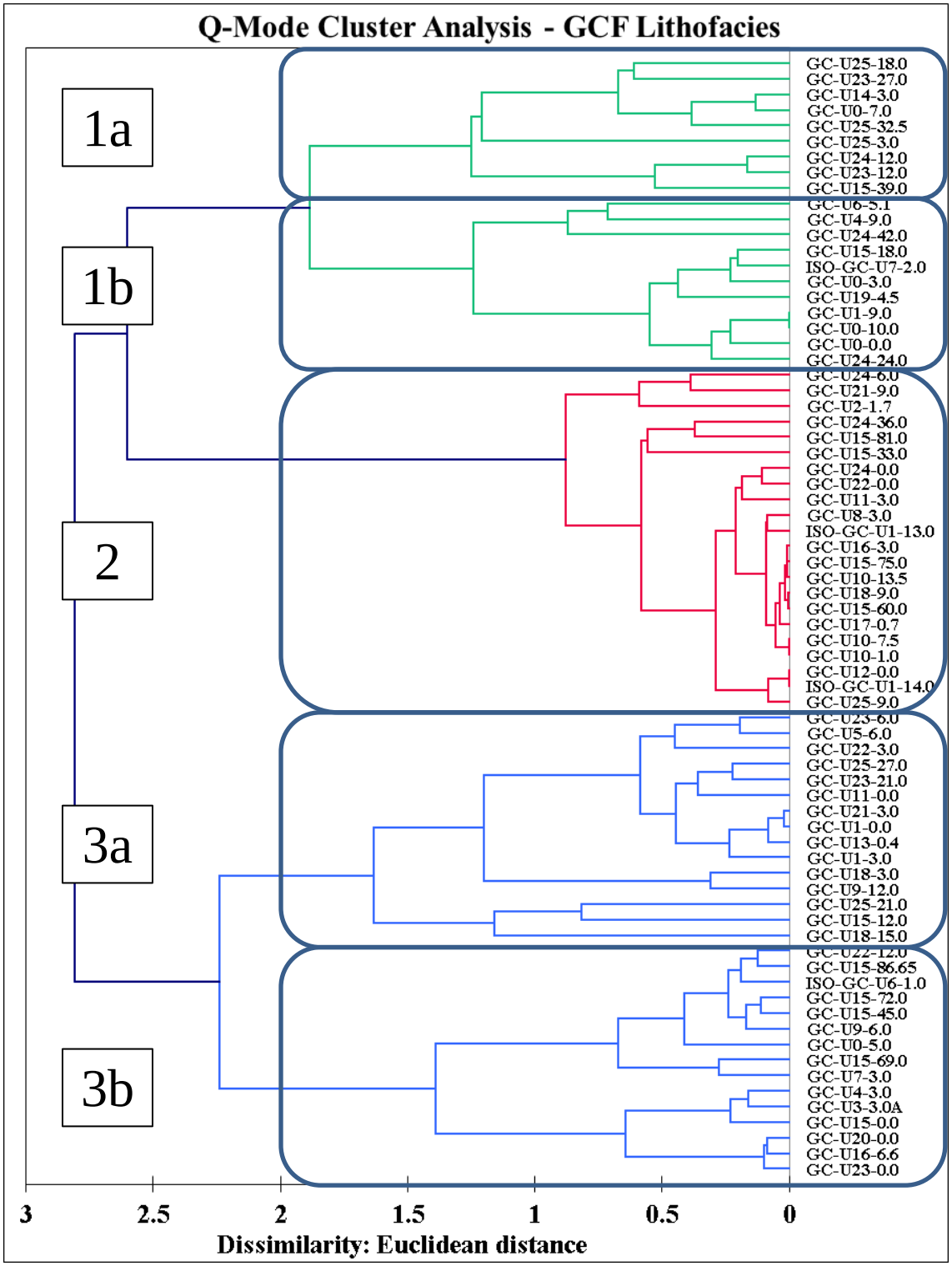

Figure 42. Garden City Formation Q-mode cluster analysis showing lithofacies. Blue boxes indicate grouping of samples based on grain types. Sample names are to the right of the dendrogram.

intraclastic wackestones, packstones, and grainstones. Fossiliferous packstones and wackestone dominate the upper cluster, while intraclastic wackestones, packstones, and grainstones dominate the lower cluster. Peloids/pellets are also prevalent throughout each of these clusters. These lithologies are generally associated with higher energy environments and likely represent lowstand and/or transgressive deposits.

Lithofacies appear to repeat in a cyclic fashion throughout the Garden City Formation. Lithofacies are distributed within these cycles with high-energy shallow water lithofacies consisting of lowstand deposits occurring at the base of the cycle, followed by transitional transgressive deposits. The upper portions of cycles contain deeper water low-energy lithofacies consisting of highstand deposits.

Garden City Formation Principal Components Analysis of Important Grain Types

R-mode PCA of the four main grain types indicates which grains occur together. Similarly to the cluster analysis of these grains, PCA shows three broad groups of grain types, with bioclasts and intraclasts occurring together, while matrix and quartz grains occur independently (Figure 43).

Q-mode PCA illustrates the grouping of samples and shows lithofacies. The majority of samples appear to group around bioclasts/intraclasts and matrix grain types with fewer samples grouping around the quartz grain type (Figure 44), which is consistent with the cluster analysis. Samples grouping around the quartz, bioclasts, and intraclasts points likely represent lowstand/transgressive deposits, while those samples grouping around the matrix point likely represent highstand deposits.

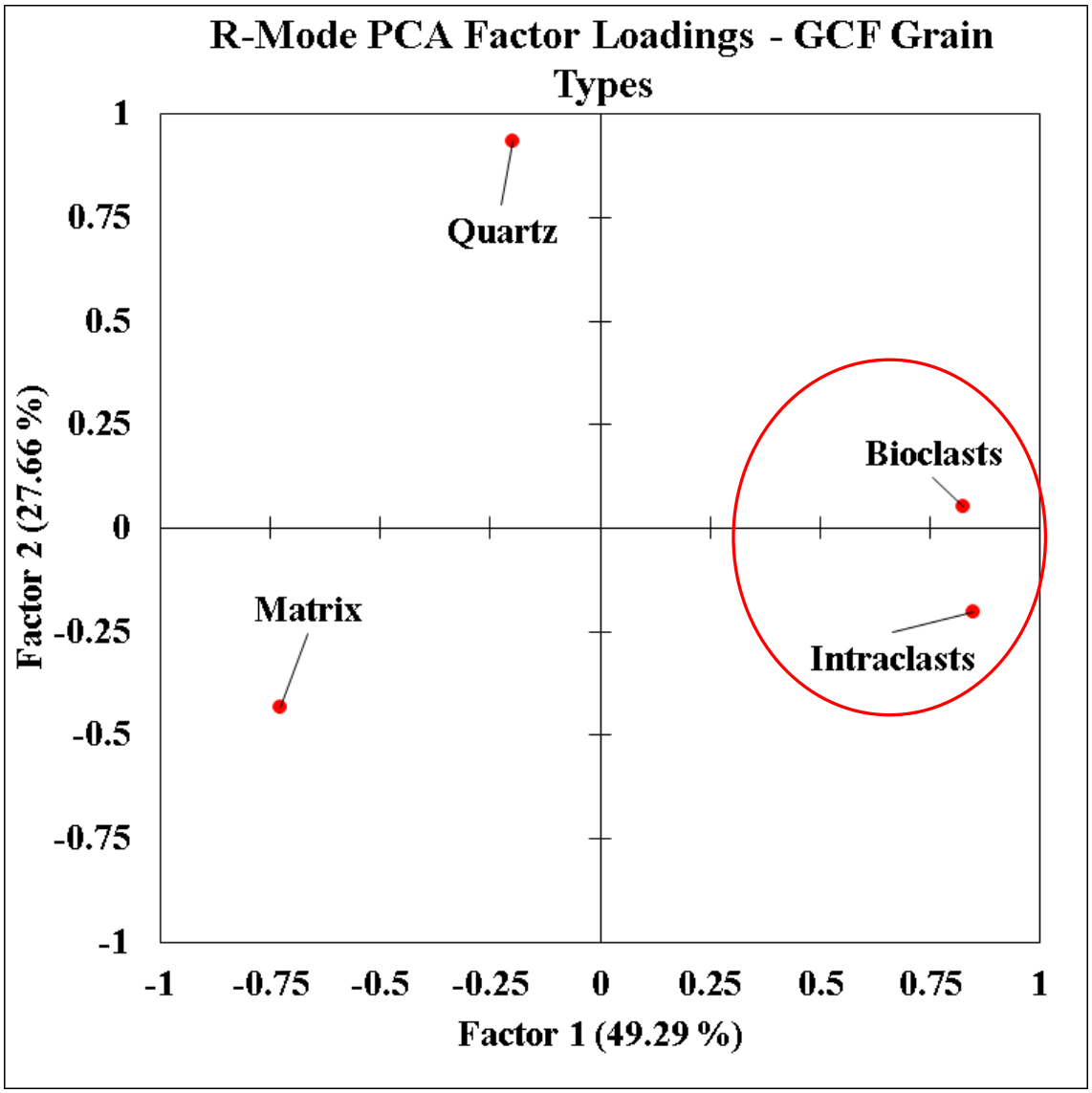

Figure 43. Garden City Formation PCA showing grain type relationships. The red circle indicates the grouping of bioclasts and intraclasts.

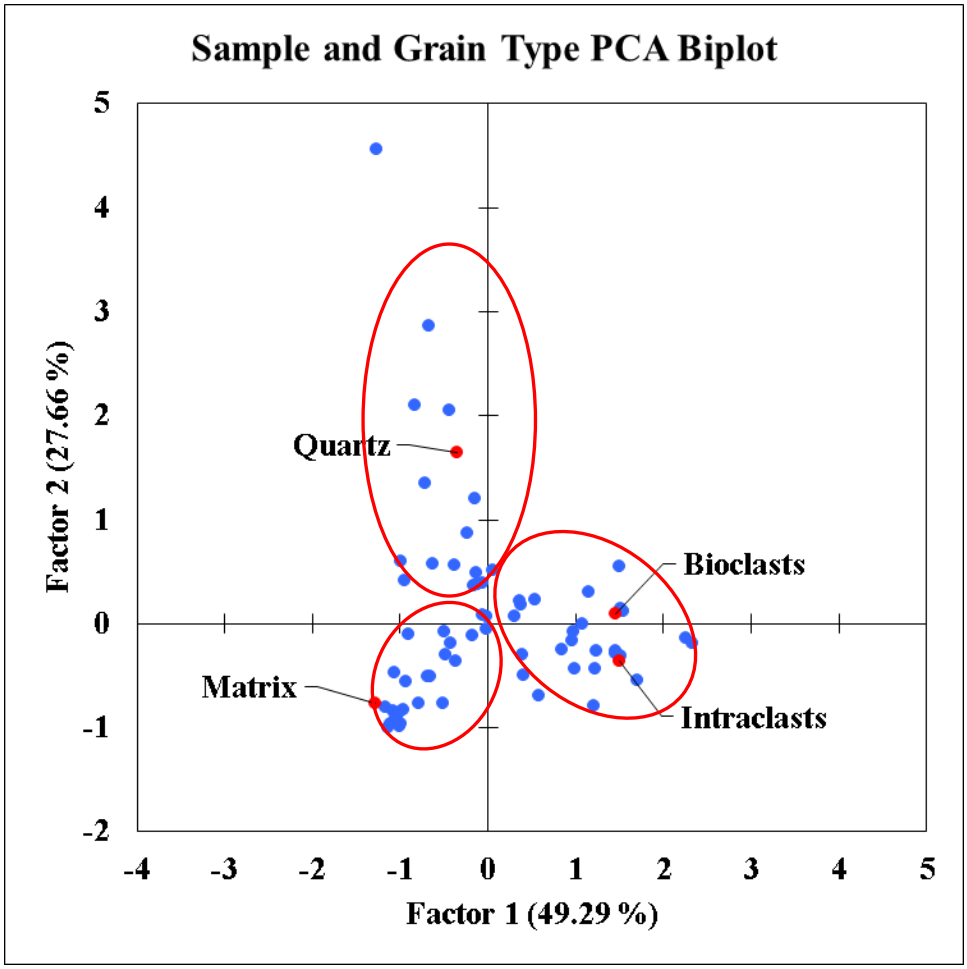

Figure 44. Garden City Formation combined sample (blue dots) and grain type (red dots) PCA biplot showing grain type and sample relationship. Red circles indicate groups of similar samples.

Pogonip Group

Pogonip Group R-Mode Cluster Analysis of Bioclasts

R-mode cluster analysis delineates communities of organisms in the Pogonip Group. These organisms include algae, brachiopods, bryozoans, calcispheres, echinoderms, gastropods, ostracods, *Nuia*, sponges, and trilobites. R-mode cluster analysis indicates that 5 groups or communities occur within the Pogonip Group (Figure 45). The uppermost cluster (1) consists of calcispheres and algae. The cluster second

from the top (2) includes trilobites, brachiopods, echinoderms, and bryozoans, while the third cluster from the bottom (3) contains *Nuia* and gastropods. The second cluster from the bottom (4) contains only ostracods and the lowermost cluster contains only sponges.

Pogonip Group Q-Mode Cluster Analysis of Bioclasts

Q-mode cluster analysis illustrates the clustering of samples which represent biofacies or similar environments. Q-mode cluster analysis indicates that there are eight biofacies, which occur within the Pogonip Group (Figure 46). Cluster 1 contains samples with abundant brachiopods and minor trilobites and echinoderms, while cluster 2 contains no fossil organisms. Cluster 3 contains abundant echinoderms with varying amounts of brachiopods and trilobites, while cluster 4 contains abundant *Nuia* with minor

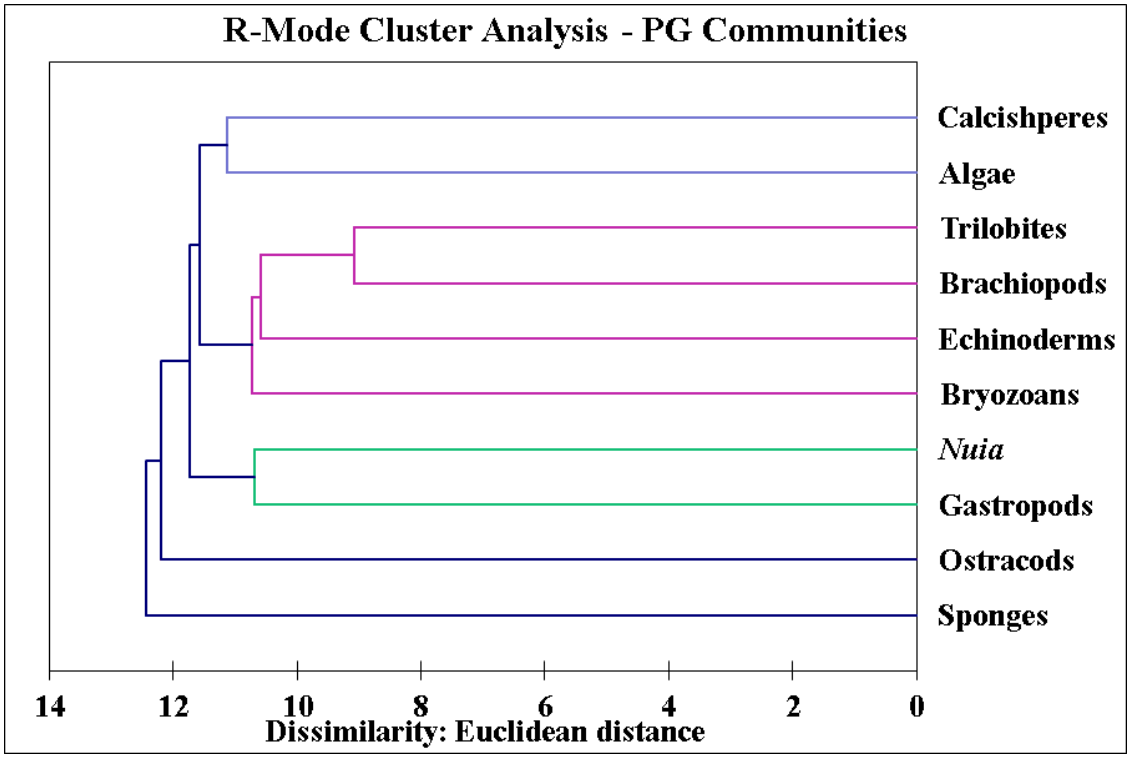

Figure 45. Pogonip Group R-mode cluster analysis showing communities.

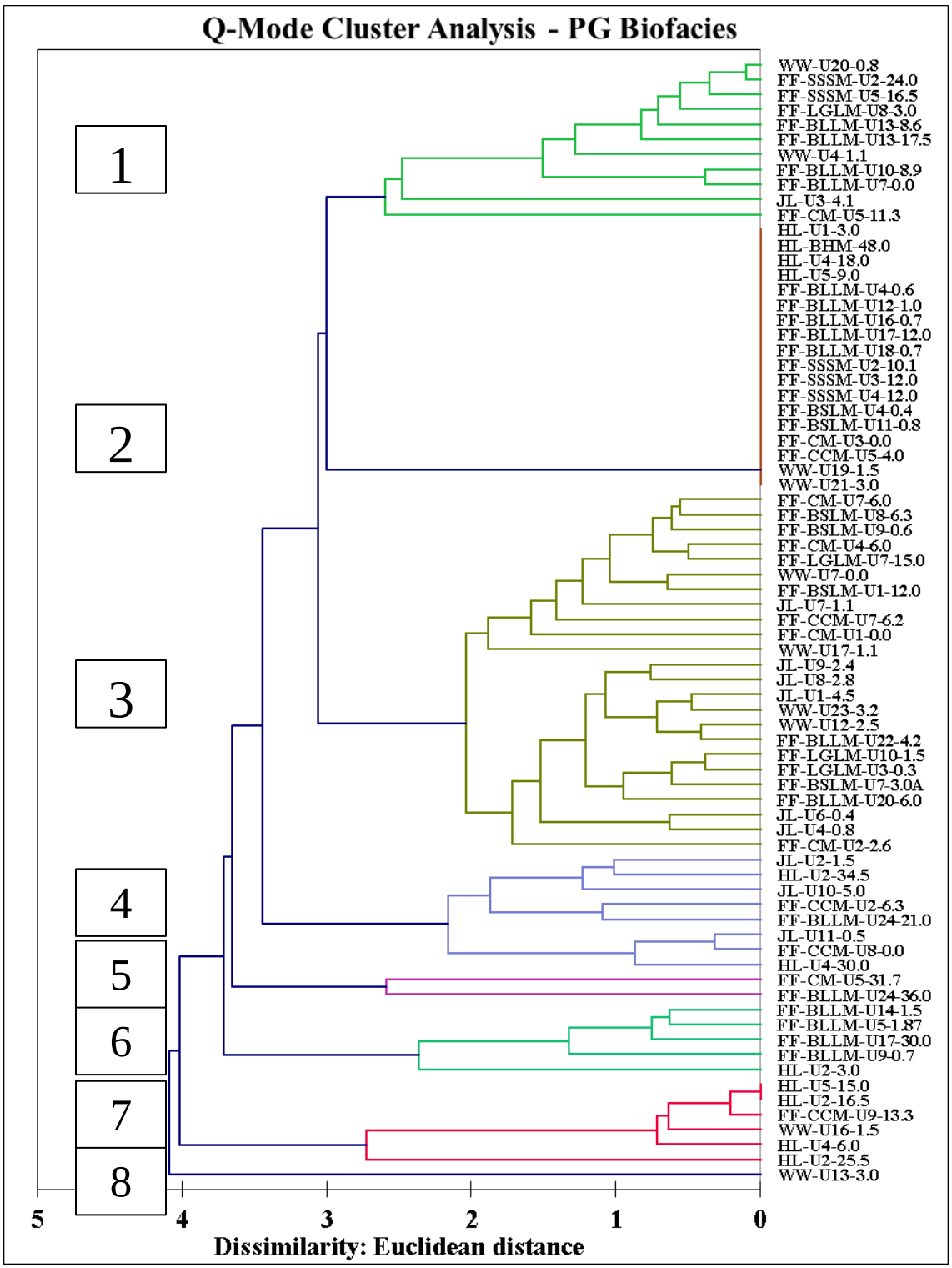

Figure 46. Pogonip Group Q-mode cluster analysis showing biofacies. Sample names are to the right of the dendrogram.

echinoderms and brachiopods. Cluster 5 contains algae with minor brachiopods and cluster 6 contains trilobites with minor brachiopods. Cluster 7 contains sponges and cluster 8 contains ostracods.

Pogonip Group Principal Components Analysis of Bioclasts

R-mode PCA for the Pogonip Group shows organisms that occur together and represent communities (Figure 47). This analysis indicates that echinoderms (brachiopods are redundant) are the most important variable affecting distribution along the factor 1 axis (x axis), while ostracods are the most important variable affecting

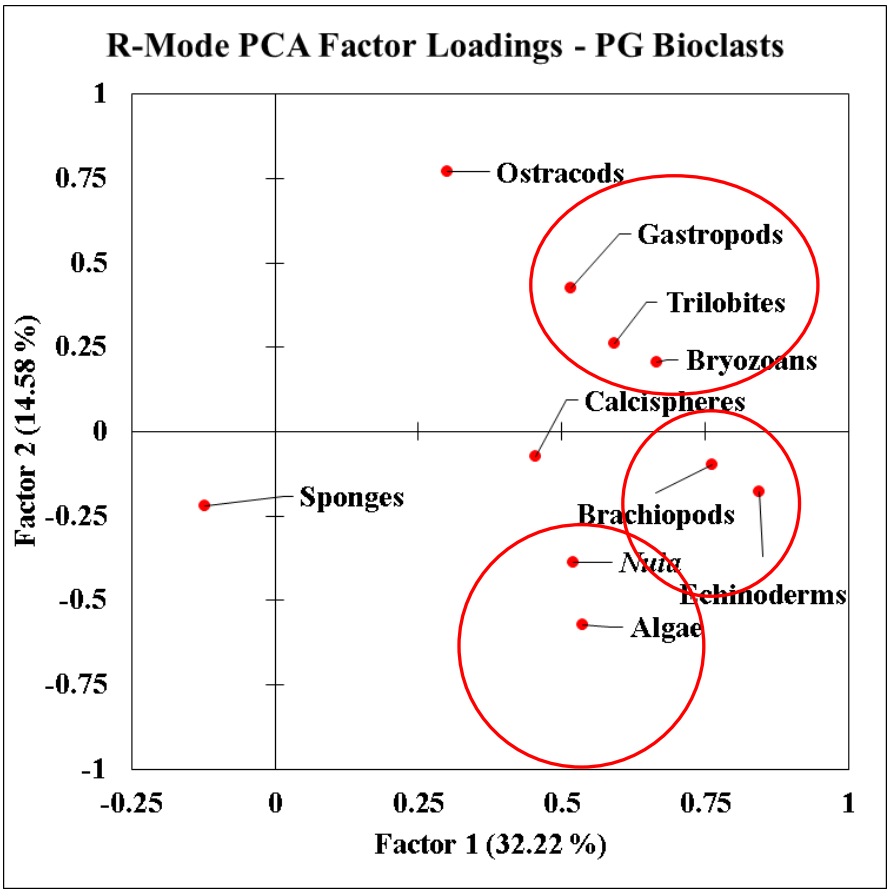

Figure 47. Pogonip Group PCA showing communities.

distribution along the factor 1 axis (y axis). This analysis groups gastropods, trilobites, and bryozoans into a community. Also, brachiopods and echinoderms group as a community, while *Nuia* and algae group as a community. Sponges and ostracods appear to group independently.

Q-mode PCA illustrates the grouping of samples containing similar bioclasts and should show biofacies. However, Q-mode PCA does not appear to produce any obvious biofacies groups except for the cluster (red circle) which represent samples without bioclasts (Figure 48).

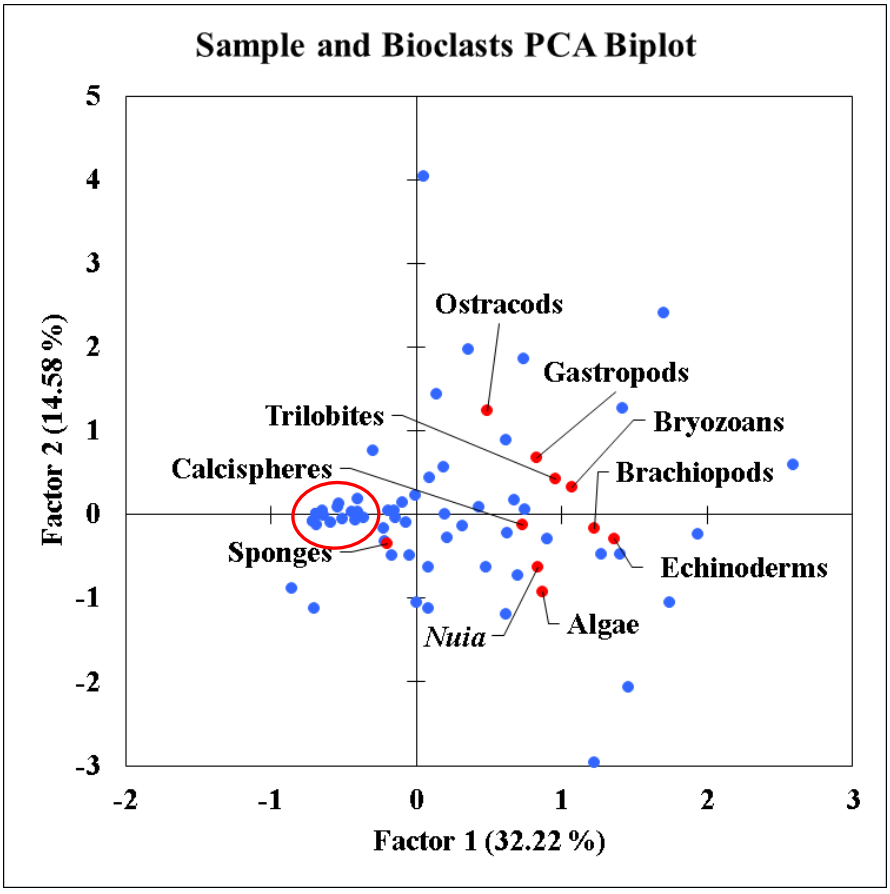

Figure 48. Pogonip Group combined sample (blue dots) and bioclast (red dots) PCA biplot showing bioclast and sample relationship. Red circle are samples with no bioclasts.

Pogonip Group R-Mode Cluster Analysis of Important Grain Types

Twenty-three different grain types were found during thin-section point count analysis. Principle components and cluster analyses were run on the point count data for the Pogonip Group. R-mode cluster analysis illustrates the relationships between important grain types. The majority of identified grains have been grouped into one of four grain types: bioclasts (all taxa), intraclasts, matrix, or quartz grains. R-mode cluster analysis indicates that these four grain types fall into 3 groups (Figure 49). Bioclasts and intraclasts group together, while matrix and quartz independently.

Pogonip Group Q-Mode Cluster Analysis of Lithofacies

Q-mode cluster analysis illustrates the clustering of samples and represent different lithofacies. This analysis indicates divides the samples into three broad

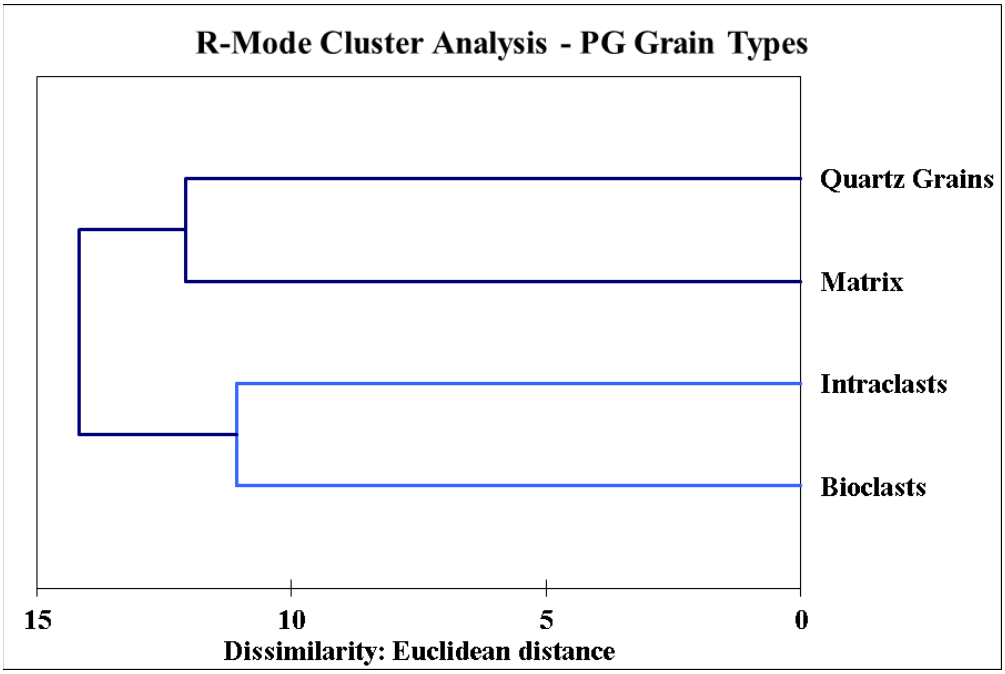

Figure 49. Pogonip Group R-mode cluster analysis showing grain type relationships.

lithofacies groups and five more specific lithofacies (Figure 50). These lithofacies appear to repeat up through the section.

The uppermost cluster contains samples with higher quartz contents and consists of two dominate subclusters. The uppermost subcluster (1a) contains more matrix-sized material and consists of siliceous wackestones associated with lower energy and deeper water environments of near shore highstand deposits. The lower subcluster (1b) consists of recrystallized wackestones and packstones that contain abundant peloids/pellets. Lithofacies containing higher amounts of sand- and silt-sized terrigenous material generally indicates closer proximity to a shoreline and terrigenous material source. Higher terrigenous material content is generally associated with lowstand deposits.

The middle cluster (2) groups samples containing primarily fine-grained matrix material and consists of low energy lithologies with low fossil content such as mudstones, and wackestones. These lithotypes are generally associated with highstand deposits. The boundstones clustered with these fine grained lithologies because they are also composed of fine-grained material, however, boundstones are considered lowstand or transgressive deposits.

The bottommost cluster contains samples with abundant intraclasts and bioclasts and is subdivided into two subclusters. The upper subcluster (3a) contains abundant intraclasts and peloids/pellets common in intraclastic wackestones and packstones. The lower subcluster (3b) contains abundant bioclastic associated with fossiliferous wackestones, packstones, or grainstones. These lithologies are generally associated with higher energy environments and likely represent lowstand and/or transgressive deposits.

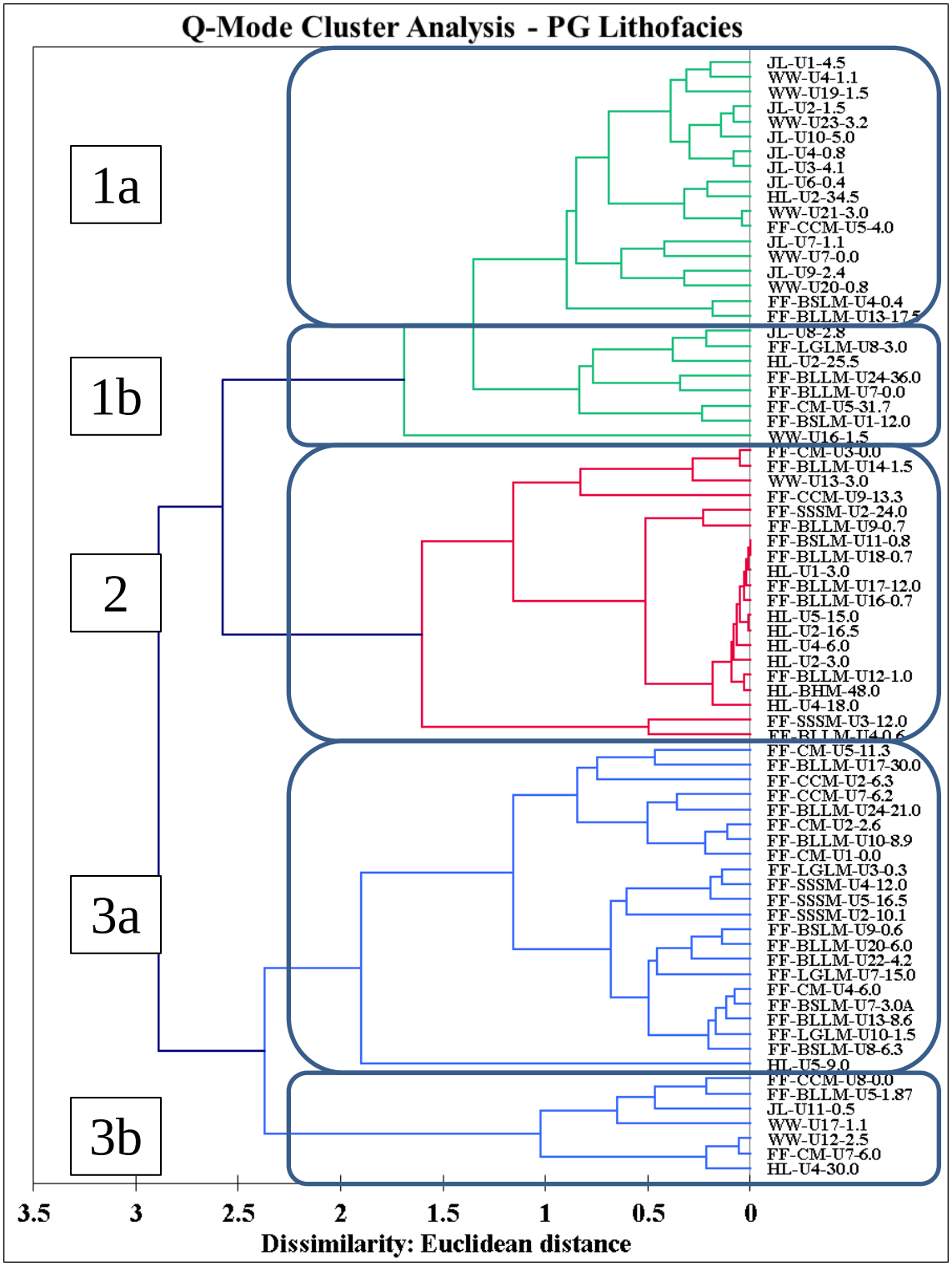

Figure 50. Pogonip Group Q-mode cluster analysis showing lithofacies. Blue boxes indicate groupings of samples based on grain types. Sample names are to the right of the dendrogram.

Lithofacies appear to repeat in a cyclic fashion throughout the Pogonip Group. These cycles contain high-energy shallow water lithofacies consisting of lowstand deposits at the base of the cycle, followed by followed by transitional transgressive deposits. The upper portions of cycles contain deeper-water low-energy lithofacies consisting of highstand deposits.

Pogonip Group Principal Components Analysis of Important Grain Types

R-mode PCA of the four main grain types indicates which grains occur together. Similarly to the cluster analysis of these grains, PCA shows bioclasts and intraclasts occurring closely together, while matrix and quartz grains occur independently (Figure 51).

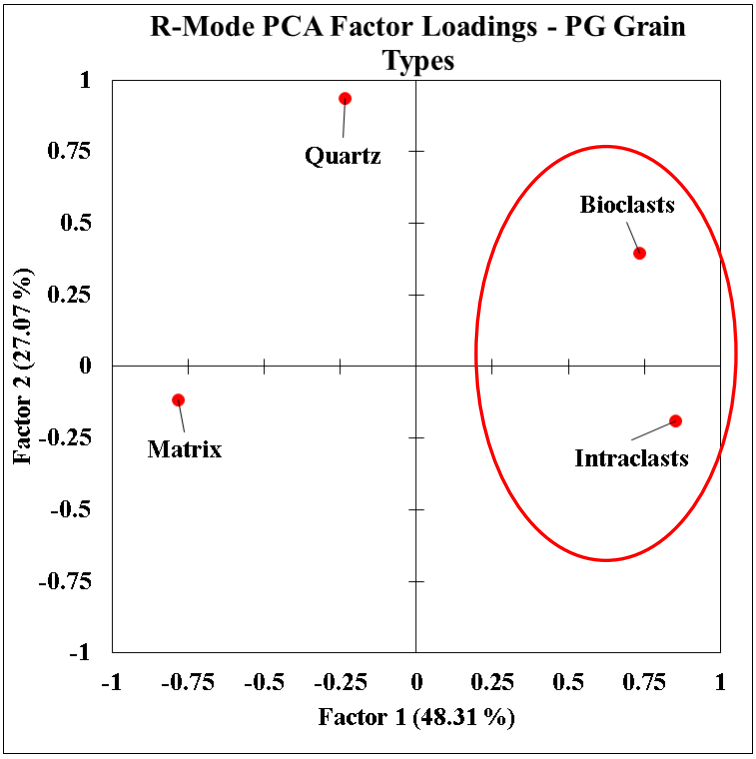

Figure 51. Pogonip Group R-mode PCA showing grain type relationships.

Q-mode PCA illustrates the grouping of samples and shows lithofacies. The majority of samples appear to group around intraclasts, matrix, and quartz grain types with fewer samples grouping around the bioclast grain type (Figure 52). Samples grouping around the quartz, bioclasts, and intraclasts points likely represent lowstand/transgressive deposits, while those samples grouping around the matrix point likely represent highstand deposits.

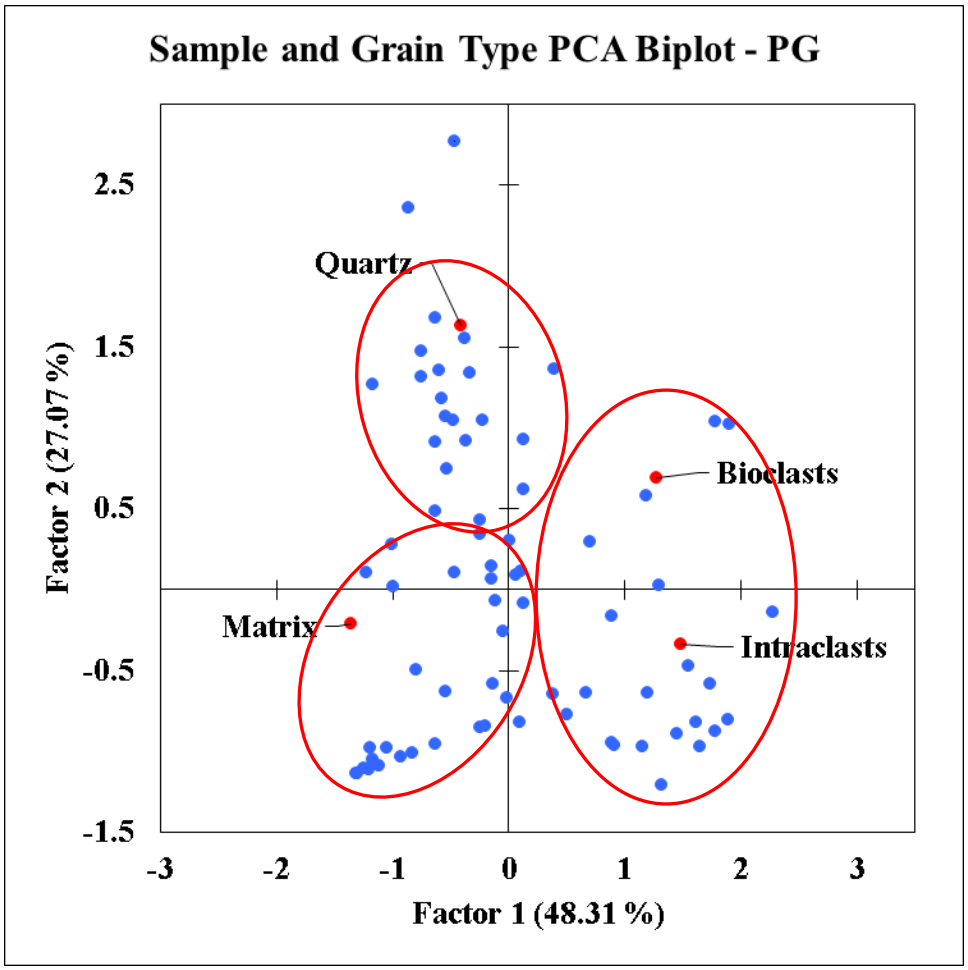

Figure 52. Pogonip Group combined sample (blue dots) and grain type (red dots) PCA biplot. Red circles indicate groups of similar samples.

Diagenesis within the Garden City Formation and Pogonip Group

Field observations and thin-section analysis indicate that the Garden City Formation and Pogonip Group have undergone various forms of carbonate diagenesis. Diagenesis encompasses all processes resulting in the alterations, cementation, lithification, and solution of carbonates and carbonate rocks between deposition and metamorphism (Flugel, 1982). The resulting changes from diagenesis can be physical and/or chemical and are influenced by local elements such as the presence of fluids, pressure, and temperature. Diagenesis generally occurs as submarine (shallow or deep ocean) or meteoric (freshwater) diagenesis and can be destructive (carbonate degradation) or constructive (carbonate aggradation).

Thin-section analysis indicates that the Garden City Formation has experienced a higher degree of diagenesis than the Pogonip Group. This assessment is based on the number of diagenetically-related grains and features encountered during thin-section point counts. Diagenetically-related grains and features include calcite crystals, chert, dolomite crystals, glauconite, pyrite/hematite, and stylolites. Garden City Formation thin-sections have more calcite/dolomite crystals, pyrite/hematite grains, and stylolites. Pogonip Group thin-sections have higher occurrences of chert and glauconite (Table 5). Diagenetic features recognized within the Garden City Formation in Green Canyon include cementation, chertification/silicification, compaction, dolomitization, dedolomitization, dissolution, micritization, and neomorphism. All photomicrographs were taken at 40x magnification.

Table 5. Diagenetic grains and features from thin-section analysis.

Diagenetic Grain/Feature	Garden City Formation	Pogonip Group
Calcite Crystal Count	4624	3747
Chert Count	202	357
Dolomite Crystal Count	1509	367
Glauconite Grain Count	0	78
Pyrite/Hematite Grain Count	43	0
Stylolite Count	434	128
TOTAL THIN SECTIONS	73	75

Cementation

Cementation is the process by which voids within sediment are filled with a chemically-precipitated cement resulting in consolidation and lithification of said sediment (Flugel, 1982). At least three phases of cementation have occurred within some of the rocks of the Garden City Formation and Pogonip Group. Phase 1 of cementation consists of the formation of an early rim cement (Figure 53). This cement exhibits a fibrous crystalline growth rim surrounding a particle which grows away from the particle and out into the pore space. Bioclasts such as trilobites and brachiopods have rim cements which indicate early cementation in a marine phreatic environment. Phase 2 of cementation occurs when available pore space is filled after initial cementation and occurs in both marine and meteoric environments. This cement appears blocky or granular with no preferred crystal orientation. Phase 3 of cementation includes the filling of post-depositional fractures, producing mineral-filled veins. Fractures are generally calcite filled, although some fractures are silica/chert filled, and occur as crumbly fractures around hard particles and sharp-edged fractures.

Syntaxial rim cement (syntaxial overgrowth) is very common within coarse-

grained packstones and grainstones of the Garden City Formation and the Pogonip Group (Figure 54). Syntaxial overgrowth occurs most commonly with crinoid bioclasts and less commonly with brachiopods, *Nuia*, and trilobites. Syntaxial rim cement is likely associated with early marine cementation (Burgess, 1979).

Chertification/Silicification

Chertification/silicification is the diagenetic process that replaces original rock components (e.g. bioclasts, cements, etc.) with chert or silica. This conversion or replacement occurs in the presence of silica-rich fluids and can happen as both an early and late diagenetic process. Chert is common within the Garden City Formation and the

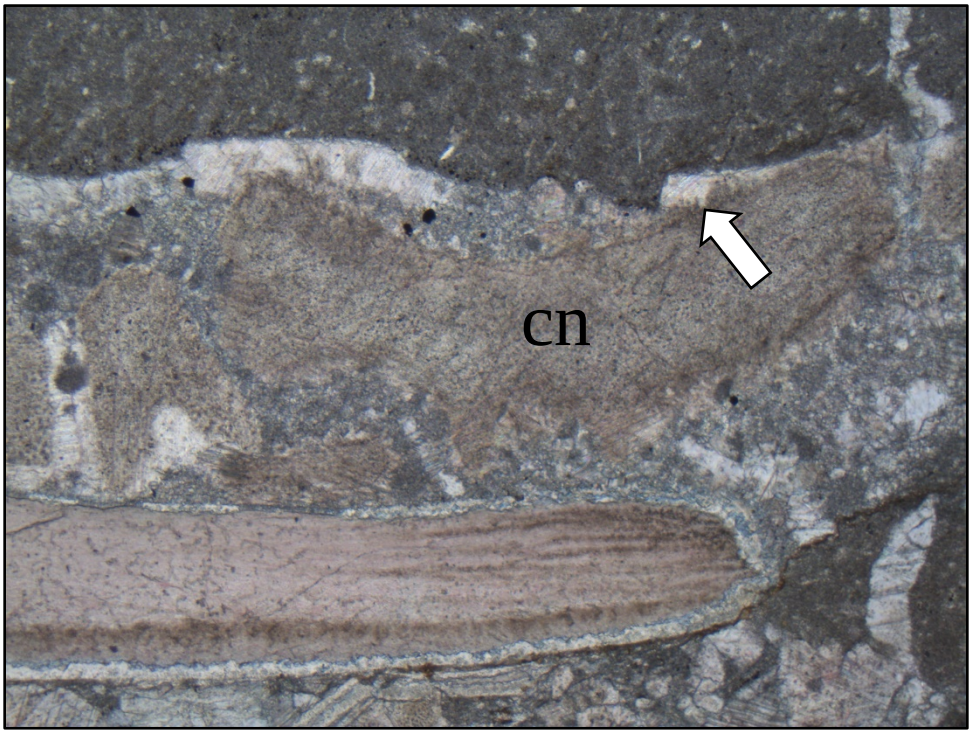

Figure 53. Plane light photomicrograph of sample GC-U21-9.0 (249 m). Showing fine fibrous cement (arrow) on a crinoid (cn) bioclast indicating early cementation. Bottom axis is 2.5 mm.

Pogonip Group and occurs as nodules, vertical and horizontal chert bodies, and as irregular chert masses. Chert also occurs within bioturbated and boundstone facies implying silica rich fluid migration and precipitation within permeable carbonate rocks. In thin-section, individual dolomite rhombohedral crystals often occur as floating particles within a chert matrix.

Partial silicification of bioclasts is also common within the Garden City Formation and Pogonip Group. The outer surfaces of trilobite and brachiopod bioclasts are most commonly partially replaced with silica (Figure 55).

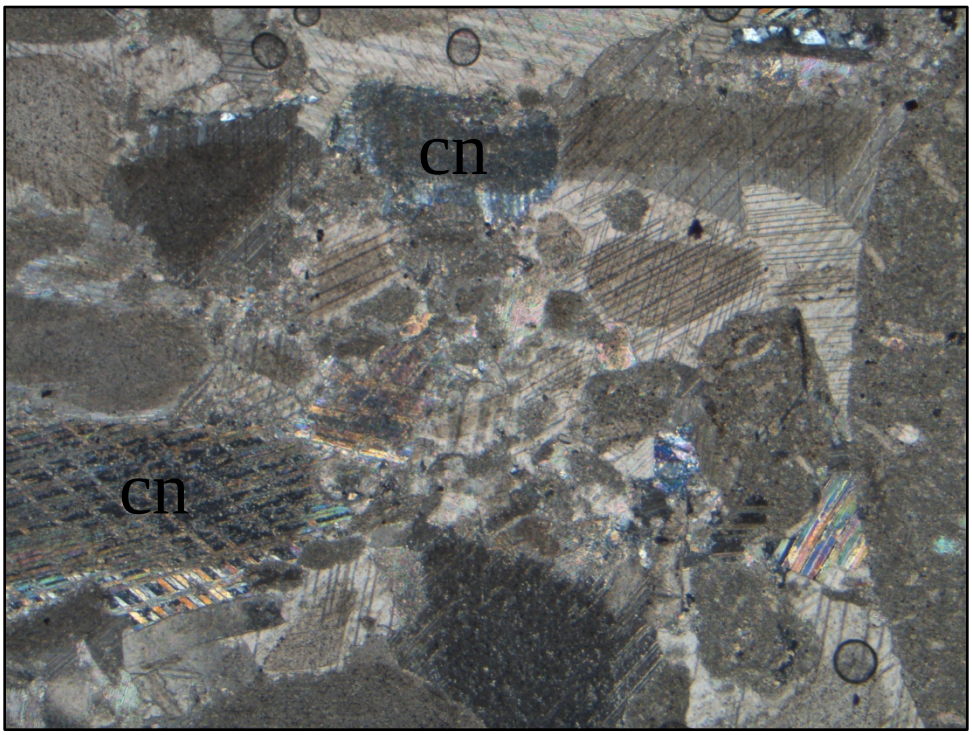

Figure 54. Polarized light photomicrograph of sample GC-U15-86.7 (199 m). Showing syntaxial rim cement (syntaxial overgrowth) around crinoid bioclasts (cn) indicating early cementation. Bottom axis is 2.5 mm.

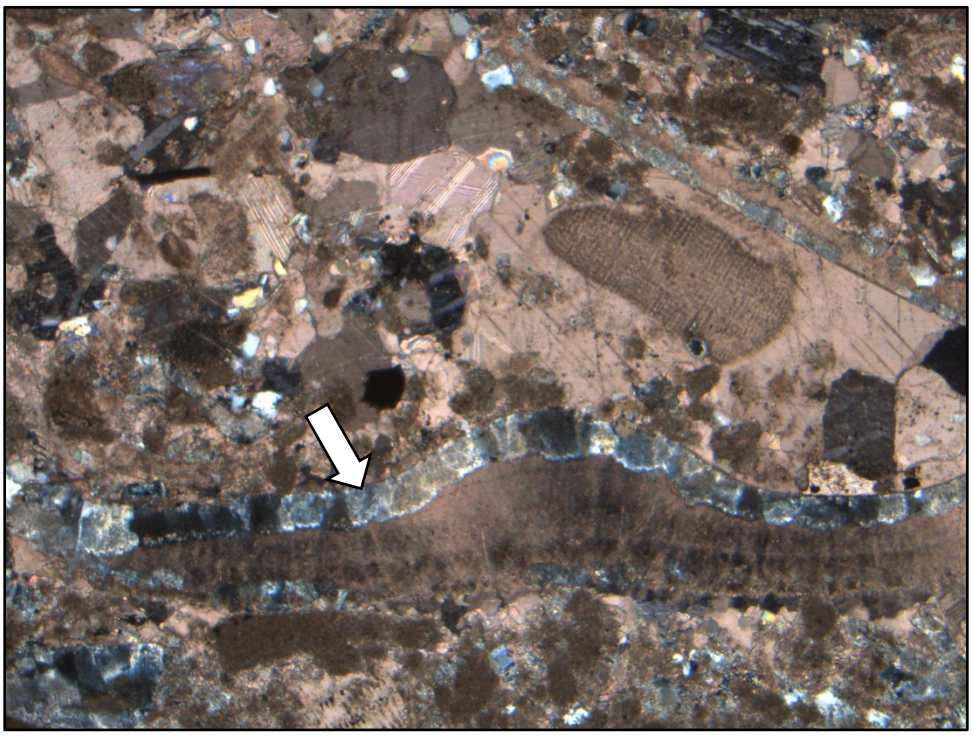

Figure 55. Plane light photomicrograph of stained sample FF-CM-U5-11.3 (608 m). Showing silicification of the outer surface of a brachiopod bioclast (arrow). Bottom axis is 2.5 mm.

Compaction

Compaction results in the reduction of rock volume by mechanical and chemical processes which act upon both individual grains and cement minerals (Flugel, 1982) and generally occurs during deep burial. The most prominent compaction features within the Garden City Formation and Pogonip Group are pressure solution features, which occur in every lithology. Pressure solution in carbonates occur when minerals dissolve when subjected to externally applied pressure and is often referred to as chemical compaction.

Intergranular compaction pressure dissolution occurs at the microscopic scale between grain surfaces and results primarily in sutured grain contacts (Figure 56), although, flattened and concavo-convex grain contacts can occur which are typically

associated with mechanical compaction. Compaction pressure dissolution is common in intraclastic conglomerates, packstones, and grainstones of the Garden City Formation and the Pogonip Group.

Dissolution seams are sub-planar features, which lack the serrated low and high amplitude peaks of stylolites (Figure 57). Dissolution seams and stylolites occur at microscopic and macroscopic scales, and require pressure perpendicular to the seam or stylolite to form. Dissolution seams are common in most marine sedimentary lithologies, but occur more commonly in wackestones and mudstones. Stylolite surfaces are common in coarse-grained lithologies and vary in amplitude. Stylolites can also be columnar or irregular in appearance. Dissolution seams and stylolites only occur after

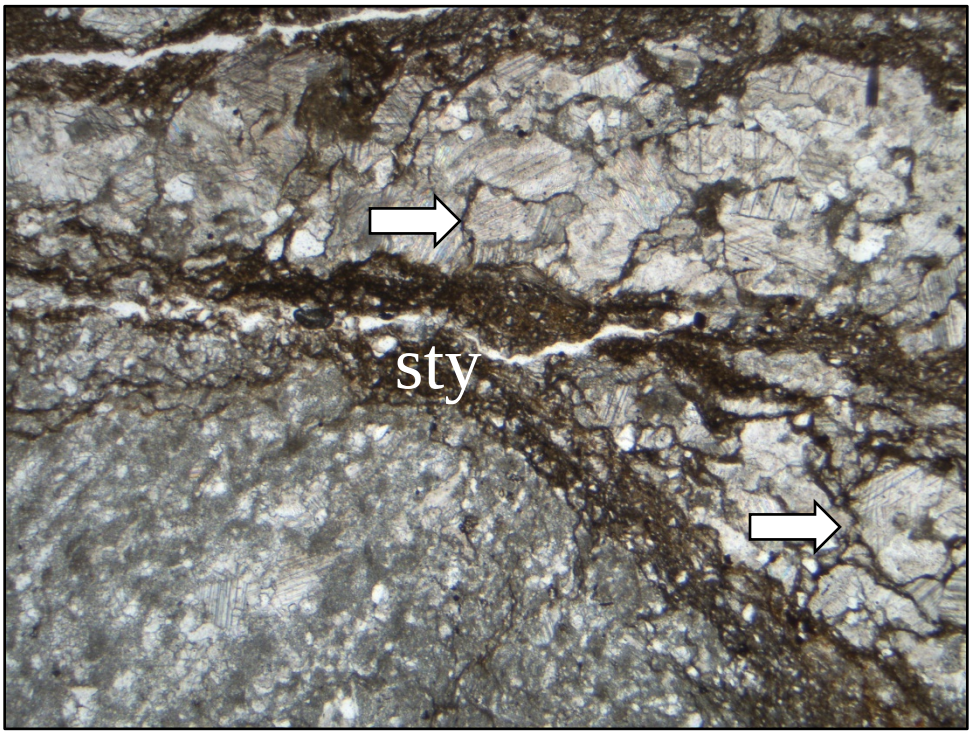

Figure 56. Plane light photomicrograph of sample GC-U23-27.0 (292 m). Showing sutured grain contacts (arrows) and stylolite (sty) compaction features. Bottom axis is 2.5 mm.

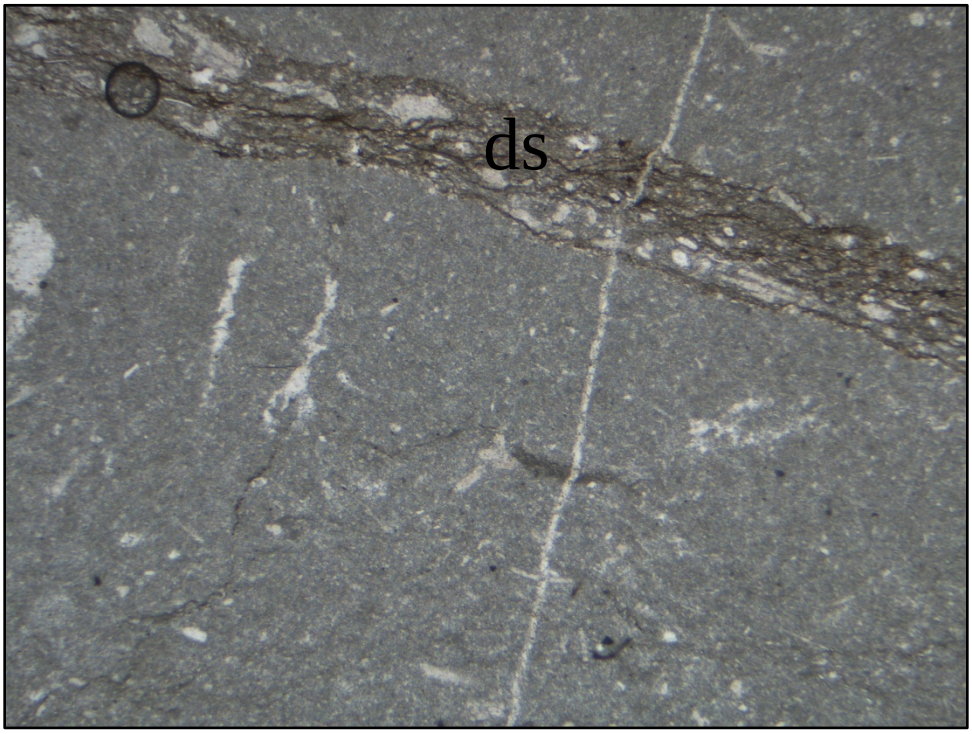

Figure 57. Plane light photomicrograph of sample ISO-GC-U1-13.0 (35 m). Showing dissolution seams (ds) within an argillaceous mudstone. Bottom axis is 2.5 mm.

lithification, and are often found as sets (or swarms), which form pressure dissolution structures.

Dolomitization and Dedolomitization

Dolomitization is the process by which calcium carbonate ($CaCO_3$) rocks or minerals are altered to dolomite ($CaMg(CO_3)_2$). This occurs when magnesium ions (Mg^{+2}) replace calcium ions (Ca^{+2}) in calcite as a result of high Mg/Ca ratio fluid -rock interaction during deep burial (Flugel, 1982). Dolomitization can also occur in evaporitic sabkha environments (Kinsman, 1973). This alteration often destroys the original depositional texture of the altered rock.

Dolomitization is found within the Pogonip Group, however, it is significantly

more common in the Garden City Formation. The lower and upper contacts of the Garden City Formation contain considerable amounts of dolomite and dolostone. The dolostones contain fine- to medium-crystalline dolomite grains and display xenotopic planar-s (subhedral) to nonplanar textures (Figure 58). Individual dolomite crystals or groups of crystals are subhedral to euhedral rhombs and range in color from clear to dark brown. Some dolomite rhombs display various types of zoning with some dolomite rhombs having clear rims and brown cores and others having brown rims and clear cores. Dedolomitization is the process of dissolution of dolomite, which is replaced by pseudomorphs of calcite. Evidence of dedolomitization is found in both the Garden City Formation and the Pogonip Group where dedolomitization is easily recognized in

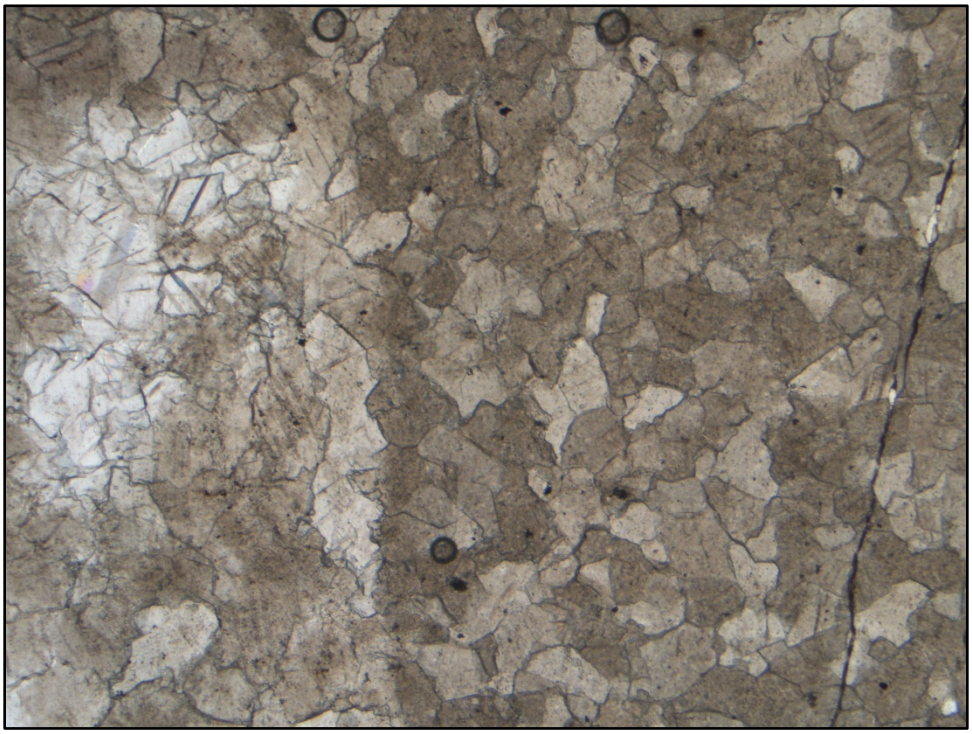

Figure 58. Plane light photomicrograph showing fine- to medium-crystalline dolomite crystals with a nonplanar texture. Bottom axis is 2.5 mm.

thin-section as red-stained calcite pseudomorphs. Chert is common in thin-sections that display dedolomitization and often calcite pseudomorphs are suspended within a chert matrix along with unaltered dolomite rhombs (Figure 59).

Micritization

Micritization can lead to the formation of a mud envelope around bioclasts (Figure 60) and can produce peloids as the result of complete replacement of bioclasts with micrite. Micritization is common in the Garden City Formation and the Pogonip Group, especially in sediments which contain *Nuia*. Often pellets/peloids and *Nuia* of the

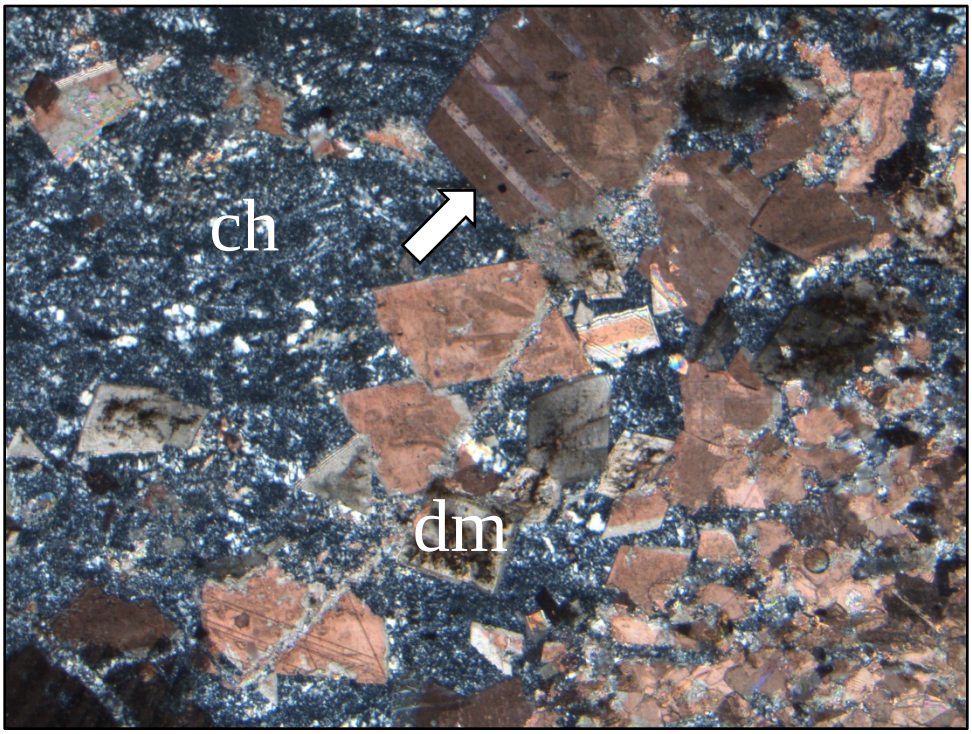

Figure 59. Polarized light photomicrographs of stained sample FF-SSSM-U2-10.1 (348 m). Showing evidence for dedolomitization. Red stained calcite pseudomorphs (arrow) are suspended within a chert matrix (ch) along with unaltered clear/brown dolomite rhombs. Bottom axis is 2.5 mm.

same shape and size occur side by side, suggesting that some *Nuia* have been completely micritized into pellets/peloids.

Neomorphism

Neomorphism occurs as recrystallization, inversion (transformation), and replacement. Recrystallization is the process by which new crystal growth occurs at the expense of existing crystals in conditions of increasing pressure and temperature while maintaining the same chemical composition. Recrystallization is common in the mudstone, wackestone, and packstone lithologies of the Garden City Formation and the Pogonip Group (Figure 61).

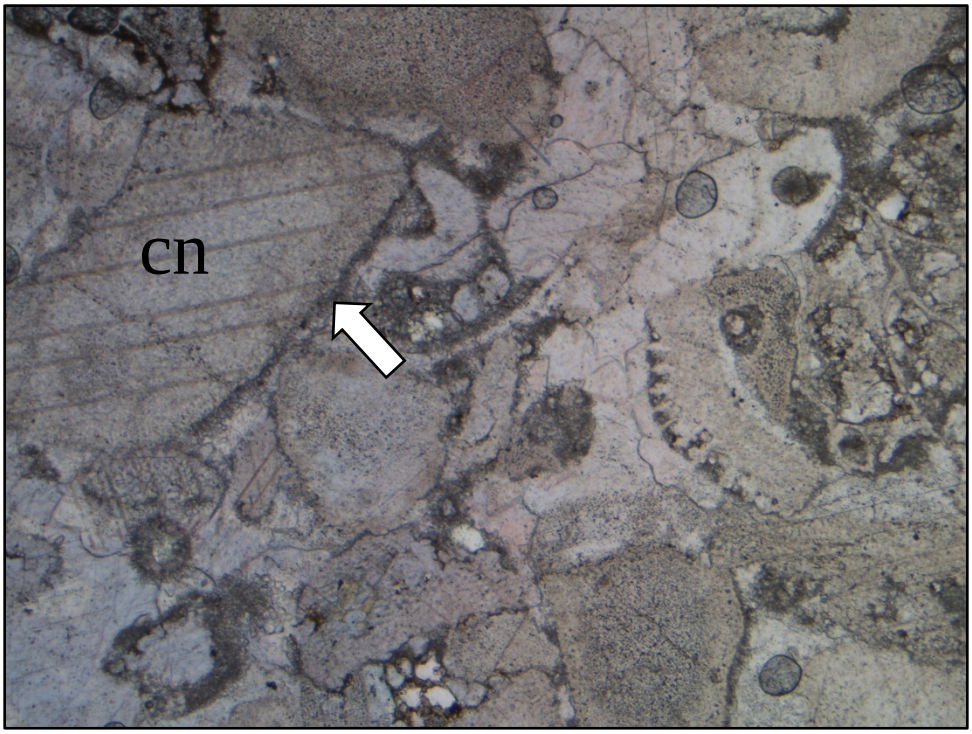

Figure 60. Plane light photomicrograph of sample FF-CM-U7-6.0 (642 m). Showing micritization of bioclasts resulting in the formation of a mud envelope (arrow) around a crinoid bioclasts (cn). Bottom axis is 2.5 mm.

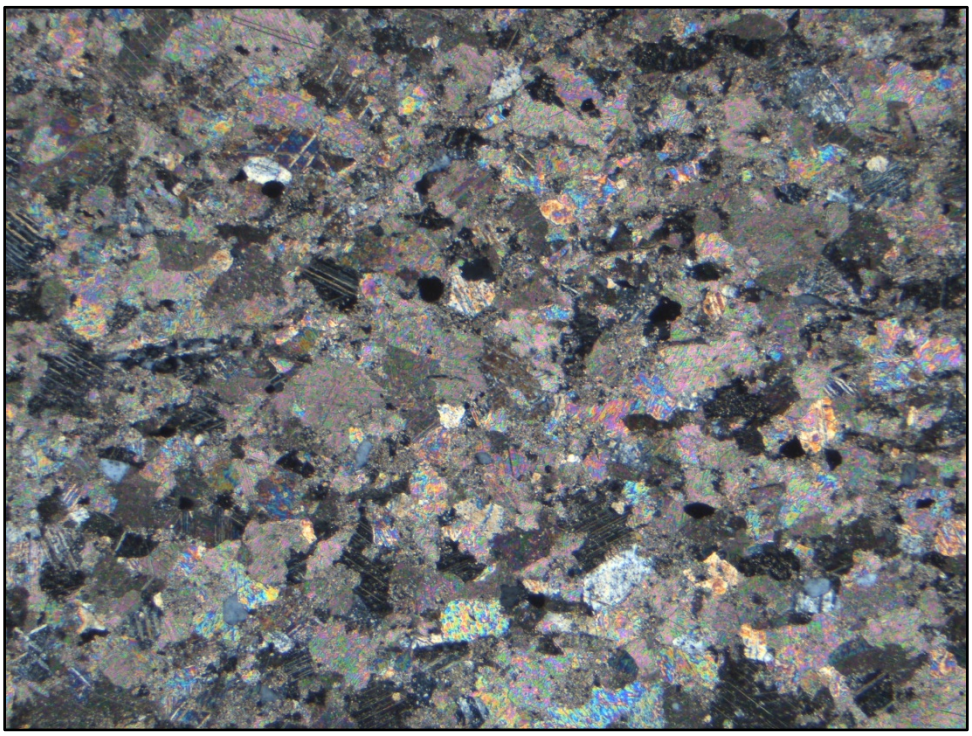

Figure 61. Polarized light photomicrographs of sample GC-U19-4.5 (237 m). Showing a recrystallized packstone (crystalline carbonate). Bottom axis is 2.5 mm.

Replacement is the process by which one mineral is removed by dissolution and is replaced by the precipitation of a different mineral with a different chemical composition. Replacement occurs commonly as dolomitization, dedolomitization, and chertification/silicification (discussed above) within the Garden City Formation and the Pogonip Group.

Pyrite and Hematite

Pyrite and hematite are present in thin-sections of the Garden City Formation and the Pogonip Group where they occur as opaque single grains or opaque clusters of grains (Figure 62). Pyrite occurs commonly in carbonates and is altered to hematite through weathering and oxidation. It often shows a cubic, pyritohedral, or octoheadral shape.

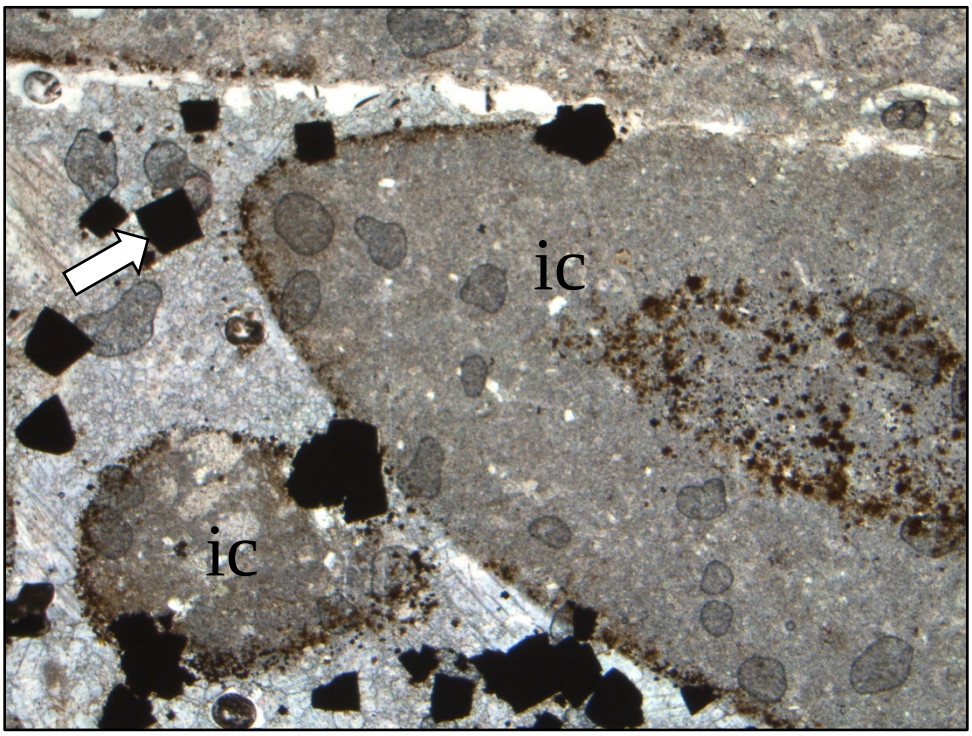

Figure 62. Plane light photomicrograph showing pyrite grains (arrow) and hematite zones on and within intraclasts (ic). Bottom axis is 2.5 mm.

Geochemistry

Garden City Formation Carbonate Carbon and Oxygen Stable Isotope Ratios

$\delta^{13}C$ values of the Garden City Formation show two major trends with increasing stratigraphic position (Figure 63). $\delta^{13}C$ values show an overall decrease from the base of the section to approximately 130 m upsection and then gradually increase through the rest of the section. Values range from -2.19 to 0.56 ‰ V-PDB with a precision of ± 0.05 ‰. $\delta^{13}C$ values fluctuate around 0.2 ‰ near the base of the Garden City Formation before decreasing to approximately -1.2 ‰ at ~31 m. A short lived positive excursion with values near 0.5 ‰ occurs at approximately 62 m and is subsequently followed by a sharp decrease in $\delta^{13}C$ values down to around -1‰. $\delta^{13}C$ values fluctuate and decrease to

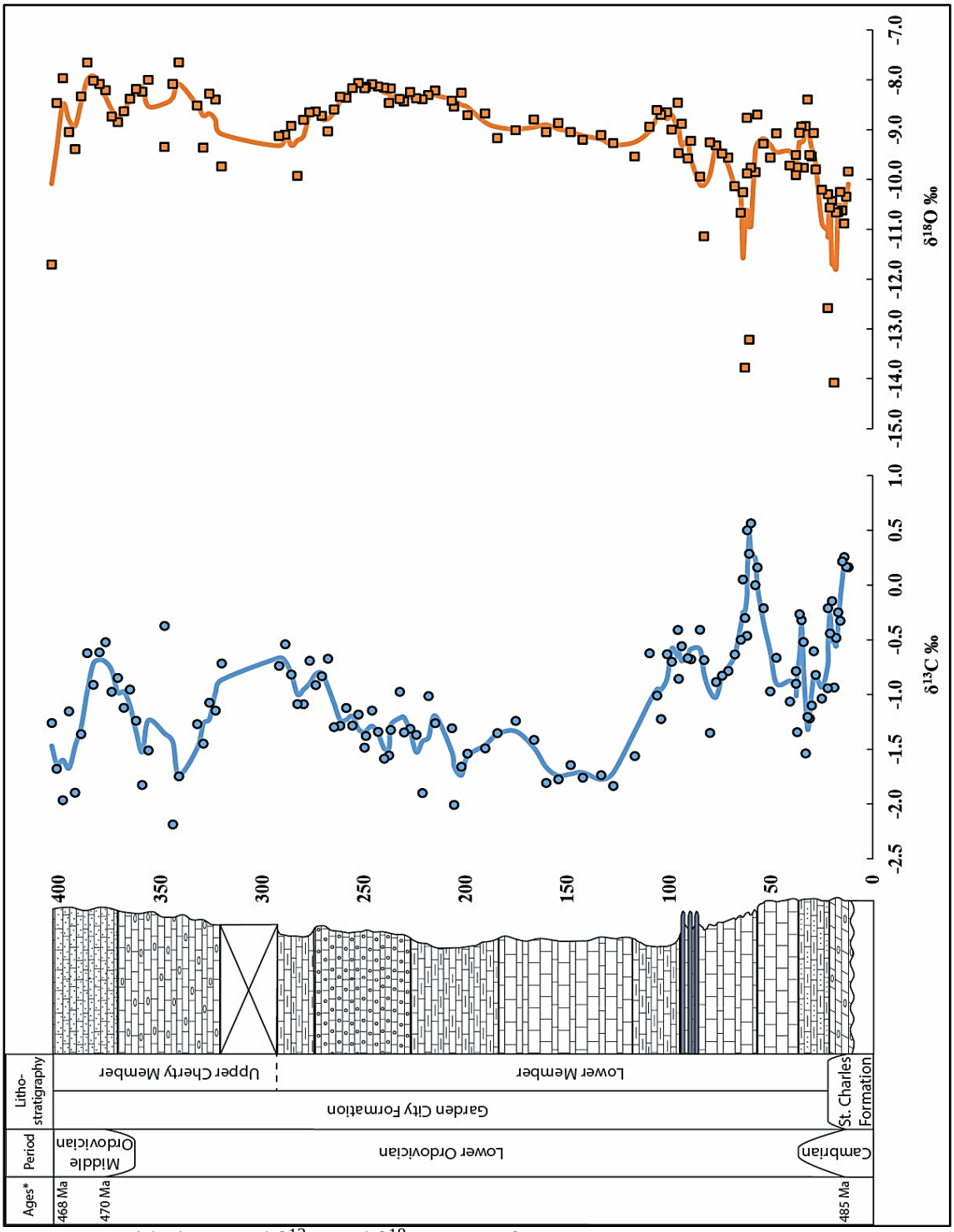

Figure 63. Lithology and $\delta^{13}C$ and $\delta^{18}O$ curves from the Garden City Formation. Blue ($\delta^{13}C$) and orange ($\delta^{18}O$) lines represent a three-point moving average of $\delta^{13}C$ and $\delta^{18}O$ data. See figure 8 for lithology types.

approximately -1.5 ‰ (at ~127 - 161 m) before steadily increasing to around -0.7 ‰ (~292 - 320 m). $\delta^{13}C$ values then decrease to around -2.0 ‰ near 362 m. $\delta^{13}C$ values increase to approximately -0.5 ‰ before decreasing and fluctuating around -2.0 and -1.2 ‰ near the Garden City Formation and Swan Peak Formation contact.

$\delta^{18}O$ of the Garden City Formation generally increases with increasing stratigraphic position (Figure 63). Values range from -14.1 to -7.7 ‰ V-PDB with a precision of ± 0.1 ‰. $\delta^{18}O$ values fluctuate between -10.0 and -11.0 ‰ near the base of the Garden City Formation. Two fluctuations with $\delta^{18}O$ values of ~14.0 ‰ occur at ~20 m and ~ 61 m. These fluctuations appear to be antithetical with positive $\delta^{13}C$ values. $\delta^{18}O$ values continue to increase upsection to ~255 m where values decrease for approximately 35 m before showing an overall increase upsection. A complete table of the Garden City Formation $\delta^{13}C$ and $\delta^{18}O$ values is located in Appendix C1.

Pogonip Group Carbonate Carbon and Oxygen Stable Isotope Ratios

$\delta^{13}C$ of the Pogonip Group show two major trends with increasing stratigraphic position (Figure 64). Values show an overall decrease from the base of the section to approximately 350 m upsection and then gradually increase through the rest of the section. $\delta^{13}C$ values range from -2.9 to 1.2 ‰ V-PDB with a precision of ± 0.05 ‰. There are two negative $\delta^{13}C$ values occurring at 45.7 and 91.3 m with $\delta^{13}C$ values of -1.8 and -2.9 ‰, respectively. Values fluctuate around 1.0 ‰ at the base of the Pogonip Group, before decreasing to approximately -0.7 ‰ near the Cambrian-Ordovician boundary. A short lived positive excursion with values greater than 1.0 ‰ occurs near

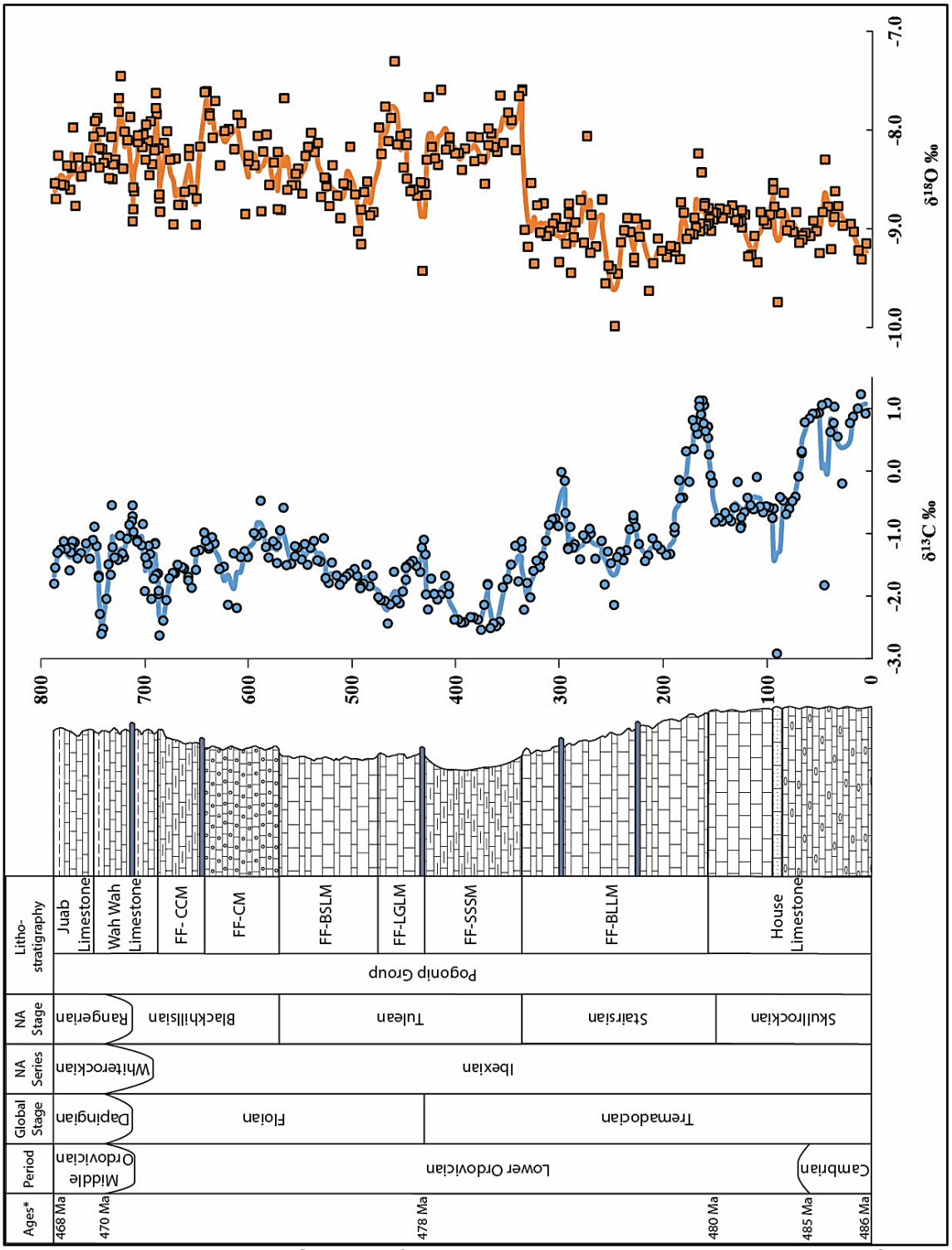

Figure 64. Lithology and $\delta^{13}C$ and $\delta^{18}O$ curves from the Pogonip Group. Blue ($\delta^{13}C$) and orange ($\delta^{18}O$) lines represent a three-point moving average of $\delta^{13}C$ and $\delta^{18}O$ data. See Figure 11 for lithology types.

the contact between the House Limestone and the Fillmore Formation (156.8 to 172.5 m) and is followed by a sharp decrease in $\delta^{13}C$ values more negative than1.0 ‰. $\delta^{13}C$ values of the Fillmore Formation fluctuate and decrease to approximately -2.5 ‰ (at ~360 m) before steadily increasing to around -1.0 ‰ (~570 m). $\delta^{13}C$ values then decrease to -2.6 ‰ near the Fillmore Formation-Wah Wah Limestone contact. $\delta^{13}C$ values of the Wah Wah Limestone increase to approximately -0.5 ‰ before decreasing to around -2.6 ‰ at the Wah Wah Limestone-Juab Limestone contact. $\delta^{13}C$ values of the Juab Limestone remain relatively constant at around -1.2 ‰.

$\delta^{18}O$ of the Pogonip Group becomes more positive with increasing stratigraphic position (Figure 64) and values range from -9.9 to -7.3 ‰ V-PDB with a precision of ± 0.1 ‰. $\delta^{18}O$ values of around -9.0 ‰ persist from the base of the Pogonip Group up to the contact between the FF-BLLM and FF-SSSM where $\delta^{18}O$ values increase (become less negative) to near -8.0 ‰. $\delta^{18}O$ values remain near -8.0 ‰ up to the FF-LGLM and FF-BSLM contact where $\delta^{18}O$ values decrease (become more negative) to around -9.0 ‰. $\delta^{18}O$ values continue to increase (become less negative) up through the Juab Limestone. Pogonip Group $\delta^{13}C$ and $\delta^{18}O$ values are located in Appendix C2.

Garden City Formation Insoluble Residue and Total Organic Carbon Analysis

In this study insoluble residue is defined as the total insoluble residue remaining after the removal of carbonate ($CaCO_3$) and organic carbon. Insoluble residue initially appears to decrease with increasing stratigraphic thickness (Figure 65), however, this trend appears to be significantly influenced by higher insoluble residue values from the base of the section. The general trend of insoluble residue above 50 m shows an increase

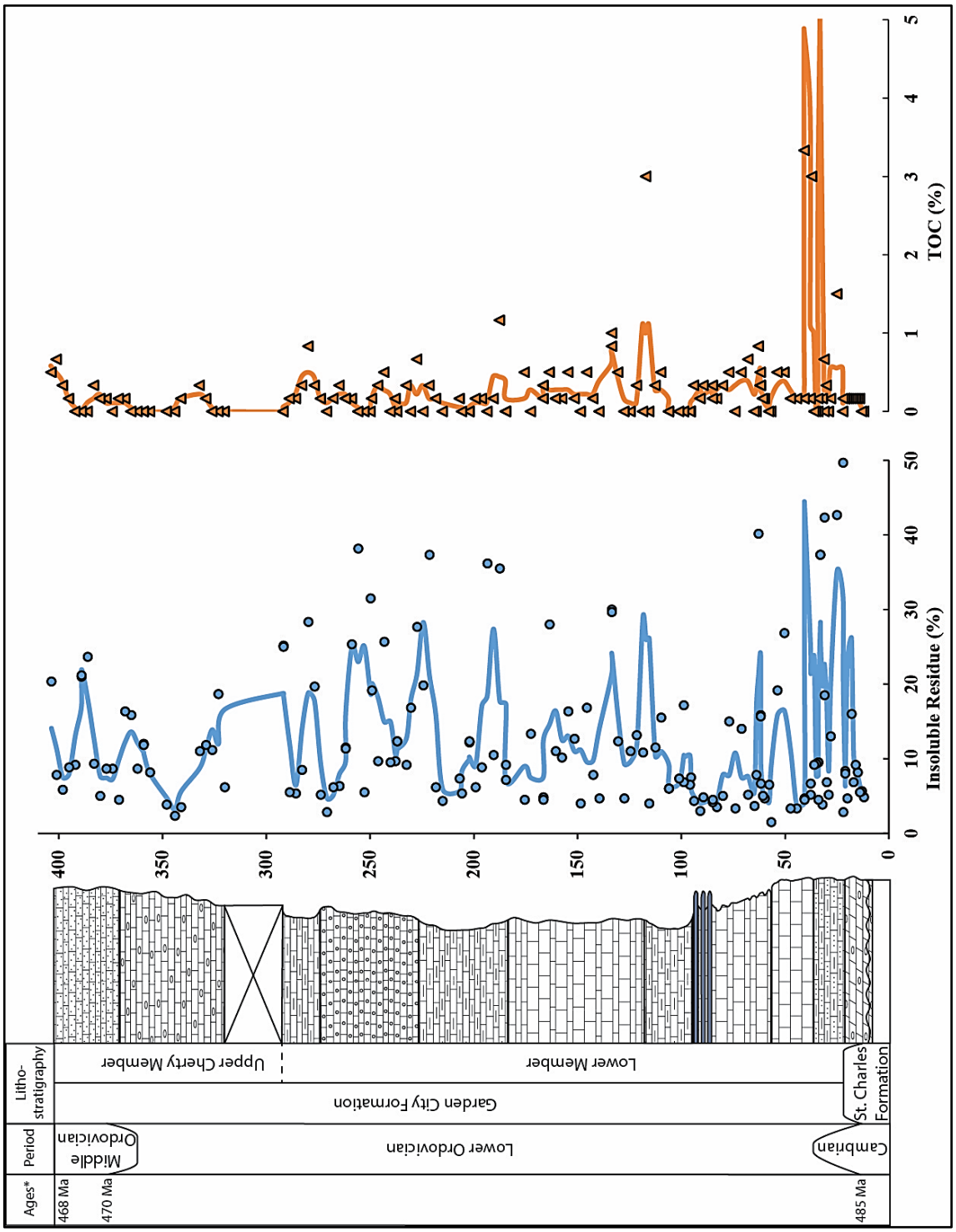

Figure 65. Lithology, insoluble residue, and TOC data from the Garden City Formation. Blue and orange lines represent a three-point moving average for insoluble residue and TOC wt. % data. See Figure 8 for lithology types.

in insoluble content. Insoluble residue ranges from1.5 to 63.8 weight percent (wt. %) with a precision of 1.0 wt. %. Fluctuations between high and low values of insoluble residue occur throughout the Garden City Formation. The lower 50 m of the Garden City Formation contain the highest insoluble residue values. This portion of the Garden City Formation consists of abundant argillaceous material that is reflected by the high insoluble residue values.

TOC decreases slightly with increase in stratigraphic section (Figure 65). This trend appears to be influenced by the high TOC values from the lower portion of the Garden City Formation. The general trend above these high values shows relatively steady TOC values upsection. TOC values range from 0.0 to 7.5 wt. % with a precision of 0.1 wt. %. There are three high TOC values occurring at 33, 37, 41, and 117 m with values of 7.5, 3.0, 3.3, and 3.0 wt. % respectively. A complete table of the Garden City Formation insoluble residue and TOC values is located in Appendix D1.

Pogonip Group Insoluble Residue and Total Organic Carbon Analysis

Insoluble residue increases upsection (Figure 66). Insoluble residue values range from 1.2 to 84.7 wt. % with a precision of 0.7 wt. %. Insoluble residue values at the base of the Pogonip Group fluctuate between 5 to 10 wt. % and gradually increase upsection to values of 10 to 30 wt. %. Fluctuations between high and low values of insoluble residue occur throughout the Pogonip Group. Prominent fluctuations between high and low values of insoluble residue occur near both member and formation contacts of the Pogonip Group.

TOC appears to increase upsection (Figure 66). TOC values range from 0.0 to 4.8

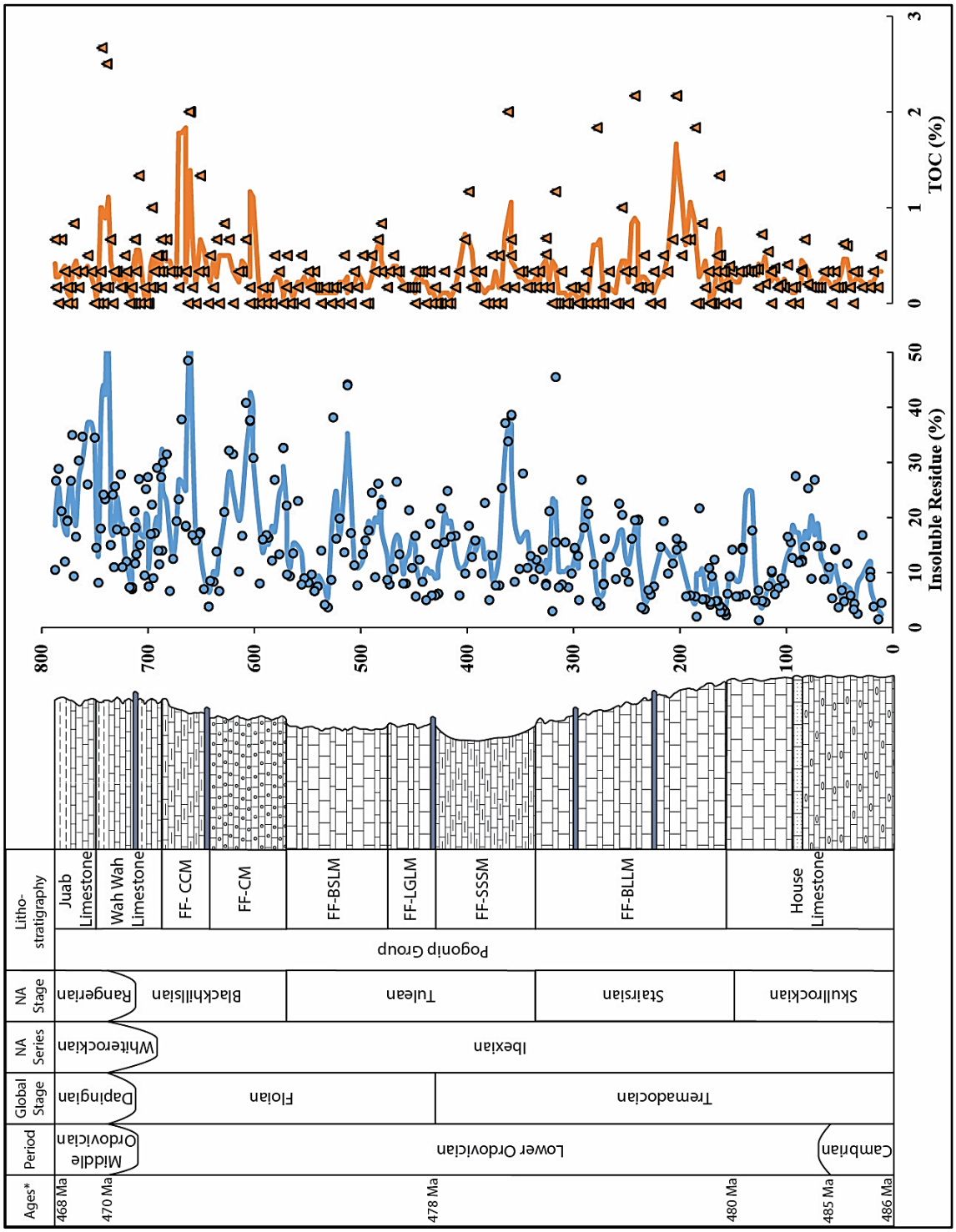

Figure 66. Lithology, insoluble residue, and TOC data from the Pogonip Group. Blue and orange lines represent a three-point moving average for insoluble residue and TOC wt. % data. See Figure 11 for lithology types.

wt. % with a 0.03 wt. %. Values are relatively constant upsection with the exception of two obvious increases in TOC occur at approximately 200 m and 650 m. Values at these locations fluctuate from ~0.5 to 2 wt. %. Increases in TOC values appear to coincide with increases in insoluble residue values. The complete data set for the Pogonip Group insoluble residue and TOC values is located in Appendix D.

Garden City Formation Conodont Biostratigraphy

A total of 539 conodont elements were extracted from samples of the lower 55 m (from 12-67 m as the lowermost 12 m is removed by erosion) of the Garden City Formation in Green Canyon. Identified species belong to conodont Fauna C and Fauna D of Ethington and Clark (1971). Identified conodont species from Fauna C include *Acanthodus lineatus* (Furnish, 1938), *Cordylodus angulatus* (Pander, 1856), *Cordylodus intermedius* (Furnish, 1938), *Loxodus bransoni* (Furnish, 1938), *Paltodus spurius* (Ethington and Clark, 1964), *Triangulodus?* n. sp., and *Utahconus bassleri* (Furnish, 1938). Virtually no conodont elements were found from 32-44 m and is likely a barren zone. Conodont species identified within Fauna D include *Scolopodus filosus* (Ethington and Clark, 1964) and *Scalpellodus n. sp. A* [= *Protopanderodus? n. sp. 1* and *P.? n. sp. 2* of Repetski (1975)] which occur at approximately 57 m in the Green Canyon Garden City Formation section.

Conodont upper Fauna B of Landing (1981) and Taylor et al. (1981a) is absent in the lower Garden City Formation in Green Canyon and Blacksmith Fork. Landing (1981) only reported conodont occurrence in the lower (remaining) 10 m of the Garden City Formation in Green Canyon which falls within conodont Fauna C. However,

conodont upper Fauna B, conodont Fauna C, and conodont Fauna D occur within the lower 50-70 m of the Garden City Formation in Hillyard Canyon and Franklin Basin (Landing, 1981). This absence of the conodont upper Fauna B in Green Canyon and Blacksmith Fork Canyon indicates that the Garden City Formation was deposited in these locations upon an erosional surface with at least 12 m of relief and that the base of the Garden City Formation is younger in the southern Bear River Range (Landing, 1981).

Meter Scale Cycles (fifth-order high-frequency parasequences)

High frequency meter-scale cycles (parasequences) are common within much of the Pogonip Group and Garden City Formation. They appear as shallowing upward slope and ledge packages that generally consist of lower slope forming shaly nodular mudstones and wackestones with minor intraformational conglomerate and upper ledge forming intraclastic packstones, grainstones, and algal boundstones (Figure 67). The lower and upper surfaces of these cycles are interpreted as minor flooding surfaces and show an abrupt contact between low-energy deeper-marine lithofacies (shales, etc.) and higher-energy shallow-marine lithofacies (packstones, etc.). The contact surfaces between many parasequences within the Pogonip Group are hardgrounds that include ferruginous (orange color rinds) stain, truncations, encrusting organisms, and trace fossils like borings and burrows (Figure 68). Hardground surfaces within the Garden City Formation are rare and difficult to recognize because they lack the obvious features of hardgrounds found within the Pogonip Group. No cycles greater than meter-scale cycles are observed within the Garden City Formation in outcrop.

Figure 67. Meter-scale (1.5 m) cycle from the Fillmore Formation. White dashed line shows upper surface and black triangle shows cycle is shallowing (coarsening) upward.

Figure 68. Bored intraclasts found within the FF-BLLM. This hardground surface likely represents the contact between parasequences. Pencil for scale (15 cm).

Larger Cycles

Pogonip Group Sequences

Nine sequences ranging from 10 to 170 m thick are recognized and named within the Pogonip Group, however, these sequences have not been ordered into third- or fourth-order sequences (Miller et al., 2003, 2012). Evans et al. (2003) and Miller et al. (2003) recognized that lowstand deposits are often preserved at sequence boundaries within the Pogonip Group instead of unconformities. Lowstand deposits occur during the lowstand systems tract when the rate of base-level rise is slower than the rate of aggradation and form during periods of extended low sea level after a drop in relative sea level (Miller et al., 2003). Lowstand deposits are shallow high-energy lithologies such as

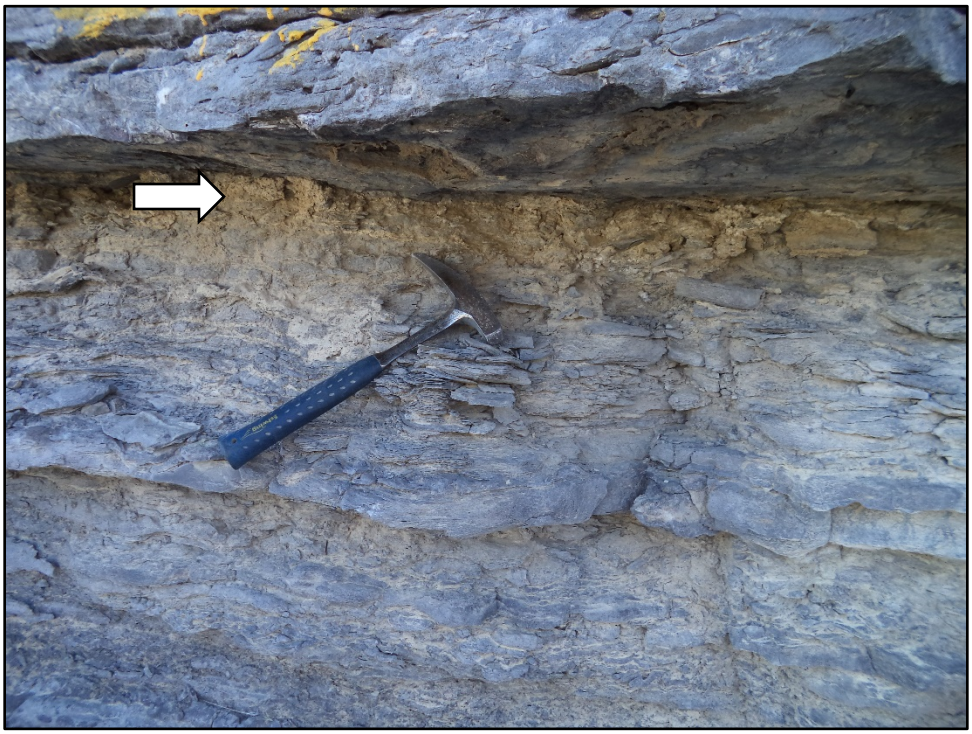

Figure 69. A sequence boundary within the lower FF-BLLM. Identified by a thin, poorly- lithified fine sandstone (arrow). Rock hammer for scale.

intraformational conglomerates and grainstones, and also include microbial reefs and carbonates with high amounts of quartz sand/silt and white to brown chert (Miller et al., 2012). Highstand deposits occur during extended periods of high sea level and include deep marine low-energy lithologies such as lime mudstones, wackestones with minor amounts of intraformational conglomerates and grainstones (Miller et al., 2012). Sequence boundaries within the Pogonip Group are often associated with algal reef horizons or thin, poorly-lithified sandstone beds (Figure 69).

DISCUSSION

Biostratigraphic Correlation

Fossil assemblage Zone A through L have been established for both the Garden City Formation and Pogonip Group by Ross (1949, 1951, 1953, and 1968) and Hintze (1951, 1953, and 1954), and can be used as a biostratigraphic correlation tool (Figure 70). Biostratigraphic studies have been conducted on the Garden City Formation in Green Canyon, however these studies are incomplete and the locations of these studies are not well described. For this reason fossil assemblage Zones A through L have been approximated using established zone boundaries from neighboring sections of Ross (1949) (Table 6) located in Hillyard Canyon, Logan Canyon, Green Canyon, Blacksmith Fork, and Mantua, Utah. The base of Zone A is not present within the Garden City Formation at Green Canyon due to the 12 m erosional relief between the Garden City Formation and the underlying St. Charles Formation.

Table 6. Estimated stratigraphic positions of Fossil Assemblage Zones A through L within the Garden City Formation in Green Canyon.

Fossil Assemblage Zone (Ross, 1951; 1968)	Stratigraphic Position (m)
A	12-21
B	21-37
C	37-57
D	57-65
E	65-85
F	85-118
G	118-256
H	256-286
I	286-300
J	300-368
K-L	368-404

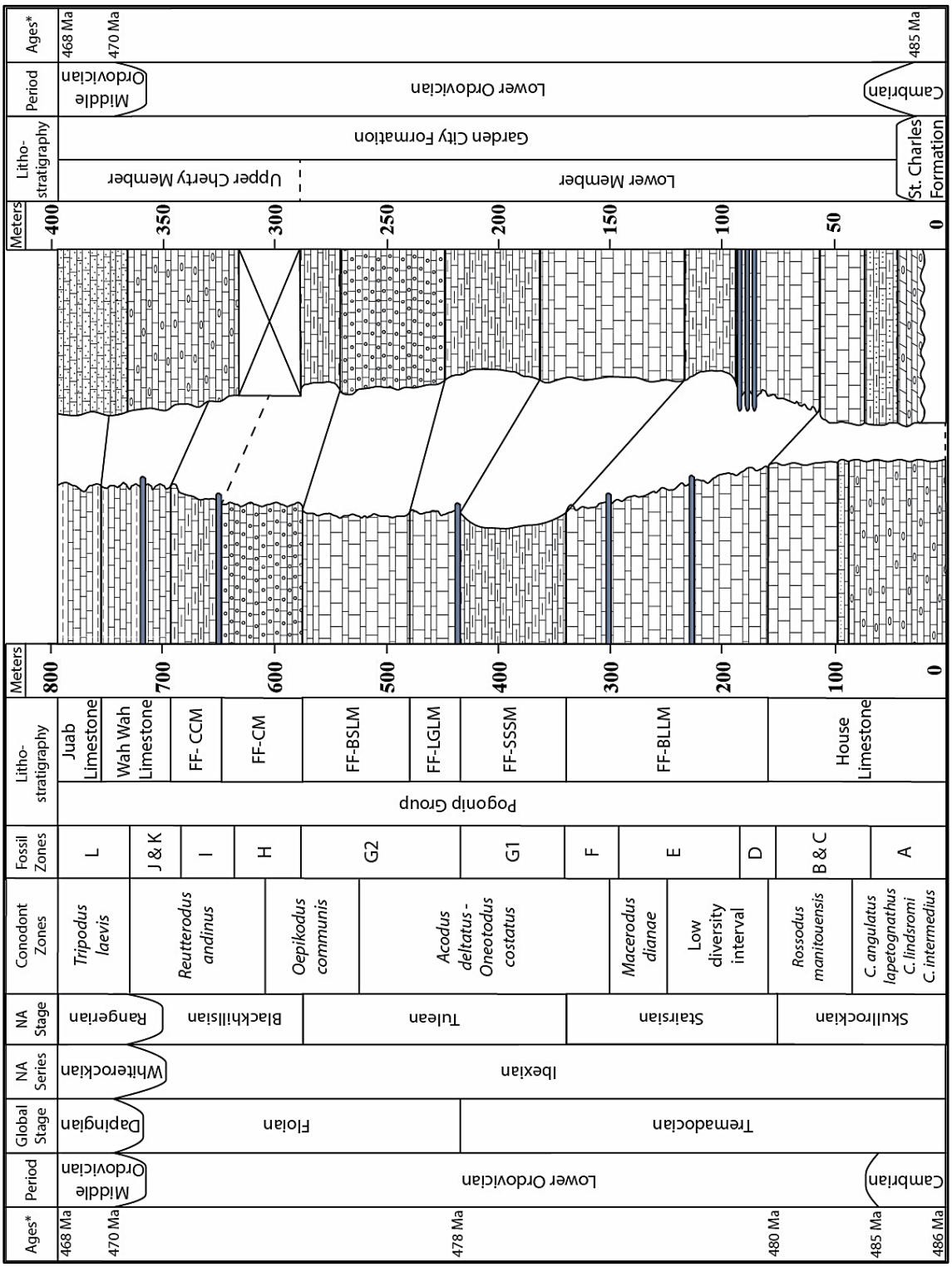

Figure 70. Biostratigraphic correlation of the Pogonip Group and the Garden City Formation. Black lines show equivalent contacts between Pogonip Group formations and the Garden City Formation. Dashed line indicates an unknown contact location.

Establishing these fossil assemblage zone boundaries is significant in that the Garden City Formation can now be subdivided into coeval units with the various members of the Pogonip Group through the correlation of fossil assemblage zones from each area. The House Limestone (0-158 m) is equivalent to the lower 60 m of Garden City Formation and the Fillmore Formation (158-687 m) is representative of 60-332 m of the Garden City Formation. The Wah Wah Limestone (687-749 m) is equivalent to the stratigraphic interval of 332-383 m of the Garden City Formation and the Juab Limestone (749-787 m) represents 383-404 m of the Garden City Formation (Figure 70). Identifying the approximate location of the Pogonip Group member equivalents within the Garden City Formation allows conodont zones to be approximated within that unit.

Chemostratigraphic Correlation

Correlation of Carbonate Carbon and Oxygen Stable Isotope Ratios

The Garden City Formation and the Pogonip Group display similar upsection trends (Figure 71). $\delta^{13}C$ values at bases of both rock units begin positive and shift into negative values shortly thereafter. $\delta^{13}C$ values then increase, resulting in a short-lived positive $\delta^{13}C$ excursion near the Skullrockian-Stairsian stage boundary. After which $\delta^{13}C$ values decrease steadily until the Tremadocian-Floian global stage boundary. $\delta^{13}C$ values then show an overall increase upsection. $\delta^{13}C$ trends of the Garden City Formation and the Pogonip Group are interpreted to correlate based on the occurrence of these $\delta^{13}C$ fluctuations within a well-established biostratigraphic framework. Although variations from local effects such as diagenesis or restricted open sea water circulation could be overprinted on the $\delta^{13}C$ signal, no such variations were evident.

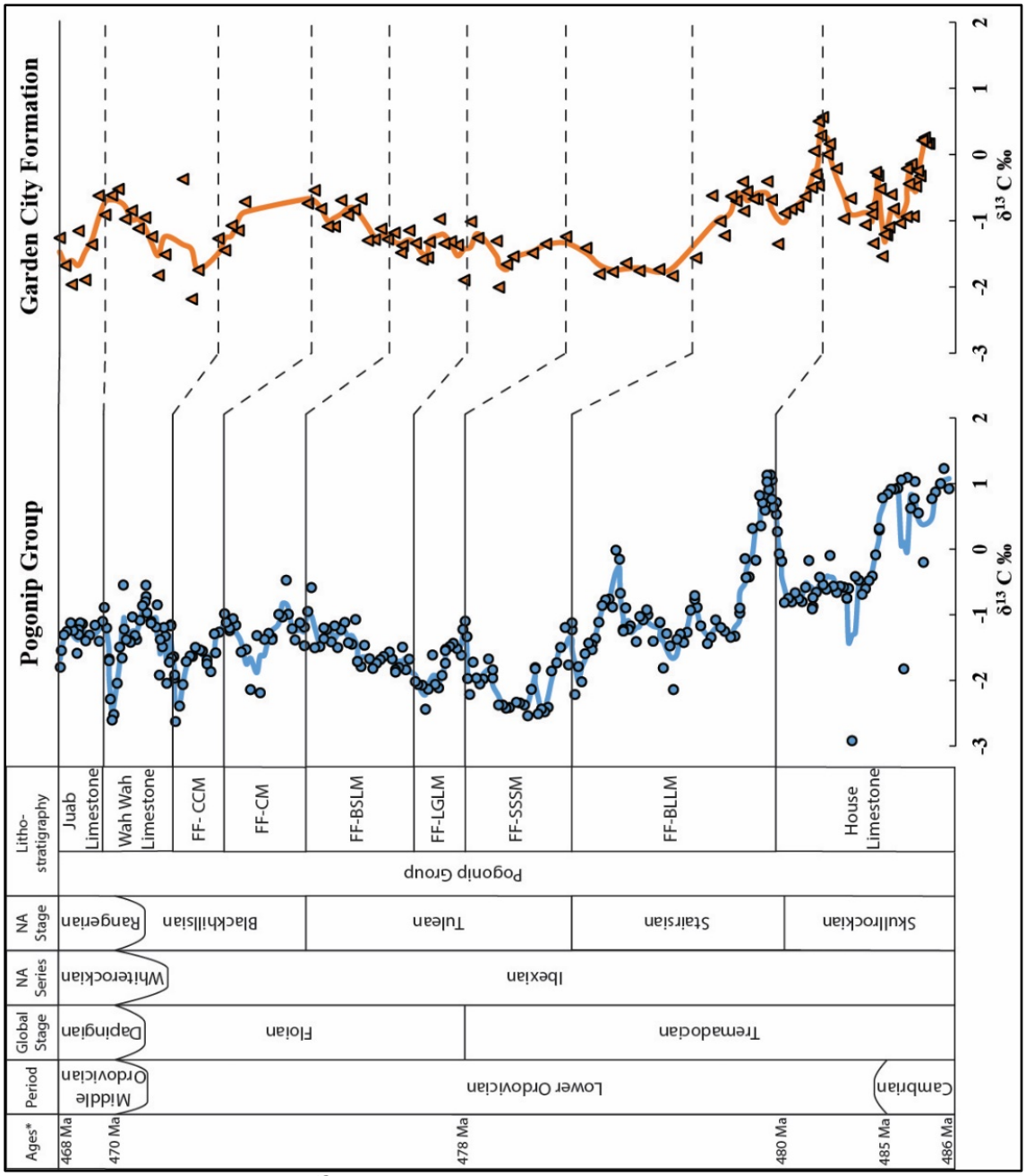

Figure 71. Correlation of $\delta^{13}C$ data from the Pogonip Group (blue points) and the Garden City Formation (orange points). Based off Pogonip Group member contacts. The blue and orange lines represent a three-point moving average of $\delta^{13}C$ data. Dashed lines represent approximate equivalent contacts within the Garden City Formation.

One interesting difference between $\delta^{13}C$ data from the Garden City Formation and the Pogonip Group is the amplitude of $\delta^{13}C$ values. The highest and lowest $\delta^{13}C$ values from the Pogonip Group show ~0.5 ‰ difference. For example: the highest and lowest $\delta^{13}C$ value for the Pogonip Group +1.2 ‰ and -2.9 ‰ versus +0.6 ‰ and -2.2 ‰ for the Garden City Formation. The cause of this apparent amplitude difference is not understood.

The $\delta^{18}O$ curves from the Garden City Formation and the Pogonip Group do not appear to follow similar trends, although, trendlines for each data set indicate an overall increase in $\delta^{18}O$ values (Figure 72). Notable differences occur near the base and at 70 m within the Garden City Formation, where abrupt negative $\delta^{18}O$ values occur. These $\delta^{18}O$ values are regularly more negative than -10.0 ‰ and reach a minimum of -14.0 ‰. In contrast, the Pogonip Group $\delta^{18}O$ isotope values never fall below -10.0 ‰. $\delta^{18}O$ values at the FF-BLLM and FF-SSSM contact abruptly increase from ~-9.0 ‰ to ~-8.0 ‰. $\delta^{18}O$ values within the Garden City Formation appear to gradually increase from -9.5 ‰ at around 100 m to -8.5 ‰ near 212 m. $\delta^{18}O$ correlation between the Garden City Formation and the Pogonip Group is unlikely because $\delta^{18}O$ values are easily altered through diagenesis than $\delta^{13}C$ values. The observed dissimilarities between the $\delta^{18}O$ the Garden City Formation and the Pogonip Group likely represent the effects of localized alteration of $\delta^{18}O$ values through diagenesis.

Statistical Comparison of Carbon and Oxygen Isotope Data

The null hypothesis H_0 was rejected for both the Mann Whitney U and Kolmogorov-Smirnov tests when comparing the complete data sets of the $\delta^{13}C$ and $\delta^{18}O$

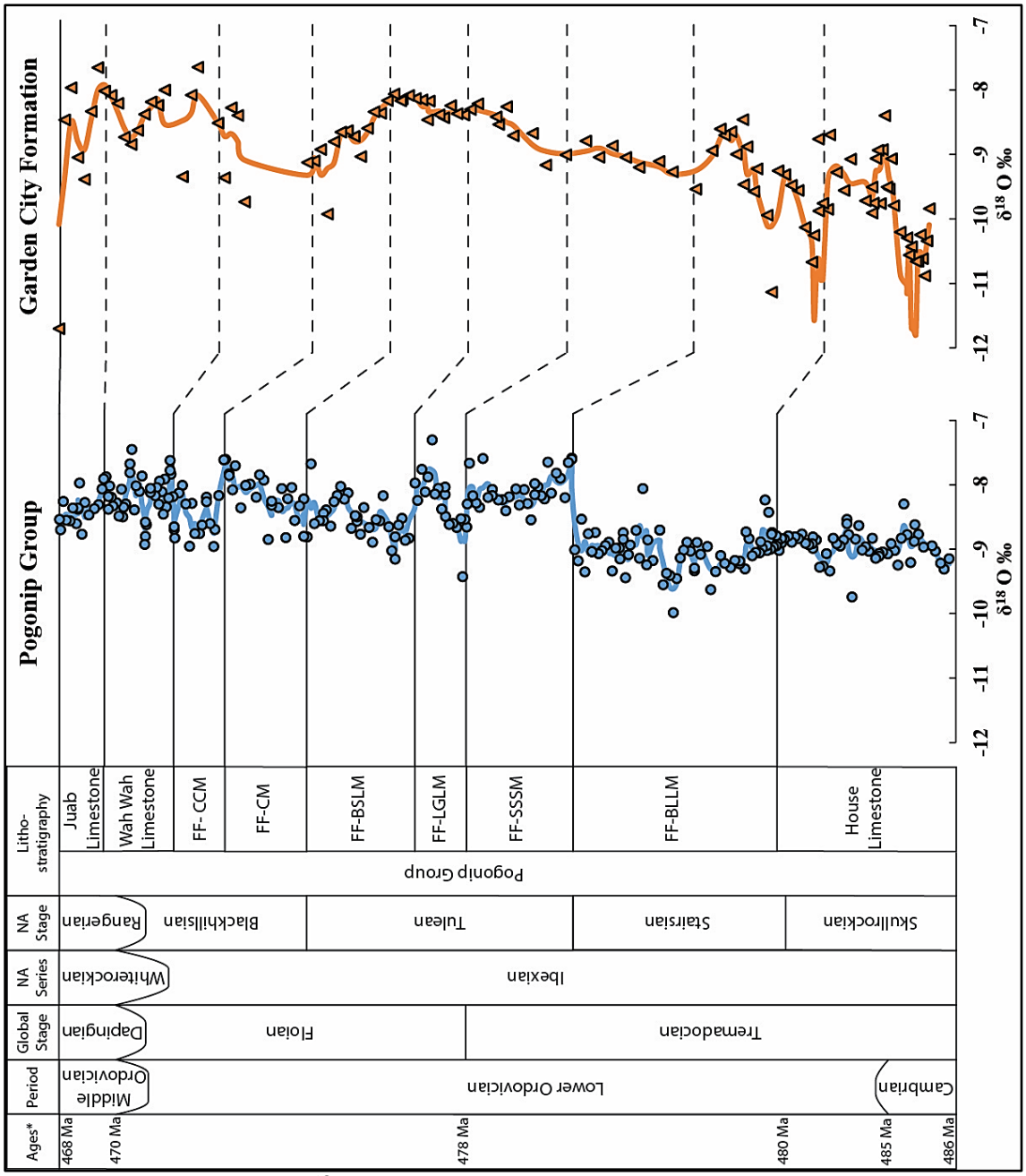

Figure 72. Correlation of $\delta^{18}O$ data from the Pogonip Group (blue points) and the Garden City Formation (orange points). Based off Pogonip Group member contacts. Four $\delta^{18}O$ values ranging from approximately -12.5 to -14.0 ‰ occur off scale on the Garden City Formation graph. The blue and orange lines represent a three-point moving average of $\delta^{18}O$ data. Dashed lines represent approximate equivalent contacts within the Garden City Formation.

from the Garden City Formation and the Pogonip Group. Rejection of H_0 for the Mann Whitney U test implies that the two data sets come from different populations. Rejection of the H_0 hypothesis for the Kolmogorov-Smirnov text implies that the two data sets exhibit different distributions.

The delineation of the equivalent Pogonip Group units within the Garden City Formation allows more detailed, unit by unit statistical analysis of $\delta^{13}C$ and $\delta^{18}O$ values using the Mann Whitney U and Kolmogorov-Smirnov tests. Member-scale statistical analysis reveals similarities and differences within the $\delta^{13}C$ and $\delta^{18}O$ values of the Garden City Formation and Pogonip Group.

The null hypotheses H_0 for both the Mann Whitney U and Kolmogorov-Smirnov tests are accepted for $\delta^{13}C$ values in all the units (and equivalents) except for the FF-SSSM, FF-BSLM, and FF-CM members of the Fillmore Formation (Table 7). This indicates that these members of the Garden City Formation and the Pogonip Group are more dissimilar than similar. The null hypothesis H_0 is rejected and the alternative hypothesis H_a is accepted for the $\delta^{18}O$ values from lower portions of the rock units, namely locations representing the House Limestone, and the FF-BLLM, FF-SSSM, and FF-CM of the Fillmore Formation (Table 7). The null hypothesis H_0 for both the Mann Whitney U and Kolmogorov-Smirnov tests were rejected for $\delta^{13}C$ and $\delta^{18}O$ values from the FF-SSSM and the FF-CM members of the Fillmore Formation. This can partially be explained for the FF-CM portion by the 28 m sampling gap within the upper portion of the Garden City Formation (292-320 m). This 28 m thick section occurs between the FF-CCM and FF-CM equivalent of the Garden City Formation.

Table 7. Statistical results of the Mann Whitney U and Kolmogorov-Smirnov tests for carbon and oxygen isotope data. Tests compare $\delta^{13}C$ and $\delta^{18}O$ values from the Pogonip Group members with member equivalent portions of the Garden City Formation. The Fillmore Formation member names abbreviated. 0 = the null hypothesis (H_0), A = the alternative hypothesis (Ha).

Member	$\delta^{13}C$		$\delta^{18}O$	
	Mann Whitney U test	**Kolmogorov-Smirnov test**	**Mann Whitney U test**	**Kolmogorov-Smirnov test**
Pogonip Group and Garden City Formation	A	A	A	A
House Limestone	0	0	A	A
FF-BLLM	A	A	A	A
FF-SSSM	A	A	A	A
FF-LGLM	0	0	0	0
FF-BSLM	A	A	0	0
FF-CM	A	A	A	A
FF-CCM	A	A	0	0
Wah Wah Limestone	0	0	0	0
Juab Limestone	0	0	0	0

Assessment of diagenesis of Stable Isotopes

Field observations and thin-section analysis have shown the presence of diagenetic features within the Garden City Formation and the Pogonip Group. This indicates that each rock units has experienced some level of diagenesis. Assessing the level of diagenesis is important because $\delta^{13}C$ and $\delta^{18}O$ isotope values can be altered through diagenesis which may inhibit regional and global correlation interpretations. Marine carbonate $\delta^{13}C$ values are often preserved during the diagenetic stabilization of unstable precursor minerals within carbonate rocks (Banner and Hanson, 1990) while marine carbonate $\delta^{18}O$ values are more commonly altered by diagenesis. Metzger and

Fike (2013) suggest that bioturbation-enhanced migration of fluids within grain pores may alter the original isotope values of seawater. High porewater:rock ratios of 1000:1 are required to alter $\delta^{13}C$ values compared to low porewater:rock ratios of 10:1 for $\delta^{18}O$ alteration (Banner and Hanson, 1990).

Diagenetically-altered isotope values of both $\delta^{13}C$ and $\delta^{18}O$ should show obvious covariation and would occur in environments with high meteoric water and rock interaction (Banner and Hanson, 1990). The cross plot of $\delta^{13}C$ and $\delta^{18}O$ data (Figure 73) indicates a weak, and likely insignificant, negative correlation from the Garden City

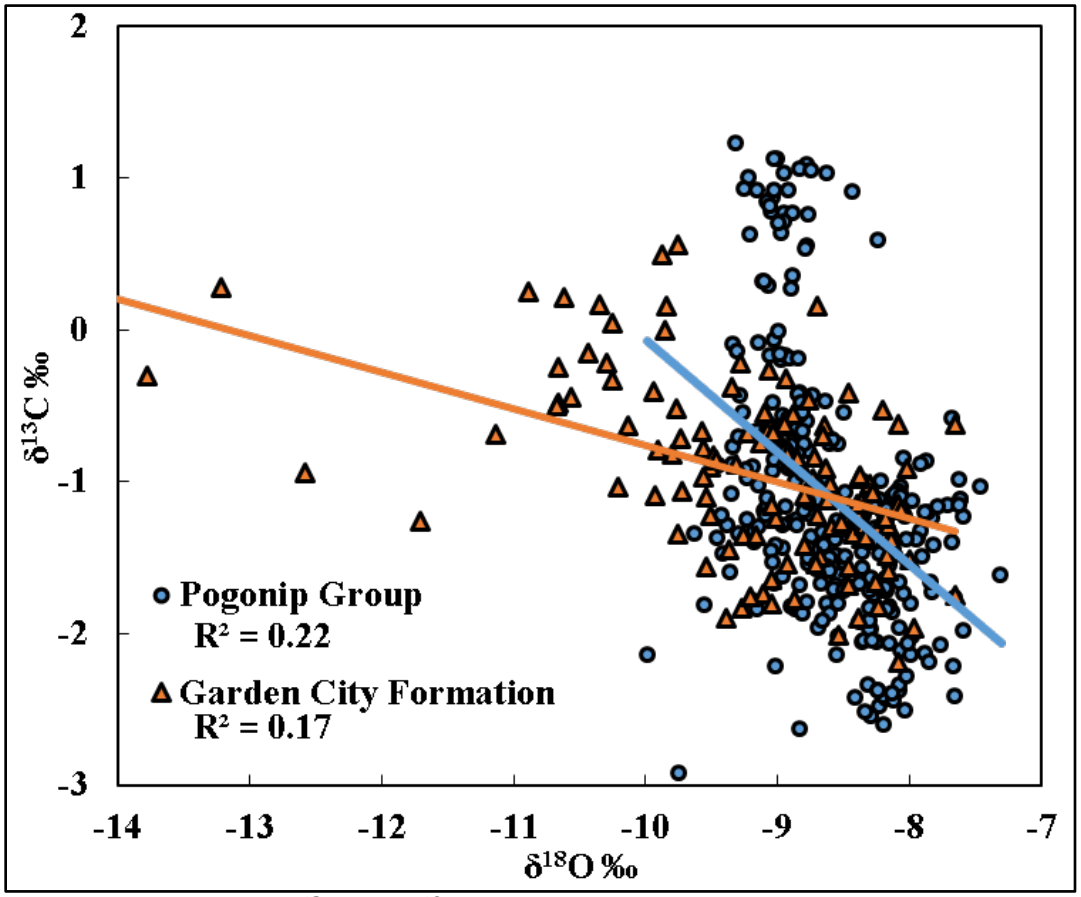

Figure 73. Cross plot of $\delta^{13}C$ and $\delta^{18}O$ from the Garden City Formation and the Pogonip Group.

Formation (R^2=0.22) and the Pogonip Group (R^2=0.17). No obvious covariation exists between the $\delta^{13}C$ and $\delta^{18}O$ data, however, it is possible for isotope values to display a strong diagenetic overprint even with a lack of covariation.

Variability of δ18O Values

Isotope trends near the base of the Garden City Formation display antithetic values where $\delta^{13}C$ decreases as $\delta^{18}O$ increases (Figure 63). The alteration of $\delta^{18}O$ values through the diagenetic process of dolomitization could have resulted in the observed increase of $\delta^{18}O$ by ~2.0 ‰. Field observations and thin -section analysis of these areas of antithetic isotope values show abundant dolostones and lithologies rich in dolomite rhombs. Other dolomitic lithotypes such as those of the upper Garden City Formation do not display the antithetic $\delta^{13}C$ and $\delta^{18}O$ values observed within the lower Garden City Formation.

The Pogonip Group does not contain any obvious antithetic isotope trends, however, there is an abrupt increase in $\delta^{18}O$ values near the contact of the FF-BLLM and FF-SSSM (Figure 64) where $\delta^{18}O$ values increase from ~ -9.0 ‰ to ~-7.5 ‰ (increase of ~1.5 ‰) over a 3 m span. Thin section analysis indicates that lithologies from this location have experienced partial recrystallization. It is possible that sediment contact with isotopically-light meteoric waters and subsequent recrystallization of those sediments could have resulted in enriched $\delta^{18}O$ values. The FF-BLLM and FF-SSSM contact has been interpreted to be a sequence boundary (Miller, 2012), where the interaction between isotopically-light meteoric water and carbonate sediments was possible during lower sea level.

Garden City Formation and Pogonip Group $\delta^{18}O$ data show an overall increasing trend from the Cambrian-Ordovician boundary up through the Middle Ordovician. This increasing trend likely represents cooling sea water temperatures through the Lower and Middle Ordovician. Reliable sea water temperatures are difficult to obtain from carbonate $\delta^{18}O$ values due to $\delta^{18}O$ value sensitivity to temperature change, hydrologic cycle change, and diagenetic alteration (Munnecke et al., 2010). However, Trotter et al. (2008) analyzed the $\delta^{18}O$ of conodont apatite oxygen to calculate sea water temperatures because conodont apatite oxygen is less affected by diagenesis than carbonate oxygen. $\delta^{18}O$ apatite values increase through the Lower and Middle Ordovician while calculated sea water temperatures decrease (Trotter et al., 2008). Correlation using $\delta^{18}O$ data will not be discussed due to its sensitivity to alteration.

Variability of δ13C Values

$\delta^{13}C$ trends from the Garden City Formation and the Pogonip Group are quite similar indicating that similar fluctuations of $\delta^{13}C$ values may result from regional effects. Both data sets show positive $\delta^{13}C$ values near the Cambrian-Ordovician boundary and at the House Limestone-Fillmore Formation contact. The local Ibex Area sea level curve produced by Miller et al. (2012) shows that these positive $\delta^{13}C$ values coincide with overall sea level fall yet other minor increases in $\delta^{13}C$ values seem to occur during overall sea level rise. According to Edwards and Saltzman (2014) the aquafacies model should link negative $\delta^{13}C$ values with sea level fall. These sea-level cycles however do not appear to influence $\delta^{13}C$ variability in any consistent way. These same positive $\delta^{13}C$ trends are present within the $\delta^{13}C$ global curve (Bergström et al., 2008) and

appear to coincide with periods of sea level rise on the global sea level curve (Haq and Schutter, 2008). These conflicting results indicate a lack of direct correlation between $\delta^{13}C$ fluctuation and sea level for the Garden City Formation and the Pogonip Group. The Ibex Area sea level curve shows an overall relative sea level drop from the Cambrian-Ordovician boundary through the lower Middle Ordovician and likely represents local fluctuations in sea level caused by localized sedimentation and subsidence rates. The global sea level curve shows an overall relative sea level rise for the same time period.

A common interpretation of positive $\delta^{13}C$ excursions is that they signify increased rates of organic carbon-burial and/or high primary productivity and negative $\delta^{13}C$ excursions indicate the collapse of primary productivity (Kump and Arthur, 1999). However, the opposite seems true within the Pogonip Group. The positive $\delta^{13}C$ values at the base of the Pogonip Group and the positive $\delta^{13}C$ excursion at the House Limestone-Fillmore Formation contact both coincide with conodont extinction events (Miller et al., 2012). The positive $\delta^{13}C$ excursion within the Garden City Formation also coincides with a conodont extinction event. The positive $\delta^{13}C$ values near the bases of the Pogonip Group and the Garden City Formation represent regression events that may have contributed to conodont extinction events. The positive $\delta^{13}C$ values associated with those regression events are not fully understood.

Overall $\delta^{13}C$ trends from the Pogonip Group and the Garden City Formation show gradually increasing $\delta^{13}C$ values from the Cambrian-Ordovician boundary through the lower Middle Ordovician. This positive trend likely indicates increased productivity,

which is also observed within the fossil record. The Great Ordovician Biodiversification Event (GOBE) occurred during the Ordovician and shows major increases in the diversity of marine organisms (Trotter et al., 2008). Thin -section analysis of the Garden City Formation and the Pogonip Group show an increased trend in the number of bioclasts upsection.

Validation of Local δ13C Data

New $\delta^{13}C$ data from this study share similar trends with $\delta^{13}C$ data from the Ibex Area by Edwards and Saltzman (2014) and are thus validated. Minors differences in $\delta^{13}C$ between data sets appears to be related to sample interval (or frequency), the sampling of different sections between studies, and varying measured section thicknesses.

Global Correlation of δ13C Data

$\delta^{13}C$ data from the Pogonip Group (this study) and the Garden City Formation (this study) display similar trends to the $\delta^{13}C$ global curve of Bergström et al. (2008) (Figure 74). These three $\delta^{13}C$ data sets show a decrease from positive to negative values near the Cambrian-Ordovician boundary followed by a positive $\delta^{13}C$ excursion. $\delta^{13}C$ values then decrease to approximately -2.0 ‰ near the Tremadocian-Floian boundary. Values then steadily increase through the remaining Lower Ordovician and into the Middle Ordovician. It is important to note that the global $\delta^{13}C$ values prior to the Tremadocian-Floian boundary are roughly the same magnitude as isotope values from the Pogonip Group and the Garden City Formation. After the Tremadocian-Floian boundary global $\delta^{13}C$ values are roughly 2.0 ‰ greater than isotope values from this study but all

data sets show similar trends.

Edwards and Saltzman (2014) have shown that Lower Ordovician $\delta^{13}C$ data from the Great Basin (the Shingle Pass area of Nevada and the Ibex Area of Utah) correlate

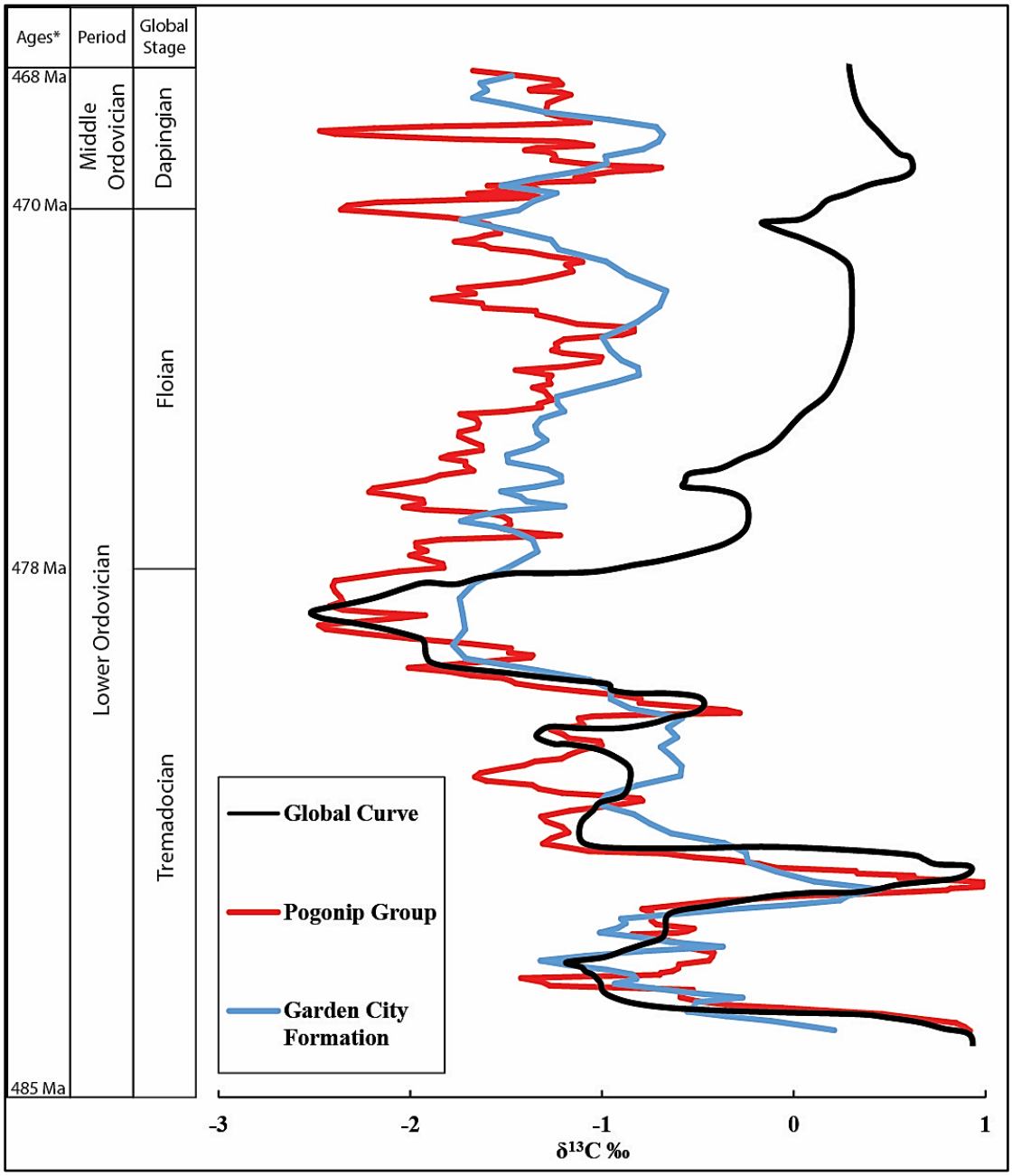

Figure 74. Global correlation of $\delta^{13}C$ curves for the Lower and Middle Ordovician. Global Curve from Bergström et al. (2009).

with $\delta^{13}C$ data from the Argentine Precordillera (Buggisch et al., 2003; Thompson and Kah, 2012) and western Newfoundland (Azmy and Lavoie, 2009). The correlation between areas is based on correlative shifts in $\delta^{13}C$ which occur at the second positive $\delta^{13}C$ excursion near the top of the *Rossodus manitouensis* Zone (Early Tremadocian), a 1.0 ‰ $\delta^{13}C$ increase within the *Oepikodus communis* Zone (Early Floian), and the Ibexian-Whiterockian series boundary. This implies that the Garden City Formation may be globally correlative with the Argentine Precordillera and western Newfoundland because of its correlation with Ibex Area.

Correlation of Insoluble Residue and TOC Data

Insoluble residue and TOC data from each area appear to show opposite qualitative trends. For example: the highest values for insoluble residue occurs in the lower beds of the Garden City Formation while the highest values for insoluble residue occurs in the upper beds of the Pogonip Group. These high and low values tend to obscure the overall trends of insoluble residue. However, when samples with extremely high or low values, those with insoluble residue values greater than 40 % and carbonate values less than 60 %, are removed from the data set overall trends are revealed. The high and low values have only been removed to reveal the obscured overall trend in insoluble residue and carbonate data and are included in all other analyses.

Trendlines for both data sets indicate an increase in insoluble residue upsection (Figure 75) and could signify an overall drop in sea level. This increase in insoluble residue is to be expected due to the implied overall regressive nature of the Sauk IV-m supersequence. The sea level curve produced by Miller et al. (2003, 2012) shows sea

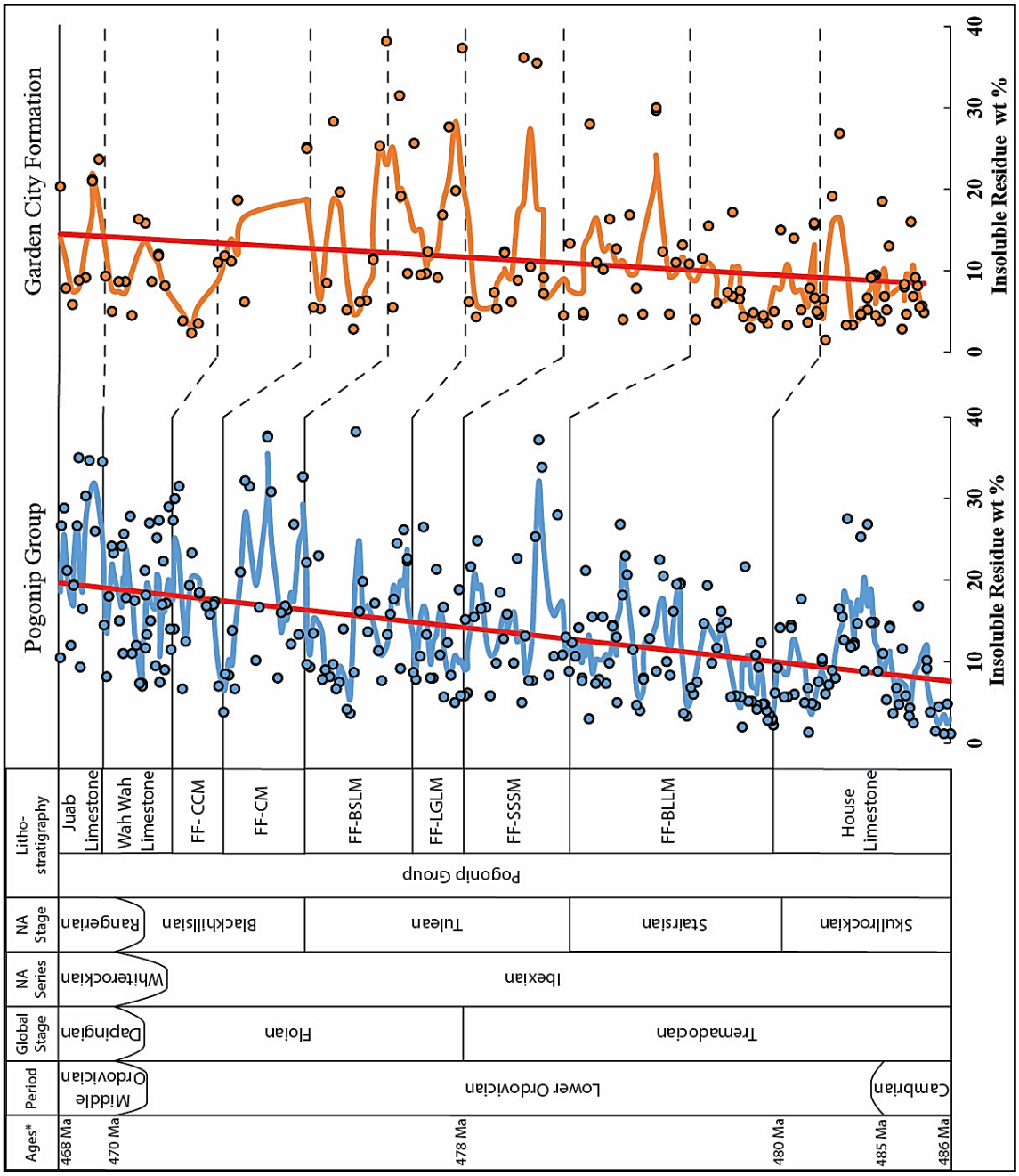

Figure 75. Insoluble residue percentages for the Pogonip Group (blue) and the Garden City Formation (orange). Insoluble residue percentage values over 40 % removed to observe the overall positive trend of the data sets. Blue and orange lines represent a three-point moving average. Red lines represent overall trends. Dashed lines represent approximate equivalent contacts within the Garden City Formation.

level gradually dropping from the Sauk III-m and Sauk IV-m supersequence boundary to the Sauk IV-m and Tippecanoe megasequence boundary.

Insoluble data obtained in this study from the same sections of the House Limestone and lower Fillmore Formation is similar to the insoluble data from Miller et al. (2003, 2012) and is thus validated. Additionally, insoluble data from the lower Garden City Formation in Green Canyon is similar to the data of Miller et al. (2003, 2012), although it contains more variability. Insoluble residues from the Pogonip Group consist primarily of fine quartz sand/silt, whereas insoluble residues from the lower Garden City Formation consists primarily of argillaceous siliciclastic material.

Trendlines for TOC data from each area show a minor overall decrease in TOC values upsection (Figure 76). An overall drop in sea level could result in the decrease in TOC which can occur with an increase in siliciclastic deposition. However, this overall decrease is minor and likely represents relatively stable preservation of little to no TOC.

Statistical Comparison of Insoluble Residue, and TOC Data

The H_0 hypothesis was rejected for both the Mann Whitney U and Kolmogorov-Smirnov tests while comparing the complete data sets of the insoluble residue and TOC data from the Garden City Formation and the Pogonip Group. Rejection of H_0 for the Mann Whitney U test implies that the two data sets come from different populations. Rejection of the H_0 hypothesis for the Kolmogorov-Smirnov text implies that the two data sets exhibit different distributions.

The delineation of the equivalent Pogonip Group members within the Garden City

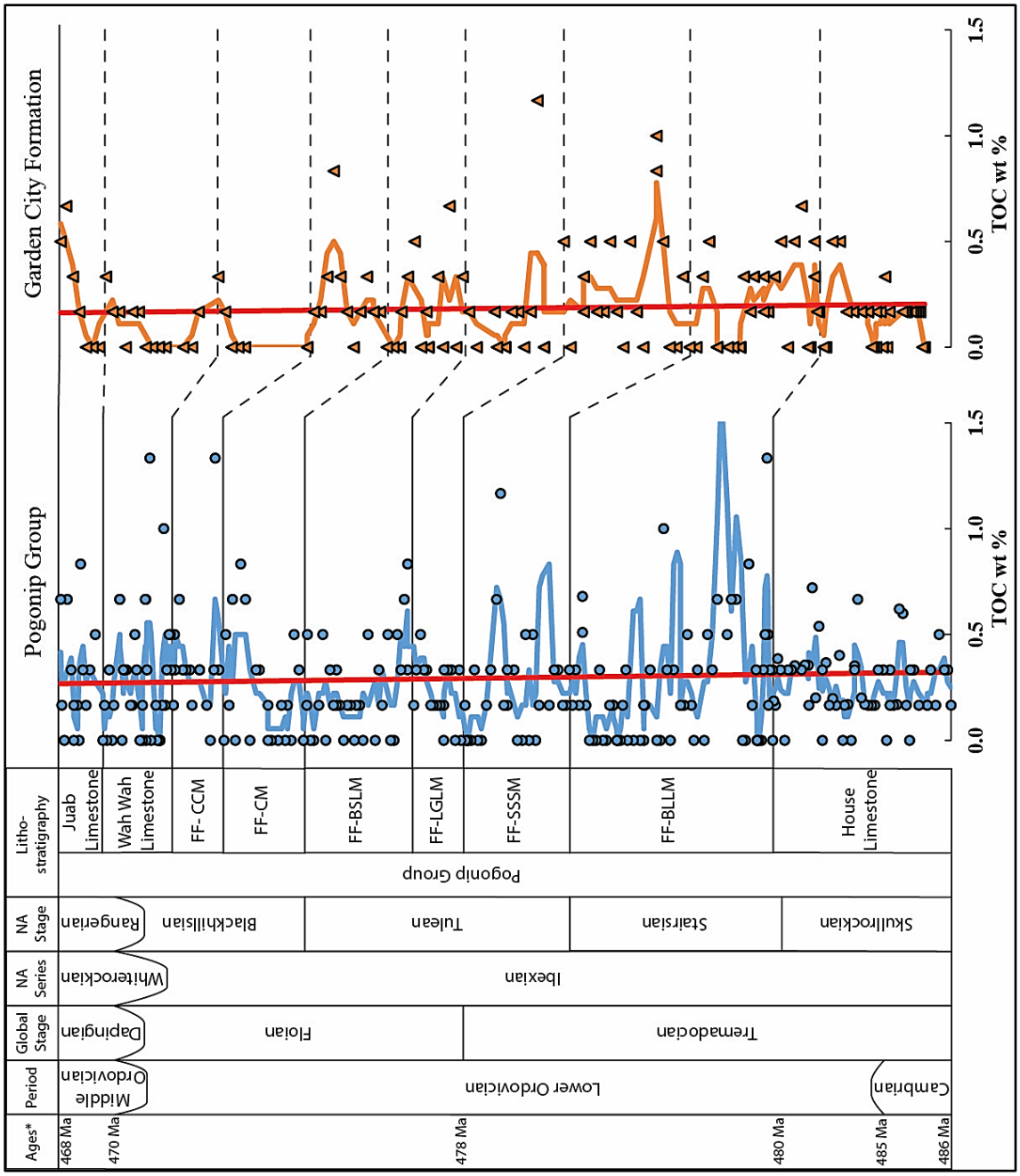

Figure 76. TOC values for the Pogonip Group (blue) and the Garden City Formation (orange). TOC values over 3 % removed to observe the overall nearly neutral trend of the data sets. Blue and orange lines represent a three-point moving average. Red lines represent overall trends. Dashed lines represent approximate equivalent contacts within the Garden City Formation.

Formation allows more detailed, unit by unit statically analysis of insoluble residue and TOC data using the Mann Whitney U and Kolmogorov-Smirnov tests. Member scale statistical analysis reveals both similarities and differences within the insoluble residue and TOC data of the Garden City Formation and Pogonip Group. Generally, the null hypotheses H0 for both the Mann Whitney U and Kolmogorov-Smirnov tests are accepted for the insoluble residue and TOC data from the lower and middle portions of the rock units (Table 8). This indicates that the lower and middle segments of the Garden City Formation and the Pogonip Group are more similar than dissimilar. However, the null hypothesis H_0 is rejected and the alternative hypothesis Ha is accepted for the insoluble residue and TOC data from upper portions of the rock units, namely locations representing the FF-CCM member of the Fillmore Formation, the Wah Wah Limestone, and the Juab Limestone (Table 8). This implies that the upper portions of the Garden City Formation and Pogonip Group contain many differences within the insoluble residue and TOC data. This can partially be explained by the fact that a continuous 28 m thick section within the upper portion of the Garden City Formation (292-320 m) was not sampled or analyzed due to covered slopes. This 28 m thick section occurs just below the FF-CCM and Wah Wah Limestone contact equivalent within the Garden City Formation.

Sequence Stratigraphic Correlation

Pogonip Group Sequence Stratigraphy

The sequence stratigraphy of the Pogonip Group has been studied by Dattilo (1993), Evans et al. (1993), and Miller et al. (2012). Nine sequences have been identified within the House Limestone, Fillmore Formation, Wah Wah Limestone, and Juab

Table 8. Statistical results of the Mann Whitney U and Kolmogorov-Smirnov tests for insoluble residue and TOC data. Tests compare insoluble residue and TOC values from the Pogonip Group members with member equivalent portions of the Garden City Formation. The Fillmore Formation member names are abbreviated. 0 = the null hypothesis (H_0), A = the alternative hypothesis (Ha).

Member	Insoluble Residue		TOC	
	Mann Whitney U test	Kolmogorov-Smirnov test	Mann Whitney U test	Kolmogorov-Smirnov test
Pogonip Group and Garden City Formation	A	A	A	A
House Limestone	0	0	A	A
FF- BLLM	A	0	0	0
FF-SSSM	0	0	0	0
FF-LGLM	0	0	0	0
FF-BSLM	0	0	0	0
FF-CM	0	0	0	0
FF-CCM	A	A	A	A
Wah Wah Limestone	A	0	A	A
Juab Limestone	A	A	0	0

Limestone (Figure 77). Miller et al. (2012) refers to these sequences are S10, S11, S12, S13, F1, F2, F3, and F4. The last sequence has not been named and will be referred to as sequence JL. S10, S11, S12, and part of S13 occur within the House Limestone. Part of S13 and all of F1, F2, and F3 occur within the Fillmore Formation. F4 includes the upper Fillmore Formation and most of the Wah Wah Limestone while sequence JL includes the uppermost Wah Wah Limestone and all of the Juab Limestone. The sequences have been divided into lowstand deposits (shallow water high-energy lithologies) and highstand deposits (deeper water low-energy lithologies).

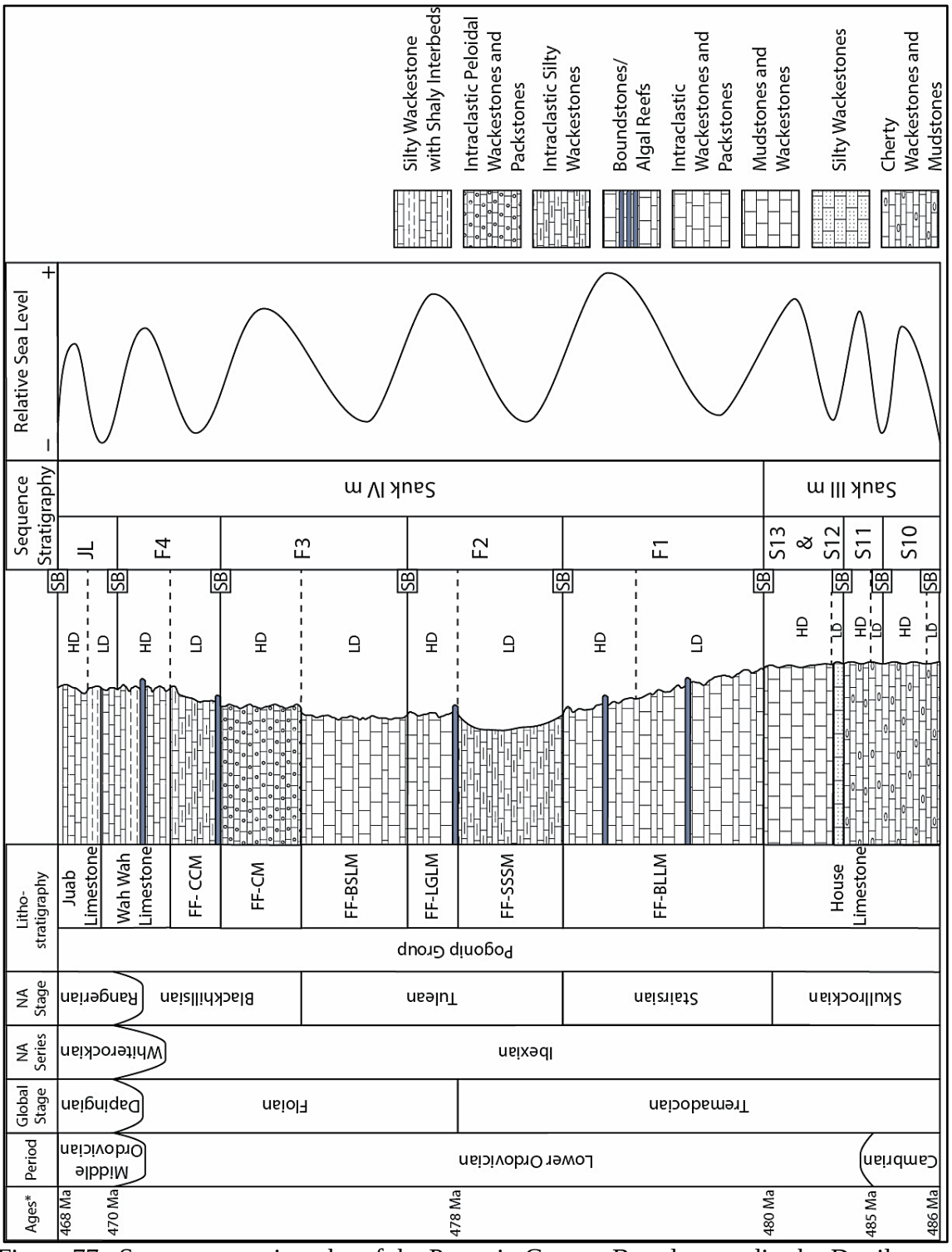

Figure 77. Sequence stratigraphy of the Pogonip Group. Based on studies by Dattilo (1993), Evans et al. (1993), and Miller et al. (2003, 2012). SB=sequence boundary, HD=highstand deposits, LD=lowstand deposits. Black dashed lines are approximate transitions from LD and HD. Sea level curve is based on Miller et al. (2012).

It is important to note that the sequence stratigraphic framework developed by Miller et al. (2003, 2012) for the Pogonip Group in the Ibex Area is somewhat nontraditional. Traditional sequence stratigraphic features such as hierarchical orders (second, third, fourth-order sequences), maximum flooding surfaces, and unconformities appear to be absent within the Pogonip Group as a result of rapid subsidence during deposition. Sequence boundaries within the Pogonip Group generally occur at or near member contact boundaries and have been approximated within the Garden City Group using correlated biostratigraphy and chemostratigraphy.

Garden City Formation Sequence Stratigraphy

The sequence stratigraphy of the Garden City Formation has been interpreted within the framework of the Pogonip Group sequence stratigraphy (Figure 78). Lowstand deposits are often preserved at sequence boundaries within the Garden City Formation instead of unconformities. Lowstand deposits include shallow high-energy lithologies, such as intraclastic wackestones, packstones, and grainstones, microbial reefs, and carbonates with high siliciclastic content. Highstand deposits include deeper water, low-energy lithologies, such as lime mudstones and wackestones with minor amounts of intraclastic wackestones and packstones.

S10 is absent in the Garden City Formation at Green Canyon due to ~12 m of erosional relief at the contact of the Garden City Formation and the underlying St. Charles Formation. Conodont Faunas A and B (Ethington and Clark, 1971), which encompasses the *Cordylodus intermedius, Cordylodus lindstromi, lapetognathus,* and *Cordylodus angulatus* Zones in the Ibex Area, are absent in the Green Canyon section of

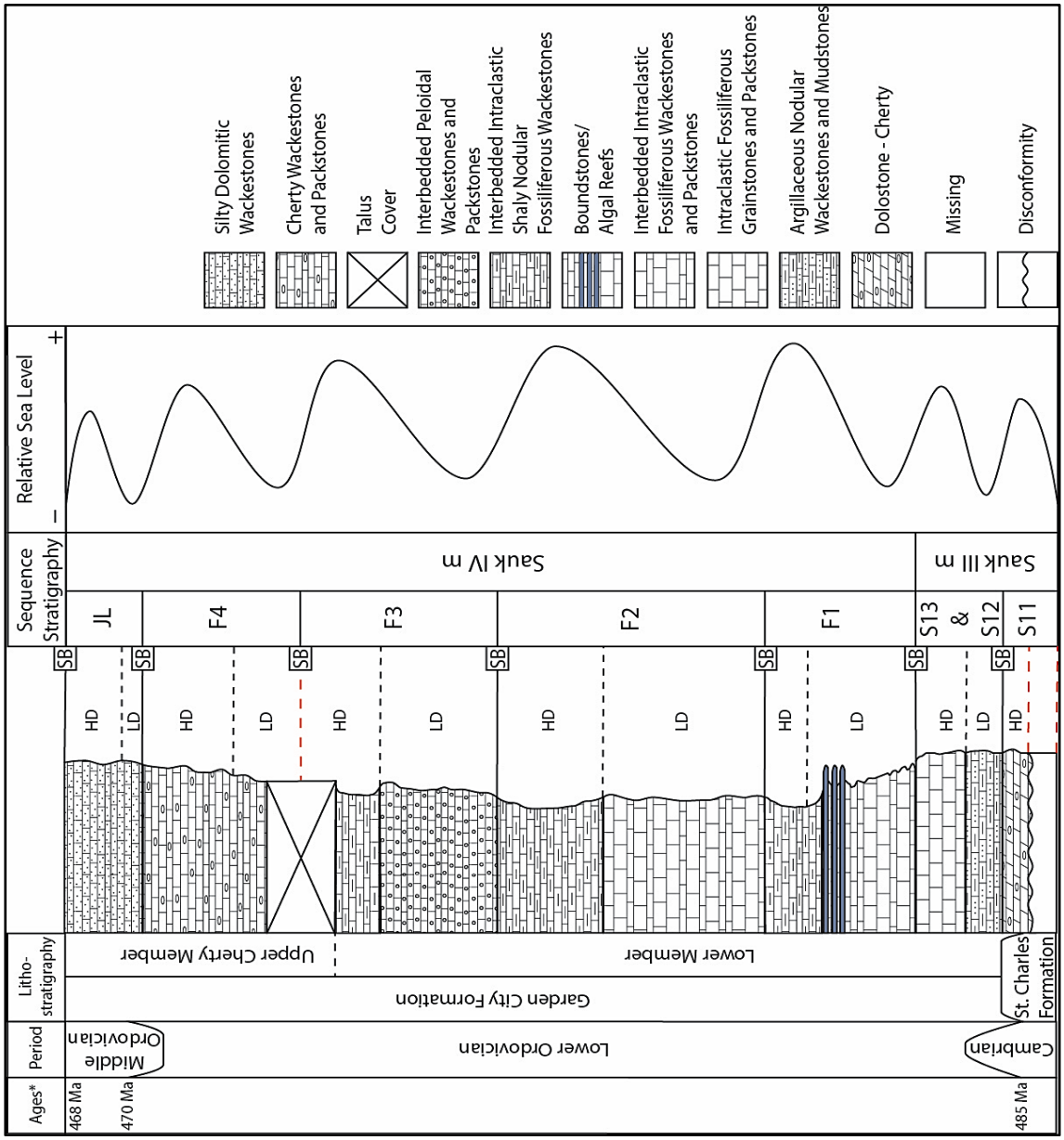

Figure 78. Sequence Stratigraphy of the Garden City Formation. Based on the sequence stratigraphic framework of the Pogonip Group. SB=sequence boundary, HD=highstand deposits, LD=lowstand deposits. Black dashed lines are approximate transitions from LD and HD. Red dashed lines indicate unknown boundary locations. Sea level curve is based on Miller et al. (2012) sea level curve for the Ibex Area.

the Garden City Formation. These conodont zones occur within S10 and part of S11 in the Pogonip Group which implies the absence of S10 and possible part of S11 in the Garden City Formation.

S11 is represented, at least in part, by the interval of 12-31 m within the Garden City Formation. It is difficult to determine where S11 begins within the Garden City Formation because the lower 10 m (12-22 m) is primarily dolostone. The basal portion of S11 coincides with overall positive $\delta^{13}C$ values within the Garden City Formation. The trend of increasing insoluble residue content within this interval, coupled with biostratigraphy and chemostratigraphy, confirms the occurrence of S11 within the Garden City Formation. Lowstand deposits are observed at the base and top of S11 within the Garden City Formation. Lithologies at the base of this sequence are primarily dolostones that transition into silty wackestones.

S12 occurs from 31-54 m of the Garden City Formation. This sequence begins with a subtle increase in insoluble residue and the top of S12 coincides with an abrupt change in $\delta^{13}C$ values from approximately -1.5 ‰ to near 0.0 ‰.

S13 is very thin and occurs from 54-61 m within the Garden City Formation. It has been identified as the Tule Valley lowstand in the Ibex Area and correlates with the *Ceratopyge* regressive event in Europe (Miller et al., 2003, 2012). This interval coincides with major conodont and trilobite extinctions, and with the positive $\delta^{13}C$ excursion observed within both rock units. The Low Diversity Interval (conodont Fauna D of Ethington and Clark (1971) begins within S13 in the Pogonip Group and was confirmed within the Garden City Formation near 57 m with the lowest occurrence of

Scolopodus filosus (Ethington and Clark, 1964). The top of S13 should represent the Sauk III-m and Sauk IV-m boundary (Miller et al., 2003, 2012).

F1 occurs from 61-118 m of the Garden City Formation. The highest positive $\delta^{13}C$ values within the second positive $\delta^{13}C$ excursion occur near the base of F1. Insoluble residue values show an overall increase while $\delta^{13}C$ values show an overall decrease through F1. F1 contains a thrombolite horizon from 83-95 m that is presumed to correlate with Miller's Reef (~ 330 m in the Pogonip Group). Lithologies at the base of the sequence in both locations are fossiliferous, silty lowstand deposits containing peloids, while lithologies near the top of the sequence represent late highstand deposits and include wackestones and intraclastic wackestones.

F2 occurs from 118-220 m of the Garden City Formation. The location F2 is based primarily on the biostratigraphy between the two areas. Insoluble residue values and $\delta^{13}C$ values show increasing values in the Garden City Formation. Lithologies within F2 show lowstand deposits occurring lower in the sequence and highstand deposits occurring at the top of the sequence.

F3 occupies interval from 220-290 m of the Garden City Formation. The top of F3 is difficult to place due to a 28 m sampling gap. Lithologies within the lower portion of sequence F3 include lowstand intraclastic fossiliferous wackestones that transition into highstand deposits such as peloidal wackestones.

F4 occurs from approximately 290-380 m of the Garden City Formation. The base of F4 is difficult to place due to the 28 m sampling gap within the Garden City Formation. However, insoluble residue values show overall increasing trends through

this sequence. The top F4 is placed at 380 m where a sharp increase in insoluble residue occurs just above beds containing increased amounts of brachiopod fossils. Lithologies within the lower portion of F4 represent lowstand deposits and include silty, fossiliferous, and intraclastic wackestones-packstones containing peloids/pellets, while upper lithologies within the sequence include mainly wackestones with minor packstones. Chert is very common within the lithologies of F4. The top of F4 is the contact between the Ibexian and Whiterockian Series and is the base of the Whiterockian Regression (Miller et al., 2003, 2012).

Sequence JL occurs from 380-404 m and shows an overall decrease in insoluble residue values. Lithologies are mainly silty, fossiliferous wackestones and sparse intraformational conglomerates. Lithologies within the upper portion of this sequence are dolomitic.

Sequence Stratigraphic Correlation

As hypothesized, eustatically-driven lithologic sequences preserved within the Pogonip Group appear to be present within the Garden City Formation. The sequence stratigraphy of the Pogonip Group and the Garden City Formation show the same transitions from shallow-water high-energy lithologies at the sequence base to deeper-water lower-energy lithologies towards the top of the sequence. PCA and cluster analysis show similar transitions in high- and low-energy lithologies. Insoluble residue values generally increase near sequence boundaries and are relatively high within lowstand deposits. This may indicate an influx of siliciclastic materials during relatively low sea levels. Insoluble residue values generally decrease toward the top of each sequence as

relative sea level increases. There do appear to be fluctuations of high insoluble residue values within the upper portion of some sequences. These rapid fluctuations could represent brief periods of minor sea level fall or storm events.

Sedimentological Responses to Subsidence Rates, Eustasy, and Regional Tectonics

Sequence stratigraphy, chemostratigraphy, and biostratigraphy have been used to show correlation between the Garden City Formation and the Pogonip Group (Figures 70, 71, and 78). However, these data provides little information as to the overall thickness and lithologic differences between units. These rock units are coeval and were deposited on the western margin of Laurentia in normal or near normal-marine conditions, yet the Pogonip Group is approximately 400 m thicker than the Garden City Formation. Thickness differences between rock units appear to be related to different subsidence rates within the Ibex Basin and the Northern Utah Basin. Subsidence curves produced by Bond et al. (1989) indicate that subsidence was occurring more rapidly near the Ibex Basic and slower in the Northern Utah Basin. Differences in subsidence rates between basins appears to have resulted in more accommodation space within the Ibex Basin, which possibly explains the approximate thickness difference of 400 m. Differences in subsidence rates can be explained by the proximity of the basins to the hinge zone of the subsiding passive margin. For example: the computer simulated model of a passive margin by Steckler (1981) illustrates that flexural bending of the craton edge moves landward as lithospheric rigidity and sediment influx increase which allows carbonate platforms to prograde onto the craton edge (Bond et al., 1989). This model shows subsidence occurring more rapidly basinward from the hinge zone. The Garden City

Formation could have been deposited closer to the hinge zone where subsidence occurs more slowly compared to more rapid basin-ward subsidence. The Pogonip Group could have been deposit farther basin-ward from the hinge zone.

Regional tectonic elements such as the Northern Utah Basin, the Toole Arch, the House Range Embayment, and the Wah Wah Arch may have influenced sedimentological interactions between basins and siliciclastic source material. The Northern Utah Basin and the Ibex Basin are geographically separated by the east-west trending Tooele Arch with the Transcontinental Arch (exposed craton) located to the east. This study has shown that the Pogonip Group contains a diverse set of lithologies, which range from shallow marine carbonates to terrigenous fine sandstones. Sandstones are absent from the Garden City Formation which consists of marine carbonates containing episodic fine detrital silt. Insoluble residue from the Pogonip Group ranges from 1.2 to 84.7 wt. % with an average of 16.0 wt. % ± 0.7 wt. %. Insoluble residue from the Garden City Formation ranges from 1.5 to 63.8 wt. % with an average of 13.4 wt. % ± 1.0 wt. %. Lithologic differences were likely influenced by sedimentologic interactions between regional tectonic elements and basin proximity to siliciclastic source material. The configuration of Laurentia combined with the location of the Tooele Arch likely contributed to an increase in terrigenous siliciclastic material within the Pogonip Group. During the Early Ordovician Laurentia was located near the equator and was rotated clockwise from its current orientation. Major ocean currents and storm path/wind directions in the Northern Hemisphere during the Early Ordovician were likely northeast to southwest due to the position of Laurentia and the Coriolis Effect. These combined

factors may have resulted in the transportation of higher volumes of siliciclastic material (fine sand, silt, and shale) into the Ibex Basin from the emergent Tooele Arch located to the north and the exposed craton located to the east, thus explaining the increased volume of sand, silt, and shale within the Pogonip Group.

CONCLUSIONS

The Garden City Formation (~403 m thick) and the Pogonip Group (~787 m thick, excluding the Kanosh Shale and Lehman Formation) are coeval Early to Middle Ordovician (~488-466 Ma) successions of mixed carbonate and siliciclastic rock units deposited under normal marine conditions on a shallow carbonate ramp on the western margin of Laurentia. The Garden City Formation was deposited in the Northern Utah Basin and is located in northeastern Utah and southeastern Idaho. The Pogonip Group was deposited in the Ibex Basin and is located in west central Utah and eastern Nevada. These two basins experienced different rates of thermal subsidence following the Neoproterozoic rifting along the western margin of Laurentia that resulted in significant thickness differences between rock units and varying lithologic expressions of eustatic change. The Garden City Formation is interpreted as being deposited closer to the hinge zone of the subsiding passive margin. This resulted in lower rates of subsidence and may explain the thickness difference between the Pogonip Group and Garden City Formation. The Tooele Arch, House Range Embayment, and Wah Wah Arch are regional tectonic elements that likely contributed to lithologic differences between the two rock units.

The Garden City Formation and the Pogonip Group are interpreted as coeval based on the correlation of established macrofossil assemblage zones and conodont zones. This correlation was verified by the lowest occurrence of conodont species *Scolopodus filosus* and *Scalpellodus n. sp. A* of the Low Diversity Interval at around 57 m in the Green Canyon Garden City Formation section. The lowest occurrence of these conodont species coincides with the second positive $\delta^{13}C$ excursion in both the Garden

City Formation and the Pogonip Group, confirming their correlative relationship.

As hypothesized, new $\delta^{13}C$ data from the Garden City Formation and the Pogonip Group are interpreted to be correlative and represent primary sea water $\delta^{13}C$ trends for the Lower and early Middle Ordovician. Trends in $\delta^{13}C$ data do not appear to reflect significant local factors influencing $\delta^{13}C$ values and likely represent global $\delta^{13}C$ trends of primary seawater chemistry. This interpretation is based on correlation with $\delta^{13}C$ trends from the Argentine Precordillera, western Newfoundland, and the $\delta^{13}C$ global curve. Fluctuations in $\delta^{13}C$ values at near the bases of the Garden City Formation and the Pogonip Group do not appear to reflect changes in sea level. These fluctuations appear to represent global changes in Ordovician sea water $\delta^{13}C$ based on the correlation of similar fluctuations in $\delta^{13}C$ values from other locations. $\delta^{18}O$ data from the Garden City Formation and the Pogonip Group do not show similar trends and are interpreted as being altered through diagenetic processes.

Insoluble residue trends from the Garden City Formation and the Pogonip Group are similar as hypothesized. Insoluble residue increases from the bottom to the top of each section suggesting a basinward progradation of craton-derived siliciclastic debris as sea level fell. This drop in sea level is representative of onset of the regressive upper portion of the Sauk III supersequence. The Pogonip Group is interpreted to have been deposited closer to siliciclastic sources based on the occurrence of thin, poorly-lithified sandstones and a slightly higher amount of insoluble residue.

Nine sequences occur within the Pogonip Group. Eight representative sequences are located within the Garden City Formation based on biostratigraphic and

chemostratigraphic correlations between the two rock units and increases in insoluble residue at sequence boundaries. These sequences are primarily expressed as deepening upward packages containing high energy silty/sandy lowstand deposits topped by lower energy highstand deposits. Important sequence boundaries mark the Sauk III-m to Sauk IV-m transition and also the Ibexian-Whiterockian Series boundary. Meter-scale cycles are common within both rock units and are likely related to Milankovitch cycles.

Statistical analysis of point count data from the Pogonip Group and Garden City Formation indicate a cyclical repetition in lithologies within sequences, which suggests that changes in eustasy resulted in the generation of sea-level related lithofacies. High-energy lithofacies with high siliciclastic content are associated with low sea-level and are found at the bottom of sequences, while lower-energy lithofacies with low quartz content associated with high sea-level are found upper portion of sequences. PCA and cluster analysis were instrumental in segregating lowstand and highstand deposits, especially lowstand and highstand intraformational conglomerates. PCA and cluster analysis indicates that intraformational conglomerates, which occur as highstand deposits, generally contain more abundant peloids/pellets than lowstand intraformational conglomerates.

This study has provided a unique opportunity to compare new and existing data sets from two coeval sedimentary basins deposited along the western margin of Laurentia. It demonstrates the usefulness of employing multiple correlative tools in order to better understand the lithologic, geochemical, and paleontological expressions of eustatic change in basins with different tectonic settings.

REFERENCES

ADRAIN, J. M., LEE, D. C., WESTROP, S. R., CHATTERTON, B. D. E., AND LANDING, E., 2003, Classification of the trilobite subfamilies Hystricurinae and Hintzecurinae subfam. nov., with new genera from the Lower Ordovician (Ibexian) of Idaho and Utah: Memoirs of the Queensland Museum, v. 48, p. 553-586.

ADRAIN, J. M., MCADAMS, N. E. B., AND WESTROP, S. R., 2009, Trilobite biostratigraphy and revised bases of the Tulean and Blackhillsian Stages of the Ibexian Series, Lower Ordovician, western United States: Memoirs of the Association of Australasian Palaeontologists, no. 37, p. 541-610.

ADRAIN, J. M., KARIM, T. S., WESTROP, S. R., AND LANDING, E., 2014, Trilobite biostratigraphy of the Stairsian Stage (upper Tremadocian) of the Ibexian Series, Lower Ordovician, western United States: Memoirs of the Association of Australasian Palaeontologists, no. 45, p. 167–214.

ALLMENDINGER, R. W., FARMER, H., HAUSER, E. C., SHARP, J. W., VON TISH, D., OLIVER, J., AND KAUFMAN, S., 1986, Phanerozoic tectonics of the Basin and Range – Colorado Plateau transition from COCORP data and geologic data, *in* Barazangi, M., and Brown, L., eds, Reflection seismology - The continental crust: American Geophysical Union Geodynamics Series, v. 14, p. 257-268.

ÁLVARO, J. J., BAULUZ, B., SUBÍAS, I., PIERRE, C. AND VIZCAÏNO, D., 2008, Carbon chemostratigraphy of the Cambrian-Ordovician transition in a midlatitude mixed platform, Montagne Noire, France: Geological Society of America Bulletin 120, p. 962-975.

AZMY, K., AND LAVOIE, D., 2009, High-resolution isotope stratigraphy of the Ordovician St. George Group of western Newfoundland, Canada: implications for global correlation: Canadian Journal of Earth Sciences, v. 46, p. 403-423.

BANNER, J. L., AND HANSON, G. N., 1990, Calculation of simultaneous isotopic and trace element variations during water interaction with applications to carbonate diagenesis: Geochimica et Cosmochimica Acta, v. 54, p. 3123-3137.

BASSETT, D., MACLEOD, K. G., MILLER, J. F., AND ETHINGTON, R. L., 2007, Oxygen isotopic composition of biogenic phosphate and the temperature of Early Ordovician seawater: Palaios, v. 22, p. 98-103.

BENNER, J. S., EKDALE, A. A., & DE GIBERT, J. M., 2004, Macroborings (Gastrochaenolites) in Lower Ordovician hardgrounds of Utah: sedimentologic, paleoecologic, and evolutionary implications: Palaios, v. 19, p. 543-550.

BERGSTRÖM, S. M., CHEN, X., GUTIÉRREZ-MARCO, J. C. AND DRONOV, A., 2009, The new chronostratigraphic classification of the Ordovician System and its relations to major regional series and stages and to $\delta^{13}C$ chemostratigraphy: Lethaia, v. 42, p. 97-107.

BERRY, W. B. N., 1962, Comparison of some Ordovician limestones: American Association of Petroleum Geologists Bulletin 46, p. 605-615.

BOND, G. C., NICKESON, P. A., AND KOMINZ, M. A., 1984, Breakup of a supercontinent between 625 Ma and 555 Ma - New evidence and implications for continental histories: Earth and Planetary Science Letters, v. 70, p. 325-345.

BOND, G. C., KOMINZ, M. A., STECKLER, M. S., AND GROTZINGER, J. P., 1989, Role of thermal subsidence, flexure, and eustasy in the evolution of Early Paleozoic passive-margin carbonate platforms, *in* Crevello, P. D. and Wilson, J. L., eds., Controls on Carbonate Platform and Basin Development: SEPM Special Publication 44, p. 39-62.

BRAITHWAITE, L. F., 1969, Graptolites from the Pogonip Group (Lower Ordovician) of western Utah [Ph. D. dissertation]: Provo, Utah, Brigham Young University, 152 p.

BRAITHWAITE, L. F., 1976, Graptolites from the lower Ordovician Pogonip Group of western Utah: Geological Society of America Special Paper 166, p. 1-106.

BUGGISCH, W., KELLER, M. AND LEHNERT, O., 2003, Carbon isotope record of late Cambrian to Early Ordovician carbonates of the Argentine Precordillera: Palaeogeography, Palaeoclimatology, Palaeoecology, v. 195, p. 357–373.

BURGESS, C. J., 1979, The development of a Lower Jurassic carbonate tidal flat, Central High Atlas, Morocco, 2: Diagenetic history: Journal of Sedimentary Research, v. 49, p. 413-427.

CATUNEANU, O., 2006, Principals of Sequence Stratigraphy: Elsevier, Oxford, 375 p. Compare to Braithwaite

CHURCH, S. B., 1991, A new Lower Ordovician species of *Calathium*, and skeletal structure of western Utah Calathids: Journal of Paleontology, v. 65, p. 602-610.

CLARK, T. H., 1935, A new Ordovician graptolite locality in Utah: Journal of Paleontology, v. 9, p. 239-246.

COOK, G. A., AND LAUER, C. M., 1968, Oxygen, *in* Clifford, A. H., ed., The Encyclopedia of the Chemical Elements: New York, Reinhold Book Corporation, p. 499–512.

CRAIG, H., 1957, Isotopic standards for carbon and oxygen and correction factors for massspectrometric analysis of carbon dioxide: Geochimica et Cosmochimica Acta, v. 12, p. 133–149.

CRAMER, B.D., SALTZMAN, M.R., 2005, Sequestration of ^{12}C in the deep ocean during the early Wenlock (Silurian) positive carbon isotope excursion: Palaeogeography, Palaeoclimatology, Palaeoecology, v. 219, p. 333-349.

DAHL, R. M., 2012, A paleoenvironmental analysis of Gastropods from the Middle Ordovician, Ibex region, Utah [MS Thesis]: Riverside, University of California, 59 p.

DATTILO, B. F., 1993, The Lower Ordovician Fillmore Formation of western Utah: Storm-dominated sedimentation on a passive margin: Brigham Young University Geology Studies, v. 39, p. 71-100.

DICKINSON, W. R., 2006, Geotectonic Evolution of the Great Basin: Geosphere, v. 2, p. 353-368.

DICKSON, J. A. D., 1965, A modified technique for carbonates in thin section: Nature, v. 205, p. 587.

DRUCE, E. C., AND JONES, P. J., 1971, Cambro-Ordovician conodonts from the Burke River structural belt, Queensland: Australian: Bureau of Mineral Resources Bulletin 110, 167 p.

DUNHAM, R. J., 1962, Classification of carbonate rocks according to depositional texture, *in* Ham, W. E., ed., Classification of Carbonate Rocks: American Association of Petroleum Geologists Memoir 1, p. 108-121.

EDWARDS, C. T., AND SALTZMAN, M. R., 2014, Carbon isotope ($\delta^{13}Ccarb$) stratigraphy of the Lower–Middle Ordovician (Tremadocian–Darriwilian) in the Great Basin, western United States: Implications for global correlation: Palaeogeography, Palaeoclimatology, Palaeoecology, v. 399, p. 1-20.

ELRICK, M., AND SNIDER, A. C., 2002, Deep-water stratigraphic cyclicity and carbonate mud mound development in the Middle Cambrian Marjum Formation, House Range, Utah, USA: Sedimentology, v. 49, p. 1021-1047.

EMBRY, A. F., AND KLOVAN, J. E., 1971, A Late Devonian reef tract on Northeastern Banks Island, NWT: Canadian Petroleum Geology Bulletin 19, p. 730-781.

EMERY, D., AND MYERS, K. J., 1996, Sequence Stratigraphy: Oxford, U. K., Blackwell, 297 p.

ETHINGTON, R. L., AND CLARK, D. L., 1964, Conodonts from the El Paso Formation (Ordovocian) of Texas and Arizona: Journal of Paleontology, v. 38, p. 685-704.

ETHINGTON, R. L., AND CLARK, D. L., 1971, Lower Ordovician conodonts in North America, *in* Sweet, W. C. and Bergstrom, S. M., eds., Symposium on Conodont Biostratigraphy: Geological Society of America Memoir 127, p. 63–82.

ETHINGTON, R. L., AND CLARK, D. L., 1981, Lower and Middle Ordovician conodonts from the Ibex area, western Millard County, Utah: Brigham Young University Geology Studies, v. 28, pt. 2, 155 p.

ETHINGTON, R. L., ENGEL, K. M., AND ELLIOTT, K. L., 1987, An abrupt change in conodont faunas in the Lower Ordovician of the Midcontinent Province, *in* Aldridge, R.J., ed., Palaeobiology of Conodonts: Chichester, U.K., Ellis Horwood Limited, p. 111-127.

EVAMY, B. D., 1963, The application of a chemical staining technique to a study of dedolomitization: Sedimentology, v. 2, p. 164-170.

EVANS, K. R., MILLER, J. F., AND DATTILO, B., 2003, Sequence stratigraphy of the Sauk sequence: 40th anniversary field trip in western Utah, *in* T. W. Swanson, ed., Western Cordillera and adjacent areas: Geological Society of America Field Guide 4, p. 17-35.

FINNEGAN, S., AND DROSER, M. L., 2005, Relative and absolute abundance of trilobites and rhynchonelliform brachiopods across the Lower/Middle Ordovician boundary, eastern Basin and Range: Paleobiology, v. 31, p. 480-502.

FLUGEL, E., 1982, Microfacies Analysis of Limestones: New York, Springer-Verlag, 418 p.

FOLK, R. L., 1965, Some aspects of recrystallization in ancient Limestones, *in* Pray, L. C., and Murray, R. C., eds., Dolomitization and Limestone Diagenesis: Society of Economic Paleontologists and Mineralogists, Special Publication 13, p. 14-48.

FRANCIS, G. G., 1972, Stratigraphy and environmental analysis of the Swan Peak Formation and Eureka Quartzite, Northern Utah [M.S. Thesis]: Logan, Utah State University, 53 p.

FURNISH, W. M., 1938, Conodonts from the Prairie du Chien beds of the upper Mississippi Valley: Journal of Paleontology, v. 12, p. 318–340.

GAHN, F. J., 2006, Garden City of echinoderms: a new early Ordovician lagerstätte from Idaho and Utah: Geological Society of America Abstracts with Programs, v. 38, no. 7, p. 383.

GEOLOGY IN: Sequence stratigraphy: http://www.geologyin.com/2015/09/sequence-stratigraphy.html

GREEN, D. C., AND HERRING, D. M., 2013, Structural architecture of the Confusion Range, west-central Utah: A Sevier Fold-thrust Belt and Frontier Petroleum Province: Utah Geological Survey Open-File Report 613, 22 p.

HANSEN, A. M., 1949, Geology of the southern Malad Range and vicinity in northern Utah [M.S. Thesis]: Madison, University of Wisconsin, 128 p.

HAQ, B. U., AND SCHUTTER, S. R., 2008, A chronology of Paleozoic sea-level changes: Science, v. 322, p. 64-68.

HAYES, J. M., STRAUSS, H., AND KAUFMAN, A. J., 1999, The abundance of ^{13}C in marine organic matter and isotopic fractionation in the global biogeochemical cycle of carbon during the past 800 Ma: Chemical Geology v. 161, p. 103–125.

HINDS, R. W., 1970, Ordovician bryozoa from the Pogonip Group of Millard County, western Utah: Brigham Young University Research Studies, v. 17, no. 1, p. 19-40.

HINTZE, L. F., 1951, Early Ordovician detailed stratigraphic sections for western Utah: Utah Geological and Mineralogical Survey Bulletin 39, 99 p.

HINTZE, L. F., 1952, Lower Ordovician trilobites from western Utah and eastern Nevada. Utah Geological and Mineralogical Survey Bulletin 48, 249 p.

HINTZE, L. F., 1954, *Presbynileus* and *Protopresbynileus*, new generic names proposed for *Pseudonileus* and *Paranileus* Hintze: Journal of Paleontology, v. 28, p. 119.

HINTZE, L. F., 1959, Ordovician regional relationships in north-central Utah and adjacent areas: Intermountain Association of?? Petroleum Geologists Guidebook 10, p. 46-53.

HINTZE, L. F., 1973, Lower and Middle Ordovician stratigraphic sections in the Ibex Area, Millard County, Utah: Geologic History of Utah: Brigham Young University Geology Studies, v. 20, no. 3, p. 21-26.

HINTZE, L. F., 1982, Ibexian Series (Lower Ordovician) type section, western Utah, U.S.A, *in* The Ordovician System in the United States of America: Ottawa, Canada and Paris, France, International Union of Geological Sciences Publication 12, p. 7-10.

HINTZE, L. F., AND DAVIS, F. D., 2002a, Geologic map of the Wah Wah Mountains North 30′ x 60′ quadrangle and part of the Garrison 30′ x 60′ quadrangle, southwest Millard County and part of Beaver County, Utah: Utah Geological Survey Map 182, scale 1:100,000.

HINTZE, L. F., AND DAVIS, F. D., 2002b, Geologic map of the Delta 30′ x 60′ quadrangle and part of the Lynndyl 30′ x 60′ quadrangle, northeast Millard County and parts of Juab, Sanpete, and Sevier Counties, Utah: Utah Geological Survey Map 184, scale 1:100,000.

HINTZE, L. F., AND DAVIS, F. D., 2002c, Geologic map of the Tule Valley 30′ x 60′ quadrangle and parts of the Ely, Fish Springs, and Kern Mountains 30′ x 60′ quadrangles, northwest Millard County, Utah: Utah Geological Survey Map 186, scale 1:100,000.

HINTZE, L. F., AND DAVIS, F. D., 2003, Geology of Millard County, Utah: Utah Geological Survey Bulletin 133, p. 69-92.

HINTZE, L. F., DAVIS, F. D., ROWLEY, P. D., CUNNINGHAM, C. G., STEVEN, T. A., AND WILLIS, G. C., 2003, Geologic map of the Richfield 30′ x 60′ quadrangle, southeast Millard County and parts of Beaver, Piute, and Sevier Counties, Utah: Utah Geological Survey Map 195, scale 1:100,000.

HINTZE, L. F., 1988, Geologic History of Utah: Brigham Young University Geology Studies Special Publication 7, 202 p.

HINTZE, L. F., AND KOWALIS, B. J., 2009, Geologic History of Utah: Brigham Young University Geology Studies, v. 9, 225 p.

HOSE, R. K., 1977, Structural geology of the Confusion Range, west-central Utah: Geological Survey Professional Paper, no.971. Washington D. C., United States Government Printing Office, 9 p.

JAMES, N. P., AND KENDALL, A. C. 1992, Introduction to carbonate and evaporite facies models, *in* Walker, R. G., and James, N. P., eds., Facies Models: Response to Sea Level Change: Geological Association of Canada, GeoText 1, p. 265-275.

JENSEN, R. G., 1967, Ordovician brachiopods from the Pogonip Group of Millard County, western Utah: Brigham Young University Geology Studies, v. 14, p. 67-100.

JOHNS, R. A., 1994, Ordovician lithistid sponges of the Great Basin: Nevada Bureau of Mines and Geology, NBMG Open-file Report 94, 199 p.

KUMP, L. R., AND ARTHUR, M. A., 1999, Interpreting carbon-isotope excursions: carbonates and organic matter: Chemical Geology, v. 161, p. 181-198.

KINSMAN, D. J. J., 1973, Dolomitization process in sabkha environment: Abstract: American Association of Petroleum Geologists Bulletin 57, no. 4, p. 788-789.

KEHOE, K. W., DAVIS, C. R., LIDDELL, W. D., AND NEWELL, D. L., 2014, Bio-, chemo- and sequence stratigraphy of Lower Ordovician units from differing depositional settings along the western margin of northern Laurentia: Geological Society of America Abstracts with Programs, v. 46, no. 6, p.152.

KOUCHINSKY, A., BENGTSON, S., GALLET, Y., KOROVNIKOV, I., PAVLOV, V., RUNNEGAR, B., AND ZIEGLER, K., 2008, The SPICE carbon isotope excursion in Siberia: a combined study of the upper Middle Cambrian–lowermost Ordovician Kulyumbe River section, northwestern Siberian Platform: Geological Magazine, v. 145, p. 609-622.

LANDING, E., 1981, Conodont biostratigraphy and thermal color alteration indices of the Upper St. Charles and Lower Garden City Formations, Bear River Range, Northern Utah and Southeastern Idaho: U.S. Department of the Interior Geological Survey, Open-File Report 81-740, 29 p.

LANE, N. G., 1970, Lower and Middle Ordovician crinoids from west-central Utah: Brigham Young University.: Geologic Studies, v. 17, p. 3-17.

LEE, D. C., AND CHATTERTON, B. D., 1997, Hystricurid trilobite larvae from the Garden City Formation (Lower Ordovician) of Idaho and their phylogenetic implications. Journal of Paleontology, v. 71, p. 862-877.

LINDSTRÖM, M., 1955, Conodonts from the lowermost Ordovician strata of south-central Sweden: Geologiska Föreningens I Stockholm, Förhandlingar, v. 76, p. 517–604.

LOWE, M., AND GALLOWAY, C. L., 1993, Provisional geologic map of the Smithfield quadrangle, Cache County, Utah: Utah Geological Survey.

MARENCO, P. J., MARENCO, K. N., LUBITZ, R. I., AND NIU, D., 2013, Contrasting long-term global and short-term local redox proxies during the Great Ordovician Biodiversification Event: a case study from Fossil Mountain, Utah, USA: Palaeogeography, Palaeoclimatology, Palaeoecology, v. 377, p. 45-51.

MARSHALL, J. D., BRENCHLEY, P. J., MASON, P., WOLFF, G. A., ASTINI, R. A., HINTS, L., AND MEIDLA, T., 1997, Global carbon isotopic events associated with mass extinctions and glaciation in the Late Ordovician. Palaeogeography, Palaeoclimatology, Palaeoecology, v. 132, p. 195-210.

METZGER, J. G., AND FIKE, D. A., 2013, Techniques for assessing spatial heterogeneity of carbonate δ13C values: implications for craton-wide isotope gradients: Sedimentology, v. 60, p. 1405-1431.

MILLER, J. F., 1969, Conodont fauna of the Notch Peak Limestone (Cambro-Ordovician), House Range, Utah: Journal of Paleontology, v. 43, p. 413-439.

MILLER, J. F., 1978, Upper Cambrian and lowest Ordovician conodont faunas of the House Range, *in* Miller, J.F., ed., Upper Cambrian to Middle Ordovician conodont faunas of western Utah: S.W. Missouri State University Geoscience Series 5, p. 1-33.

MILLER, J. F., 1988, Conodonts as biostratigraphic tools for redefinition and correlation of the Cambrian-Ordovician boundary: Geological Magazine, v. 125, p. 347-362.

MILLER, J. F., TAYLOR, M. E., STITT, J. H., ETHINGTON, R. L., HINTZE, L. F., AND TAYLOR, J. F., 1982, Potential Cambrian-Ordovician boundary stratotype sections in the western United States, *in* Bassett, M.G., and Dean, W.T., eds., The Cambrian-Ordovician boundary; Sections, Fossil Distributions, and Correlations: National Museum of Wales (Cardiff), Geological Series 3, p. 155-180.

MILLER, J. F., EVANS, K. R., LOCH, J. D., ETHINGTON, R. L., AND STITT, J. H., 2001, New lithostratigraphic units in the Notch Peak and House formations (Cambrian–Ordovician), Ibex area, western Millard County, Utah: Brigham Young University Geology Studies, v. 46, p. 35-69.

MILLER, J. M., EVANS, K. R., LOCH, J. D., ETHINGTON, R. L., STITT, J. H., HOLMER, L., AND POPOV, L. E., 2003, Stratigraphy of the Sauk III interval (Cambrian–Ordovician) in the Ibex Area, western Millard County, Utah and central Texas: Brigham Young University, Geology Studies, v. 47, p. 23-118.

MILLER, J. F., ETHINGTON, R. L., EVANS, K. R., HOLMER, L. E., LOCH, J. D., POPOV, L. E., REPETSKI, J. E., RIPPERDAN, R. L., AND TAYLOR, J. F., 2006, Proposed stratotype for the base of the highest Cambrian stage at the first appearance datum of *Cordylodus andresi*, Lawson Cove section, Utah, U.S.A.: Palaeoworld 15, no. 3, p. 385-405.

MILLER, J. F., EVANS, K. R., AND DATTILO, B. F., 2012, The great American carbonate bank in the Miogeocline of Western Central Utah: tectonic influences on sedimentation, *in* Derby, J. R., Fritz, S. A., Longacre, W. A., and Sembach, C.A., eds., The Great American Carbonate Bank: The Geology and Economic Resources of the Cambrian-Ordovician Sauk Megasequence of Laurentia: American Association of Petroleum Geologists Memoir 98, p. 796-854.

MITCHUM, R. M., JR., 1977, Seismic Stratigraphy and global changes of sea level, part 11: Glossary of terms used in seismic stratigraphy, *in* Payton, C. E., ed., Seismic Stratigraphy-Applications to Hydrocarbon Exploration: American Association of Petroleum Geologists Memoir 26, p. 205-212.

MORGAN, S. K., 1988, Petrology of passive-margin eperic sea sediments: The Garden City Formation, north-central Utah [M.S. thesis]: Logan, Utah State University, 168 p.

MORGAN, W. A., 2012, Sequence stratigraphy of the great American carbonate bank, *in* Derby, J. R., Fritz, R. D., Longacre, S. A., Morgan, W. A., and Sternbach, C. A., eds., The Great American Carbonate Bank: The Geology and Economic Resources of the Cambrian- Ordovician Sauk Megasequence of Laurentia: American Association of Petroleum Geologists Memoir 98, p. 37-79.

MUNNECKE, A., CALNER, M., HARPER, D. A., AND SERVAIS, T., 2010, Ordovician and Silurian sea–water chemistry, sea level, and climate: A synopsis: Palaeogeography, Palaeoclimatology, Palaeoecology, v. 296, p. 389-413.

NEUMANN, A. C., AND LAND, L. S., 1975, Lime mud deposition and calcareous algae in the Bight of Abaco, Bahamas: A budget: Journal of Sedimentary Petrology, v. 45, p. 763-786.

OAKS, R. Q., JR., JAMES, W. C., FRANCIS, G. G., AND SCHULINGKAMP, W. J., 1977, Summary of Middle Ordovician stratigraphy and tectonics, northern Utah, southern and central Idaho, *in* Keisey, E. L., Lawson, D. E., Norwood, E. R., Wach, P. H., and Hale, L. A., eds., Rocky Mountain Thrust Belt Geology and Resources: Wyoming Geological Association Guidebook, 29th Annual Field Conference, p. 101-118.

OSLEGER, D. A., AND READ, J. F., 1993, Comparative analysis of methods used to define eustatic variations in outcrop: Late Cambrian interbasinal sequence development: American Journal of Science, v. 293, p. 157-216.

OSLEGER, D. A., AND MONTAÑEZ, I. P., 1996, Cross-platform architecture of a sequence boundary in mixed siliciclastic-carbonate lithofacies, Middle Cambrian, southern Great Basin, USA: Sedimentology, v. 43, p. 197-217.

PALMER, A. R., 1981, Subdivision of the Sauk sequence, *in* Taylor, M. E., ed., Short Papers for the Second Symposium on the Cambrian System: U.S. Geological Survey Open-File Report 81-743, p. 160-162.

PANDER, C. H., 1856, Monographie der fossilen Fische des silurischen Systems der russisch-baltischen Gouvernements: St. Petersburg, Buchdruckerei der Kaiserlichen Akademie der Wissenschaften, 91 p.

PEARCE, H., 2012, A study of the bioherms of the Early Ordovician Garden City Formation and a literature review of Early Ordovician organic buildups [M.S. Thesis]: Logan, Utah State University, 67 p.

POOLE, F. G., STEWART, J. H., PALMER, A. R., SANDBERG, C. A., MADRID, R. J., ROSS, R. J., JR., HINTZE, L. F., MILLER, M. M., AND WRUCKE, C. T., 1992, Latest Precambrian to latest Devonian time: Development of a continental margin, *in* Burchfiel, B. C., Lipman, P. W., and Zoback, M. L., eds., The Cordilleran Orogen: Conterminous U. S.: Boulder, Colorado, Geological Society of America, Geology of North America, v. G-3, p. 9-56.

POSAMENTIER, H. W., JERVEY, M. T., AND VAIL, P. R., 1988, Eustatic controls on clastic deposition I – Conceptual framework, *in* Wilgus, C.K., Hastings, B.S., Kendall, C.G. St. C., Posamentier, H.W., Ross, C.A., and Van Wagoner, J.C., eds., Sea Level Changes – An Integrated Approach: Society of Economic Paleontologists and Mineralogists Special Publication, v. 42, p. 110-124.

REPETSKI, J. E., 1975, Conodonts from the El Paso Group (Lower Ordovician) of West Texas [unpublished Ph. D. thesis]: Colombia, University of Missouri, 245 p.

RIGBY, J. K., 1958, Geology of the Stansbury Mountains, eastern Tooele County, Utah: Utah Geological Society: Guidebook to the Geology of Utah, no. 13, p. 1-135.

RIGBY, J. K., 1962, Canadian and Chazyan receptaculitids from Utah and Nevada: Geological Society of America Special Paper 68, p. 51-52.

RIGBY, J. K., 1965, Evolution of Lower and Middle Ordovician sponge reefs in western Utah: Geological Society of America Special Paper 87, p. 137.

RIGBY, J. K., 1971, Sponges and reef and related facies through time: Proceedings of North American Paleontological Convention, Chicago, pt. J, p. 1374-1388.

RIGBY, J.K., AND GILLAND, J.K., 1977, A new fossil sponge from the Ordovician Garden City limestone of southeastern Idaho: Western North American Naturalist, v. 37, p. 475-480.

RIPPERDAN, R. L., AND MILLER, J. F., 1995, Carbon isotope ratios from the Cambrian-Ordovician boundary section at Lawson Cove, Ibex area, Utah, *in* Cooper, J.D., Droser, M.L., and Finney, S.C., eds., Ordovician Odyssey: Short Papers for the Seventh International Symposium on the Ordovician System: Pacific Section Society for Sedimentary Geology, p. 129-132.

RIPPERDAN, R. L., MAGARITZ, M., NICOLL, R. S., AND SHERGOLD, J. H., 1992, Simultaneous changes in carbon isotopes, sea level, and conodont biozones within the Cambrian–Ordovician boundary interval at Black Mountain, Australia: Geology, v. 20, p. 1039-1042.

ROSS, R. J., 1949, Stratigraphy and trilobite faunal zones of the Garden City Formation, northeastern Utah: American Journal of Science, v. 247, p. 472-491.

ROSS, R. J., JR., 1951, Stratigraphy of the Garden City Formation in northeastern Utah, and its trilobite faunas: Peabody Museum of Natural History, Yale University, Bulletin 6, 161 p.

ROSS, R. J., JR., 1953, Additional Garden City (Early Ordovician) trilobites: Journal of Paleontology, v. 27, p. 633-646.

ROSS, R. J., 1968, Brachiopods from the Upper Part of the Garden City Formation (Ordovician) North-central Utah. US Government Printing Office, p. 1-11.

ROSS, R. J., JR., and 27 others, 1982, The Ordovician System in the United States: correlation chart and explanatory notes. No. 12. International Union of Geological Sciences, 73 p.

ROSS, R. J., JR., AND ETHINGTON, R. L., 1992, North American Whiterock Series suited for global correlation, *in* Webby, B.D., and Laurie, J.R., eds., Global Perspectives on Ordovician Geology (Proceedings of the Sixth International Symposium on the Ordovician System, Sydney, Australia): Rotterdam, Netherlands, A.A. Balkema, p. 153-170.

ROSS, R. J., JR., VALUSEK, J. E., AND JAMES, N. P., 1988, *Nuia* and its environmental significance, *in* Wolberg, D.L., ed., Contributions to Paleozoic Paleontology and Stratigraphy in Honor of Rousseau H. Flower: New Mexico Bureau of Mines and Mineral Resources Memoir 44, p. 115-121.

ROSS, R. J., JR, HINTZE, L. F., ETHINGTON, R. L., MILLER, J. F., TAYLOR, M. E., AND REPETSKI, J. E., 1997, The Ibexian, lowermost series in the North American Ordovician: United States Geological Survey Professional Paper 1579, 50 p.

ROSS JR., R. J., JAMES, N. P., HINTZE, L. F., AND POOLE, F. G., 1989, Architecture and evolution of a Whiterockian (Early Middle Ordovician) carbonate platform, Basin Ranges of western U.S.A., *in* Crevello, P.D., Wilson, J.L., Sarg, J.F., and Read, J.F., eds., Controls on Carbonate Platform and Basin Development, Society of Economic Paleontologists and Mineralogists Special Publication 44, p. 167–185.

ROSS, C. A., AND ROSS, J. R. P., 1995, North American Ordovician depositional sequences and correlations, *in* Cooper, J. D., ed., Ordovician Odyssey: Short Papers for the Seventh International Symposium on the Ordovician System: Pacific Section Society for Sedimentary Geology Publication 77, p. 309-313.

ROSS JR., R. J., HINTZE, L. F., ETHINGTON, R. L., MILLER, J. F., TAYLOR, M. E., REPETSKI, J. E., SPRINKLE, J., AND GUENSBURG, T. E., 1997, The Ibexian, lowermost series in the North American Ordovician, *in* Taylor, M. E., ed., Early Paleozoic Biochronology of the Great Basin, Western United States: U.S. Geological Survey Professional Paper 1579, 50 p.

RUDDIMAN, W. F., 2001, Earth's Climate: past and future: New York, W. H. Freeman and Company, 359 p.

SCHAEFFER, F. E., 1960, Stratigraphy of the Silver Island Mountains, *in* Schaeffer, F. E., ed., Geology of the Silver Island Mountains Box Elder and Tooele Counties, Utah and Elko County, Nevada, p. 15- 113.

SCHUMACHER, B. A., 2002, Methods for the determination of total organic carbon (TOC) in soils and sediments: Ecological Risk Assessment Support Center, 23 p.

SEARS, J. W., AND PRICE, R. A., 2003, Tightening the Siberian connection to western Laurentia: Geological Society of America Bulletin 115, p. 943-953.

SPRINKLE, J., 2007, New eocrinoids from the Lower Ordovician Garden City Formation, northeastern Utah and southeastern Idaho: Geological Society of America Abstracts with Programs, v. 39, no. 6, p. 74.

SPRINKLE, J., AND GUENSBURG, T. E., 1997, Echinoderm biostratigraphy, Appendix 4, *in* Ross, R.J., Jr., Hintze, L.F., Ethington, R. L., Miller, J.F., Taylor, M.E., and Repetski, J.E., The Ibexian, Lowermost Series in the North American Ordovician: U.S. Geological Survey Professional Paper 1579-A, p. 49-50.

STECKLER, M. S., 1981, Thermal and mechanical evolution of Atlantic-type margins [unpublished Ph. D. thesis]: New York, Columbia University, 261 p.

STOKES, W. L., 1986, Geology of Utah: Utah Museum of Natural History, University of Utah and Utah Geological and Mineral Survey, Occasional Paper 6, 280 p.

TAYLOR, M. E., AND LANDING, E., 1981, Upper St. Charles and Lower Garden City Formation, Blacksmith Fork Canyon, southern Bear River Range, Utah, *in* Taylor, M.E., and Palmer, A.R., eds., Cambrian Stratigraphy and Paleontology of the Great Basin and Vicinity, Western United States: Guidebook for Field Trip 1, 2nd International Symposium on the Cambrian Systems, p. 141-149.

TAYLOR, M. E., LANDING, E., AND GILLETT, S. L., 1981a, The Cambrian-Ordovician transition in the Bear River Range, Utah-Idaho: A preliminary evaluation, *in* Taylor, M.E., ed., Short Papers for the Second International Symposium on the Cambrian System: U.S. Geological Survey Open-File Report 81- 743, p. 222-227.

TAYLOR, M. E., GILLETT, S., LANDING, E., AND REPETSKI, J. E., 1981b, Newly discovered disconformity: Lower Paleozoic, Bear River Range, Utah-Idaho: U.S. Geological Survey Professional Paper 1275, 192 p.

TAYLOR, M. E., AND LANDING, E., 1982, Biostratigraphy of the Cambrian-Ordovician transition in the Bear River Range, Utah and Idaho, western United States, *in* Bassett, M.G., and Dean, W.T., eds., The Cambrian-Ordovician Boundary; Sections, Fossil Distributions, and Correlations: National Museum of Wales (Cardiff), Geological Series 3, p. 181-191.

TAYLOR, J. F., REPETSKI, J. E., AND ORNDORFF, R. C., 1992, The Stonehenge transgression: A rapid submergence of the central Appalachian platform in the Early Ordovician, *in* B. D. Webby and J. R. Laurie, eds., Global Perspectives on Ordovician Geology: Rotterdam, Balkema, p. 409-418.

TAYLOR, M. E., (ed.). 1997, Early Paleozoic Biochronology of the Great Basin, Wastern United States: U. S. Geological Survey Professional Paper 1579, p. 1-115.

THOMPSON, C. K., AND KAH, L.C., 2012, Sulphur isotope evidence for widespread euxinia and a fluctuating oxycline in Early to Middle Ordovician greenhouse oceans: Palaeogeography, Palaeoclimatology, Palaeoecology, v. 313, p. 189-214.

TROTTER, J. A., WILLIAMS, I. S., BARNES, C. R., LÉCUYER, C., AND NICOLL, R.S., 2008, Did cooling oceans trigger Ordovician biodiversification? Evidence from conodont thermometry: Science, v. 321, p. 550-554.

VAIL, P. R., MITCHUM, R. M. JR., AND THOMPSON, S., III, 1977, Seismic stratigraphy and global changes of sea level, part 4: Global Cycles of Relative Changes of Sea Level: Section 2. Application of Seismic Reflection Configuration to Stratigraphic Interpretation: American Association of Petroleum Geologists Memoir 26, p. 83-98.

VAN WAGONER, J. C., 1995, Overview of sequence stratigraphy of foreland basin deposits: Terminology, summary of papers, and glossary of sequence stratigraphy, *in* Van Wagoner, J. C., and Bertman, G. T., eds., Sequence Stratigraphy of Foreland Basin Deposits, American Association of Petroleum Geologists Memoir 64, p. ix-xxi.

WALKER, R. G., AND JAMES, N. P., eds., 1992, Facies Models: Response to Sea Level Change: Geological Association of Canada, Geotext 1, 409 p.

WENZEL, B., AND JOACHIMSKI, M. M., 1996, Carbon and oxygen isotopic composition of Silurian brachiopods (Gotland/Sweden): paleooceanographic implications: Palaeogeography, Palaeoclimatology, Palaeoecology, v. 122, p. 143-166.

WILSON, M. A., PALMER, T. J., GUENSBURG, T. E., FINTON, C. D., AND KAUFMAN, L. E., 1992, The development of an Early Ordovician hardground community in response to rapid sea-floor calcite precipitation: Lethaia, v. 25, p. 19-34.

WYATT, D., 1979, Carbonate mud mounds from the Lower Ordovician Wah Wah Limestone of the Ibex area, western Millard County, western Utah: Brigham Young University Geology Studies, v. 26, no. 2, p. 101-114.

YONKEE, W.A., AND WEIL, A.B., 2011, Evolution of the Wyoming salient of the Sevier fold-thrust belt, northern Utah to western Wyoming, *in* Sprinkel, D.A., Yonkee, W.A., and Chidsey, T.C. Jr., eds., Sevier Thrust Belt: Northern and Central Utah and Adjacent Areas: Utah Geological Association Publication 40, p. 1-56

APPENDICES

Appendix A. Green Canyon Garden City Formation Section

Green Canyon Garden City Formation Section

This section is located in the Bear River Range approximately 1.4 km up Green Canyon on the eastern flank of the Bear River Range (Sec. 19 & 20, T12N, R2 E, Smithfield, UT 7.5' Quadrangle, 1998). It was measured and described during the summer of 2014 by K.W. Kehoe and C.R. Davis in order to study Early and Middle Ordovician strata exposed above the Cambrian St. Charles Formation and below the Middle Ordovician Swan Peak Formation.

The base of the section is located at UTM zone 12 grid coordinates 436523 m E, 4624636 m N. This section trends uphill to the east northeast and the top of the section is located at UTM zone 12 gird coordinates 437030 m E, 4624937 m N. Access to the base of the section is by Green Canyon Drive (E 1900 N) which transitions into Forest Service Road 050.

SWAN PEAK FORMATION
Abrupt unconformable contact

TOTAL STRATA MEASURED (excluding the 12 m of erosional relief at the base of the Garden City Formation) OF THE GARDEN CITY FORMATION: 391.5 m

		Stratigraphic Position (m)	
Unit	*Description*	*Unit*	*Cumulative*
GC-25	Primarily medium- to thick-bedded wackestones. Additional lithologies include fossiliferous wackestones and packstones, and dolomitic mudstones, wackestones, and packstones.	32.5 m	403.6 m
GC-24	Primarily medium- to thick-bedded lime mudstones. Additional lithologies include fossiliferous wackestones and packstones, and recrystallized wackestones and packstones. Chert is common through this unit. Unit GC-U24 marks the beginning of the informal Upper Cherty Member of the Garden City Formation. Be consistent throughout	51.0 m	371.1 m
GC-23	Primarily thin- to medium- bedded intraformational conglomerates and laminated mudstone. Additional lithologies include fossiliferous wackestones and packstones.	55.3 m	320.1 m
GC-22	Primarily thin- to medium- bedded laminated mudstones and intraformational conglomerates. Additional lithologies include fossiliferous wackestones and packstones.	15.0 m	264.8 m
GC-21	Primarily thin- to thick-bedded wackestones with silty interbeds and intraformational conglomerates. Additional lithologies include fossiliferous wackestones.	9.6 m	249.8 m
GC-20	Primarily thin- to medium- bedded intraformational conglomerates. Intraclasts increase in size up through this unit.	2.4 m	240.2 m
GC-19	Primarily thin- to medium-bedded intraformational conglomerates and wackestones with black chert nodules. Additional lithologies include recrystallized packstones.	5.3 m	237.8 m
GC-18	Primarily thin- to thick-bedded lime mudstones with interbedded wackestones. Additional lithologies include intraformational conglomerates and fossiliferous packstones.	17.1 m	232.5 m
GC-	Primarily medium- to thick-bedded lime mudstones.	1.0 m	215.4 m

17	Additional lithologies include dolomitic wackestones.		
GC-16	Primarily thin- to thick-bedded lime mudstones. Additional lithologies include intraclastic fossiliferous wackestones and packstones.	15.2 m	214.4 m
GC-15	Primarily thin- to thick-bedded intraformational conglomerates, nodular shaly limestones, and shale interbeds. Additional lithologies include fossiliferous wackestones and packstones (dolomitic), lime mudstones, and recrystallized wackestones and mudstones.	86.7 m	199.2 m
GC-14	Primarily medium- to thick-bedded nodular wackestones. Additional lithologies include recrystallized silty wackestones.	5.8 m	112.5 m
GC-13	Primarily medium- to thick-bedded recrystallized limestones. Additional lithologies include fossiliferous packstones.	1.1 m	106.7 m
GC-12	Primarily medium- to thick-bedded intraformational conglomerates with interbedded wackestones. Additional lithologies include lime mudstones.	4.5 m	105.6 m
GC-11	Primarily medium- to thick-bedded wackestone and nodular lime mudstone. Additional lithologies include intraclastic fossiliferous packstones and argillaceous wackestones. Some elongate black chert bodies are also present in unit GC-U11.	5.3 m	101.1 m
GC-10	Primarily microbial/thrombolytic boundstones. There are 6 distinct boundstone horizons (algal reefs) each separated by bioturbated wackestone/nodular limestones interbeds. The algal reefs often have irregular undulating undersides which appear to have compressed and distorted the underlying wackestone beds. Individual algal mounds are rounded in shape and measure approximately 1.6 m high, 3 m wide, and vary in length from 1.5 to 3 m.	13.9 m	95.8 m
GC-9	Primarily medium- to thick-bedded wackestones and nodular limestones with silty/shaley layers. Additional lithologies include intraclastic fossiliferous packstones and wackestones.	13.9 m	91.9 m
GC-8	Primarily lime mudstones and wackestones. Additional lithologies include recrystallized wackestones and mudstones. Sedimentary structures include cross stratification in interbeds of wackestone.	3.2 m	68.0 m
GC-7	Primarily thin- to medium-bedded lime mudstones. Additional lithologies include recrystallized cherty packstones and intraformational conglomerates.	3.0 m	64.8 m

GC-6	Primarily thin- to medium- bedded coarse-grained limestones which grade into wackestones and packstones near the top of the unit. Additional lithologies include intraclastic fossiliferous wackestones and packstones, and recrystallized packstones.	5.1 m	61.8 m
GC-5	Primarily thin- to medium-bedded dolomitic packstones, wackestones, and lime mudstones. Many beds are heavily bioturbated and nodular. Fossils include brachiopods, crinoids, and trilobites.	6.0 m	56.7 m
GC-4	Similar to unit GC-U1 and contains primarily medium- to thick-bedded silty lime mudstones interbedded with thin beds of intraformational conglomerates. The argillaceous laminations are thinner than those of GC-U1 and additional lithologies include dolomitic packstones and intraclastic fossiliferous wackestones, packstones, and grainstones. Large intraclasts similar to those of GC-U2 are also found within this unit.	9.4 m	50.7 m
GC-3	Primarily thin- to medium bedded lime mudstones with shale interbeds and intraformational conglomerates. A 5 cm green shale separates GC-U3 and GC-U4. Additional lithologies include fossiliferous wackestones and packstones. Fossils include brachiopods, crinoids, and trilobites.	3.6 m	41.3 m
GC-2	Primarily thin- to thick-bedded intraformational conglomerates interbedded with lime mudstones. Intraclasts range from mm to decameter (dm) in size and often are coated with silty brown mud. Additional lithologies include fossiliferous wackestones with packstone lenses and recrystallized mudstones. Fossils include brachiopods, crinoids, and trilobites. Sedimentary structures include fine to medium argillaceous laminations, black chert beds, and ripples superimposed on mega-ripples.	1.7 m	37.7 m
GC-1	Primarily medium- to thick-bedded silty nodular lime mudstones, wackestones, and intraformational conglomerates. Intraclasts range from mm to cm in size and other lithologies include fossiliferous wackestones with packstone lenses, recrystallized silty mudstones, and argillaceous mudstones. Fossils include brachiopods, crinoids, and trilobites. Sedimentary structures include trace fossils (bioturbation), black chert nodules, fine to medium argillaceous laminations, and hummocky surfaces.	13.9 m	36.0 m

GC-0	Primarily thick-bedded coarse grained dolostones interbedded with sparse argillaceous silty mudstones and thin beds of intraformational conglomerates. Black and white chert nodules are present within this unit. Lowermost exposed outcrop of the Garden City Formation in this section in Green Canyon. Note: Cumulative thickness includes the 12 m of erosional relief at the base of the Garden City Formation.	10.1 m	22.1 m

Disconformity with approximately 12 m of erosional relief.
SAINT CHARLES FORMATION

Appendix B1. Garden City Formation Thin-Section Point Count Data

Sample Name	SC-0.0	SC-3.0	SC-5.0	SC-7.0	SC-10.0	GC-U1-0.0	GC-U1-3.0
Stratigraphic position (m)	12.0	15.0	17.0	19.0	22.0	22.1	25.0
Matrix	0	0	0	152	0	50	25
Algae	0	0	0	0	0	0	0
Brachiopods	0	0	0	0	0	4	22
Bryozoans	0	0	0	0	0	0	0
Calcispheres	0	0	0	0	0	0	0
Calcite Crystals	0	0	213	45	0	196	194
Cephalopods	0	0	0	0	0	0	0
Chert	0	0	0	0	0	0	6
Dolomite Crystals	296	280	0	0	292	7	17
Echinoderms	0	0	1	0	0	13	11
Intraclasts	0	0	72	0	0	0	0
Gastropods	0	0	0	0	0	0	0
Ostracods	0	0	0	0	0	0	0
Peloids/Pellets	0	0	0	0	0	0	0
Nuia	0	0	1	0	0	0	0
Pyrite/ Hematite	0	0	1	8	0	12	0
Quartz Grains	4	12	1	94	7	0	0
Radiolarians	0	0	0	0	0	0	0
Sponges/Spicules	0	0	11	0	0	0	0
Stylolites	0	8	0	0	0	1	3
Trilobites	0	0	0	0	0	11	20
Unknown Bioclasts	0	0	0	0	0	0	0
Veins	0	0	0	1	1	6	2

Sample Name	GC-U1-9.0	ISO-GC-U1-13.0	ISO-GC-U1-14.0	GC-U2-1.7	GC-U3-3.0A	GC-U4-3.0	GC-U4-9.0
Stratigraphic position (m)	31.0	35.0	36.0	37.7	40.7	44.4	50.4
Matrix	0	266	271	209	0	0	0
Algae	0	0	0	0	0	0	0
Brachiopods	0	0	2	27	19	13	4
Bryozoans	0	0	0	0	0	0	0
Calcispheres	0	0	0	0	0	0	0
Calcite Crystals	291	7	0	6	11	8	154
Cephalopods	0	0	0	0	0	0	0
Chert	0	0	0	0	0	0	0
Dolomite Crystals	0	0	0	2	0	0	118
Echinoderms	0	0	9	12	97	123	11
Intraclasts	0	0	0	16	130	146	0
Gastropods	0	0	0	0	0	0	0
Ostracods	0	0	0	0	0	0	0
Peloids/Pellets	0	0	0	1	9	1	0
Nuia	0	0	0	0	20	0	0
Pyrite/ Hematite	0	0	0	0	0	0	0
Quartz Grains	7	2	0	10	0	0	7
Radiolarians	0	0	0	0	0	0	0
Sponges/Spicules	0	4	2	0	0	0	0
Stylolites	0	19	13	1	0	0	0
Trilobites	0	0	1	5	14	9	6
Unknown Bioclasts	0	0	0	9	0	0	0
Veins	2	2	2	2	0	0	0

Sample Name	GC-U5-6.0	ISO-GC-U6-1.0	GC-U6-5.1	ISO-GC-U7-2.0	GC-U7-3.0	GC-U8-3.0	GC-U9-6.0
Stratigraphic position (m)	56.7	57.7	61.8	63.8	64.8	67.8	74.0
Matrix	11	26	10	0	102	157	15
Algae	0	1	1	0	0	0	0
Brachiopods	37	0	3	1	0	0	14
Bryozoans	0	2	0	0	0	0	0
Calcispheres	0	0	0	0	0	0	0
Calcite Crystals	174	39	138	237	46	110	77
Cephalopods	0	0	0	0	0	0	0
Chert	0	0	65	13	1	0	2
Dolomite Crystals	30	0	34	17	0	0	0
Echinoderms	4	6	0	2	0	1	3
Intraclasts	0	166	0	0	131	0	114
Gastropods	0	0	0	0	0	0	0
Ostracods	0	0	0	0	0	0	0
Peloids/Pellets	23	4	0	0	0	0	39
Nuia	0	0	0	2	11	1	8
Pyrite/ Hematite	0	0	0	0	0	0	0
Quartz Grains	1	1	0	20	0	0	2
Radiolarians	0	0	0	0	0	0	0
Sponges/Spicules	0	0	0	0	0	2	0
Stylolites	0	0	2	5	2	8	0
Trilobites	14	12	3	2	0	0	5
Unknown Bioclasts	6	43	42	0	4	8	6
Veins	0	0	2	1	3	13	15

Sample Name	GC-U9-12.0	GC-U10-1.0	GC-U10-7.5	GC-U10-13.5	GC-U11-0.0	GC-U11-3.0	GC-U12-0.0
Stratigraphic position (m)	80.0	82.9	89.4	95.4	95.8	98.8	101.1
Matrix	143	261	266	235	30	156	277
Algae	9	0	0	0	2	0	0
Brachiopods	7	0	0	0	9	0	0
Bryozoans	2	0	0	0	4	0	0
Calcispheres	0	0	2	0	0	0	0
Calcite Crystals	22	17	12	15	24	91	3
Cephalopods	0	0	0	0	0	0	0
Chert	0	0	0	0	0	0	0
Dolomite Crystals	10	0	0	4	24	0	0
Echinoderms	50	4	2	1	55	0	14
Intraclasts	38	0	0	0	36	0	0
Gastropods	10	0	0	0	0	0	0
Ostracods	0	0	0	0	0	0	0
Peloids/Pellets	0	0	0	0	3	26	0
Nuia	0	0	0	1	34	0	0
Pyrite/ Hematite	0	0	0	0	0	0	0
Quartz Grains	0	0	0	0	0	0	0
Radiolarians	0	0	0	0	0	0	0
Sponges/Spicules	0	0	0	0	0	0	0
Stylolites	0	7	10	22	0	15	6
Trilobites	4	0	0	0	5	0	0
Unknown Bioclasts	5	0	0	0	72	4	0
Veins	0	11	8	22	2	8	0

Sample Name	GC-U13-0.4	GC-U14-3.0	GC-U15-0.0	GC-U15-12.0	GC-U15-18.0	GC-U15-33.0	GC-U15-39.0
Stratigraphic position (m)	106.0	109.7	112.5	124.5	130.5	145.5	151.5
Matrix	18	121	33	61	14	103	102
Algae	0	0	3	0	0	0	0
Brachiopods	16	1	26	5	0	0	0
Bryozoans	0	0	3	2	0	0	0
Calcispheres	0	0	0	0	0	0	0
Calcite Crystals	34	124	16	196	184	164	147
Cephalopods	0	0	0	0	0	0	0
Chert	0	0	0	2	0	0	0
Dolomite Crystals	0	0	0	0	0	0	0
Echinoderms	138	0	75	6	0	0	1
Intraclasts	0	0	97	0	0	0	0
Gastropods	0	0	0	0	0	0	0
Ostracods	8	0	0	0	0	0	0
Peloids/Pellets	7	0	9	0	78	0	0
Nuia	0	0	1	0	0	0	0
Pyrite/ Hematite	0	0	0	0	0	0	0
Quartz Grains	6	46	6	0	15	0	4
Radiolarians	0	0	0	0	0	0	0
Sponges/Spicules	0	0	0	0	0	0	0
Stylolites	12	2	12	20	7	7	46
Trilobites	20	0	9	3	1	0	0
Unknown Bioclasts	41	0	10	3	0	0	0
Veins	0	6	0	2	1	26	0

Sample Name	GC-U15-45.0	GC-U15-60.0	GC-U15-69.0	GC-U15-72.0	GC-U15-75.0	GC-U15-81.0	GC-U15-86.65
Stratigraphic position (m)	157.5	172.5	181.5	184.5	187.5	193.5	199.2
Matrix	24	252	67	7	267	253	18
Algae	0	0	0	0	0	0	1
Brachiopods	10	0	1	10	0	2	11
Bryozoans	1	0	0	0	0	0	2
Calcispheres	0	0	0	0	0	0	0
Calcite Crystals	30	28	17	36	31	25	26
Cephalopods	0	0	0	0	0	0	0
Chert	0	0	0	0	0	0	0
Dolomite Crystals	45	0	0	17	0	0	0
Echinoderms	8	0	4	17	0	0	24
Intraclasts	152	0	205	182	0	0	202
Gastropods	0	0	0	0	0	0	0
Ostracods	0	0	0	0	0	0	0
Peloids/Pellets	0	0	0	0	0	0	0
Nuia	0	0	0	0	0	0	0
Pyrite/ Hematite	1	3	0	0	1	0	0
Quartz Grains	3	0	0	3	0	8	0
Radiolarians	0	0	0	0	0	0	0
Sponges/Spicules	0	0	0	0	0	0	0
Stylolites	0	14	0	6	1	6	4
Trilobites	16	2	1	1	0	2	3
Unknown Bioclasts	9	1	5	10	0	4	7
Veins	1	0	0	11	0	0	2

Sample Name	GC-U16-3.0	GC-U16-6.6	GC-U17-0.7	GC-U18-3.0	GC-U18-9.0	GC-U18-15.0	GC-U19-4.5
Stratigraphic position (m)	202.2	205.8	215.1	218.4	224.4	230.4	237.0
Matrix	276	21	241	122	257	76	28
Algae	0	5	0	10	0	19	0
Brachiopods	0	7	0	13	0	10	0
Bryozoans	0	1	0	1	0	0	0
Calcispheres	0	0	0	5	0	0	0
Calcite Crystals	18	22	3	23	32	33	232
Cephalopods	0	0	0	0	0	0	0
Chert	0	2	0	0	0	0	0
Dolomite Crystals	0	4	36	1	0	5	0
Echinoderms	0	63	0	38	0	0	0
Intraclasts	0	119	0	34	0	0	0
Gastropods	0	0	0	0	0	0	0
Ostracods	0	0	0	0	0	0	0
Peloids/Pellets	0	4	0	25	0	49	0
Nuia	0	0	0	6	0	12	0
Pyrite/ Hematite	0	0	0	0	0	0	0
Quartz Grains	0	0	0	2	0	10	38
Radiolarians	0	0	0	0	2	0	0
Sponges/Spicules	0	1	0	1	0	0	0
Stylolites	3	10	2	2	5	13	0
Trilobites	0	4	0	2	0	0	0
Unknown Bioclasts	0	17	0	15	0	50	0
Veins	3	20	18	0	4	23	2

Sample Name	GC-U20-0.0	GC-U21-3.0	GC-U21-9.0	GC-U22-0.0	GC-U22-3.0	GC-U22-12.0	GC-U23-0.0
Stratigraphic position (m)	237.8	243.2	249.2	249.8	252.8	261.8	264.8
Matrix	26	34	221	281	8	53	45
Algae	8	1	0	0	9	6	4
Brachiopods	14	15	0	0	40	10	16
Bryozoans	5	0	0	0	10	2	3
Calcispheres	0	0	0	0	0	0	0
Calcite Crystals	11	70	20	7	65	30	26
Cephalopods	0	0	0	0	0	0	0
Chert	0	5	0	0	5	2	1
Dolomite Crystals	16	21	0	0	14	2	14
Echinoderms	51	21	38	2	40	4	23
Intraclasts	129	0	9	0	48	136	78
Gastropods	0	0	0	0	0	0	0
Ostracods	0	0	0	0	0	0	0
Peloids/Pellets	15	55	0	0	17	18	43
Nuia	0	47	0	0	2	3	1
Pyrite/ Hematite	0	0	4	0	0	0	0
Quartz Grains	0	3	0	4	5	1	0
Radiolarians	0	0	0	0	0	0	0
Sponges/Spicules	0	0	0	0	0	0	1
Stylolites	3	7	4	1	6	7	11
Trilobites	4	0	0	0	2	6	10
Unknown Bioclasts	16	21	0	0	29	20	24
Veins	2	0	4	5	0	0	0

Sample Name	GC-U23-6.0	GC-U23-12.0	GC-U23-21.0	GC-U23-27.0	GC-U24-0.0	GC-U24-6.0	GC-U24-12.0
Stratigraphic position (m)	270.8	276.8	285.8	291.8	320.1	326.1	332.1
Matrix	30	192	40	113	222	140	215
Algae	0	0	0	0	0	0	0
Brachiopods	16	0	15	0	0	4	5
Bryozoans	0	0	0	0	0	1	0
Calcispheres	0	0	0	0	0	0	0
Calcite Crystals	67	70	16	65	66	121	32
Cephalopods	0	0	0	0	0	0	0
Chert	0	0	0	0	0	0	0
Dolomite Crystals	1	0	2	1	0	6	1
Echinoderms	20	0	7	0	0	5	3
Intraclasts	13	0	16	0	0	0	0
Gastropods	0	0	0	0	0	0	0
Ostracods	0	0	0	0	0	1	0
Peloids/Pellets	64	0	20	84	0	0	0
Nuia	14	0	51	0	0	2	0
Pyrite/ Hematite	0	1	2	0	0	0	0
Quartz Grains	4	20	1	17	4	1	25
Radiolarians	0	0	0	0	0	0	0
Sponges/Spicules	0	0	102	0	0	14	0
Stylolites	10	16	5	20	4	1	17
Trilobites	3	0	2	0	2	2	0
Unknown Bioclasts	31	0	14	0	1	2	0
Veins	27	1	7	0	1	0	2

Sample Name	GC-U24-24.0	GC-U24-36.0	GC-U24-42.0	GC-U25-3.0	GC-U25-9.0	GC-U25-18.0	GC-U25-21.0
Stratigraphic Position (m)	344.1	356.1	362.1	374.1	380.1	389.1	392.1
Matrix	16	217	28	156	224	184	169
Algae	0	0	0	0	3	3	0
Brachiopods	6	0	2	12	1	7	6
Bryozoans	0	0	0	2	0	0	0
Calcispheres	0	0	0	2	3	0	0
Calcite Crystals	163	44	104	31	27	5	16
Cephalopods	0	0	0	3	0	0	0
Chert	0	4	91	0	0	0	0
Dolomite Crystals	8	8	29	0	28	37	3
Echinoderms	1	7	0	8	3	20	62
Intraclasts	0	0	0	0	0	0	0
Gastropods	0	0	0	9	0	0	0
Ostracods	0	0	0	6	2	0	1
Peloids/Pellets	99	0	11	0	0	0	14
Nuia	0	0	0	0	0	0	1
Pyrite/ Hematite	0	0	0	0	0	1	0
Quartz Grains	6	12	1	19	0	36	16
Radiolarians	0	0	0	0	0	0	0
Sponges/Spicules	0	0	18	0	3	0	0
Stylolites	0	2	14	12	0	0	0
Trilobites	1	3	0	4	2	3	3
Unknown Bioclasts	0	1	1	36	1	0	0
Veins	0	2	1	0	3	4	9

Sample Name	GC-U25-27.0	GC-U25-32.5
Stratigraphic Position (m)	398.1	403.6
Matrix	66	156
Algae	0	0
Brachiopods	3	7
Bryozoans	0	0
Calcispheres	0	0
Calcite Crystals	0	17
Cephalopods	0	0
Chert	3	0
Dolomite Crystals	67	12
Echinoderms	108	31
Intraclasts	32	0
Gastropods	0	0
Ostracods	1	0
Peloids/Pellets	5	0
Nuia	0	4
Pyrite/ Hematite	0	9
Quartz Grains	1	62
Radiolarians	0	0
Sponges/Spicules	0	0
Stylolites	0	0
Trilobites	5	2
Unknown Bioclasts	9	0
Veins	0	0

Appendix B2. Pogonip Group Thin-Section Point Count Data

Sample Name	HL-BHM-48.0	HL-U1-3.0	HL-U2-3.0	HL-U2-16.5	HL-U2-25.5	HL-U2-34.5	HL-U4-6.0
Stratigraphic Position (m)	33.0	39.7	50.9	64.4	73.4	82.4	101.7
Matrix	219	277	256	276	17	68	281
Algae	0	0	0	0	0	0	0
Brachiopods	0	0	0	0	2	2	1
Bryozoans	0	0	0	0	0	0	0
Calcispheres	0	0	0	0	0	0	0
Calcite Crystals	78	0	17	11	186	165	0
Chert	0	0	0	0	21	0	0
Dolomite Crystals	0	0	0	7	23	0	0
Echinoderms	0	0	0	0	0	3	0
Intraclasts	0	0	0	0	0	0	0
Gastropods	0	0	0	0	0	0	0
Glauconite	0	0	0	0	0	0	0
Ostracods	0	0	0	0	0	0	0
Peloids/Pellets	0	0	0	0	1	1	0
Nuia	0	0	0	0	3	5	0
Quartz Grains	0	0	2	0	43	50	4
Sponges/Spicules	0	0	3	3	3	0	4
Stylolites	0	0	15	0	0	0	10
Trilobites	0	0	4	0	1	3	0
Unknown Bioclasts	3	0	0	0	0	3	0
Veins	0	23	3	3	0	0	0

Sample Name	HL-U4-18.0	HL-U4-30.0	HL-U5-9.0	HL-U5-15.0	FF-BLLM-U4-0.6	FF-BLLM-U5-1.87	FF-BLLM-U7-0.0
Stratigraphic Position (m)	113.7	125.7	135.2	141.2	162.8	164.5	167.7
Matrix	156	0	46	291	75	101	56
Algae	0	0	0	0	0	0	0
Brachiopods	0	34	0	0	0	10	12
Bryozoans	0	0	0	0	0	0	0
Calcispheres	0	0	0	0	0	0	0
Calcite Crystals	136	57	92	0	75	40	115
Chert	0	0	102	0	0	6	5
Dolomite Crystals	8	0	34	0	18	26	20
Echinoderms	0	25	0	0	0	5	4
Intraclasts	0	0	0	0	0	0	0
Gastropods	0	0	0	0	0	0	0
Glauconite	0	0	0	0	0	0	0
Ostracods	0	0	0	0	0	0	0
Peloids/Pellets	0	13	8	0	132	48	12
Nuia	0	134	0	0	0	0	0
Quartz Grains	0	2	10	0	0	12	30
Sponges/Spicules	0	0	0	3	0	0	0
Stylolites	0	1	0	6	0	0	4
Trilobites	0	0	0	0	0	24	6
Unknown Bioclasts	0	34	8	0	0	28	36
Veins	0	0	0	0	0	0	0

Sample Name	FF-BLLM-U9-0.7	FF-BLLM-U10-8.9	FF-BLLM-U12-1.0	FF-BLLM-U13-8.6	FF-BLLM-U13-17.5	FF-BLLM-U14-1.5	FF-BLLM-U16-0.7
Stratigraphic Position (m)	172.5	181.7	185.4	194.3	203.1	215.3	229.6
Matrix	179	39	198	42	115	219	267
Algae	0	1	0	4	0	0	0
Brachiopods	0	27	0	19	8	1	0
Bryozoans	0	1	0	0	0	0	0
Calcispheres	0	0	0	0	0	0	0
Calcite Crystals	99	26	63	103	62	21	28
Chert	0	18	0	0	3	0	0
Dolomite Crystals	0	31	0	0	0	0	0
Echinoderms	0	11	0	2	0	0	0
Intraclasts	0	100	0	68	0	6	0
Gastropods	0	0	0	0	0	0	0
Glauconite	0	0	0	0	0	0	0
Ostracods	0	0	0	0	0	0	0
Peloids/Pellets	0	0	3	15	13	0	0
Nuia	0	0	0	0	0	0	0
Quartz Grains	21	1	0	7	40	45	2
Sponges/Spicules	0	0	0	0	0	0	0
Stylolites	0	2	0	0	0	0	0
Trilobites	1	11	0	0	2	3	0
Unknown Bioclasts	0	31	0	40	57	5	0
Veins	0	1	3	0	0	0	3

Sample Name	FF-BLLM-U17-12.0	FF-BLLM-U17-30.0	FF-BLLM-U18-0.7	FF-BLLM-U20-6.0	FF-BLLM-U22-4.2	FF-BLLM-U24-21.0	FF-BLLM-U24-36.0
Stratigraphic Position (m)	242.2	260.2	271.7	287.6	295.0	319.9	334.9
Matrix	258	41	298	62	90	5	14
Algae	0	0	0	3	1	4	32
Brachiopods	0	3	0	9	8	8	27
Bryozoans	0	0	0	0	0	0	0
Calcispheres	0	0	0	2	0	0	0
Calcite Crystals	33	166	0	21	84	21	127
Chert	0	18	0	41	0	0	1
Dolomite Crystals	0	0	0	0	0	0	0
Echinoderms	0	0	0	12	12	54	0
Intraclasts	0	0	0	109	60	147	0
Gastropods	0	0	0	0	0	0	0
Glauconite	0	0	0	0	0	0	0
Ostracods	0	0	0	0	0	0	0
Peloids/Pellets	0	38	0	24	17	6	10
Nuia	0	0	0	0	1	44	1
Quartz Grains	0	3	0	0	8	4	69
Sponges/Spicules	0	0	0	0	0	0	0
Stylolites	6	0	0	6	0	0	0
Trilobites	0	5	0	0	4	1	1
Unknown Bioclasts	0	26	0	11	14	6	18
Veins	3	0	2	0	1	0	0

Sample Name	FF-SSSM-U2-10.1	FF-SSSM-U2-24.0	FF-SSSM-U3-12.0	FF-SSSM-U4-12.0	FF-SSSM-U5-16.5	FF-LGLM-U3-0.3	FF-LGLM-U7-15.0
Stratigraphic Position (m)	347.5	361.4	376.2	392.4	418.4	433.4	463.7
Matrix	24	134	66	40	15	43	76
Algae	0	0	0	0	0	0	2
Brachiopods	0	2	0	0	11	4	7
Bryozoans	0	0	0	0	0	0	0
Calcispheres	0	0	0	0	0	0	0
Calcite Crystals	96	150	141	45	23	64	45
Chert	138	0	0	0	0	0	0
Dolomite Crystals	14	0	0	0	0	0	0
Echinoderms	0	0	0	0	1	7	21
Intraclasts	12	0	0	178	192	148	60
Gastropods	0	0	0	0	0	0	0
Glauconite	0	0	0	0	0	0	0
Ostracods	0	0	0	0	0	0	0
Peloids/Pellets	7	0	6	8	35	25	35
Nuia	0	0	0	0	0	0	0
Quartz Grains	0	12	0	7	13	9	0
Sponges/Spicules	0	0	0	0	0	0	0
Stylolites	0	2	33	4	6	0	4
Trilobites	0	0	0	0	1	0	0
Unknown Bioclasts	3	0	51	18	2	0	49
Veins	6	0	3	0	1	0	1

Sample Name	FF-LGLM-U8-3.0	FF-LGLM-U10-1.5	FF-BSLM-U1-12.0	FF-BSLM-U4-0.4	FF-BSLM-U7-3.0A	FF-BSLM-U8-6.3	FF-BSLM-U9-0.6
Stratigraphic Position (m)	469.2	475.2	489.6	512.5	531.0	543.4	553.1
Matrix	52	44	78	201	28	45	77
Algae	0	0	0	0	2	2	0
Brachiopods	10	18	2	0	14	4	4
Bryozoans	0	3	6	0	0	4	0
Calcispheres	0	0	0	0	0	0	0
Calcite Crystals	54	27	82	0	32	52	54
Chert	2	0	0	0	0	0	0
Dolomite Crystals	2	0	2	0	2	0	0
Echinoderms	2	29	16	0	26	26	21
Intraclasts	0	153	0	0	168	150	110
Gastropods	0	0	0	0	0	0	0
Glauconite	0	0	0	0	0	0	0
Ostracods	0	0	0	0	0	0	0
Peloids/Pellets	62	23	54	0	8	2	20
Nuia	0	3	0	0	4	0	0
Quartz Grains	28	0	34	99	0	2	0
Sponges/Spicules	0	0	0	0	0	0	0
Stylolites	0	0	6	0	0	0	0
Trilobites	0	0	0	0	4	3	4
Unknown Bioclasts	88	0	14	0	12	10	6
Veins	0	0	6	0	0	0	4

Sample Name	FF-BSLM-U11-0.8	FF-CM-U1-0.0	FF-CM-U2-2.6	FF-CM-U3-0.0	FF-CM-U4-6.0	FF-CM-U5-11.3	FF-CM-U5-31.7
Stratigraphic Position (m)	569.8	572.8	583.5	588.7	595.1	607.9	628.3
Matrix	296	16	17	246	18	68	72
Algae	0	10	8	0	4	2	13
Brachiopods	0	7	26	0	8	17	0
Bryozoans	0	17	9	0	0	4	2
Calcispheres	0	1	0	0	0	0	0
Calcite Crystals	0	34	39	3	30	34	70
Chert	0	1	0	0	0	0	0
Dolomite Crystals	0	0	0	0	0	0	0
Echinoderms	0	32	20	0	37	13	5
Intraclasts	0	111	134	0	173	56	0
Gastropods	0	0	0	0	0	0	0
Glauconite	0	0	0	0	0	0	0
Ostracods	0	0	0	0	0	0	0
Peloids/Pellets	0	40	20	0	8	39	62
Nuia	0	0	4	0	4	0	0
Quartz Grains	0	2	0	51	2	33	32
Sponges/Spicules	0	0	0	0	0	12	0
Stylolites	0	3	0	0	0	1	0
Trilobites	0	2	2	0	0	14	0
Unknown Bioclasts	0	23	21	0	14	7	42
Veins	4	1	0	0	2	0	2

Sample Name	FF-CM-U7-6.0	FF-CCM-U2-6.3	FF-CCM-U5-4.0	FF-CCM-U7-6.2	FF-CCM-U8-0.0	FF-CCM-U9-13.3	WW-U4-1.1
Stratigraphic Position (m)	641.5	650.8	662.3	671.2	673.2	686.8	691.5
Matrix	58	16	34	83	177	181	110
Algae	0	0	0	13	0	0	5
Brachiopods	16	8	0	7	0	2	11
Bryozoans	0	8	0	0	0	0	0
Calcispheres	0	0	0	1	0	0	0
Calcite Crystals	30	44	74	16	11	36	41
Chert	0	0	0	0	0	0	0
Dolomite Crystals	4	0	36	0	0	0	31
Echinoderms	192	32	0	34	2	0	1
Intraclasts	0	48	0	73	0	0	0
Gastropods	0	0	0	3	0	0	0
Glauconite	0	78	0	0	0	0	0
Ostracods	0	0	0	0	0	0	0
Peloids/Pellets	0	0	52	17	0	0	15
Nuia	0	46	0	10	91	0	1
Quartz Grains	0	4	102	14	11	52	77
Sponges/Spicules	0	0	0	0	0	29	0
Stylolites	0	0	2	0	6	0	0
Trilobites	0	2	0	1	1	0	1
Unknown Bioclasts	0	14	0	28	1	0	5
Veins	0	0	0	0	0	0	2

Sample Name	WW-U7-0.0	WW-U12-2.5	WW-U13-3.0	WW-U16-1.5	WW-U17-1.1	WW-U19-1.5	WW-U20-0.8
Stratigraphic Position (m)	700.2	715.0	720.2	725.6	733.0	737.2	740.3
Matrix	163	64	226	129	126	104	130
Algae	0	0	0	2	7	0	0
Brachiopods	3	46	0	3	10	0	41
Bryozoans	5	6	0	0	2	0	0
Calcispheres	0	0	0	0	1	0	0
Calcite Crystals	21	36	4	82	60	111	37
Chert	0	0	0	0	0	0	0
Dolomite Crystals	0	0	0	0	0	0	3
Echinoderms	22	68	2	6	18	0	0
Intraclasts	1	9	0	0	26	0	4
Gastropods	0	0	0	0	1	0	0
Glauconite	0	0	0	0	0	0	0
Ostracods	1	0	12	0	0	0	1
Peloids/Pellets	0	3	4	0	1	4	0
Nuia	3	0	0	0	5	0	0
Quartz Grains	61	7	52	39	20	78	82
Sponges/Spicules	0	0	0	30	8	0	0
Stylolites	6	0	0	0	0	0	1
Trilobites	0	23	0	0	0	0	1
Unknown Bioclasts	11	38	0	8	13	1	0
Veins	3	0	0	1	2	2	0

Sample Name	WW-U21-3.0	WW-U23-3.2	JL-U1-4.5	JL-U2-1.5	JL-U3-4.1	JL-U4-0.8	JL-U6-0.4
Stratigraphic Position (m)	743.3	748.6	753.1	756.7	761.6	767.7	771.1
Matrix	18	134	134	150	151	145	115
Algae	0	0	0	0	0	0	0
Brachiopods	0	10	5	8	5	4	11
Bryozoans	0	0	0	0	2	0	0
Calcispheres	0	0	1	2	0	0	0
Calcite Crystals	22	56	15	12	18	43	41
Chert	0	0	0	0	0	0	1
Dolomite Crystals	106	0	0	0	0	0	0
Echinoderms	0	11	5	7	2	4	10
Intraclasts	0	0	0	0	0	0	22
Gastropods	0	0	0	0	2	0	0
Glauconite	0	0	0	0	0	0	0
Ostracods	0	0	0	0	3	2	4
Peloids/Pellets	0	8	0	7	0	0	14
Nuia	0	0	0	10	0	0	0
Quartz Grains	154	77	138	88	98	93	76
Sponges/Spicules	0	0	0	0	0	0	0
Stylolites	0	0	0	3	1	0	0
Trilobites	0	4	2	6	4	3	5
Unknown Bioclasts	0	0	0	2	0	2	0
Veins	0	0	0	5	14	4	1

Sample Name	JL-U7-1.1	JL-U8-2.8	JL-U9-2.4	JL-U10-5.0	JL-U11-0.5
Stratigraphic Position (m)	772.5	775.7	778.1	786.4	787.3
Matrix	161	113	132	146	159
Algae	3	0	0	0	0
Brachiopods	5	14	14	8	3
Bryozoans	1	6	3	0	2
Calcispheres	0	1	0	0	0
Calcite Crystals	15	21	57	12	9
Chert	0	0	0	0	0
Dolomite Crystals	0	0	0	0	0
Echinoderms	16	15	14	8	5
Intraclasts	0	40	0	0	3
Gastropods	0	3	2	0	5
Glauconite	0	0	0	0	0
Ostracods	2	3	3	0	0
Peloids/Pellets	0	4	2	2	0
Nuia	3	0	0	12	70
Quartz Grains	79	66	65	102	33
Sponges/Spicules	0	0	0	0	0
Stylolites	0	0	0	0	0
Trilobites	6	7	3	2	7
Unknown Bioclasts	5	2	3	8	3
Veins	4	5	2	0	1

Appendix C1. Garden City Formation $\delta^{13}C$ and $\delta^{18}O$ Isotopic Analysis Data

Sample Name	Stratigraphic Position (m)	$\delta^{13}C$ (PDB)	$\delta^{18}O$ (PDB)
GC-U0-0.0	12.0	0.16	-9.84
GC-U0-1.0	13.0	0.17	-10.35
GC-U0-2.0	14.0	0.26	-10.89
GC-U0-3.0	15.0	0.21	-10.62
GC-U0-4.0	16.0	-0.33	-10.25
GC-U0-5.0	17.0	-0.25	-10.66
GC-U0-6.0	18.0	-0.48	-10.66
GC-U0-7.0	19.0	-0.94	-14.08
GC-U0-8.0	20.0	-0.15	-10.43
GC-U0-9.0	21.0	-0.44	-10.57
GC-U0-10.0	22.0	-0.21	-10.30
GC-U1-0.0	22.1	-0.94	-12.58
GC-U1-3.0B	25.0	-1.04	-10.20
GC-U1-6.0	28.0	-0.82	-9.80
ISO-GC U1- 7.0	29.0	-0.60	-9.07
ISO-GC-U1-8.0	30.0	-1.10	-9.54
GC-U1-9.0	31.0	-1.22	-9.51
ISO-GC-U1-10.0	32.0	-1.20	-8.40
ISO-GC-U1-11.0-D	33.0	-1.54	-8.93
GC-U1-12.0	34.0	-0.52	-9.76
ISO-GC-U1-13.0	35.0	-0.32	-8.94
ISO-GC-U1-14.0	36.0	-0.27	-9.06
GC-U2-1.1	37.1	-1.34	-9.76
GC-U2-1.7A	37.7	-0.79	-9.91
GC-U3-0.0	37.7	-0.90	-9.51
GC-U3-3.0B	40.7	-1.06	-9.72
GC-U4-6.0A	47.4	-0.66	-9.08
GC-U4-9.0	50.4	-0.97	-9.56
GC-U5-3.0	53.7	-0.21	-9.28
GC-U5-6.0	56.7	0.16	-8.70
ISO-GC-U6-1.0	57.7	0.00	-9.85
GC-U6-3.15	59.9	0.56	-9.76
ISO-GC-U6-4.0	60.7	0.29	-13.22
ISO-GC-U6-5.0	61.7	0.50	-9.88
GC-U6-5.1	61.8	-0.46	-8.76
ISO-GC-U7-1.0	62.8	-0.30	-13.77
ISO-GC-U7-2.0	63.8	0.05	-10.25

Sample Name	Stratigraphic Position (m)	$\delta^{13}C$ (PDB)	$\delta^{18}O$ (PDB)
GC-U7-3.0	64.8	-0.50	-10.67
GC-U8-3.0	67.8	-0.63	-10.14
GC-U9-3.0	71.0	-0.78	-9.56
GC-U9-6.0	74.0	-0.83	-9.48
GC-U9-9.0	77.0	-0.89	-9.32
GC-U9-12.0A	80.0	-1.35	-9.26
GC-U10-1.0	82.9	-0.68	-11.14
GC-U10-3.0	84.9	-0.41	-9.94
GC-U10-7.5	89.4	-0.68	-9.23
GC-U10-9.0	90.9	-0.67	-9.58
GC-U10-12.0	93.9	-0.56	-8.88
GC-U10-13.5	95.4	-0.86	-9.47
GC-U11-0.0A	95.8	-0.41	-8.46
GC-U11-3.0	98.8	-0.70	-9.00
GC-U12-0.0A	101.1	-0.63	-8.65
GC-U12-3.0	104.1	-1.22	-8.70
GC-U13-0.4	106.0	-1.01	-8.61
GC-U14-3.0	109.7	-0.62	-8.94
GC-U15-4.5	117.0	-1.56	-9.54
GC-U15-15.0	127.5	-1.83	-9.27
GC-U15-21.0	133.5	-1.74	-9.11
GC-U15-30.0	142.5	-1.76	-9.20
GC-U15-36.0	148.5	-1.64	-9.05
GC-U15-42.0A	154.5	-1.78	-8.87
GC-U15-48.0A	160.5	-1.81	-9.05
GC-U15-54.0	166.5	-1.41	-8.79
GC-U15-63.0A	175.5	-1.24	-9.01
GC-U15-72.0	184.5	-1.35	-9.17
GC-U15-78.0A	190.5	-1.49	-8.67
GC-U15-86.65	199.2	-1.54	-8.71
GC-U16-3.0	202.2	-1.66	-8.26
GC-U16-6.6	205.8	-2.01	-8.54
GC-U16-7.7	206.9	-1.31	-8.42
GC-U17-0.7	215.1	-1.26	-8.21
GC-U18-3.0	218.4	-1.02	-8.31
GC-U18-6.0	221.4	-1.90	-8.39
GC-U18-9.0	224.4	-1.37	-8.37

Sample Name	Stratigraphic Position (m)	$\delta^{13}C$ (PDB)	$\delta^{18}O$ (PDB)
GC-U18-12.0	227.4	-1.31	-8.24
GC-U18-15.0	230.4	-1.35	-8.43
GC-U19-0.0	232.5	-0.98	-8.38
GC-U19-4.5	237.0	-1.32	-8.17
GC-U20-0.0	237.8	-1.56	-8.46
GC-U20-2.4	240.2	-1.59	-8.16
GC-U21-3.0-D	243.2	-1.34	-8.13
GC-U21-6.0	246.2	-1.15	-8.09
GC-U21-9.0	249.2	-1.38	-8.14
GC-U22-0.0	249.8	-1.48	-8.17
GC-U22-3.0	252.8	-1.18	-8.06
GC-U22-6.0	255.8	-1.28	-8.17
GC-U22-9.0	258.8	-1.12	-8.36
GC-U22-12.0	261.8	-1.29	-8.34
GC-U23-0.0	264.8	-1.30	-8.60
GC-U23-3.0	267.8	-0.67	-9.03
GC-U23-6.0	270.8	-0.83	-8.72
GC-U23-9.0	273.8	-0.91	-8.63
GC-U23-12.0	276.8	-0.69	-8.65
GC-U23-15.0	279.8	-1.09	-8.80
GC-U23-18.0	282.8	-1.09	-9.93
GC-U23-21.0	285.8	-0.82	-8.92
GC-U23-24.0	288.8	-0.54	-9.10
GC-U23-27.0	291.8	-0.74	-9.13
GC-U24-0.0	320.1	-0.72	-9.74
GC-U24-3.0	323.1	-1.15	-8.40
GC-U24-6.0	326.1	-1.08	-8.28
GC-U24-9.0	329.1	-1.45	-9.36
GC-U24-12.0	332.1	-1.27	-8.52
GC-U24-21.0	341.1	-1.75	-7.65
GC-U24-24.0	344.1	-2.19	-8.08
GC-U24-28.5	348.1	-0.37	-9.35
GC-U24-36.0	356.1	-1.51	-8.00
GC-U24-39.0	359.1	-1.83	-8.24
GC-U24-42.0	362.1	-1.24	-8.19
GC-U24-45.0	365.1	-0.96	-8.38
GC-U24-48.0	368.1	-1.12	-8.63

Sample Name	Stratigraphic Position (m)	$\delta^{13}C$ (PDB)	$\delta^{18}O$ (PDB)
GC-U24-51.0	371.1	-0.85	-8.85
GC-U25-3.0	374.1	-0.97	-8.73
GC-U25-6.0	377.1	-0.52	-8.21
GC-U25-9.0	380.1	-0.62	-8.08
GC-U25-12.0	383.1	-0.91	-8.02
GC-U25-15.0	386.1	-0.62	-7.65
GC-U25-18.0	389.1	-1.36	-8.33
GC-U25-21.0	392.1	-1.90	-9.39
GC-U25-24.0	395.1	-1.15	-9.05
GC-U25-27.0	398.1	-1.97	-7.97
GC-U25-30.0	401.1	-1.68	-8.46
GC-U25-32.5	403.6	-1.26	-11.71

Appendix C2. Pogonip Group $\delta^{13}C$ and $\delta^{18}O$ Isotopic Analysis Data

Sample Name	Stratigraphic Position (m)	$\delta^{13}C$ (PDB)	$\delta^{18}O$ (PDB)
HL-BHM-15.0	0.0	Not Analyzed	Not Analyzed
HL-BHM-18.0	3.0	Not Analyzed	Not Analyzed
HL-BHM-21.0	6.0	0.92	-9.15
HL-BHM-25.5	10.5	1.23	-9.31
HL-BHM-28.5	13.5	1	-9.22
HL-BHM-33.0	18.0	0.87	-9.03
HL-BHM-36.0	21.0	0.77	-8.95
HL-BHM-43.5	28.5	-0.2	-8.97
HL-BHM-48.0	33.0	0.55	-8.77
HL-BHM-51.0	36.0	1.03	-8.62
HL-BHM-51.7	36.7	0.77	-8.88
HL-U1-3.0	39.7	0.63	-9.21
HL-U1-6.0	42.7	1.09	-8.78
HL-U1-9.0	45.7	-1.83	-8.30
HL-U1-11.2	47.9	1.06	-8.83
HL-U2-3.0	50.9	0.93	-9.25
HL-U2-6.0	53.9	0.92	-9.02
HL-U2-9.0	56.9	0.92	-8.92
HL-U2-12.0	59.9	0.84	-9.07
HL-U2-16.5	64.4	0.78	-9.04
HL-U2-19.5	67.4	0.29	-9.07
D-HL-U2-19.5	67.4	0.32	-9.11
HL-U2-22.5	70.4	-0.09	-9.14
HL-U2-25.5	73.4	-0.41	-8.83
HL-U2-28.5	76.4	-0.48	-9.03
HL-U2-31.5	79.4	-0.60	-8.96
HL-U2-34.5	82.4	-0.69	-9.02
HL-U2-37.4	85.3	-0.47	-8.64
HL-U3-3.0	88.3	-0.42	-8.84
HL-U3-6.0	91.3	-2.92	-9.74
HL-U3-9.0	94.3	-0.60	-8.78
HL-U3-10.4	95.7	-0.75	-8.54
D-HL-U3-10.4	95.7	-0.75	-8.60
HL-U4-3.0	98.7	-0.58	-8.86
HL-U4-6.0	101.7	-0.57	-8.95

Sample Name	Stratigraphic Position (m)	$\delta^{13}C$ (PDB)	$\delta^{18}O$ (PDB)
HL-U4-9.0	104.7	-0.66	-8.92
HL-U4-12.0	107.7	-0.57	-8.83
HL-U4-15.0	110.7	-0.10	-9.34
HL-U4-18.0	113.7	-0.61	-9.07
HL-U4-21.0	116.7	-0.54	-9.26
HL-U4-24.0	119.7	-0.43	-9.28
HL-U4-27.0	122.7	-0.66	-8.86
HL-U4-30.0	125.7	-0.87	-8.99
D-HL-U4-30.0	125.7	-0.74	-8.81
HL-U4-30.5	126.2	-0.91	-8.92
HL-U5-3.0	129.2	-0.17	-8.93
HL-U5-6.0	132.2	-0.58	-8.91
HL-U5-9.0	135.2	-0.80	-8.77
HL-U5-12.0	138.2	-0.76	-8.84
HL-U5-15.0	141.2	-0.67	-8.81
HL-U5-18.0	144.2	-0.81	-8.89
HL-U5-21.0	147.2	-0.75	-8.80
HL-U5-24.6	150.8	-0.81	-8.84
HL-U5-27.0	153.2	-0.18	-8.91
D-HL-U5-27.0	153.2	-0.18	-8.84
HL-U5-29.1	155.3	-0.07	-9.02
HL-U6-1.5	156.8	0.27	-8.90
HL-U6-2.5	157.8	0.53	-8.79
FF-BLLM-U1-0.0	157.8	0.71	-8.95
FF-BLLM-U1-2.4	160.2	0.64	-8.97
FF-BLLM-U2-1.3	161.5	1.05	-8.74
FF-BLLM-U3-0.0	161.9	0.76	-8.77
FF-BLLM-U4-0.6	162.8	1.13	-9.00
FF-BLLM-U5-1.7	164.5	0.91	-8.43
FF-BLLM-U6-1.5	166.0	1.13	-9.02
D-FF-BLLM-U6-1.5	166.0	1.03	-8.95
FF-BLLM-U7-0.0	167.7	0.59	-8.24
FF-BLLM-U7-2.3	170.0	0.71	-8.99
FF-BLLM-U8-1.5	171.5	0.36	-8.89
FF-BLLM-U9-0.7	172.5	0.82	-9.06
FF-BLLM-U10-3.0	175.9	-0.17	-9.05
FF-BLLM-U10-6.0	178.9	0.32	-9.10

Sample Name	Stratigraphic Position (m)	$\delta^{13}C$ (PDB)	$\delta^{18}O$ (PDB)
FF-BLLM-U10-8.9	181.7	-0.42	-8.84
FF-BLLM-U11-2.7	184.4	-0.43	-8.73
FF-BLLM-U12-1.0	185.4	-0.15	-9.31
FF-BLLM-U13-4.3	190.0	-0.98	-9.23
D-FF-BLLM-U13-4.3	190.0	-0.90	-9.19
FF-BLLM-U13-8.6	194.3	-1.33	-9.18
FF-BLLM-U13-12.3	198.0	-1.34	-9.29
FF-BLLM-U13-17.5	203.1	-1.25	-9.22
FF-BLLM-U13-21.0	206.7	-1.19	-9.10
FF-BLLM-U13-25.5	211.2	-1.08	-9.35
FF-BLLM-U14-1.5	215.3	-1.35	-9.63
FF-BLLM-U14-4.5	218.3	-1.44	-8.96
FF-BLLM-U14-10.5	224.3	-1.17	-9.08
FF-BLLM-U15-2.5	227.4	-0.89	-8.90
FF-BLLM-U16-0.7	229.6	-0.77	-9.34
D-FF-BLLM-U16-0.7	229.6	-0.71	-9.30
FF-BLLM-U17-3.0	233.2	-0.93	-9.03
FF-BLLM-U17-6.0	236.2	-1.27	-8.89
FF-BLLM-U17-9.0	239.2	-1.42	-9.02
FF-BLLM-U17-12.0	242.2	-1.29	-9.14
FF-BLLM-U17-15.0	245.2	-1.37	-9.46
FF-BLLM-U17-18.0	248.2	-2.14	-9.99
FF-BLLM-U17-21.0	251.2	-1.47	-9.41
FF-BLLM-U17-24.0	254.2	-1.29	-9.38
FF-BLLM-U17-27.0	257.2	-1.81	-9.55
FF-BLLM-U17-30.0	260.2	-1.12	-8.71
D-FF-BLLM-U17-30.0	260.2	-1.11	-8.70
FF-BLLM-U17-36.0	266.2	-1.40	-9.18
FF-BLLM-U17-40.5	270.7	-1.00	-8.86
FF-BLLM-U18-0.7	271.7	-0.92	-9.24
FF-BLLM-U19-3.0	274.9	-1.08	-8.06
FF-BLLM-U19-6.0	277.9	-1.03	-9.14
FF-BLLM-U19-9.0	280.9	-1.41	-8.71
FF-BLLM-U20-4.5	286.1	-1.17	-8.94
FF-BLLM-U20-6.0	287.6	-1.22	-9.09
FF-BLLM-U21-1.8	290.3	-0.89	-9.45

Sample Name	Stratigraphic Position (m)	$\delta^{13}C$ (PDB)	$\delta^{18}O$ (PDB)
FF-BLLM-U22-1.5	292.3	-1.22	-8.75
D-FF-BLLM-U22-1.5	292.3	-1.25	-8.85
FF-BLLM-U22-4.2	295.0	-0.67	-9.15
FF-BLLM-U23-0.6	295.6	-0.16	-8.98
FF-BLLM-U23-3.9	298.9	-0.01	-8.99
FF-BLLM-U24-3.0	301.9	-0.88	-9.34
FF-BLLM-U24-6.0	304.9	-0.76	-8.89
FF-BLLM-U24-9.0	307.9	-0.77	-8.95
FF-BLLM-U24-12.0	310.9	-0.86	-9.02
FF-BLLM-U24-15.0	313.9	-1.11	-9.07
FF-BLLM-U24-18.0	316.9	-1.36	-8.74
FF-BLLM-U24-21.0	319.9	-1.46	-9.04
D-FF-BLLM-U24-21.0	319.9	-1.53	-9.04
FF-BLLM-U24-24.0	322.9	-1.43	-8.76
FF-BLLM-U24-27.0	325.9	-1.59	-9.35
FF-BLLM-U24-30.0	328.9	-2.02	-8.54
FF-BLLM-U24-33.0	331.9	-1.79	-9.18
FF-BLLM-U24-36.0	334.9	-2.22	-9.01
FF-SSSM-U1-2.6	337.4	-1.23	-7.59
D-FF-SSSM-U1-2.6	337.4	-1.12	-7.61
FF-SSSM-U2-3.0	340.4	-1.77	-7.66
FF-SSSM-U2-6.0	343.4	-1.20	-8.20
FF-SSSM-U2-10.1	347.5	-1.50	-7.90
FF-SSSM-U2-13.5	350.9	-1.73	-7.82
FF-SSSM-U2-18.0	355.4	-1.86	-8.13
FF-SSSM-U2-21.0	358.4	-2.41	-7.65
FF-SSSM-U2-24.0	361.4	-2.48	-8.22
FF-SSSM-U2-26.8	364.2	-2.44	-8.17
FF-SSSM-U3-3.0	367.2	-2.51	-8.03
FF-SSSM-U3-5.7	369.9	-1.81	-7.99
D-FF-SSSM-U3-5.7	369.9	-1.82	-8.15
FF-SSSM-U3-9.0	373.2	-2.14	-8.54
FF-SSSM-U3-12.0	376.2	-2.54	-8.29
FF-SSSM-U3-15.0	379.2	-2.38	-8.08
FF-SSSM-U4-3.0	383.4	-2.34	-8.32
FF-SSSM-U4-6.0	386.4	-2.34	-8.07

Sample Name	Stratigraphic Position (m)	$\delta^{13}C$ (PDB)	$\delta^{18}O$ (PDB)
FF-SSSM-U4-12.0	392.4	-2.42	-8.19
FF-SSSM-U4-15.0	395.4	-2.42	-8.40
FF-SSSM-U4-18.0	398.4	-2.38	-8.23
FF-SSSM-U4-21.5	401.9	-2.38	-8.24
FF-SSSM-U5-5.3	407.2	-1.96	-8.07
D-FF-SSSM-U5-5.3	407.2	-1.84	-8.17
FF-SSSM-U5-9.0	410.9	-1.67	-8.20
FF-SSSM-U5-13.5	415.4	-1.98	-7.59
FF-SSSM-U5-16.5	418.4	-2.05	-8.35
FF-SSSM-U5-19.5	421.4	-1.97	-8.29
FF-SSSM-U5-22.5	424.4	-1.72	-8.17
FF-SSSM-U5-25.5	427.4	-2.22	-7.67
FF-SSSM-U5-27.3	429.2	-1.97	-8.30
FF-LGLM-U1-0.6	429.8	-1.33	-8.66
FF-LGLM-U2-1.5	431.3	-1.10	-8.54
FF-LGLM-U3-0.3	433.4	-1.22	-9.43
FF-LGLM-U4-0.8	434.9	-1.61	-8.53
FF-LGLM-U5-2.6	438.5	-1.52	-8.66
FF-LGLM-U5-6.0	441.9	-1.44	-8.60
FF-LGLM-U5-9.0	444.9	-1.48	-8.62
FF-LGLM-U5-12.4	448.3	-1.53	-8.49
FF-LGLM-U6-0.4	448.7	-1.55	-8.15
D-FF-LGLM-U6-0.4	448.7	-1.74	-8.04
FF-LGLM-U7-3.0	451.7	-1.93	-8.38
FF-LGLM-U7-6.0	454.7	-2.11	-8.06
FF-LGLM-U7-9.0	457.7	-2.06	-8.15
FF-LGLM-U7-11.4	460.1	-1.61	-7.31
FF-LGLM-U7-15.0	463.7	-2.13	-7.88
FF-LGLM-U7-17.5	466.2	-2.44	-8.11
FF-LGLM-U8-3.0	469.2	-2.07	-7.76
FF-LGLM-U9-0.0	472.9	-2.06	-8.24
FF-LGLM-U10-1.5	475.2	-2.02	-7.98
FF-BSLM-U1-3.0	480.6	-1.68	-8.83
FF-BSLM-U1-6.0	483.6	-1.84	-8.86
FF-BSLM-U1-9.0	486.6	-1.49	-8.52
FF-BSLM-U1-12.0	489.6	-1.80	-8.63
FF-BSLM-U1-15.0	492.6	-1.84	-9.16

Sample Name	Stratigraphic Position (m)	$\delta^{13}C$ (PDB)	$\delta^{18}O$ (PDB)
D-FF-BSLM-U1-15.0	492.6	-1.87	-8.81
FF-BSLM-U1-18.0	495.6	-1.68	-9.03
FF-BSLM-U2-0.0	498.1	-1.57	-8.65
FF-BSLM-U3-4.5	503.1	-1.64	-8.17
FF-BSLM-U3-7.5	506.1	-1.68	-8.56
FF-BSLM-U3-10.7	509.3	-1.74	-8.54
FF-BSLM-U4-0.4	512.5	-1.82	-8.89
FF-BSLM-U5-3.0	515.5	-1.67	-8.67
FF-BSLM-U5-7.5	520.0	-1.46	-8.36
FF-BSLM-U5-10.5	523.0	-1.79	-8.77
FF-BSLM-U5-13.5	526.0	-1.71	-8.57
D-FF-BSLM-U5-13.5	526.0	-1.71	-8.50
FF-BSLM-U6-1.0	527.7	-1.07	-8.48
FF-BSLM-U7-3.0	531.0	-1.45	-8.68
FF-BSLM-U7-6.0	534.0	-1.43	-8.13
FF-BSLM-U7-9.2	537.2	-1.12	-8.22
FF-BSLM-U8-3.4	540.6	-1.23	-8.03
FF-BSLM-U8-6.3	543.4	-1.50	-8.17
FF-BSLM-U8-9.0	546.2	-1.17	-8.26
FF-BSLM-U8-12.0	549.2	-1.41	-8.65
FF-BSLM-U9-0.6	553.1	-1.22	-8.39
FF-BSLM-U10-2.5	555.6	-1.20	-8.44
D-FF-BSLM-U10-2.5	555.6	-1.36	-8.56
FF-BSLM-U10-6.0	559.1	-1.48	-8.56
FF-BSLM-U10-10.5	563.6	-1.50	-8.61
FF-BSLM-U10-13.5	566.6	-0.59	-7.68
FF-BSLM-U11-0.8	569.8	-0.95	-8.81
FF-CM-U1-0.0	572.8	-1.47	-8.22
FF-CM-U1-3.0	572.8	-1.19	-8.80
FF-CM-U1-6.8	576.6	-1.12	-8.33
FF-CM-U1-11.1	580.9	-1.38	-8.56
FF-CM-U2-2.6	583.5	-1.22	-8.05
FF-CM-U2-6.0	586.9	-0.99	-8.22
FF-CM-U3-0.0	588.7	-0.47	-8.82
FF-CM-U4-3.0	592.1	-1.03	-8.06
FF-CM-U4-6.0	595.1	-0.99	-8.36
FF-CM-U5-4.5	601.1	-1.35	-8.32

Sample Name	Stratigraphic Position (m)	$\delta^{13}C$ (PDB)	$\delta^{18}O$ (PDB)
D-FF-CM-U5-4.5	601.1	-1.38	-8.26
FF-CM-U5-7.5	604.1	-1.28	-8.85
FF-CM-U5-11.3	607.9	-1.37	-7.93
FF-CM-U5-15.0	611.6	-2.19	-7.85
FF-CM-U5-18.0	614.6	-1.32	-8.20
FF-CM-U5-23.4	620.0	-2.14	-7.99
FF-CM-U5-27.3	623.9	-1.53	-8.01
FF-CM-U5-31.7	628.3	-1.57	-8.36
FF-CM-U5-36.4	633.0	-1.16	-7.71
FF-CM-U6-1.5	635.5	-1.06	-8.08
FF-CM-U7-3.0	638.5	-1.24	-7.83
D-FF-CM-U7-3.0	638.5	-1.20	-7.86
FF-CM-U7-6.0	641.5	-1.12	-7.61
FF-CCM-U1-1.5	643.0	-0.98	-7.62
FF-CCM-U2-3.0	647.5	-1.26	-8.17
FF-CCM-U2-6.3	650.8	-1.58	-8.70
FF-CCM-U3-0.3	651.9	-1.29	-8.96
FF-CCM-U4-2.8	655.1	-1.87	-8.61
FF-CCM-U4-6.0	658.3	-1.69	-8.19
D-FF-CCM-U4-6.0	658.3	-1.75	-8.26
FF-CCM-U5-4.0	662.3	-1.56	-8.63
FF-CCM-U6-0.9	664.5	-1.54	-8.76
FF-CCM-U7-3.5	668.5	-1.50	-8.76
FF-CCM-U7-6.2	671.2	-1.64	-8.29
FF-CCM-U8-0.0	673.2	-1.63	-8.96
FF-CCM-U9-3.0	676.5	-1.71	-8.30
FF-CCM-U9-6.0	679.5	-2.06	-8.01
FF-CCM-U9-9.0	682.5	-2.39	-8.13
FF-CCM-U9-12.6	686.1	-2.63	-8.83
FF-CCM-U9-13.3	686.8	-1.97	-8.69
D-FF-CCM-U9-13.3	686.8	-1.92	-8.65
WW-U1-0.8B	687.6	-1.64	-8.19
WW-U2-0.9	689.5	-1.66	-7.84
WW-U3-0.4	690.2	-1.15	-7.63
D-WW-U3-0.4	690.2	-1.17	-7.78
WW-U4-1.1	691.5	-1.72	-8.21
WW-U5-0.0	693.7	-2.05	-8.35

Sample Name	Stratigraphic Position (m)	$\delta^{13}C$ (PDB)	$\delta^{18}O$ (PDB)
WW-U5-1.3	695.0	-1.33	-7.91
WW-U5-2.6	696.3	-1.19	-8.46
WW-U6-1.2	697.5	-1.49	-8.11
WW-U6-3.2	699.5	-1.38	-7.95
WW-U7-0.0	700.2	-1.92	-8.30
WW-U7-1.8	702.0	-0.85	-8.04
WW-U9-0.0	703.2	-1.19	-8.17
WW-U10-4.0	707.5	-1.10	-8.12
D-WW-U10-4.0	707.5	-1.13	-8.06
WW-U10-7.5	711.0	-0.97	-8.62
WW-U11-0.9	711.9	-0.72	-8.58
WW-U11-1.0	712.0	-0.55	-8.80
WW-U12-0.0	712.5	-0.80	-8.93
WW-U12-2.5	715.0	-0.86	-7.87
WW-U13-0.0	717.2	-1.08	-8.10
WW-U13-3.0	720.2	-1.38	-8.02
WW-U14-1.5	721.7	-1.32	-8.39
WW-U15-0.4	723.9	-1.03	-7.45
WW-U16-1.5	725.6	-1.40	-7.68
D-WW-U16-1.5	725.6	-1.42	-7.82
WW-U16-5.1	729.2	-1.38	-8.30
WW-U16-7.0	731.1	-1.22	-8.35
WW-U16-7.8	731.9	-0.55	-8.50
WW-U17-1.1	733.0	-1.66	-8.07
WW-U18-1.5	735.1	-1.49	-8.49
WW-U19-1.5	737.2	-2.05	-8.28
WW-U20-0.8	740.3	-2.52	-8.33
WW-U21-1.5	741.8	-2.61	-8.20
WW-U21-3.0	743.3	-2.29	-8.02
WW-U22-1.1	744.4	-1.67	-8.38
D-WW-U22-1.1	744.4	-1.70	-8.18
WW-U23-1.5	746.5	-1.20	-7.88
WW-U23-3.2	748.6	-0.89	-7.91
JL-U1-1.5	750.1	-1.10	-8.07
JL-U1-4.5	753.1	-1.40	-8.31
JL-U2-1.5	756.7	-1.16	-8.37
JL-U3-4.1	761.6	-1.31	-8.47

Sample Name	Stratigraphic Position (m)	$\delta^{13}C$ (PDB)	$\delta^{18}O$ (PDB)
JL-U3-7.5	765.0	-1.40	-8.28
JL-U4-0.8	767.7	-1.14	-8.77
JL-U5-1.2	769.8	-1.12	-7.97
JL-U6-0.4	771.1	-1.23	-8.38
D-JL-U6-0.4	771.1	-1.30	-8.36
JL-U7-1.1	772.5	-1.59	-8.60
JL-U8-2.8	775.7	-1.24	-8.36
JL-U9-2.4	778.1	-1.12	-8.56
JL-U9-5.7	781.4	-1.26	-8.55
JL-U10-2.7	784.1	-1.31	-8.26
JL-U10-5.0	786.4	-1.54	-8.70
JL-U11-0.5	787.3	-1.80	-8.54

Appendix D1. Garden City Formation Insoluble Residue, Carbonate, and Total Organic Carbon Data

Sample Name	SC-0.0	SC-1.0	SC-2.0	SC-3.0	SC-4.0	SC-5.0	SC-6.0
Stratigraphic Position (m)	12.0	13.0	14.0	15.0	16.0	17.0	18.0
Container Mass (g)	74.7	75.7	73.8	74.2	74.7	74.4	74.9
Sample Mass (g)	6.0	6.0	6.0	6.0	6.0	6.0	6.0
Container and Sample Mass (g)	80.7	81.7	79.8	80.2	80.7	80.4	80.9
Sample Mass after HCl (g)	0.3	0.3	0.3	0.5	0.6	0.4	1.0
Sample Mass after H_2O_2 (g)	0.0	0.0	0.0	0.0	0.0	0.0	0.0
Carbonate %	95.2	94.3	94.3	91.7	90.7	93.0	83.8
Organic Carbon %	0.0	0.0	0.2	0.2	0.2	0.2	0.2
Inorganic Insoluble Residue %	4.8	5.7	5.5	8.2	9.2	6.8	16.0

Sample Name	SC-7.0	SC-8.0	D-SC-9.0	SC-9.0	SC-10.0	GC-U1-0.0	GC-U1-3.0B
Stratigraphic Position (m)	19.0	20.0	21.0	21.0	22.0	22.1	25.0
Container Mass (g)	74.9	73.2	75.2	74.5	74.7	74.0	76.0
Sample Mass (g)	6.0	6.0	6.0	6.0	6.0	6.0	6.0
Container and Sample Mass (g)	80.9	79.2	81.2	80.5	80.7	80.0	82.0
Sample Mass after HCl (g)	3.4	0.3	0.5	0.5	0.2	3.0	2.6
Sample Mass after H_2O_2 (g)	0.0	0.0	0.0	0.0	0.0	0.0	0.1
Carbonate %	44.2	95.2	91.5	91.8	97.0	50.3	55.8
Organic Carbon %	0.2	0.2	0.2	0.2	0.2	0.0	1.5
Inorganic Insoluble Residue %	55.7	4.7	8.3	8.0	2.8	49.7	42.7

Sample Name	GC-U1-6.0	ISO-GC U1-7.0	ISO-GC-U1-8.0	ISO-GC-U1-9.0	GC-U1-9.0	ISO-GC-U1-10.0	D-ISO-GC-U1-11.0-D
Stratigraphic Position (m)	28.0	29.0	30.0	31.0	31.0	32.0	33.0
Container Mass (g)	73.8	75.0	73.5	74.1	72.6	75.5	75.2
Sample Mass (g)	6.0	6.0	6.0	6.0	6.0	6.0	6.0
Container and Sample Mass (g)	79.8	81.0	79.5	80.1	78.6	81.5	81.2
Sample Mass after HCl (g)	0.8	0.3	0.4	2.6	1.1	0.2	2.7
Sample Mass after H_2O_2 (g)	0.0	0.0	0.0	0.0	0.0	0.0	0.5
Carbonate %	86.8	94.8	92.8	57.0	81.5	96.0	55.0
Organic Carbon %	0.2	0.0	0.3	0.7	0.0	0.2	7.7
Inorganic Insoluble Residue %	13.0	5.2	6.8	42.3	18.5	3.8	37.3

Sample Name	ISO-GC-U1-11.0-D	ISO-GC-U1-12.0	GC-U1-12.0	ISO-GC-U1-13.0	ISO-GC-U1-14.0	GC-U2-1.1	GC-U2-1.7A
Stratigraphic Position (m)	33.0	34.0	34.0	35.0	36.0	37.1	37.7
Container Mass (g)	74.2	73.8	75.7	73.6	75.1	75.2	74.8
Sample Mass (g)	6.0	6.0	6.0	6.0	6.0	6.0	6.0
Container and Sample Mass (g)	80.2	79.8	81.7	79.6	81.1	81.2	80.8
Sample Mass after HCl (g)	2.7	0.6	0.3	0.6	0.6	3.3	0.3
Sample Mass after H_2O_2 (g)	0.5	0.0	0.0	0.0	0.0	0.2	0.0
Carbonate %	55.2	90.5	95.3	90.7	90.8	44.3	94.7
Organic Carbon %	7.5	0.0	0.2	0.0	0.0	3.0	0.2
Inorganic Insoluble Residue %	37.3	9.5	4.5	9.3	9.2	52.7	5.2

Sample Name	GC-U3-0.0	GC-U3-3.0B/A	GC-U3-3.0B	GC-U3-3.0A	D-GC-U3-3.0A	GC-U4-3.0	GC-U4-6.0A
Stratigraphic Position (m)	37.7	40.7	40.7	40.7	40.7	44.4	47.4
Container Mass (g)	71.3	75.6	73.6	74.8	74.4	74.4	74.1
Sample Mass (g)	6.0	6.0	6.0	6.0	6.0	6.0	6.0
Container and Sample Mass (g)	77.3	81.6	79.6	80.8	80.4	80.4	80.1
Sample Mass after HCl (g)	0.4	4.4	4.0	0.3	0.3	0.2	0.2
Sample Mass after H_2O_2 (g)	0.0	0.7	0.2	0.0	0.0	0.0	0.0
Carbonate %	93.2	26.2	32.8	95.2	95.3	96.5	96.5
Organic Carbon %	0.2	11.2	3.3	0.2	0.2	0.2	0.2
Inorganic Insoluble Residue %	6.7	62.7	63.8	4.7	4.5	3.3	3.3

Sample Name	GC-U4-9.0	GC-U5-3.0	GC-U5-6.0	ISO-GC-U6-1.0	GC-U6-3.15	ISO-GC-U6-4.0	ISO-GC-U6-5.0
Stratigraphic Position (m)	50.4	53.7	56.7	57.7	59.9	60.7	61.7
Container Mass (g)	75.0	74.7	73.8	75.1	74.5	74.8	75.4
Sample Mass (g)	6.0	6.0	6.0	6.0	6.0	6.0	6.0
Container and Sample Mass (g)	81.0	80.7	79.8	81.1	80.5	80.8	81.4
Sample Mass after HCl (g)	1.6	1.2	0.1	0.4	0.3	0.3	0.4
Sample Mass after H_2O_2 (g)	0.0	0.0	0.0	0.0	0.0	0.0	0.0
Carbonate %	72.7	80.3	98.5	93.5	95.2	94.8	93.0
Organic Carbon %	0.5	0.5	0.0	0.0	0.2	0.2	0.3
Inorganic Insoluble Residue %	26.8	19.2	1.5	6.5	4.7	5.0	6.7

Sample Name	GC-U6-5.1	D-GC-U6-5.1	ISO-GC-U7-1.0	ISO-GC-U7-2.0	GC-U7-3.0	GC-U8-3.0	GC-U9-3.0
Stratigraphic Position (m)	61.8	61.8	62.8	63.8	64.8	67.8	71.0
Container Mass (g)	73.9	75.1	74.6	75.2	74.0	73.6	75.0
Sample Mass (g)	6.0	6.0	6.0	6.0	6.0	6.0	6.0
Container and Sample Mass (g)	79.9	81.1	80.6	81.2	80.0	79.6	81.0
Sample Mass after HCl (g)	1.0	1.0	2.5	0.5	0.2	0.3	0.9
Sample Mass after H_2O_2 (g)	0.0	0.0	0.0	0.0	0.0	0.0	0.0
Carbonate %	83.8	83.8	59.0	92.2	96.3	94.2	85.5
Organic Carbon %	0.3	0.5	0.8	0.0	0.0	0.7	0.5
Inorganic Insoluble Residue %	15.8	15.7	40.2	7.8	3.7	5.2	14.0

Sample Name	GC-U9-6.0	GC-U9-9.0	GC-U9-12.0A	GC-U10-1.0	GC-U10-3.0	D-GC-U10-3.0	GC-U10-7.5
Stratigraphic Position (m)	74.0	77.0	80.0	82.9	84.9	84.9	89.4
Container Mass (g)	75.0	74.7	73.8	74.4	74.3	74.7	75.6
Sample Mass (g)	6.0	6.0	6.0	6.0	6.0	6.0	6.0
Container and Sample Mass (g)	81.0	80.7	79.8	80.4	80.3	80.7	81.6
Sample Mass after HCl (g)	0.2	0.9	0.3	0.2	0.3	0.3	0.3
Sample Mass after H_2O_2 (g)	0.0	0.0	0.0	0.0	0.0	0.0	0.0
Carbonate %	96.7	84.5	94.7	96.3	95.5	95.3	94.8
Organic Carbon %	0.0	0.5	0.3	0.2	0.3	0.2	0.3
Inorganic Insoluble Residue %	3.3	15.0	5.0	3.5	4.2	4.5	4.8

Sample Name	GC-U10-9.0	GC-U10-12.0	GC-U10-13.5	GC-U11-0.0A	GC-U11-3.0	GC-U11-3.0B	GC-U12-0.0A
Stratigraphic Position (m)	90.9	93.9	95.4	95.8	98.8	98.8	101.1
Container Mass (g)	74.9	74.9	74.2	74.3	73.8	73.9	74.4
Sample Mass (g)	6.0	6.0	6.0	6.0	6.0	6.0	6.0
Container and Sample Mass (g)	80.9	80.9	80.2	80.3	79.8	79.9	80.4
Sample Mass after HCl (g)	0.2	0.3	0.5	0.4	1.0	0.4	0.4
Sample Mass after H_2O_2 (g)	0.0	0.0	0.0	0.0	0.0	0.0	0.0
Carbonate %	96.8	95.3	92.5	93.5	82.8	93.2	92.7
Organic Carbon %	0.2	0.3	0.0	0.0	0.0	0.0	0.0
Inorganic Insoluble Residue %	3.0	4.3	7.5	6.5	17.2	6.8	7.3

Sample Name	GC-U13-0.4	D-GC-U13-0.4	GC-U14-3.0	GC-U15-0.0	GC-U15-3.0	GC-U15-4.5	GC-U15-6.0
Stratigraphic Position (m)	106.0	106.0	109.7	112.5	115.5	117.0	118.5
Container Mass (g)	73.7	74.5	75.1	73.6	73.1	73.0	74.2
Sample Mass (g)	6.0	6.0	6.0	6.0	6.0	6.0	6.0
Container and Sample Mass (g)	79.7	80.5	81.1	79.6	79.1	79.0	80.2
Sample Mass after HCl (g)	0.4	0.4	1.0	0.7	0.2	4.0	0.7
Sample Mass after H_2O_2 (g)	0.0	0.0	0.0	0.0	0.0	0.2	0.0
Carbonate %	94.0	94.0	84.0	88.2	96.0	34.0	89.2
Organic Carbon %	0.0	0.0	0.5	0.3	0.0	3.0	0.0
Inorganic Insoluble Residue %	6.0	6.0	15.5	11.5	4.0	63.0	10.8

Sample Name	GC-U15-9.0	GC-U15-12.0	GC-U15-15.0	GC-U15-18.0	D-GC-U15-21.0	GC-U15-21.0	GC-U15-27.0
Stratigraphic Position (m)	121.5	124.5	127.5	130.5	133.5	133.5	139.5
Container Mass (g)	73.8	75.0	74.0	73.9	74.9	73.1	75.6
Sample Mass (g)	6.0	6.0	6.0	6.0	6.0	6.0	6.0
Container and Sample Mass (g)	79.8	81.0	80.0	79.9	80.9	79.1	81.6
Sample Mass after HCl (g)	0.8	0.7	0.3	0.8	1.8	1.8	0.3
Sample Mass after H_2O_2 (g)	0.0	0.0	0.0	0.0	0.0	0.1	0.0
Carbonate %	86.5	89.0	95.3	87.2	69.2	69.3	95.3
Organic Carbon %	0.3	0.0	0.0	0.5	0.8	1.0	0.0
Inorganic Insoluble Residue %	13.2	11.0	4.7	12.3	30.0	29.7	4.7

Sample Name	GC-U15-30.0	GC-U15-33.0	GC-U15-36.0	GC-U15-39.0	GC-U15-42.0A	GC-U15-45.0	GC-U15-48.0A
Stratigraphic Position (m)	142.5	145.5	148.5	151.5	154.5	157.5	160.5
Container Mass (g)	74.1	74.1	74.3	74.9	74.7	74.5	74.7
Sample Mass (g)	6.0	6.0	6.0	6.0	6.0	6.0	6.0
Container and Sample Mass (g)	80.1	80.1	80.3	80.9	80.7	80.5	80.7
Sample Mass after HCl (g)	0.5	1.0	0.2	0.8	1.0	0.6	0.7
Sample Mass after H_2O_2 (g)	0.0	0.0	0.0	0.0	0.0	0.0	0.0
Carbonate %	92.0	82.7	96.0	87.2	83.2	89.7	88.8
Organic Carbon %	0.2	0.5	0.0	0.2	0.5	0.2	0.2
Inorganic Insoluble Residue %	7.8	16.8	4.0	12.7	16.3	10.2	11.0

Sample Name	GC-U15-51.0	D-GC-U15-54.0	GC-U15-54.0	GC-U15-60.0	GC-U15-63.0A	GC-U15-69.0	GC-U15-72.0
Stratigraphic Position (m)	163.5	166.5	166.5	172.5	175.5	184.5	184.5
Container Mass (g)	73.3	75.2	73.7	74.3	73.6	73.7	74.8
Sample Mass (g)	6.0	6.0	6.0	6.0	6.0	6.0	6.0
Container and Sample Mass (g)	79.3	81.2	79.7	80.3	79.6	79.7	80.8
Sample Mass after HCl (g)	1.7	0.3	0.3	0.8	0.3	0.6	0.4
Sample Mass after H_2O_2 (g)	0.0	0.0	0.0	0.0	0.0	0.0	0.0
Carbonate %	71.5	95.0	95.2	86.7	95.0	90.8	92.8
Organic Carbon %	0.5	0.2	0.3	0.0	0.5	0.0	0.0
Inorganic Insoluble Residue %	28.0	4.8	4.5	13.3	4.5	9.2	7.2

Sample Name	GC-U15-75.0	GC-U15-78.0A	GC-U15-81.0	GC-U15-83.65	GC-U15-86.65	D-GC-U16-3.0	GC-U16-3.0
Stratigraphic Position (m)	187.5	190.5	193.5	196.2	199.2	202.2	202.2
Container Mass (g)	73.4	74.9	74.7	74.7	73.8	74.4	75.0
Sample Mass (g)	6.0	6.0	6.0	6.0	6.0	6.0	6.0
Container and Sample Mass (g)	79.4	80.9	80.7	80.7	79.8	80.4	81.0
Sample Mass after HCl (g)	2.2	0.6	2.2	0.5	0.4	0.7	0.7
Sample Mass after H_2O_2 (g)	0.1	0.0	0.0	0.0	0.0	0.0	0.0
Carbonate %	63.3	89.3	63.8	91.0	93.7	87.8	87.7
Organic Carbon %	1.2	0.2	0.0	0.2	0.2	0.0	0.0
Inorganic Insoluble Residue %	35.5	10.5	36.2	8.8	6.2	12.2	12.3

Sample Name	GC-U16-6.6	GC-U16-7.7	GC-U17-0.7	GC-U18-3.0	GC-U18-6.0	GC-U18-9.0	GC-U18-12.0
Stratigraphic Position (m)	205.8	206.9	215.1	218.4	221.4	224.4	227.4
Container Mass (g)	74.0	73.6	74.1	73.7	73.2	73.8	75.6
Sample Mass (g)	6.0	6.0	6.0	6.0	6.0	6.0	6.0
Container and Sample Mass (g)	80.0	79.6	80.1	79.7	79.2	79.8	81.6
Sample Mass after HCl (g)	0.3	0.5	0.3	0.4	2.3	1.2	1.7
Sample Mass after H_2O_2 (g)	0.0	0.0	0.0	0.0	0.0	0.0	0.0
Carbonate %	94.7	92.5	95.7	93.7	62.3	80.2	71.7
Organic Carbon %	0.0	0.2	0.0	0.2	0.3	0.0	0.7
Inorganic Insoluble Residue %	5.3	7.3	4.3	6.2	37.3	19.8	27.7

Sample Name	GC-U18-15.0	GC-U19-0.0	D-GC-U19-4.5	GC-U19-4.5	GC-U20-0.0	GC-U20-2.4	GC-U21-3.0-D
Stratigraphic Position (m)	230.4	232.5	237.0	237.0	237.8	240.2	243.2
Container Mass (g)	74.8	74.0	75.3	72.5	72.7	73.9	75.5
Sample Mass (g)	6.0	6.0	6.0	6.0	6.0	6.0	6.0
Container and Sample Mass (g)	80.8	80.0	81.3	78.5	78.7	79.9	81.5
Sample Mass after HCl (g)	1.0	0.6	0.7	0.7	0.6	0.6	1.6
Sample Mass after H_2O_2 (g)	0.0	0.0	0.0	0.0	0.0	0.0	0.0
Carbonate %	83.2	90.5	87.7	87.7	90.2	90.5	73.8
Organic Carbon %	0.0	0.3	0.0	0.0	0.2	0.0	0.5
Inorganic Insoluble Residue %	16.8	9.2	12.3	12.3	9.7	9.5	25.7

Sample Name	GC-U21-6.0	GC-U21-9.0	GC-U22-0.0	GC-U22-3.0	GC-U22-6.0	GC-U22-9.0	GC-U22-12.0
Stratigraphic Position (m)	246.2	249.2	249.8	252.8	255.8	258.8	261.8
Container Mass (g)	74.3	73.5	74.8	74.8	73.9	72.5	75.0
Sample Mass (g)	6.0	6.0	6.0	6.0	6.0	6.0	6.0
Container and Sample Mass (g)	80.3	79.5	80.8	80.8	79.9	78.5	81.0
Sample Mass after HCl (g)	0.6	1.2	1.9	0.3	2.3	1.5	0.7
Sample Mass after H_2O_2 (g)	0.0	0.0	0.0	0.0	0.0	0.0	0.0
Carbonate %	90.0	80.7	68.5	94.5	61.8	74.5	88.3
Organic Carbon %	0.3	0.2	0.0	0.0	0.0	0.2	0.2
Inorganic Insoluble Residue %	9.7	19.2	31.5	5.5	38.2	25.3	11.5

Sample Name	D-GC-U22-12.0	GC-U23-0.0	GC-U23-3.0	GC-U23-6.0	GC-U23-9.0	GC-U23-12.0	GC-U23-15.0
Stratigraphic Position (m)	261.8	264.8	267.8	270.8	273.8	276.8	279.8
Container Mass (g)	75.3	74.8	74.4	74.4	74.1	74.1	75.0
Sample Mass (g)	6.0	6.0	6.0	6.0	6.0	6.0	6.0
Container and Sample Mass (g)	81.3	80.8	80.4	80.4	80.1	80.1	81.0
Sample Mass after HCl (g)	0.7	0.4	0.4	0.2	0.3	1.2	1.8
Sample Mass after H_2O_2 (g)	0.0	0.0	0.0	0.0	0.0	0.0	0.0
Carbonate %	88.5	93.3	93.7	97.2	94.7	80.0	70.8
Organic Carbon %	0.2	0.3	0.2	0.0	0.2	0.3	0.8
Inorganic Insoluble Residue %	11.3	6.3	6.2	2.8	5.2	19.7	28.3

Sample Name	GC-U23-18.0	GC-U23-21.0	GC-U23-24.0	D-GC-U23-27.0	GC-U23-27.0	GC-U24-0.0	GC-U24-3.0
Stratigraphic Position (m)	282.8	285.8	288.8	291.8	291.8	320.1	323.1
Container Mass (g)	74.1	73.5	75.3	74.1	75.2	75.0	75.1
Sample Mass (g)	6.0	6.0	6.0	6.0	6.0	6.0	6.0
Container and Sample Mass (g)	80.1	79.5	81.3	80.1	81.2	81.0	81.1
Sample Mass after HCl (g)	0.5	0.3	0.3	1.5	1.5	0.4	1.1
Sample Mass after H_2O_2 (g)	0.0	0.0	0.0	0.0	0.0	0.0	0.0
Carbonate %	91.2	94.5	94.3	74.8	75.0	93.8	81.3
Organic Carbon %	0.3	0.2	0.2	0.0	0.0	0.0	0.0
Inorganic Insoluble Residue %	8.5	5.3	5.5	25.2	25.0	6.2	18.7

Sample Name	GC-U24-6.0	GC-U24-9.0	GC-U24-12.0	GC-U24-21.0	GC-U24-24.0	GC-U24-28.5	GC-U24-36.0
Stratigraphic Position (m)	326.1	329.1	332.1	341.1	344.1	348.1	356.1
Container Mass (g)	74.7	75.3	73.8	74.9	74.8	73.4	74.6
Sample Mass (g)	6.0	6.0	6.0	6.0	6.0	6.0	6.0
Container and Sample Mass (g)	80.7	81.3	79.8	80.9	80.8	79.4	80.6
Sample Mass after HCl (g)	0.7	0.7	0.7	0.2	0.1	0.2	0.5
Sample Mass after H_2O_2 (g)	0.0	0.0	0.0	0.0	0.0	0.0	0.0
Carbonate %	88.8	88.0	88.7	96.3	97.7	96.2	91.8
Organic Carbon %	0.0	0.2	0.3	0.2	0.0	0.0	0.0
Inorganic Insoluble Residue %	11.2	11.8	11.0	3.5	2.3	3.8	8.2

Sample Name	D-GC-U24-39.0	GC-U24-39.0	GC-U24-42.0	GC-U24-45.0	GC-U24-48.0	GC-U24-51.0	GC-U25-3.0
Stratigraphic Position (m)	359.1	359.1	362.1	365.1	368.1	371.1	374.1
Container Mass (g)	74.4	74.1	73.9	75.1	73.7	73.4	73.8
Sample Mass (g)	6.0	6.0	6.0	6.0	6.0	6.0	6.0
Container and Sample Mass (g)	80.4	80.1	79.9	81.1	79.7	79.4	79.8
Sample Mass after HCl (g)	0.7	0.7	0.5	0.9	1.0	0.3	0.5
Sample Mass after H_2O_2 (g)	0.0	0.0	0.0	0.0	0.0	0.0	0.0
Carbonate %	88.0	88.2	91.3	84.2	83.5	95.3	91.3
Organic Carbon %	0.0	0.0	0.0	0.0	0.2	0.2	0.0
Inorganic Insoluble Residue %	12.0	11.8	8.7	15.8	16.3	4.5	8.7

Sample Name	GC-U25-6.0	GC-U25-9.0	GC-U25-12.0	GC-U25-15.0	D-GC-U25-18.0	GC-U25-18.0	GC-U25-21.0
Stratigraphic Position (m)	377.1	380.1	383.1	386.1	389.1	389.1	392.1
Container Mass (g)	74.4	75.4	73.3	73.9	73.7	73.8	74.0
Sample Mass (g)	6.0	6.0	6.0	6.0	6.0	6.0	6.0
Container and Sample Mass (g)	80.4	81.4	79.3	79.9	79.7	79.8	80.0
Sample Mass after HCl (g)	0.5	0.3	0.6	1.4	1.3	1.3	0.5
Sample Mass after H_2O_2 (g)	0.0	0.0	0.0	0.0	0.0	0.0	0.0
Carbonate %	91.2	94.8	90.3	76.3	79.0	78.8	90.8
Organic Carbon %	0.2	0.2	0.3	0.0	0.0	0.0	0.0
Inorganic Insoluble Residue %	8.7	5.0	9.3	23.7	21.0	21.2	9.2

Sample Name	GC-U25-24.0	GC-U25-27.0	GC-U25-30.0	GC-U25-32.5
Stratigraphic Position (m)	395.1	398.1	401.1	403.6
Container Mass (g)	75.7	74.2	74.5	73.6
Sample Mass (g)	6.0	6.0	6.0	6.0
Container and Sample Mass (g)	81.7	80.2	80.5	79.6
Sample Mass after HCl (g)	0.5	0.4	0.5	1.3
Sample Mass after H_2O_2 (g)	0.0	0.0	0.0	0.0
Carbonate %	91.0	93.8	91.5	79.2
Organic Carbon %	0.2	0.3	0.7	0.5
Inorganic Insoluble Residue %	8.8	5.8	7.8	20.3

Appendix D2. Pogonip Group Inorganic Insoluble Residue, Carbonate, and Total Organic Carbon Data

Sample Name	HL-BHM-15.0	HL-BHM-18.0	HL-BHM-21.0	HL-BHM-25.5	HL-BHM-28.5	HL-BHM-33.0	HL-BHM-36.0
Stratigraphic Position (m)	0.0	3.0	6.0	10.5	13.5	18.0	21.0
Container Mass (g)	73.9	74.4	73.8	75.0	73.7	74.3	75.0
Sample Mass (g)	6.0	6.0	6.0	6.0	6.0	6.0	6.0
Container and Sample Mass (g)	79.9	80.4	79.8	81.0	79.7	80.3	81.0
Sample Mass after HCl (g)	0.1	0.3	0.1	0.3	0.1	0.3	0.6
Sample Mass after H_2O_2 (g)	0.0	0.0	0.0	0.0	0.0	0.0	0.0
Carbonate %	98.7	94.8	98.5	95.0	98.3	95.8	89.7
Organic Carbon %	0.2	0.3	0.3	0.5	0.2	0.3	0.2
Inorganic Insoluble Residue %	1.2	4.8	1.2	4.5	1.5	3.8	10.2

Sample Name	D-HL-BHM-36.0	HL-BHM-43.5	HL-BHM-48.0	HL-BHM-51.0	HL-BHM-51.7	HL-U1-3.0	HL-U1-6.0
Stratigraphic Position (m)	21.0	28.5	33.0	36.0	36.7	39.7	42.7
Container Mass (g)	75.1	75.1	75.3	74.2	73.6	74.7	74.4
Sample Mass (g)	6.0	6.0	6.0	6.0	6.0	6.0	5.0
Container and Sample Mass (g)	81.1	81.1	81.3	80.2	79.6	80.7	79.4
Sample Mass after HCl (g)	0.6	1.0	0.2	0.3	0.2	0.4	0.6
Sample Mass after H_2O_2 (g)	0.0	0.0	0.0	0.0	0.0	0.0	0.0
Carbonate %	90.7	83.0	97.2	95.3	96.7	94.0	87.8
Organic Carbon %	0.2	0.2	0.3	0.3	0.0	0.2	0.6
Inorganic Insoluble Residue %	9.2	16.8	2.5	4.3	3.3	5.8	11.6

Sample Name	HL-U1-9.0	HL-U1-11.2	HL-U2-3.0	HL-U2-6.0	D-HL-U2-6.0	HL-U2-9.0	HL-U2-12.0
Stratigraphic Position (m)	45.7	47.9	50.9	53.9	53.9	56.9	59.9
Container Mass (g)	74.8	74.5	75.6	73.9	74.6	74.9	75.2
Sample Mass (g)	4.8	5.9	6.0	6.0	6.0	4.9	6.0
Container and Sample Mass (g)	79.6	80.4	81.6	79.9	80.6	79.8	81.2
Sample Mass after HCl (g)	0.3	0.4	0.2	0.9	0.9	0.3	0.7
Sample Mass after H_2O_2 (g)	0.0	0.0	0.0	0.0	0.0	0.0	0.0
Carbonate %	94.6	93.1	96.2	85.5	85.5	94.7	88.7
Organic Carbon %	0.6	0.2	0.2	0.3	0.2	0.0	0.3
Inorganic Insoluble Residue %	4.8	6.8	3.7	14.2	14.3	5.3	11.0

Sample Name	HL-U2-16.5	HL-U2-19.5	HL-U2-22.5	HL-U2-25.5	HL-U2-28.5	HL-U2-31.5	HL-U2-34.5
Stratigraphic Position (m)	64.4	67.4	70.4	73.4	76.4	79.4	82.4
Container Mass (g)	74.2	74.9	73.4	73.7	73.8	74.7	73.9
Sample Mass (g)	6.0	6.0	6.0	6.0	5.9	5.0	6.0
Container and Sample Mass (g)	80.2	80.9	79.4	79.7	79.7	79.7	79.9
Sample Mass after HCl (g)	0.5	0.9	0.9	1.6	0.5	1.3	0.9
Sample Mass after H_2O_2 (g)	0.0	0.0	0.0	0.0	0.0	0.0	0.0
Carbonate %	90.8	85.0	85.0	73.0	91.0	74.5	84.7
Organic Carbon %	0.3	0.2	0.2	0.2	0.2	0.2	0.7
Inorganic Insoluble Residue %	8.8	14.8	14.8	26.8	8.9	25.3	14.7

Sample Name	HL-U2-37.4	D-HL-U2-37.4	HL-U3-3.0	HL-U3-6.0	HL-U3-9.0	HL-U3-10.4	HL-U4-3.0
Stratigraphic Position (m)	85.3	85.3	88.3	91.3	94.3	95.7	98.7
Container Mass (g)	74.3	74.1	74.9	71.6	71.3	74.4	73.1
Sample Mass (g)	5.7	6.0	6.0	5.9	6.0	6.0	5.0
Container and Sample Mass (g)	80.0	80.1	80.9	77.5	77.3	80.4	78.1
Sample Mass after HCl (g)	0.7	0.7	0.7	1.6	0.8	0.9	0.8
Sample Mass after H_2O_2 (g)	0.0	0.0	0.0	0.0	0.0	0.0	0.0
Carbonate %	87.3	87.7	88.2	72.3	87.2	84.5	83.1
Organic Carbon %	0.4	0.3	0.0	0.2	0.2	0.0	0.4
Inorganic Insoluble Residue %	12.3	12.0	11.8	27.5	12.7	15.5	16.5

Sample Name	HL-U4-6.0	HL-U4-9.0	HL-U4-12.0	HL-U4-15.0	D-HL-U4-18.0	HL-U4-18.0	HL-U4-21.0
Stratigraphic Position (m)	101.7	104.7	107.7	110.7	113.7	113.7	116.7
Container Mass (g)	73.1	74.2	74.5	74.8	74.8	74.8	75.1
Sample Mass (g)	6.0	5.0	6.0	5.4	6.0	6.0	5.6
Container and Sample Mass (g)	79.1	79.2	80.5	80.3	80.8	80.8	80.6
Sample Mass after HCl (g)	0.5	0.5	0.4	0.3	0.6	0.6	0.5
Sample Mass after H_2O_2 (g)	0.0	0.0	0.0	0.0	0.0	0.0	0.0
Carbonate %	91.8	90.9	92.7	93.6	89.7	89.7	91.9
Organic Carbon %	0.2	0.2	0.2	0.4	0.3	0.0	0.5
Inorganic Insoluble Residue %	8.0	8.9	7.2	6.1	10.0	10.3	7.6

Sample Name	HL-U4-24.0	HL-U4-27.0	HL-U4-30.0	HL-U4-30.5	HL-U5-3.0	HL-U5-6.0	HL-U5-9.0
Stratigraphic Position (m)	119.7	122.7	125.7	126.2	129.2	132.2	135.2
Container Mass (g)	73.8	75.3	74.3	74.8	75.0	74.9	74.1
Sample Mass (g)	5.0	5.6	6.0	5.6	5.6	6.0	6.0
Container and Sample Mass (g)	78.7	80.9	80.3	80.4	80.6	80.9	80.1
Sample Mass after HCl (g)	0.2	0.3	0.1	0.4	0.3	1.1	3.1
Sample Mass after H_2O_2 (g)	0.0	0.0	0.0	0.0	0.0	0.0	0.0
Carbonate %	95.2	94.4	98.5	92.9	94.7	82.0	48.5
Organic Carbon %	0.2	0.7	0.2	0.4	0.4	0.3	0.3
Inorganic Insoluble Residue %	4.6	4.9	1.3	6.7	5.0	17.7	51.2

Sample Name	HL-U5-12.0	HL-U5-15.0	D-HL-U5-15.0	HL-U5-18.0	HL-U5-21.0	HL-U5-24.6	HL-U5-27.0
Stratigraphic Position (m)	138.2	141.2	141.2	144.2	147.2	150.8	153.2
Container Mass (g)	73.8	74.4	74.1	73.6	73.8	74.1	75.3
Sample Mass (g)	5.7	6.0	6.0	6.0	6.0	6.0	5.2
Container and Sample Mass (g)	79.5	80.4	80.1	79.6	79.8	80.1	80.5
Sample Mass after HCl (g)	0.4	0.9	0.9	0.4	0.3	0.9	0.5
Sample Mass after H_2O_2 (g)	0.0	0.0	0.0	0.0	0.0	0.0	0.0
Carbonate %	93.6	85.2	85.5	94.0	94.3	85.5	90.3
Organic Carbon %	0.4	0.3	0.3	0.3	0.0	0.3	0.4
Inorganic Insoluble Residue %	6.0	14.5	14.2	5.7	5.7	14.2	9.3

Sample Name	HL-U5-29.1	HL-U6-1.5	FF-BLLM-U1-0.0	HL-U6-2.5	FF-BLLM-U1-2.4	FF-BLLM-U2-1.3	FF-BLLM-U3-0.0
Stratigraphic Position (m)	155.3	156.8	157.8	157.8	160.2	161.5	161.9
Container Mass (g)	74.0	74.8	75.2	74.8	73.8	75.4	74.1
Sample Mass (g)	6.0	5.4	6.0	6.0	6.0	6.0	6.0
Container and Sample Mass (g)	80.0	80.2	81.2	80.8	79.8	81.4	80.1
Sample Mass after HCl (g)	0.4	0.1	0.2	0.2	0.2	0.2	0.2
Sample Mass after H_2O_2 (g)	0.0	0.0	0.0	0.0	0.0	0.0	0.0
Carbonate %	93.7	97.6	96.8	97.0	96.2	97.0	96.7
Organic Carbon %	0.2	0.2	0.3	0.0	0.3	0.2	0.5
Inorganic Insoluble Residue %	6.2	2.2	2.8	3.0	3.5	2.8	2.8

Sample Name	FF-BLLM-U4-0.6	FF-BLLM-U5-1.7	FF-BLLM-U6-1.5	FF-BLLM-U7-0.0	FF-BLLM-U7-2.3	D-FF-BLLM-U8-1.5	FF-BLLM-U8-1.5
Stratigraphic Position (m)	162.8	164.5	166.0	167.7	170.0	171.5	171.5
Container Mass (g)	74.7	73.6	66.4	65.8	74.0	74.7	75.4
Sample Mass (g)	6.0	6.0	6.0	6.0	6.0	6.0	6.0
Container and Sample Mass (g)	80.7	79.6	72.4	71.8	80.0	80.7	81.4
Sample Mass after HCl (g)	0.3	0.3	0.3	0.7	0.6	0.3	0.3
Sample Mass after H_2O_2 (g)	0.1	0.0	0.0	0.0	0.0	0.0	0.0
Carbonate %	94.7	94.7	94.8	87.7	90.7	95.8	95.3
Organic Carbon %	1.3	0.5	0.3	0.0	0.0	0.0	0.0
Inorganic Insoluble Residue %	4.0	4.8	4.8	12.3	9.3	4.2	4.7

Sample Name	FF-BLLM-U9-0.7	FF-BLLM-U10-3.0	FF-BLLM-U10-6.0	FF-BLLM-U10-8.9	FF-BLLM-U11-2.7	FF-BLLM-U12-1.0	FF-BLLM-U13-4.3
Stratigraphic Position (m)	172.5	175.9	178.9	181.7	184.4	185.4	190.0
Container Mass (g)	75.2	74.3	73.6	73.8	73.9	75.0	74.1
Sample Mass (g)	6.0	6.0	6.0	6.0	6.0	6.0	6.0
Container and Sample Mass (g)	81.2	80.3	79.6	79.8	79.9	81.0	80.1
Sample Mass after HCl (g)	0.7	0.3	0.4	1.3	0.1	0.5	0.4
Sample Mass after H_2O_2 (g)	0.0	0.0	0.0	0.0	0.0	0.1	0.0
Carbonate %	88.8	94.7	94.0	78.3	98.0	92.5	93.5
Organic Carbon %	0.3	0.2	0.8	0.0	0.0	1.8	0.7
Inorganic Insoluble Residue %	10.8	5.2	5.2	21.7	2.0	5.7	5.8

Sample Name	FF-BLLM-U13-8.6	FF-BLLM-U13-12.3	D-FF-BLLM-U13-17.5	FF-BLLM-U13-17.5	FF-BLLM-U13-21.0	FF-BLLM-U13-25.5	FF-BLLM-U14-1.5
Stratigraphic Position (m)	194.3	198.0	203.1	203.1	206.7	211.2	215.3
Container Mass (g)	75.3	75.2	75.2	74.8	75.6	73.7	74.8
Sample Mass (g)	6.0	6.0	6.0	6.0	6.0	6.0	6.0
Container and Sample Mass (g)	81.3	81.2	81.2	80.8	81.6	79.7	80.8
Sample Mass after HCl (g)	0.4	0.9	1.0	1.1	0.7	0.6	1.2
Sample Mass after H_2O_2 (g)	0.0	0.0	0.1	0.1	0.0	0.0	0.0
Carbonate %	93.7	84.7	83.7	81.7	87.7	89.8	80.2
Organic Carbon %	0.7	0.5	2.2	2.2	0.7	0.3	0.5
Inorganic Insoluble Residue %	5.7	14.8	14.2	16.2	11.7	9.8	19.3

Sample Name	FF-BLLM-U14-4.5	FF-BLLM-U14-10.5	FF-BLLM-U15-2.5	FF-BLLM-U16-0.7	FF-BLLM-U17-3.0	FF-BLLM-U17-6.0	D-FF-BLLM-U17-9.0
Stratigraphic Position (m)	218.3	224.3	227.4	229.6	233.2	236.2	239.2
Container Mass (g)	73.3	72.2	73.3	73.5	74.2	74.8	74.2
Sample Mass (g)	6.0	6.0	6.0	6.0	6.0	6.0	6.0
Container and Sample Mass (g)	79.3	78.2	79.3	79.5	80.2	80.8	80.2
Sample Mass after HCl (g)	0.9	0.5	0.4	0.4	0.2	0.2	1.2
Sample Mass after H_2O_2 (g)	0.0	0.0	0.0	0.0	0.0	0.0	0.0
Carbonate %	85.3	92.2	94.0	93.0	96.2	96.2	80.2
Organic Carbon %	0.0	0.3	0.0	0.2	0.5	0.2	0.2
Inorganic Insoluble Residue %	14.7	7.5	6.0	6.8	3.3	3.7	19.7

Sample Name	FF-BLLM-U17-9.0	FF-BLLM-U17-12.0	FF-BLLM-U17-15.0	FF-BLLM-U17-18.0	FF-BLLM-U17-21.0	FF-BLLM-U17-24.0	FF-BLLM-U17-27.0
Stratigraphic Position (m)	239.2	242.2	245.2	248.2	251.2	254.2	257.2
Container Mass (g)	74.5	75.1	74.3	74.1	74.7	74.9	74.4
Sample Mass (g)	6.0	6.0	6.0	6.0	6.0	6.0	6.0
Container and Sample Mass (g)	80.5	81.1	80.3	80.1	80.7	80.9	80.4
Sample Mass after HCl (g)	1.2	1.3	1.0	0.5	0.6	1.3	1.4
Sample Mass after H_2O_2 (g)	0.0	0.1	0.0	0.0	0.0	0.1	0.0
Carbonate %	80.3	78.3	83.5	91.7	89.7	78.5	77.5
Organic Carbon %	0.2	2.2	0.3	0.0	0.3	1.0	0.0
Inorganic Insoluble Residue %	19.5	19.5	16.2	8.3	10.0	20.5	22.5

Sample Name	FF-BLLM-U17-30.0	FF-BLLM-U17-36.0	FF-BLLM-U17-40.5	FF-BLLM-U18-0.7	D-FF-BLLM-U18-0.7	FF-BLLM-U19-3.0	FF-BLLM-U19-6.0
Stratigraphic Position (m)	260.2	266.2	270.7	271.7	271.7	274.9	277.9
Container Mass (g)	74.8	75.5	75.2	66.4	74.5	74.0	73.9
Sample Mass (g)	6.0	6.0	6.0	6.0	6.0	6.0	6.0
Container and Sample Mass (g)	80.8	81.5	81.2	72.4	80.5	80.0	79.9
Sample Mass after HCl (g)	0.5	0.8	1.0	0.5	0.5	0.2	0.4
Sample Mass after H_2O_2 (g)	0.0	0.0	0.0	0.0	0.0	0.0	0.1
Carbonate %	91.2	86.8	83.7	92.0	92.0	96.0	93.5
Organic Carbon %	0.0	0.3	0.2	0.0	0.2	0.0	1.8
Inorganic Insoluble Residue %	8.8	12.8	16.2	8.0	7.8	4.0	4.7

Sample Name	FF-BLLM-U19-9.0	FF-BLLM-U20-4.5	FF-BLLM-U20-6.0	FF-BLLM-U21-1.8	FF-BLLM-U22-1.5	FF-BLLM-U22-4.2	FF-BLLM-U23-0.6
Stratigraphic Position (m)	280.9	286.1	287.6	290.3	292.3	295.0	295.6
Container Mass (g)	74.4	74.7	74.8	73.7	74.7	73.8	72.4
Sample Mass (g)	6.0	6.0	6.0	6.0	6.0	6.0	6.0
Container and Sample Mass (g)	80.4	80.7	80.8	79.7	80.7	79.8	78.4
Sample Mass after HCl (g)	0.7	1.2	1.4	1.1	1.6	0.3	0.8
Sample Mass after H_2O_2 (g)	0.0	0.0	0.0	0.0	0.0	0.0	0.0
Carbonate %	88.5	79.3	76.7	81.7	73.2	95.0	87.0
Organic Carbon %	0.0	0.0	0.3	0.2	0.0	0.0	0.0
Inorganic Insoluble Residue %	11.5	20.7	23.0	18.2	26.8	5.0	13.0

Sample Name	D-FF-BLLM-U23-3.9	FF-BLLM-U23-3.9	FF-BLLM-U24-3.0	FF-BLLM-U24-6.0	FF-BLLM-U24-9.0	FF-BLLM-U24-12.0	FF-BLLM-U24-15.0
Stratigraphic Position (m)	298.9	298.9	301.9	304.9	307.9	310.9	313.9
Container Mass (g)	73.3	73.1	73.5	74.9	74.0	74.3	74.9
Sample Mass (g)	6.0	6.0	6.0	6.0	6.0	6.0	6.0
Container and Sample Mass (g)	79.3	79.1	79.5	80.9	80.0	80.3	80.9
Sample Mass after HCl (g)	0.9	0.9	0.6	0.4	0.9	0.5	0.4
Sample Mass after H_2O_2 (g)	0.0	0.0	0.0	0.0	0.0	0.0	0.0
Carbonate %	85.5	85.3	90.0	92.7	84.5	91.8	92.7
Organic Carbon %	0.2	0.2	0.2	0.0	0.0	0.3	0.0
Inorganic Insoluble Residue %	14.3	14.5	9.8	7.3	15.5	7.8	7.3

Sample Name	FF-BLLM-U24-18.0	FF-BLLM-U24-18.0 A	FF-BLLM-U24-21.0	FF-BLLM-U24-24.0	FF-BLLM-U24-27.0	D-FF-BLLM-U24-27.0	FF-BLLM-U24-30.0
Stratigraphic Position (m)	316.9	316.9	319.9	322.9	325.9	325.9	328.9
Container Mass (g)	74.8	74.7	74.1	73.9	73.8	74.8	74.1
Sample Mass (g)	6.0	6.0	6.0	6.0	5.9	5.9	6.0
Container and Sample Mass (g)	80.8	80.7	80.1	79.9	79.7	80.7	80.1
Sample Mass after HCl (g)	0.9	2.8	0.2	1.3	0.5	0.5	0.9
Sample Mass after H_2O_2 (g)	0.0	0.1	0.0	0.0	0.0	0.0	0.0
Carbonate %	84.5	53.3	97.0	78.7	91.5	91.7	85.7
Organic Carbon %	0.0	1.2	0.0	0.2	0.5	0.7	0.2
Inorganic Insoluble Residue %	15.5	45.5	3.0	21.2	8.0	7.7	14.2

Sample Name	FF-BLLM-U24-33.0	FF-BLLM-U24-36.0	FF-SSSM-U1-2.6	FF-SSSM-U2-3.0	FF-SSSM-U2-6.0	FF-SSSM-U2-10.1	FF-SSSM-U2-13.5
Stratigraphic Position (m)	331.9	334.9	337.4	340.4	343.4	347.5	350.9
Container Mass (g)	74.7	74.1	74.1	73.2	73.6	74.3	76.1
Sample Mass (g)	6.0	6.0	6.0	6.0	6.0	6.0	6.0
Container and Sample Mass (g)	80.7	80.1	80.1	79.2	79.6	80.3	82.1
Sample Mass after HCl (g)	0.7	0.8	0.5	0.8	0.7	1.7	0.7
Sample Mass after H_2O_2 (g)	0.0	0.0	0.0	0.0	0.0	0.0	0.0
Carbonate %	89.0	87.5	90.8	86.8	89.0	71.7	89.0
Organic Carbon %	0.3	0.2	0.3	0.2	0.2	0.3	0.3
Inorganic Insoluble Residue %	10.7	12.3	8.8	13.0	10.8	28.0	10.7

Sample Name	FF-SSSM-U2-18.0	D-FF-SSSM-U2-21.0	FF-SSSM-U2-21.0	FF-SSSM-U2-24.0	FF-SSSM-U2-26.8	FF-SSSM-U3-3.0	FF-SSSM-U3-5.7
Stratigraphic Position (m)	355.4	358.4	358.4	361.4	364.2	367.2	369.9
Container Mass (g)	75.3	75.1	75.4	62.4	74.9	74.7	74.2
Sample Mass (g)	6.0	6.0	6.0	6.0	6.0	6.0	6.0
Container and Sample Mass (g)	81.3	81.1	81.4	68.4	80.9	80.7	80.2
Sample Mass after HCl (g)	0.5	2.4	2.3	2.2	2.2	1.5	0.5
Sample Mass after H_2O_2 (g)	0.0	0.0	0.0	0.1	0.0	0.0	0.0
Carbonate %	91.5	60.8	60.8	64.2	62.7	74.7	91.8
Organic Carbon %	0.2	0.7	0.5	2.0	0.2	0.0	0.5
Inorganic Insoluble Residue %	8.3	38.5	38.7	33.8	37.2	25.3	7.7

Sample Name	FF-SSSM-U3-9.0	FF-SSSM-U3-12.0	FF-SSSM-U3-15.0	FF-SSSM-U4-3.0	FF-SSSM-U4-6.0	D-FF-SSSM-U4-12.0	FF-SSSM-U4-12.0
Stratigraphic Position (m)	373.2	376.2	379.2	383.4	386.4	392.4	392.4
Container Mass (g)	75.3	74.6	74.4	73.7	75.8	74.4	74.3
Sample Mass (g)	6.0	6.0	6.0	6.0	6.0	6.0	6.0
Container and Sample Mass (g)	81.3	80.6	80.4	79.7	81.8	80.4	80.3
Sample Mass after HCl (g)	0.5	0.8	0.3	1.4	0.6	1.0	1.0
Sample Mass after H_2O_2 (g)	0.0	0.0	0.0	0.0	0.0	0.0	0.0
Carbonate %	92.3	86.3	95.0	77.3	89.8	84.0	83.8
Organic Carbon %	0.0	0.5	0.0	0.0	0.3	0.2	0.3
Inorganic Insoluble Residue %	7.7	13.2	5.0	22.7	9.8	15.8	15.8

Sample Name	FF-SSSM-U4-15.0	FF-SSSM-U4-18.0	FF-SSSM-U4-21.5	FF-SSSM-U5-5.3	FF-SSSM-U5-9.0	FF-SSSM-U5-13.5	FF-SSSM-U5-16.5
Stratigraphic Position (m)	395.4	398.4	401.9	407.2	410.9	415.4	418.4
Container Mass (g)	73.4	74.1	75.8	74.7	73.9	75.6	74.0
Sample Mass (g)	6.0	6.0	6.0	6.0	6.0	6.0	6.0
Container and Sample Mass (g)	79.4	80.1	81.8	80.7	79.9	81.6	80.0
Sample Mass after HCl (g)	0.8	1.2	0.6	0.4	1.0	1.0	1.5
Sample Mass after H_2O_2 (g)	0.0	0.1	0.0	0.0	0.0	0.0	0.0
Carbonate %	87.0	80.3	89.5	93.8	83.2	83.5	75.2
Organic Carbon %	0.2	1.2	0.7	0.3	0.2	0.0	0.0
Inorganic Insoluble Residue %	12.8	18.5	9.8	5.8	16.7	16.5	24.8

Sample Name	FF-SSSM-U5-19.5	FF-SSSM-U5-22.5	D-FF-SSSM-U5-25.5	FF-SSSM-U5-25.5	FF-SSSM-U5-27.3	FF-LGLM-U1-0.6	FF-LGLM-U3-0.3
Stratigraphic Position (m)	421.4	424.4	427.4	427.4	429.2	429.8	433.4
Container Mass (g)	74.7	75.6	74.2	73.9	73.8	75.4	74.7
Sample Mass (g)	6.0	6.0	6.0	6.0	6.0	6.0	6.0
Container and Sample Mass (g)	80.7	81.6	80.2	79.9	79.8	81.4	80.7
Sample Mass after HCl (g)	1.0	1.3	0.4	0.4	0.9	0.4	0.4
Sample Mass after H_2O_2 (g)	0.0	0.0	0.0	0.0	0.0	0.0	0.0
Carbonate %	84.2	78.3	93.8	93.8	84.8	94.0	94.2
Organic Carbon %	0.3	0.0	0.0	0.0	0.0	0.2	0.0
Inorganic Insoluble Residue %	15.5	21.7	6.2	6.2	15.2	5.8	5.8

Sample Name	FF-LGLM-U4-0.8	FF-LGLM-U5-2.6	FF-LGLM-U5-6.0	FF-LGLM-U5-9.0	FF-LGLM-U5-12.4	D-FF-LGLM-U6-0.4	FF-LGLM-U6-0.4
Stratigraphic Position (m)	434.9	438.5	441.9	444.9	448.3	448.7	448.7
Container Mass (g)	73.8	73.4	73.6	75.0	75.5	75.3	73.4
Sample Mass (g)	6.0	6.0	6.0	6.0	6.0	6.0	6.0
Container and Sample Mass (g)	79.8	79.4	79.6	81.0	81.5	81.3	79.4
Sample Mass after HCl (g)	1.1	0.3	0.5	0.8	0.4	1.0	1.0
Sample Mass after H_2O_2 (g)	0.0	0.0	0.0	0.0	0.0	0.0	0.0
Carbonate %	80.8	95.0	91.3	87.3	94.0	83.3	83.2
Organic Carbon %	0.3	0.0	0.3	0.3	0.3	0.0	0.2
Inorganic Insoluble Residue %	18.8	5.0	8.3	12.3	5.7	16.7	16.7

Sample Name	FF-LGLM-U7-3.0	FF-LGLM-U7-6.0	FF-LGLM-U7-9.0	FF-LGLM-U7-11.4	FF-LGLM-U7-15.0	FF-LGLM-U7-17.5	FF-LGLM-U8-3.0
Stratigraphic Position (m)	451.7	454.7	457.7	460.1	463.7	466.2	469.2
Container Mass (g)	74.8	73.5	73.2	73.6	73.9	73.6	74.4
Sample Mass (g)	6.0	6.0	6.0	6.0	6.0	6.0	6.0
Container and Sample Mass (g)	80.8	79.5	79.2	79.6	79.9	79.6	80.4
Sample Mass after HCl (g)	0.7	1.3	0.5	0.5	0.8	1.6	0.7
Sample Mass after H_2O_2 (g)	0.0	0.0	0.0	0.0	0.0	0.0	0.0
Carbonate %	89.0	78.5	91.8	91.8	86.3	73.2	88.8
Organic Carbon %	0.2	0.2	0.2	0.2	0.3	0.3	0.5
Inorganic Insoluble Residue %	10.8	21.3	8.0	8.0	13.3	26.5	10.7

Sample Name	FF-LGLM-U9-0.0	FF-LGLM-U10-1.5	D-FF-BSLM-U1-3.0	FF-BSLM-U1-3.0	FF-BSLM-U1-6.0	FF-BSLM-U1-9.0	FF-BSLM-U1-12.0
Stratigraphic Position (m)	472.9	475.2	480.6	480.6	483.6	486.6	489.6
Container Mass (g)	74.2	62.3	74.5	74.4	74.5	74.3	74.2
Sample Mass (g)	6.0	6.0	6.0	6.0	6.0	6.0	6.0
Container and Sample Mass (g)	80.2	68.3	80.5	80.4	80.5	80.3	80.2
Sample Mass after HCl (g)	0.5	0.5	1.4	1.4	1.6	0.6	1.5
Sample Mass after H_2O_2 (g)	0.0	0.0	0.0	0.0	0.0	0.0	0.0
Carbonate %	91.8	91.2	77.0	76.8	73.2	90.5	75.0
Organic Carbon %	0.3	0.2	0.3	0.8	0.7	0.3	0.5
Inorganic Insoluble Residue %	7.8	8.7	22.7	22.3	26.2	9.2	24.5

Sample Name	FF-BSLM-U1-15.0	FF-BSLM-U1-18.0	FF-BSLM-U2-0.0	FF-BSLM-U3-4.5	FF-BSLM-U3-7.5	FF-BSLM-U3-10.7	D-FF-BSLM-U4-0.4
Stratigraphic Position (m)	492.6	495.6	498.1	503.1	506.1	509.3	512.5
Container Mass (g)	73.2	73.9	75.8	74.9	75.5	71.3	74.8
Sample Mass (g)	6.0	6.0	6.0	6.0	6.0	6.0	6.0
Container and Sample Mass (g)	79.2	79.9	81.8	80.9	81.5	77.3	80.8
Sample Mass after HCl (g)	1.1	1.0	0.8	0.5	0.7	1.0	2.7
Sample Mass after H_2O_2 (g)	0.0	0.0	0.0	0.0	0.0	0.0	0.0
Carbonate %	82.3	84.2	86.2	92.2	88.3	82.8	55.7
Organic Carbon %	0.0	0.0	0.5	0.2	0.3	0.0	0.2
Inorganic Insoluble Residue %	17.7	15.8	13.3	7.7	11.3	17.2	44.2

Sample Name	FF-BSLM-U4-0.4	FF-BSLM-U5-3.0	FF-BSLM-U5-7.5	FF-BSLM-U5-10.5	FF-BSLM-U5-13.5	FF-BSLM-U6-1.0	FF-BSLM-U7-3.0
Stratigraphic Position (m)	512.5	515.5	520.0	523.0	526.0	527.7	531.0
Container Mass (g)	73.7	73.6	75.8	75.4	73.8	73.2	73.2
Sample Mass (g)	6.0	6.0	6.0	6.0	6.0	6.0	6.0
Container and Sample Mass (g)	79.7	79.6	81.8	81.4	79.8	79.2	79.2
Sample Mass after HCl (g)	2.6	0.9	1.2	1.0	2.3	0.5	0.2
Sample Mass after H_2O_2 (g)	0.0	0.0	0.0	0.0	0.0	0.0	0.0
Carbonate %	55.8	85.8	80.2	83.7	61.7	91.3	96.2
Organic Carbon %	0.2	0.5	0.0	0.2	0.2	0.0	0.2
Inorganic Insoluble Residue %	44.0	13.7	19.8	16.2	38.2	8.7	3.7

Sample Name	FF-BSLM-U7-6.0	FF-BSLM-U7-9.2	FF-BSLM-U8-3.4	FF-BSLM-U8-6.3	D-FF-BSLM-U8-6.3	FF-BSLM-U8-9.0	FF-BSLM-U8-12.0
Stratigraphic Position (m)	534.0	537.2	540.6	543.4	543.4	546.2	549.2
Container Mass (g)	73.7	72.7	75.6	75.5	74.6	74.5	73.8
Sample Mass (g)	6.0	6.0	6.0	6.0	6.0	6.0	6.0
Container and Sample Mass (g)	79.7	78.7	81.6	81.5	80.6	80.5	79.8
Sample Mass after HCl (g)	0.3	0.8	0.5	0.4	0.4	0.6	0.5
Sample Mass after H_2O_2 (g)	0.0	0.0	0.0	0.0	0.0	0.0	0.0
Carbonate %	95.7	86.0	92.3	93.2	93.0	90.2	91.5
Organic Carbon %	0.2	0.0	0.2	0.2	0.3	0.2	0.3
Inorganic Insoluble Residue %	4.2	14.0	7.5	6.7	6.7	9.7	8.2

Sample Name	FF-BSLM-U9-0.6	FF-BSLM-U10-2.5	FF-BSLM-U10-6.0	FF-BSLM-U10-10.5	FF-BSLM-U10-13.5	FF-BSLM-U11-0.8	FF-CM-U1-0.0
Stratigraphic Position (m)	553.1	555.6	559.1	563.6	566.6	569.3	569.8
Container Mass (g)	75.6	73.6	75.6	74.4	73.5	65.9	75.7
Sample Mass (g)	6.0	6.0	6.0	6.0	6.0	6.0	6.0
Container and Sample Mass (g)	81.6	79.6	81.6	80.4	79.5	71.9	81.7
Sample Mass after HCl (g)	0.5	0.5	1.4	0.8	0.6	0.6	1.3
Sample Mass after H_2O_2 (g)	0.0	0.0	0.0	0.0	0.0	0.0	0.0
Carbonate %	91.0	91.7	76.8	86.5	90.7	89.8	77.7
Organic Carbon %	0.0	0.5	0.2	0.0	0.0	0.5	0.2
Inorganic Insoluble Residue %	9.0	7.8	23.0	13.5	9.3	9.7	22.2

Sample Name	D-FF-CM-U1-3.0	FF-CM-U1-3.0	FF-CM-U1-6.8	FF-CM-U1-11.1	FF-CM-U2-2.6	FF-CM-U2-6.0	FF-CM-U3-0.0
Stratigraphic Position (m)	572.8	572.8	576.6	580.9	583.5	586.9	588.7
Container Mass (g)	74.7	75.0	74.0	75.1	75.6	72.5	74.6
Sample Mass (g)	6.0	6.0	6.0	6.0	6.0	6.0	6.0
Container and Sample Mass (g)	80.7	81.0	80.0	81.1	81.6	78.5	80.6
Sample Mass after HCl (g)	2.0	2.0	0.8	1.6	0.7	1.0	1.0
Sample Mass after H_2O_2 (g)	0.0	0.0	0.0	0.0	0.0	0.0	0.0
Carbonate %	67.3	67.3	86.3	72.7	87.8	83.5	83.2
Organic Carbon %	0.0	0.0	0.3	0.5	0.0	0.2	0.0
Inorganic Insoluble Residue %	32.7	32.7	13.3	26.8	12.2	16.3	16.8

Sample Name	FF-CM-U4-3.0	FF-CM-U4-6.0	FF-CM-U5-4.5	FF-CM-U5-4.8	FF-CM-U5-7.5	D-FF-CM-U5-7.5	FF-CM-U5-11.3
Stratigraphic Position (m)	592.1	595.1	601.1	601.4	604.1	604.1	607.9
Container Mass (g)	74.2	74.5	73.9	74.6	75.2	74.6	74.1
Sample Mass (g)	6.0	6.0	6.0	6.0	6.0	6.0	6.0
Container and Sample Mass (g)	80.2	80.5	79.9	80.6	81.2	80.6	80.1
Sample Mass after HCl (g)	1.0	0.5	1.8	3.4	2.3	2.3	2.5
Sample Mass after H_2O_2 (g)	0.0	0.0	0.0	0.2	0.0	0.0	0.0
Carbonate %	83.8	92.0	69.2	43.7	62.5	62.2	58.5
Organic Carbon %	0.2	0.0	0.0	3.3	0.0	0.2	0.7
Inorganic Insoluble Residue %	16.0	8.0	30.8	53.0	37.5	37.7	40.8

Sample Name	FF-CM-U5-15.0	FF-CM-U5-18.0	FF-CM-U5-23.4	FF-CM-U5-27.3	FF-CM-U5-31.7	FF-CM-U5-36.4	FF-CM-U6-1.5
Stratigraphic Position (m)	611.6	614.6	620.0	623.9	628.3	633.0	635.5
Container Mass (g)	73.1	73.4	73.5	74.2	73.7	74.6	76.0
Sample Mass (g)	6.0	6.0	6.0	6.0	6.0	6.0	6.0
Container and Sample Mass (g)	79.1	79.4	79.5	80.2	79.7	80.6	82.0
Sample Mass after HCl (g)	1.0	0.6	1.9	2.0	1.3	0.4	0.9
Sample Mass after H_2O_2 (g)	0.0	0.0	0.0	0.0	0.0	0.0	0.0
Carbonate %	83.0	89.5	68.5	67.2	78.2	93.3	85.5
Organic Carbon %	0.3	0.3	0.0	0.7	0.8	0.0	0.7
Inorganic Insoluble Residue %	16.7	10.2	31.5	32.2	21.0	6.7	13.8

Sample Name	FF-CM-U7-3.0	D-FF-CM-U7-6.0	FF-CCM-U1-1.5	FF-CCM-U2-3.0	FF-CCM-U2-6.3	FF-CCM-U3-0.3	FF-CCM-U4-2.8
Stratigraphic Position (m)	638.5	641.5	643.0	647.5	650.8	651.9	655.1
Container Mass (g)	74.8	75.3	74.2	73.6	74.5	74.0	73.3
Sample Mass (g)	6.0	6.0	6.0	6.0	6.0	6.0	6.0
Container and Sample Mass (g)	80.8	81.3	80.2	79.6	80.5	80.0	79.3
Sample Mass after HCl (g)	0.5	0.5	0.2	0.4	1.1	1.0	1.0
Sample Mass after H_2O_2 (g)	0.0	0.0	0.0	0.0	0.1	0.0	0.0
Carbonate %	91.5	91.0	96.2	92.7	81.3	82.7	84.2
Organic Carbon %	0.2	0.5	0.0	0.3	1.3	0.3	0.0
Inorganic Insoluble Residue %	8.3	8.5	3.8	7.0	17.3	17.0	15.8

Sample Name	FF-CCM-U4-6.0	FF-CCM-U5-2.0	FF-CCM-U5-3.0	FF-CCM-U5-4.0	FF-CCM-U6-0.9	D-FF-CCM-U6-0.9	FF-CCM-U7-3.5
Stratigraphic Position (m)	658.3	660.3	661.3	662.3	664.5	664.5	668.5
Container Mass (g)	75.3	73.8	75.1	75.2	75.0	74.9	74.3
Sample Mass (g)	6.0	6.0	6.0	6.0	6.0	6.0	6.0
Container and Sample Mass (g)	81.3	79.8	81.1	81.2	81.0	80.9	80.3
Sample Mass after HCl (g)	1.0	4.7	4.5	2.9	1.1	1.1	2.6
Sample Mass after H_2O_2 (g)	0.0	0.1	0.1	0.0	0.0	0.0	0.3
Carbonate %	83.0	21.8	25.8	51.5	81.3	81.2	57.3
Organic Carbon %	0.2	2.0	2.0	0.0	0.3	0.3	4.8
Inorganic Insoluble Residue %	16.8	76.2	72.2	48.5	18.3	18.5	37.8

Sample Name	FF-CCM-U7-6.2	FF-CCM-U8-0.0	FF-CCM-U9-3.0	FF-CCM-U9-6.0	FF-CCM-U9-9.0	FF-CCM-U9-12.6	FF-CCM-U9-13.3
Stratigraphic Position (m)	671.2	673.2	676.5	679.5	682.5	686.1	686.8
Container Mass (g)	73.8	73.9	74.7	73.7	73.7	73.2	73.5
Sample Mass (g)	6.0	6.0	6.0	6.0	6.0	6.0	6.0
Container and Sample Mass (g)	79.8	79.9	80.7	79.7	79.7	79.2	79.5
Sample Mass after HCl (g)	1.4	1.2	0.8	0.4	1.9	1.8	0.9
Sample Mass after H_2O_2 (g)	0.0	0.0	0.0	0.0	0.0	0.0	0.0
Carbonate %	76.5	80.3	87.2	93.0	67.8	69.7	85.5
Organic Carbon %	0.2	0.3	0.3	0.3	0.7	0.3	0.5
Inorganic Insoluble Residue %	23.3	19.3	12.5	6.7	31.5	30.0	14.0

Sample Name	WW-U1-0.8A	WW-U1-0.8B	WW-U2-0.9	WW-U3-0.4	WW-U4-1.1	WW-U5-0.0	WW-U5-1.3
Stratigraphic Position (m)	687.6	687.6	689.5	690.2	691.5	693.7	695.0
Container Mass (g)	74.8	74.8	73.9	73.8	74.0	74.6	75.0
Sample Mass (g)	6.0	6.0	6.0	6.0	6.0	6.0	6.0
Container and Sample Mass (g)	80.8	80.8	79.9	79.8	80.0	80.6	81.0
Sample Mass after HCl (g)	3.2	1.6	0.7	0.9	1.8	1.1	0.6
Sample Mass after H_2O_2 (g)	0.0	0.0	0.0	0.0	0.0	0.0	0.0
Carbonate %	46.3	72.5	88.2	85.5	70.5	82.5	90.8
Organic Carbon %	0.7	0.2	0.3	0.5	0.5	0.3	0.2
Inorganic Insoluble Residue %	53.0	27.3	11.5	14.0	29.0	17.2	9.0

Sample Name	WW-U5-2.6	WW-U6-1.2	WW-U6-3.2	D-WW-U6-3.2	WW-U7-0.0	WW-U7-1.8	WW-U9-0.0
Stratigraphic Position (m)	696.3	697.5	699.5	699.5	700.2	702.0	703.2
Container Mass (g)	74.1	73.9	74.5	75.1	73.4	73.9	73.3
Sample Mass (g)	6.0	6.0	6.0	6.0	6.0	6.0	6.0
Container and Sample Mass (g)	80.1	79.9	80.5	81.1	79.4	79.9	79.3
Sample Mass after HCl (g)	1.4	1.0	0.5	0.4	1.6	1.5	0.6
Sample Mass after H_2O_2 (g)	0.1	0.0	0.0	0.0	0.0	0.0	0.0
Carbonate %	76.7	82.8	92.5	92.5	72.7	74.8	90.3
Organic Carbon %	1.0	0.2	0.0	0.0	0.0	0.0	0.2
Inorganic Insoluble Residue %	22.3	17.0	7.5	7.5	27.3	25.2	9.5

Sample Name	WW-U10-4.0	WW-U10-5.0	WW-U10-7.5	WW-U11-0.9	WW-U11-1.0	WW-U12-0.0	WW-U12-2.5
Stratigraphic Position (m)	707.5	708.5	711.0	711.9	712.0	712.5	715.0
Container Mass (g)	73.7	75.0	74.0	74.1	74.6	74.3	75.6
Sample Mass (g)	6.0	6.0	6.0	6.0	6.0	6.0	6.0
Container and Sample Mass (g)	79.7	81.0	80.0	80.1	80.6	80.3	81.6
Sample Mass after HCl (g)	0.9	1.7	0.8	1.1	0.7	1.3	0.4
Sample Mass after H_2O_2 (g)	0.0	0.1	0.0	0.0	0.0	0.0	0.0
Carbonate %	85.0	71.7	86.3	81.8	87.7	78.2	92.8
Organic Carbon %	0.0	1.3	0.3	0.0	0.7	0.7	0.2
Inorganic Insoluble Residue %	15.0	27.0	13.3	18.2	11.7	21.2	7.0

Sample Name	D-WW-U12-2.5	WW-U13-0.0	WW-U13-3.0	WW-U14-1.5	WW-U15-0.4	WW-U16-1.5	WW-U16-5.1
Stratigraphic Position (m)	715.0	717.2	720.2	721.7	723.9	725.6	729.2
Container Mass (g)	74.7	74.1	74.7	74.2	74.0	75.0	74.2
Sample Mass (g)	6.0	6.0	6.0	6.0	6.0	6.0	6.0
Container and Sample Mass (g)	80.7	80.1	80.7	80.2	80.0	81.0	80.2
Sample Mass after HCl (g)	0.4	0.4	0.7	1.1	0.7	1.7	1.1
Sample Mass after H_2O_2 (g)	0.0	0.0	0.0	0.0	0.0	0.0	0.0
Carbonate %	92.7	92.7	87.7	82.0	88.8	72.0	81.8
Organic Carbon %	0.0	0.0	0.3	0.5	0.2	0.2	0.3
Inorganic Insoluble Residue %	7.3	7.3	12.0	17.5	11.0	27.8	17.8

Sample Name	WW-U16-7.0	WW-U16-7.8	WW-U17-1.1	D-WW-U18-1.5	WW-U18-1.5	WW-U19-1.5	WW-U19-3.0
Stratigraphic Position (m)	731.1	731.9	733.0	735.1	735.1	737.2	738.7
Container Mass (g)	73.8	74.0	74.0	74.9	74.7	74.2	74.2
Sample Mass (g)	6.0	6.0	6.0	6.0	6.0	6.0	6.0
Container and Sample Mass (g)	79.8	80.0	80.0	80.9	80.7	80.2	80.2
Sample Mass after HCl (g)	1.6	0.7	1.5	0.9	0.9	3.4	4.9
Sample Mass after H_2O_2 (g)	0.0	0.0	0.0	0.0	0.0	0.0	0.2
Carbonate %	74.0	88.7	75.8	84.3	84.3	43.5	17.7
Organic Carbon %	0.3	0.3	0.0	0.7	0.7	0.2	2.5
Inorganic Insoluble Residue %	25.7	11.0	24.2	15.0	15.0	56.3	79.8

Sample Name	WW-U20-0.8	WW-U21-1.5	WW-U21-3.0	WW-U22-1.1	WW-U23-1.5	WW-U23-3.2	JL-U1-1.5
Stratigraphic Position (m)	740.3	741.8	743.3	744.4	746.5	748.6	750.1
Container Mass (g)	74.4	73.9	75.0	75.6	73.4	75.1	73.8
Sample Mass (g)	6.0	6.0	6.0	6.0	6.0	6.0	6.0
Container and Sample Mass (g)	80.4	79.9	81.0	81.6	79.4	81.1	79.8
Sample Mass after HCl (g)	1.4	1.5	5.2	1.1	0.5	0.9	2.1
Sample Mass after H_2O_2 (g)	0.0	0.0	0.2	0.0	0.0	0.0	0.0
Carbonate %	76.5	75.8	12.7	81.7	91.8	85.3	65.5
Organic Carbon %	0.2	0.0	2.7	0.3	0.0	0.2	0.0
Inorganic Insoluble Residue %	23.3	24.2	84.7	18.0	8.2	14.5	34.5

Sample Name	JL-U1-4.5	JL-U2-1.5	JL-U3-4.1	JL-U3-7.5	JL-U4-0.8	JL-U5-1.2	JL-U6-0.4
Stratigraphic Position (m)	753.1	756.7	761.6	765.0	767.7	769.8	771.1
Container Mass (g)	75.0	75.2	75.1	72.6	73.9	73.8	74.8
Sample Mass (g)	6.0	6.0	6.0	6.0	6.0	6.0	6.0
Container and Sample Mass (g)	81.0	81.2	81.1	78.6	79.9	79.8	80.8
Sample Mass after HCl (g)	3.1	1.6	2.1	1.8	1.0	0.6	2.1
Sample Mass after H_2O_2 (g)	0.0	0.0	0.0	0.0	0.0	0.0	0.0
Carbonate %	48.8	73.5	65.0	69.5	83.2	89.8	65.0
Organic Carbon %	0.3	0.5	0.3	0.2	0.3	0.8	0.0
Inorganic Insoluble Residue %	50.8	26.0	34.7	30.3	16.5	9.3	35.0

Sample Name	JL-U7-1.1	D-JL-U8-2.8	JL-U8-2.8	JL-U9-2.4	JL-U9-5.7	JL-U10-2.7	JL-U10-5.0
Stratigraphic Position (m)	772.5	775.7	775.7	778.1	781.4	784.1	786.4
Container Mass (g)	73.9	74.4	74.8	74.2	73.7	73.6	74.8
Sample Mass (g)	6.0	6.0	6.0	6.0	6.0	6.0	6.0
Container and Sample Mass (g)	79.9	80.4	80.8	80.2	79.7	79.6	80.8
Sample Mass after HCl (g)	1.6	1.2	1.2	0.7	1.3	1.7	1.6
Sample Mass after H_2O_2 (g)	0.0	0.0	0.0	0.0	0.0	0.0	0.0
Carbonate %	73.2	80.5	80.5	87.7	78.2	71.2	73.2
Organic Carbon %	0.2	0.0	0.2	0.3	0.7	0.0	0.2
Inorganic Insoluble Residue %	26.7	19.5	19.3	12.0	21.2	28.8	26.7

Sample Name	JL-U11-0.5
Stratigraphic Position (m)	787.3
Container Mass (g)	73.4
Sample Mass (g)	6.0
Container and Sample Mass (g)	79.4
Sample Mass after HCl (g)	0.7
Sample Mass after H_2O_2 (g)	0.0
Carbonate %	88.8
Organic Carbon %	0.7
Inorganic Insoluble Residue %	10.5